UNIL | Université de Lausanne

Unicentre
CH-1015 Lausanne
http://serval.unil.ch

Year : 2015

CHARACTERIZATION OF LOCAL AND SYSTEMIC IMMUNE-MODULATION IN MELANOMA PATIENTS

Natacha Bordry

Natacha Bordry, 2015, characterization of local and systemic immune-modulation in melanoma patients

Originally published at : Thesis, University of Lausanne

Posted at the University of Lausanne Open Archive http://serval.unil.ch
Document URN : urn:nbn:ch:serval-BIB_9F9512EEBA1F7

Droits d'auteur
L'Université de Lausanne attire expressément l'attention des utilisateurs sur le fait que tous les documents publiés dans l'Archive SERVAL sont protégés par le droit d'auteur, conformément à la loi fédérale sur le droit d'auteur et les droits voisins (LDA). A ce titre, il est indispensable d'obtenir le consentement préalable de l'auteur et/ou de l'éditeur avant toute utilisation d'une oeuvre ou d'une partie d'une oeuvre ne relevant pas d'une utilisation à des fins personnelles au sens de la LDA (art. 19, al. 1 lettre a). A défaut, tout contrevenant s'expose aux sanctions prévues par cette loi. Nous déclinons toute responsabilité en la matière.

Copyright
The University of Lausanne expressly draws the attention of users to the fact that all documents published in the SERVAL Archive are protected by copyright in accordance with federal law on copyright and similar rights (LDA). Accordingly it is indispensable to obtain prior consent from the author and/or publisher before any use of a work or part of a work for purposes other than personal use within the meaning of LDA (art. 19, para. 1 letter a). Failure to do so will expose offenders to the sanctions laid down by this law. We accept no liability in this respect.

UNIL | Université de Lausanne
Faculté de biologie
et de médecine

Ecole Doctorale
Doctorat MD-PhD

Imprimatur

Vu le rapport présenté par le jury d'examen, composé de

Président	Monsieur	Prof. Pedro **Romero**
Directeur de thèse	Monsieur	Prof. Daniel **Speiser**
Co-Directeur de thèse	Madame	Prof. Melody **Swartz**
Experts	Monsieur	Prof. Olivier **Michielin**
	Monsieur	Prof. Wolf Hervé **Fridman**
	Monsieur	Prof. Pierre-Yves **Dietrich**

le Conseil de Faculté autorise l'impression de la thèse de

Madame Natacha BORDRY

Médecin diplômé de la Confédération hélvétique

intitulée

CHARACTERIZATION OF LOCAL AND SYSTEMIC IMMUNE-MODULATION IN MELANOMA PATIENTS

Lausanne, le 9 octobre 2015

pour Le Doyen
de la Faculté de Biologie et de Médecine

Prof. Pedro Romero

UNIL | Université de Lausanne

Faculté de biologie
et de médecine

Ludwig Cancer Research Centre
Department of Oncology, University Hospital, Lausanne, Vaud (CHUV)

CHARACTERIZATION OF LOCAL AND SYSTEMIC IMMUNE-MODULATION IN MELANOMA PATIENTS

Thèse de doctorat

MD - PhD
présentée à la

Faculté de biologie et de médecine
de l'Université de Lausanne

par

Natacha BORDRY

Médecin diplômé de la Confédération Helvétique

Jury

Prof. Pedro Romero, président et répondant MD-PhD
Prof. Daniel Speiser, directeur de thèse
Prof. Melody Swartz, co-directeur de thèse
Prof. Olivier Michielin, expert
Prof. Wolf Hervé Fridman, expert
Prof. Pierre-Yves Dietrich, expert

Lausanne 2015

TABLE OF CONTENTS

ABBREVATIONS

ALM	Acral lentiginous melanoma
Arg-1	Arginase 1
APC	Antigen-presenting cells
BCR	B-cell receptor
CCL	Chemokine ligand
CCR	Chemokine receptor
CD	Cluster of differentiation
CGH	Comparative genomic hybridization
CSF-1	Colony stimulating factor-1
CSF-1R	Colony stimulating factor-1 receptor
CT	Center of tumor
CTL	Cytotoxic T lymphocyte
CTLA-4	Cytotoxic T lymphocytes-associated antigen 4
DAB	3,3'-Diaminobenzidine
DAMP	Danger associated molecular pattern
DC	Dendritic cell
DNA	Deoxyribonucleic acid
ELISA	Enzyme-linked immunosorbent assay
ELISPOT	Enzyme-linked immunospot
EM	Effector memory
EMRA	Effector memory RA
FACS	Fluorescence activated cell sorting
FasL	Fas ligand
FDA	Food and Drug Administration
FDC	Follicular dendritic cell
FFPE	Formalin-fixed paraffin-embedded
FGF	Fibroblast growth factor
FISH	Fluorescence in situ hybridization
FoxP3	Forkhead box 3
FPA	Focal Plane Array
FRC	Fibroblastic reticular cell
FTIR	Fourier transform infrared
HCA	Hierarchical cluster analysis
HEV	High endothelial venule
HGF	Hepatocyte growth factor
HPF	High power field
IDO	indolamin-2,3-dioxygenase
IF	Immunofluorescence
IFN-γ	Interferon gamma
IGF	Insulin-like growth factor
IHC	Immunohistochemistry
IL	interleukin
IM	Invasive margin
iNOS	Inducible nitric oxide synthase
IR	Infrared
LEC	Lymphatic endothelial cells
LCM	Laser capture microdissection
LDH	Lactate deshydrogenase
LMM	Lentigo maligna melanoma
LN	Lymph node
LVD	lymphatic vessel density

LYVE-1	Lymphatic vessel endothelial hyaluronan receptor-1
MCT	Mercury cadmium telluride
MDSC	Myeloid-derived suppressor cell
MHC	Major histocompatibility complex
NK	Natural killer
NM	Nodular melanoma
NSLN	Non-sentinel lymph node
PAMP	Pathogen associated molecular patterns
PCA	Principal component analysis
PCR	Polymerase chain reaction
PDGF	platelet-derived growth factor
PD-1	Programmed death-1
PD-L1	Programmed death ligand-1
PLS-DA	Partial least square discriminant analysis
PMBC	Peripheral blood mononuclear cell
PPR	Pattern recognition receptor
Prox-1	Prospero homebox-1
qRT-PCR	real time quantitative polymerase chain reaction
RT-PCR	Reverse transcription-polymerase chain reaction
SLN	Sentinel lymph node
S/N	Signal to Noise
SSM	Superficial spreading melanoma
TAM	Tumor-associated macrophage
TCR	T cell receptor
TGF-β	Transforming growth factor- β
Th	T helper
TIL	Tumor-infiltrating lymphocytes
TME	Tumor microenvironment
TNF-α	Tumor necrosis factor-α
Tregs	Regulatory T cell
TSA	Tyramide signal amplfication
VEGF-C	Vascular endothelial growth factor-C
VEGF-D	Vascular endothelial growth factor-D
VEGFR3	Vascular endothelial growth factor receptor-3
VEGFR2	Vascular endothelial growth factor receptor-2
WHO	World Health Organization

REMERCIEMENTS

Je voudrais tout d'abord remercier sincèrement et chaleureusement mon professeur de thèse, Daniel Speiser. Par sa grande sensibilité et son intelligence, il a su me guider et m'aiguiller au mieux durant toute ma thèse. Il m'a initiée, proposé et introduite dans différents projets translationnels afin que je puisse développer mes connaissances sur la biologie fondamentale tout en utilisant mes compétences cliniques. Sans sa présence et son soutien quotidiens, ces projets collaboratifs n'auraient certainement pas été possibles. Sa joie de vivre, son enthousiasme et sa passion ont été bien souvent un rempart contre le découragement et la démotivation qui m'ont parfois guettée dans les moments difficiles de mon doctorat. Enfin, nos conversations sur la place de la recherche fondamentale et translationnelle dans la prise en charge globale du patient et sur la nécessité d'une collaboration cordiale, honnête et respectueuse entre chercheurs mais aussi entre médecins m'ont permis de développer les compétences nécessaires pour mener à bien cette thèse et de pouvoir par la suite l'intégrer dans ma pratique clinique. Il m'est aussi important de remercier ma co-directrice de thèse Melody Swartz sans qui tout cela n'aurait pas été possible. Sa confiance et son intérêt dès notre première rencontre alors que je n'avais aucune expérience dans la recherche ont été un précieux atout et m'ont permis de pouvoir obtenir une bourse MD-PhD. Merci aussi pour son soutien, son enthousiasme et sa générosité.

Je remercie aussi les membres de mon comité de thèse, Pedro Romero, Olivier Michielin, Wolf Hervé Fridman et Pierre-Yves Dietrich pour leurs précieux conseils, leur aide et leur présence durant toutes les étapes de mon doctorat.

Cette thèse n'est pas uniquement le fruit de mon travail mais bien celui de différentes collaborations. Je voudrais surtout souligner ici que tout ce travail n'aurait pas pu se faire sans la participation et l'aide de nombreuses personnes.

Je tiens donc à remercier tout d'abord, Maria pour son inestimable aide dans une très grande partie de mon travail, ses encouragements, sa présence et sa passion. Elle a permis le développement d'une excellente collaboration entre le laboratoire de Daniel Speiser et Melody Swartz, et notre très bonne entente (et nos nombreuses heures passées ensemble) nous ont permis de tisser de beaux liens d'amitié. Nos diverses conférences, nos week-ends ou nos pauses café m'ont aidée à me ressourcer et à oublier nos déboires avec nos expériences. Merci aussi à Manuel, pour son aide, son enthousiasme à créer cette STM dream team et tous les bons moments que nous avons passés ensemble.

Un énorme merci aussi à Kaat, pour son aide dans les derniers moments de ma thèse quand j'ai été submergée par le reste du travail à finir. Sa bonne humeur, sa gentillesse et sa disponibilité m'ont été infiniment précieuse dans ces moments difficiles de ma thèse. Je suis heureuse de savoir que ce projet se continuera avec elle et je ne doute pas qu'elle le mènera à bien avec brio.

Je voudrais remercier notamment Natalie, pour notre très bonne collaboration, son enthousiasme, sa gentillesse, et son investissement dans la rédaction de notre manuscrit sur CSF-1. Merci aussi à Carola Ries et Sabine Hoves pour leur collaboration et leur soutien pour ce projet.

Cette thèse a principalement été axée sur le développement de techniques d'immunohistochimie et l'étude des marqueurs dans les tissus humains. Ce travail n'aurait donc pas été possible sans le travail et la disponibilité de nos collaborateurs du Département de Pathologie du CHUV. Je voudrais donc tout particulièrement remercier Susana Leubat, Véronique Noguet, Marie Carmen Silva et Alain Michel pour leur extraordinaire implication et soutien dans ce travail en plus de leurs activités cliniques. Un très grand merci aussi à Periklis, Esther et Katia pour leur disponibilité et leur aide dans la conception et la réalisation de ce travail de recherche.

Un grand merci aussi aux associées de recherches cliniques Laurène, Samia et Hélène qui m'ont aidée dans la recherche des tissus des patients, dans l'analyse des données cliniques et bien évidemment aussi pour tout ce que nous avons partagé. Cette thèse n'aurait aussi certainement pas vu le jour sans leur travail.

Je voudrais encore remercier nos collaborateurs de Bruxelles, Eric Goormaghtigh et Noémie Wald avec qui j'ai eu de la chance de collaborer sur un projet très prometteur. Je les remercie pour leur implication, leur disponibilité, leur enthousiasme et leur gentillesse.

Merci aussi aux personnes de la Dermatologie et plus particulièrement à Patrick Perrier, François Kuonen, Daniel Hohl, Isabelle Surbeck, Laurence Feldmeyer et Olivier Gaide pour leur aide et implication dans l'élaboration du protocole clinique pour les mélanomes primaires.

Un énorme merci aussi à Philippe. Si je suis arrivée jusqu'au bout, c'est certainement en très grande partie grâce à lui. Ses excellentes connaissances, sa rigueur, son intégrité, son soutien et son professionnalisme m'ont été indispensable durant toute l'élaboration de cette thèse. Merci aussi pour tout ce que nous avons partagé et j'ai été heureuse de découvrir la belle personne que tu es.

Je voudrais remercier tout particulièrement Tim qui a passé de nombreuses heures en plus de son travail à corriger mes documents et ma thèse. Son implication, sa justesse, son expertise et sa disponibilité m'ont énormément aidée et m'ont permis de rendre un travail de qualité. Merci aussi pour tous ces très beaux moments que nous avons vécus et partagés ensemble au labo comme à l'extérieur pendant ces années, je ne les oublierai pas.

Bien évidemment à Mathilde pour sa passion, son énergie et sa magnifique amitié. Pour les innombrables heures où elle m'a écouté, réconforté et encouragé. Son enthousiasme, sa détermination, son implication dans son travail ont été un exemple et une source d'inspiration pour moi. Elle a réussi l'impensable: me faire apprécier et aimer la recherche pour ce qu’elle est et à sa juste valeur. Elle a changé le cours de ma thèse et encore bien plus ensuite. La personne vive, lumineuse, entière, inspirante et riche que tu es m’a tant apporté et je pense qu’elle sera l’avenir de la recherche moderne.

A Damien aussi pour sa présence, son rire (incroyable), sa spontanéité et son soutien sans faille. J’ai adoré nos petites pauses cafés à discuter de la vie et de bien d’autres choses encore.

Merci aussi à Anais et Hélène pour nos fous-rires, “nos délires” et ce que nous avons construit ensemble depuis notre rencontre. Vous avez été mes premières belles rencontres lors de ce doctorat, une bouffée d’air frais, de joie et d’amour dans ce monde que j’ai eu de la peine à apprivoiser à mes débuts.

Ma thèse n’aurait pas été là même sans toute la grande famille du Ludwig et plus particulièrement Alex, Bérengère, Romain, Greg, Amandine, Rebecca, Carla, Amélie, Gwen, Natalia et Amaia, j’ai partagé de superbes moments avec vous. Nos fous rires et nos moments de folies ont été un souffle et un bol d’air frais durant toute ma thèse. Vous êtes de merveilleuses personnes que j’ai eu beaucoup de plaisir à connaître et à découvrir. Je garderai des souvenirs mémorables de tout ce que nous avons partagé pendant ces trois ans et je sais que vous allez beaucoup me manquer.

Enfin je voudrais remercier ma famille et mes amis pour leur soutien, leur présence et leur amour dans tous les moments qui ont jalonné ma thèse.

RÉSUMÉ DESTINÉ A UN LARGE PUBLIC

Le mélanome cutané est un des cancers les plus agressifs et dont l'incidence augmente le plus en Suisse. Une fois métastatique, le pronostic de survie moyenne avec les thérapies actuelles est d'environ huit mois, avec moins de 5% de survie à cinq ans. Les récents progrès effectués dans la compréhension de la biologie de la cellule tumorale mais surtout dans l'importance du système immunitaire dans le contrôle de ce cancer ont permis le développement de nouveaux traitements novateurs et prometteurs. Ces thérapies, appelées immunothérapies, reposent sur la stimulation et l'augmentation de la réponse immunitaire à la tumeur. Alors que les derniers essais cliniques ont démontré l'efficacité de ces traitements chez les patients avec des stades avancés de la maladie, le contrôle de la maladie à long-terme est seulement atteint chez une minorité des patients. La suppression locale et systémique de la réponse immunitaire spécifique anti-tumorale apparaitrait comme une des raisons expliquant la persistance d'un mauvais pronostic clinique chez ces patients. Des études sur les souris ont montré que les vaisseaux lymphatiques joueraient un rôle primordial dans ce processus en induisant une tolérance immune, ce qui permettrait à la tumeur d'échapper au contrôle du système immunitaire et métastatiser plus facilement. Ces excitantes découvertes n'ont pas encore été établi et prouvé chez l'homme. Dans cette thèse, nous montrons pour la première fois que les vaisseaux lymphatiques sont directement impliqués dans la modulation de la réponse immunitaire au niveau local et systémique dans le mélanome chez l'homme. Ces récentes découvertes montrent le potentiel de combiner des thérapies visant le système lymphatique avec les immunothérapies actuellement utilisées afin d'améliorer le pronostic des patients atteint du mélanome.

SUMMARY

Cutaneous melanoma is one of the most invasive and metastatic human cancers and causes 75% of skin cancer mortality. Current therapies such as surgery and chemotherapy fail to control metastatic disease, and relapse occurs frequently due to microscopic residual lesions. It is, thus, essential to develop and optimize novel therapeutic strategies to improve curative responses in these patients. In recent decades, tumor immunologists have revealed the development of spontaneous adaptive immune responses in melanoma patients, leading to the accumulation of highly differentiated tumor-specific T cells at the tumor site. This remains one of the most powerful prognostic markers to date. Immunotherapies that augment the natural function of these tumor-specific T cells have since emerged as highly attractive therapeutic approaches to eliminate melanoma cells. While recent clinical trials have demonstrated great progress in the treatment of advanced stage melanoma, long-term disease control is still only achieved in a minority of patients. Local and systemic immune suppression by the tumor appears to be responsible, in part, for this poor clinical evolution. These facts underscore the need for a better analysis and characterization of immune-related pathways within the tumor microenvironment (TME), as well as at the systemic level. The overall goal of this thesis is, thus, to obtain greater insight into the complexity and heterogeneity of the TME in human melanoma, as well as to investigate immune modulation beyond the TME, which ultimately influences the immune system throughout the whole body. To achieve this, we established two main objectives: to precisely characterize local and systemic immune modulation (i) in untreated melanoma patients and (ii) in patients undergoing peptide vaccination or checkpoint blockade therapy with anti-cytotoxic T-lymphocyte-asisctaed protein-4 (CTLA-4) antibody. In the first and main part of this thesis, we analyzed lymphatic vessels in relation to anti-tumor immune responses in tissues from vaccinated patients using a combination of immunohistochemistry (IHC) techniques, whole slide scanning/analysis, and an automatic quantification system. Strikingly, we found that increased lymphatic vessel density was associated with high expression of immune

suppressive molecules, low functionality of tumor-infiltrating CD8$^+$ T cells and decreased cytokine production by tumor-antigen specific CD8$^+$ T cells in the blood. These data revealed a previously unappreciated local and systemic role of lymphangiogenesis in modulating T cell responses in human cancer and support the use of therapies that target lymphatic vessels combined with existing and future T cell based therapies. In the second objective, we describe a metastatic melanoma patient who developed pulmonary sarcoid-like granulomatosis following repetitive vaccination with peptides and CpG. We demonstrated that the onset of this pulmonary autoimmune adverse event was related to the development of a strong and long-lasting tumor-specific CD8$^+$ T cell response. This constitutes the first demonstration that a new generation tumor vaccine can induce the development of autoimmune adverse events. In the third objective, we assessed the use of Fourier Transform Infrared (FTIR) imaging to identify melanoma cells and lymphocyte subpopulations in lymph node (LN) metastasis tissues, thanks to a fruitful collaboration with researchers in Brussels. We demonstrated that the different cell types in metastatic LNs have different infrared spectral features allowing automated identification of these cells. This technic is therefore capable of distinguishing known and novel biological features in human tissues and has, therefore, significant potential as a tool for histopathological diagnosis and biomarker assessment. Finally, in the fourth objective, we investigated the role of colony-stimulating factor-1 (CSF-1) in modulating the anti-tumor response in ipilimumab-treated patients using IHC and *in vitro* co-cultures, revealing that melanoma cells produce CSF-1 via CTL-derived cytokines when attacked by cytotoxic T lymphocytes (CTLs), resulting in the recruitment of immunosuppressive monocytes. These findings support the combined use of CSF-1R blockade with T cell based immunotherapy for melanoma patients. Taken together, our results reveal the existence of novel mechanisms of immune modulation and thus promote the optimization of combination immunotherapies against melanoma.

RÉSUMÉ

Le mélanome cutané est un des cancers humains les plus invasifs et métastatiques et est responsable de 75% de la mortalité liée aux cancers de la peau. Les thérapies comme la chirurgie et la chimiothérapie ont échoué à contrôler le mélanome métastatique, par ailleurs les rechutes sous ces traitements ont été montrées fréquentes. Il est donc essentiel de développer et d'optimiser de nouvelles stratégies thérapeutiques pour améliorer les réponses thérapeutiques de ces patients. Durant les dernières décennies, les immunologistes spécialisés dans les tumeurs ont démontré qu'un patient atteint du mélanome pouvait développer spontanément une réponse immune adaptative à sa tumeur et que l'accumulation de cellules T spécifiques tumorales au sein même de la tumeur était un des plus puissants facteurs pronostiques. Les immunothérapies qui ont pour but d'augmenter les fonctions naturelles de ces cellules T spécifiques tumorales ont donc émergé comme des approches thérapeutiques très attractives pour éliminer les cellules du mélanome. Alors que les derniers essais cliniques ont démontré un progrès important dans le traitement des formes avancées du mélanome, le contrôle de la maladie à long-terme est seulement atteint chez une minorité des patients. La suppression immune locale et systémique apparaitrait comme une des raisons expliquant la persistance d'un mauvais pronostic clinique chez ces patients. Ces considérations soulignent la nécessité de mieux analyser et caractériser les voies immunitaires non seulement au niveau local dans le microenvironement tumoral mais aussi au niveau systémique dans le sang des patients. Le but de cette thèse est d'obtenir une plus grande connaissance de la complexité et de l'hétérogénéité du microenvironement tumoral dans les mélanomes mais aussi d'investiguer la modulation immunitaire au delà du microenvironement tumoral au niveau systémique. Afin d'atteindre ce but, nous avons établi deux objectifs principaux : caractériser précisément la modulation locale et systémique du système immunitaire (i) chez les patients atteints du mélanome qui n'ont pas reçu de traitement et (ii) chez les patients qui ont été traités soit par des vaccins soit par des thérapies qui bloquent les points de contrôles. Dans la première et

majeure partie de cette thèse, nous avons analysé les vaisseaux lymphatiques en relation avec la réponse immunitaire anti-tumorale dans les tissus des patients vaccinés grâce à des techniques d'immunohistochimie et de quantification informatisé et automatique des marquages. Nous avons trouvé qu'une densité élevée de vaisseaux lymphatiques dans la tumeur était associée à une plus grande expression de molécules immunosuppressives ainsi qu'à une diminution de la fonctionnalité des cellules T spécifiques tumoral dans la tumeur et dans le sang des patients. Ces résultats révèlent un rôle jusqu'à là inconnu des vaisseaux lymphatiques dans la modulation directe du système immunitaire au niveau local et systémique dans les cancers de l'homme. Cette recherche apporte finalement des preuves du potentiel de combiner des thérapies visant le système lymphatique avec des autres immunothérapies déjà utilisées en clinique. Dans le second objectif, nous rapportons le cas d'un patient atteint d'un mélanome avec de multiples métastases qui a développé à la suite de plusieurs vaccinations répétées et consécutives avec des peptides et du CpG, un évènement indésirable sous la forme d'une granulomatose pulmonaire sarcoid-like. Nous avons démontré que l'apparition de cet évènement était intimement liée au développement d'une réponse immunitaire durable et spécifique contre les antigènes de la tumeur. Par là-même, nous prouvons pour la première fois que la nouvelle génération de vaccins est aussi capable d'induire des effets indésirables auto-immuns. Pour le troisième objectif, nous avons voulu savoir si l'utilisation de la spectroscopie infrarouge à transformée de Fourier (IRTF) était capable d'identifier les cellules du mélanome ainsi que les différents sous-types cellulaires dans les ganglions métastatiques. Grâce à nos collaborateurs de Bruxelles, nous avons pu établir que les diverses composantes cellulaires des ganglions atteints par des métastases du mélanome présentaient des spectres infrarouges différents et qu'elles pouvaient être identifiées d'une façon automatique. Cette nouvelle technique permettrait donc de distinguer des caractéristiques biologiques connues ou nouvelles dans les tissus humains qui auraient des retombées pratiques importantes dans le diagnostic histopathologique et dans l'évaluation des biomarqueurs. Finalement dans le dernier objectif,

nous avons investigué le rôle du facteur de stimulation des colonies (CSF-1) dans la modulation de la réponse immunitaire anti-tumorale chez les patients qui ont été traités par l'Ipilimumab. Nos expériences in vivo au niveau des tissus tumoraux et nos co-cultures in vitro nous ont permis de démontrer que les cytokines secrétées par les cellules T spécifiques anti-tumorales induisaient la sécrétion de CSF-1 dans les cellules du mélanome ce qui résultait en un recrutement de monocytes immunosuppresseurs. Dans son ensemble, cette thèse révèle donc l'existence de nouveaux mécanismes de modulation de la réponse immunitaire anti-tumorale et propose de nouvelles optimisations de combinaison d'immunothérapies contre le mélanome.

INTRODUCTION

1 Immune response

The immune system may protect the host from potential tissue damage as seen during infection and cancer. The immune system is made up of two major arms, the innate and adaptive immune systems. The innate immune system is universal among animals and includes ancient forms of host defense against infection, while the adaptive immune system is more specialized and can be found only in vertebrates.

1.1 Innate immune response

Innate immunity provides the initial line of defense against microbes. Innate immune responses are induced by recognition of molecular structures common to related groups of microbes, and may not distinguish minor differences between invading pathogens. The innate immune system comprises several cell types, principally neutrophils, professional antigen-presenting cells (APCs) (i.e. macrophages, monocytes, dendritic cells (DC) and B cells) and natural killer (NK) cells. These cells express non-clonally distributed receptors called pattern recognition receptors (PRRs) that recognize pathogen-associated molecular patterns (PAMPs) found in microbes, or danger-associated molecular patterns (DAMPs) that are found in self-tissues (1). The binding of these molecules to their receptors on innate immune cells induces signal transduction, secretion of cytokines and chemokines, and maturation of DCs that promote the recruitment and activation of cells of the adaptive immune system.

1.2 Adaptive immune response

In contrast to innate immunity, more highly evolved defense mechanisms are stimulated by exposure to infectious agents and increase in magnitude and defensive capacity with each successive exposure to a particular microbe. Since this form of immunity develops as a response to infection or inflammation and adapts during the course of the response, it is called adaptive immunity. The adaptive immune system is composed of two parts, called humoral immunity and cell-mediated immunity. The humoral response is mediated by B cells and is directed against extracellular pathogens such as bacteria, while the cellular response is directed against intracellular pathogens such as viruses. B and T cells express specific B cell receptors (BCR) and T cell-receptors (TCR) capable of recognizing a very large variety of potential pathogens. However, the repertoire of antigens recognized by any single BCR or TCR is very limited.

Peptide antigens are presented on major histocompatibility complex (MHC) class I or II molecules on the cell surface. Cytosolic antigens are presented on MHC class I (present in almost any normal cell) and are recognized by TCRs of $CD8^+$ T cells, while antigens in the endosomal compartment are presented on MHC class II (usually by APCs) and are recognized by TCRs of $CD4^+$ T cells. CD4 and CD8 are two mutually exclusive co-receptors expressed by T cells. CD8 T cells have strong cytotoxic functions and are specialized to kill infected cells. CD4 T cells, also called T helper cells, support CD8 T cells in targeting and eliminating foreign antigens by producing cytokines such as the survival factor IL-2. CD4 T cells differentiate to specialized populations with dedicated functions, by polarizing into Th1, Th2, Th17, Th9, T_{FH} and Treg cells. The presentation of a cognate antigenic peptide on MHC molecules by APCs and subsequent ligation of the TCR on naïve T lymphocytes in the lymph node (LN) is the first step in the induction of an adaptive immune response and is called priming (2). The successful development of the cellular immune response depends on this interaction. Once a T cell is activated, it proliferates, differentiates into effector cells and migrates to the inflamed tissues to eliminate cells displaying cognate antigen on the cell surface. After the T cell response reaches a peak the majority of the effector cells die, generally following the elimination of infected cells. Importantly, a minority of activated T cells survive and become memory cells which are able to reactivate more quickly and strongly upon antigenic re-encounter.

2 Anti-tumor immune response

Cancer is the leading cause of death in developed countries (3). As described by Hanahan and Weinberg, cancer cells progressively acquire “hallmarks”, which allow them to survive, proliferate and eventually lead to clinically-detectable disease (4). Cancer cells are able to acquire these hallmarks in large part due to their genomic instability, and Darwinian selection of the most aggressive cells. Besides the properties that enable cancer cells to proliferate endlessly and resist cell death, cancer cells promote inflammatory mechanisms in the tumor microenvironment (TME) (5). Tumor-promoting inflammation is a powerful asset for the tumor as it facilitates access to necessary growth factors, as well as active prevention of tumor destruction by immune cells (6, 7).

In the last decade, particular attention has been given to understanding the complex interactions between a developing tumor and the host immune system. It is known that the immune system operates as a significant barrier to tumor formation and progression in humans. Several studies have illustrated that a functional cancer immunosurveillance process actually exists. Firstly, immunosuppressed transplant recipients display higher incidence of nonviral cancer compared to an age-matched immunocompetent control population. A 4-fold increase in the incidence of *in situ* melanoma can be found in patients that have undergone transplants (8). Furthermore, in patients that have received organ transplants, melanoma constituted 5.2% of post-transplant skin cancers compared with an incidence of 2.7% in the general population (9).

Secondly, cancer patients can also develop spontaneous adaptive and innate immune responses against cancer. Indeed, $CD8^+$ and $CD4^+$ T cell responses to tumor antigen have been detected in the blood circulation as well as at tumor sites in patients (10, 11). It has also been found that tumor specific T cells can recognize tumor-derived epitopes and can kill tumor cells displaying these epitopes *in vitro* (12). The increased peripheral precursor frequency in cancer patients compared to healthy donors, as well as the proof of generation of memory cells at sites of antigen expression have been considered as hallmarks of immunization (13). Although these responses may not always be able to prevent the development of cancer they may, nevertheless, function to attenuate tumor growth.

Finally, recent evidence points to the importance of the density of tumor-infiltrating lymphocytes (TILs) in relation to clinical outcome of cancer patients (14-16). The distribution of lymphocytes, as well as the quantification of the density and location of immune cells within the tumor (also termed immunoscore) has been shown to have a high prognostic impact (17-19). Specifically, high infiltration of memory Th1 and CD8$^+$ T cells into the tumor microenvironment has been reported to correlate with favorable clinical impact in a large array of different types of tumors such as melanoma, head and neck, breast, ovarian, esophageal, prostate, lung, pancreatic, anal and urothelial cancer (20). The clinical impact of other T cell populations remains less clear.

Taken together, these considerations highlight the important role that the immune system plays in protecting the host from tumor development and progression.

2.1 Immune escape mechanisms and tumor microenvironment

In spite of the development of an immune response to tumors and the accumulation of highly differentiated tumor-specific T cells at the tumor site, patients still frequently experience poor clinical evolution of their disease. This observation shed light on the existence of immune evasion mechanisms.

Tumor escape mechanisms are numerous and diverse. Some changes occur directly at the level of the tumor cells (e.g. loss/down-regulation of antigen presentation, disruption of the antigen processing machinery) while others involve modulation and disruption of the host immune system.

Cancer cells may hamper the development of an anti-tumor immune response by negatively modulating T cell activation and proliferation and effector functions. These properties of T cells are necessary to protect the host from cancer or infections. Tumors develop several strategies to inhibit effector T cells. First, via expression of inhibitory surface receptors such as programmed-cell death ligand (PD-L1) and Fas ligand (FasL) (21). Second, via the production of certain cytokines such as transforming growth factor beta (TGF-β) (22) and, third, via the depletion of nutrients in the local environment such as arginine and tryptophan. The production of Indoleamine 2,3-dioxygenase (IDO), inducible nitric oxide synthase (iNOS) and arginase by cancer cells, as well as other cells such as macrophages and DCs, degrades tryptophan and arginine leading to functional T cell deficiency (23, 24). Other mechanisms by which tumors suppress T cells include inhibition of proinflammatory signals, attraction of immune suppressive cells such as T regulatory cells (Tregs) and myeloid-derived suppressor cells (MDSC), and inhibition of DC maturation and $CD4^+$ T helper cells (25).

Over the past decades, it has been illustrated that tumor cells do not act in isolation, but are able to orchestrate fibroblasts, endothelial cells, pericytes, leukocytes, soluble factors and the extra-cellular matrix into a tumor-promoting microenvironment (TME). In this environment, malignant behavior is supported by the promotion of neoplastic transformation, tumor growth and invasion, protection from host immunity, development of therapeutic resistance, and establishment of niches for dormant metastases (26). There is increasing evidence that tumor evasion mechanisms (as described above) are, indeed, initiated and maintained by a constitutive interaction between tumors and the TME in mouse as well as in human cancers (27).

It has become clear that the TME is an inhospitable milieu for mounting an anti-tumor immune response. A thorough analysis of the immune suppressive mechanisms present in the TME is, thus, essential to better understand tumor/host interactions, upon which one can design novel immunotherapies that harness the full potential of the anti-tumor immune response.

These principles apply to the majority of human cancers. However, we now know that cancer is an extremely heterogeneous disease in terms of, for example, the degree of genetic mutation of tumor cells or the extent of intratumoral infiltration by immune cells. Even within a single diagnostic group such as ‘colorectal cancer’ or ‘breast cancer’ there may be huge diversity. We have chosen to study human melanoma, a disease with frequent involvement of inflammatory mechanisms and immune cell infiltration.

3 Melanoma

Melanoma is a solid malignant tumor originating from the specialized pigmented cells known as melanocytes. Melanocytes are essential to protect the skin from the damaging effects of UV radiation by secreting the brown pigment, melanin. Melanoma arises most frequently from melanocytes in the skin, but melanoma may also develop from the eyes or mucosa.

3.1 Epidemiology and risk factors

Cutaneous melanoma is one of the most invasive and metastatic human cancers and causes 75% of skin cancer mortality. Worldwide about 160,000 new cases of melanoma are diagnosed annually and melanoma incidence has risen 3-8% per year since the mid-1960s (28). At current rates, the lifetime risk for Caucasian men to develop invasive melanoma is 1 in 39 and 1 in 58 in women. This contrasts dramatically with a lifetime risk of 1 in 1500 for people born in 1935 (29). Of all cancers, cutaneous melanoma ranks with the fifth incidence among men and seventh among women and is the second leading cause of lost productive years (30). Therefore, this cancer has become an increasingly significant public heath problem.

Geographical latitude, severe episodic sunburn in early life, and tanning bed exposure are important factors associated with melanoma (31). Other risk factors are a family history, immunosuppression, previous melanoma and the presence of multiple clinically atypical nevi. The locations on the body at which the disease most frequently occurs reflects its primary cause, UV exposure, as well as a relationship with the amount of skin pigmentation (32).

3.2 Pathogenesis

The pathogenesis of human melanocyte transformation remains to be fully understood. Ultraviolet solar radiation promotes malignant change in the skin via direct mutagenic effects on DNA. Specifically, the cellular constituents of the skin are stimulated to produce growth factors, cutaneous immune defenses are suppressed, and production of reactive oxygen species is promoted, leading to deoxyribonucleic acid (DNA) damage and suppression of apoptosis (28). Melanocytes progress through a series of steps toward malignant transformation by accumulating genetic abnormalities. Clark et al, proposed a model based on histopathological and clinical features that depict the proliferation of melanocytes in the process of forming nevi (e.g. benign nevi) and the subsequent development of dysplasia (e.g. dysplastic nevi), hyperplasia (e.g. radial-growth phase in the epidermis), invasion (e.g. vertical growth phase in the dermis) and metastasis (e.g. metastatic melanoma) (33). The frequency of the progression of nevi toward malignant lesions is still unknown and the majority of dysplastic nevi will not result in melanoma. Several models of the genetic basis of melanoma development and progression are based on Clark’s multi-step model. However, some studies have challenged this model by showing that melanoma may arise *de novo* from non-melanocytic nevi (34).

3.3 Diagnosis

The most important factor for successful management of melanoma is early diagnosis. Melanoma is usually diagnosed by phenotypical pigmentation alterations. The mnemonic “ABCD” (Asymmetry, Border irregularity, Color variegation, Diameter >6 mm) created 20 years ago have helped both clinicians and laypersons to recognize melanoma in its early clinical presentation (35). Nevertheless, any significant change in existing nevi or skin lesions should raise clinical suspicion because some melanomas do not display the classical features. Indeed, in some studies more than 50% of nodular melanoma were predominantly amelanotic (red or pink) (28). During the last decade, new computer-based technologies have improved diagnostic sensitivity and specificity (29).

Pathologic examination remains the gold standard for diagnosis. The heterogeneous histological appearance of malignant melanoma has led to the frequent use of immunohistochemistry to achieve accurate and reliable diagnosis. The three antibodies S100, HMB45 and Melan-A are currently the most frequently used combination for melanocytic lesion diagnosis. S100 is the most sensitive marker of melanocytes but lacks specificity, whereas HMB45 (monoclonal antibody against group 100 protein) is a more specific marker that lacks sensitivity. Melan-A exhibits a sensitivity between that of S100 and HMB45 (36). Finally, the anatomopathological analyses of melanoma tissues allow to define the type of melanoma, the thickness, the ulceration and the mitotic rate.

3.4 Melanoma classification

Primary melanoma can present different growth patterns and incidence of these growth patterns varies according to sex, age and race. The four major growth subtypes (based on microscopic growth patterns) are superficial spreading melanoma (SSM), lentigo maligna melanoma (LMM), nodular melanoma (NM) and acral lentiginous melanoma (ALM) (37). This classification has been widely used both by clinicians and researchers, and the current World

Health Organization (WHO) classification of skin tumors is based on this system. Other systems of classification have also emerged in order to integrate clinicopathological features with somatic genetic alterations (34). Accounting for almost two thirds of all primary melanoma, SSM is the most common subtype and it is most frequent on sites with acute-intermittent sun exposure whereas LMM is known to be related to chronic sun exposure. In contrast, ALM is mainly found on palm of hands and sole of feet and are therefore not linked to sun exposure. Although used clinically as descriptive tools, the different classifications have no prognostic value or therapeutic implications (34).

3.5 Prognosis

Evaluating the prognosis of the patient by an appropriate evaluation and staging of the cancer is essential for treatment planning, stratification and assessment of clinical trials. Primary tumor thickness (also known as the Breslow depth), ulceration, and a mitotic rate higher than $1/mm^2$ (assessed by the anatomopatholical analysis of the excised lesion) are factors associated with decreased survival rate and are the most widely used prognostic indicators for survival in malignant melanoma. However, these factors are still inaccurate for a significant number of patients. Up to 15% of patients with invasive thin tumors (< 1 mm) still develop metastatic disease (38). Similarly, a substantial proportion of patients with thick melanoma (≥ 4 mm) will have relatively long-term survival (58% for > 5 years) (39). Currently, clinical prognosis is based on the TNM classification, which describes the severity of the melanoma based on the size and extent of the tumor and whether or not it has spread to distant organs. TNM stages are ranking from stage I (localized melanoma) to stage IV (melanoma with distant metastasis) (40). It has been shown that patient survival is highly dependent on the stage of the disease. Yet, some disparities among stage are also observed, suggesting metastases may begin as a clinically silent event early in the development of a primary tumor.

As with other cancers, death is due to the development of distant metastases. Specifically, cutaneous melanoma is distinguished by its propensity for early metastatic spread via lymphatic vessels to regional lymph nodes, even at the early stages of tumor invasion. Lymph-node metastases, as detected by analysis of the sentinel lymph node (SLN) (first node draining the primary tumor), is one of the major determinants for the staging and clinical management of melanoma (41), although disease will recur in 22% of lymph-node-negative patients (42).

Altogether, these results point out that there is an urgent need to identify more refined and dynamic prognostic indicators. The TME at the time of diagnosis, or of surgery, is a hallmark of how the patient and the tumor have interacted. Furthermore, different elements of the TME may impact the clinical evolution of cancer differently. Therefore, the analysis and characterization of the various components of the TME within the tumor could be one of the most promising and powerful prognostic markers (43). In this line, several studies have shown that the immunoscore and the immune contexture have a strong clinical impact and can predict response to immunotherapies (44).

3.6 Treatments

Complete surgical excision with wide margins represents the therapy of choice for primary melanomas. Additionally, radical lymphadenectomy can be undertaken when the SLN(s) is (are) positive or when one or more lymph node(s) is (are) clinically positive (palpable nodal enlargement or abnormal features on ultrasound imaging). For progressing disease, other treatments include chemotherapy (Dacarbazine), IL-2 or IFN-α therapies. However, these usually fail to control the disease and relapses occur frequently due to microscopic residual lesions. Therefore, targeted therapies and immunotherapies have emerged as promising anti-cancer strategies.

3.6.1 Targeted therapies

Targeted therapies specifically target molecular alterations in melanoma. About half of cutaneous melanomas harbor a mutation of BRAF, primarily V600E, leading to activation of the MAPK pathway. Small molecule inhibitors of the MAPK pathway (e.g. BRAF or MEK inhibitors) have demonstrated remarkable clinical activity with responses in approximately half of the patients in phase II and III clinical trials leading to increased overall survival (45, 46). Unfortunately, due to several modes of treatment resistance, the majority of responding patients will experience disease progression within an average time of six months (47, 48). However, combination regimens of BRAF-MEK inhibitors have been shown to overcome these resistance mechanisms at least partially, and thus significantly improve the progression free-survival time (49-51).

3.6.2 Immune checkpoint blockade therapies

Monoclonal antibodies that block immune-inhibitory pathways (e.g. anti-cytotoxic T-lymphocyte–associated antigen 4 (CTLA-4) and anti-programmed death 1 (PD-1) receptor) or their ligands (e.g. PD-L1) aim to enhance T cell responses against tumor cells and can induce durable objective clinical responses. The significant proportion of patients with advanced unresectable melanoma who respond to such treatments attests to the potency of anti-melanoma immunity in tumor rejection (15% for anti-CTLA-4 therapy and 35-40% for anti-PD-L1 therapy) (52-54). Moreover, combination treatment with anti-CTLA-4 and anti-PD-1 antibodies results in even increased rates of objective clinical responses (around 60%) (55, 56) and represents, along with sequential therapies, the future of melanoma therapy (57). However, because of their capacity to overcome immune tolerance their toxicities are usually high, resulting in frequent autoimmune adverse events (58, 59).

Anti-CTLA-4 therapy

CTLA-4 is a molecule expressed on the surface of CD4 and CD8 T cells as well as $CD25^{+}FoxP3^{+}$ regulatory T cells. CTLA-4 competes with CD28 to bind to its ligands B7-1 (CD80) and B7-2 (CD86) on APCs. Therefore, CTLA-4 acts as an inhibitory molecule that limits activation of T cells and prevents them from prolonged activity (60).

Two anti-CTLA-4 monoclonal antibodies, generated by different companies, have been tested in clinical trials in metastatic melanoma patients: Tremelimumab (Pfizer) and Ipilimumab/Yervoy (Bristol Myers Squibb), but only the latter was successful in phase III studies (61). Two important phase III studies have tested the clinical efficacy of Ipilimumab in advanced metastatic melanoma patients. In the first clinical trial, previously treated metastatic melanoma patients received either Ipilimumab, gp100 vaccine or the combination of both, in a randomized, double-blind manner (52). Treatment with Ipilimumab led to an improvement of median overall survival rates (10.0 and 10.1 months) compared with the gp100 vaccine-only treated group (6.4 months). In the second trial, metastatic melanoma patients that had not previously been treated received either dacarbazine or Ipilimumab in combination with dacarbazine in a double-blind manner (62). As in the first trial, Ipilimumab increased overall survival rates from 9.1 to 11.2 months. In the two trials, adverse events (mainly skin and gastro-intestinal auto-immune reactions) were noted in nearly all the patients. Based on these two exciting reports Ipilimumab was approved by the European Union (2010) and the Food and Drug Administration (FDA) (March 2011).

Unfortunately, the clinical benefit following immune checkpoint blockade of CTLA-4 is limited to a fraction (about 15%) of treated patients, and the mechanisms of action are still poorly understood. Moreover, no reliable biomarkers of clinical efficacy are available to date. The identification of biomarkers that are associated with clinical responses to Ipilimumab may help to identify patients likely to benefit from the treatment.

Although other immunotherapies such as blockade of the PD-1/PD-L1 pathway or adoptive T cell therapy are in part very successful (63), they are not further described here as this thesis does not deal with patients who received these therapies.

3.6.3 Anti-tumor vaccination

Various vaccine formulations are currently used, with different forms of antigen (e.g. proteins, peptides, tumor lysates) and different delivery systems (e.g. dendritic cells, other antigen presenting cells, nanoparticles, recombinant viruses). Furthermore, adjuvants are essential components of vaccines. Indeed, they increase the immunogenicity of antigens by triggering the activation and maturation of dendritic cells (64). Peptide cancer vaccines have the potential benefits of being highly specific, stable and relatively easy to produce (65, 66). Furthermore, their low toxicity profiles suggest that they may be attractive options for cancer patients.

Many studies of vaccine monotherapy conducted in patients with advanced cancers have yielded evidence of melanoma-specific immunization, but have failed to produce significant clinical response rates (about 5%) (67). Nevertheless, vaccines capable of inducing melanoma-specific immune activation still hold promise for eliminating or stabilizing microscopic or “minimal residual” disease (68). Despite the fact that significant technical and scientific progress has been achieved in the fields of vaccinology, much remains to be accomplished both in terms of efficacy and applicability (69). As for the combination of immune checkpoint blockade, co-treatment with tumor cell vaccines and other immunotherapies has been shown to improve clinical prognosis (70). Further characterization and assessment of primary tumors as well as metastatic tissues of these patients will not only extend our knowledge on the TME but also potentially identify novel cancer immunotherapeutic targets, which will improve the design of new combination therapies.

3.6.4 The LUD 00-018 study

Research groups at the Ludwig Institute of Cancer Research, the CHUV and UNIL have conducted a cancer vaccine study. Between 2003 and 2011, a phase I clinical trial (LUD 00-018 study, ClinicalTrials.gov Identifier NCT00112229) was completed to evaluate whether melanoma-specific immune responses could be induced through vaccination with melanoma antigenic peptide and adjuvants in patients diagnosed with stage III or IV melanoma. 29 melanoma patients were included and vaccinated with Melan-A analog (ELA) or native (EAA) peptide ± Tyrosinase (YMD) peptide, CpG-B-7909 and Montanide ISA-51 adjuvants in order to stimulate tumor antigenic specific CD8+ T lymphocytes.

At the beginning of the study, the patients were asked for their previous medical history (including other treatments received before this clinical trial), their age, the type and localization of their primary tumor. Their immune cell phenotypes were also determined at baseline. Patient survival and tumor response were assessed as readout for disease evolution. Furthermore, each patient was tested for the development of a specific immune response induced by the vaccination of the study: Melan-A-specific T cells and their functionality were measured by tetramer staining, enzyme-linked immunospot (ELISPOT) assay and intracellular cytokine staining for IFN-γ, IL-2, CD107a and TNF-α evaluation. Finally, the adverse events and the toxicity were also reported and were a part of the safety criteria.

Results from this trial clearly demonstrated the immunogenic potency of vaccines composed of Melan-A peptide, CpG-B-7909 and Montanide ISA-51 in the induction of strong antigen-specific CD8+ T lymphocyte responses, thereby supporting the continued development of this vaccine strategy (66). However, careful study of the characteristics of the tumor tissues and immune responses of these patients is required for a more complete understanding, which may support the improvement of future cancer vaccines. Indications of immune escape mechanisms or immune modulation in the local TME may explain the limited clinical responses seen in vaccinated patients. As emphasized below, lymphatic vessels represent one potential key player.

4 Lymphatic vessels

4.1 Structure

The lymphatic system is a systemic network of vessels and lymph nodes (LNs). In many ways, the lymphatic system complements the functions of the blood vascular system by regulating tissue fluid balance, facilitating interstitial protein transport, as well as serving immunological functions (71, 72). Lymphatic vessels have a distinct structure compared to blood vessels (Figure 1). Lymphatic capillaries have a thin endothelial wall and a wide lumen, which make them structurally optimal for the absorption or uptake of fluids, proteins and cells. Lymphatic endothelial cells (LECs) do not form adherent or tight junctions and their basement membrane is incomplete or nonexistent. Furthermore, the lymphatic vascular network, unlike the blood vascular system, lacks a central pump such that the transport of lymph depends solely on skeletal muscle contraction and respiratory movement.

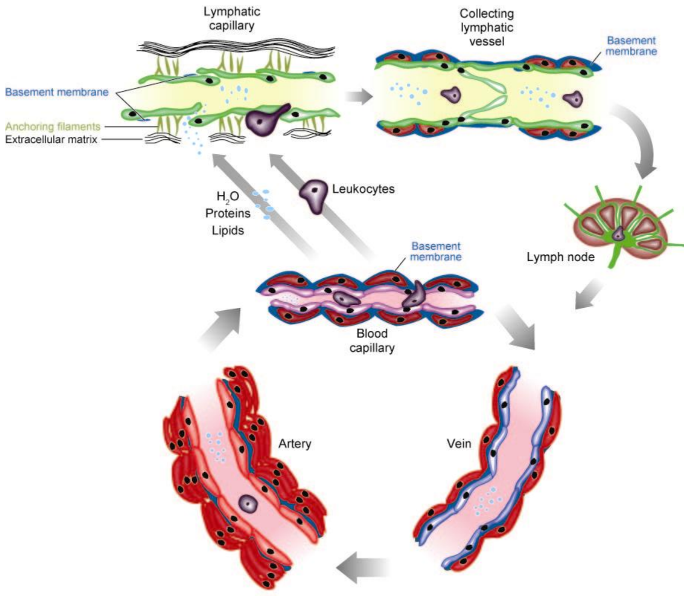

Karpanen T, Alitalo K. 2008.
Annu. Rev. Pathol. Mech. Dis. 3:367–97

Figure 1 Structure of the lymphatic vessels compared with blood vessels (Adapted from Karpanen *et al*, 2008).

This particular system provides an environment for cells that is optimal for their survival since the shear stress is negligible. Lymphatic capillaries are connected to extracellular matrix fibers through anchoring filaments. When tissue pressure increases, the contraction of these anchoring fibers opens the capillaries to enable lymph fluid and immune cells to enter the lymphatic vascular system (73). Lymph first enters the peripheral capillaries before draining to precollecting lymphatic vessels, which merge into larger lymphatic vessels surrounded by a basement membrane and valves that prevent retrograde lymph flow. Lymph passes through several sequential LN and finally reaches the thoracic duct, from where it returns to the venous circulation (74).

LNs are small organs of the lymphatic system that are widely distributed through the body and along the course of lymphatic vessels. Lymph nodes are key players in the development of an adaptive immune response and have several important functions such as recruiting naïve lymphocytes from the blood, collecting antigen and DCs from peripheral tissues and to provide the environment for antigen-specific tolerance or productive primary and secondary effector responses. Lymph nodes are structured in two different compartments, the cortex and the medulla, that can be distinguished histologically (Figure 2).

The cortex can be further subdivided into the paracortex (the T cell zone) and the more superficial B cell zone, composed of primary follicles containing germinal centers after antigen stimulation. The T cell zone contains specialized blood vessels knows as high endothelial venules (HEV) from which lymphocytes enter LNs. Interaction between antigen-specific T cells and APCs takes place in this region. The paracortex is arranged in paracortical cords that are bordered by cortical sinuses (endothelial lined lymphatic spaces) (Figure 2). The follicles in the B cells zones are rounded areas mainly composed of B cells but also of follicular dendritic cells (FDC), T cells, macrophages and reticular cells. The medulla is a labyrinth of lymph-draining sinuses that are separated by medullary cords, which contain many plasma cells and some macrophages and memory T cells. A dense network of reticular fibers maintains this compartmentalized structure and ensures an efficient crosstalk between T cells and APCs (75). FDC produce CXCL13 which attracts and retains B cells in the B cell zone whereas CCL19 and CCL21 produced by fibroblastic reticular cells (FRC) aim to attract T cells and APCs in the T cell zone (76).

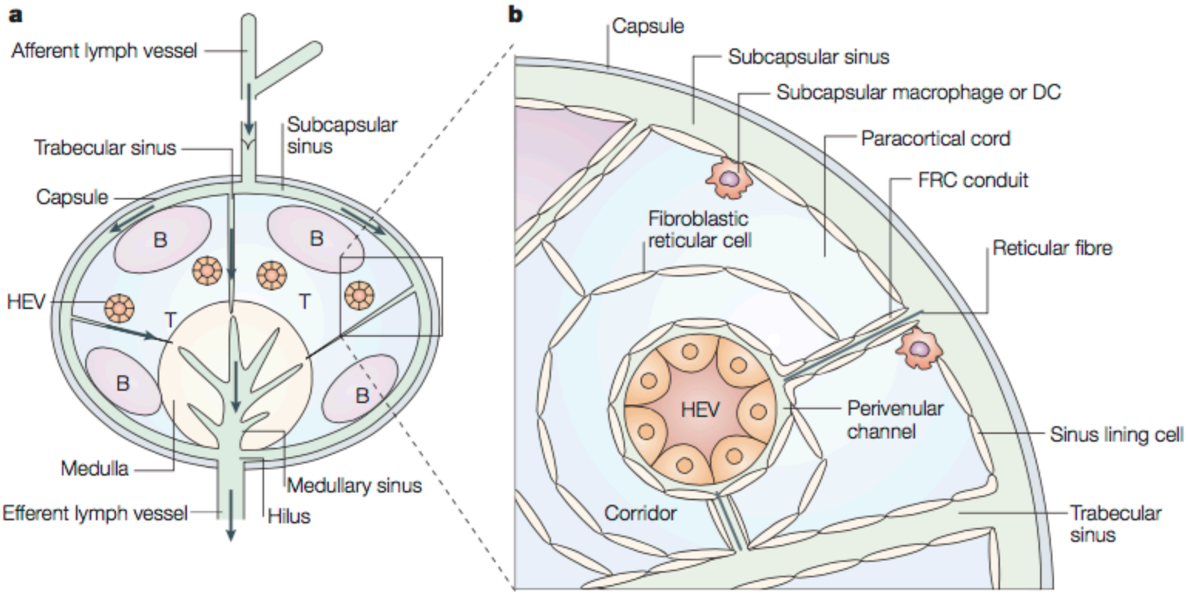

Figure 2 Structure of a lymph node. **a)** Schematic diagram showing the major structural components of a lymph node. The lymph fluid drains into the lymph nodes from afferent lymph vessels. From here the lymph is drained towards the subcapsular sinus, trabecular sinuses and medullary sinuses. **b)** Schematic representation of a paracotrical cord. The T cell area is represented in light blue, B-cell follicle in pink and lymph-filled sinuses in green. The cord is composed of reticular fibres and fibroblastic reticular cells (FRCs). A high endothelial venule (HEV) is found in the center of each cord and is surrounded by concentric layers of FRCs. (Adapted from Von Adrian *et al*, 2003)

The lymph fluid drains into the LN from afferent lymphatic vessels. From there, it goes into the subcapsular sinus (the hollow space below the fibrous capsule that surrounds the LN), then to the trabecular sinuses into the LN parenchyma, then on to the medullary network of sinuses and finally exits the LN via the efferent lymphatic vessel. Lymph channels inside the LN are surrounded by FRC, macrophages and DCs, which can remove microorganisms or debris from the lymph as well as process antigen for presentation to B and T cells (Figure 2).

4.2 Formation

The formation of *de novo* lymphatic vessels (termed lymphangiogenesis) is a dynamic process during embryogenesis and is largely absent under physiological postnatal conditions. Indeed, in the adult, lymphangiogenesis only takes place during certain pathological conditions such as inflammation, tissue repair and tumor growth (74). Lymphangiogenesis involves several molecular mechanisms. During embryogenesis, or under physiological conditions, lymphatic vessel endothelial hyaluronan receptor 1 (Lyve-1) is the first indicator of lymphatic endothelial competence (77). Prospero homebox protein 1 (Prox-1) expression begins thereafter in a polarized manner. Prox-1 is the master regulator of lymphatic endothelial fate and differentiation. Endothelial cells expressing this gene start budding and migrating in the surrounding extracellular matrix from the vein under the influence of vascular endothelial growth factor-C (VEGF-C) and begin to form lymph sacs (78). Then, the differentiated LECs start to express podoplanin, which activates platelet aggregation and leads to the separation of the lymphatic system from the blood vascular system (79). Finally, further centrifugal growth of the lymphatic vessel network ensues, driven by VEGF-C and vascular endothelial growth factor receptor-3 (VEGFR-3), and results in the differentiation to lymphatic capillaries and collecting lymphatic vessels.

4.3 Lymphangiogenic factors

The first and most studied prolymphangiogenic factors are VEGF-C, vascular endothelial growth factor-D (VEGF-D) and their associated tyrosine kinase receptor, namely VEGFR-3. VEGF-C and VEGF-D are initially produced as prepropeptides and need to be processed in order to be fully mature. As they mature they increase their affinity for VEGFR-3 (80). The binding of these two proteins to their receptor induces the dimerization of VEGFR-3 expressed on the lymphatic endothelium leading to proliferation, migration and survival of LECs (81). More recent data have suggested that VEGF-C/VEGF-D can also bind to vascular endothelial factor receptor-2 (VEGFR-2) presented on blood endothelial cells, and thus are also implicated in angiogenesis (82). Furthermore, VEGFR-2 is also expressed on LEC and has been implicated in lymphangiogenesis (83). These recent discoveries demonstrate the complexity and the similarities in the regulation of lymphangiogenesis and angiogenesis.

Genetic mouse models have demonstrated that VEGF-C (but not VEGF-D) is required for lymphatic development during embryogenesis and is postulated to intervene in the maintenance of lymphatic endothelial differentiation in adults (84). Further prolymphangiogeneic factors have recently been identified including angiopoietin, platelet-derived growth factor (PDGF), hepatocyte growth factor (HGF), fibroblast growth factor (FGF) and insulin-like growth factor (IGF). Negative regulators of lymphangiogenesis such as TGF-β have also been described (74).

4.4 Lymphatic markers and quantification

Selection of optimal markers of the lymphatic endothelium is clearly a critical step in the assessment of lymphatic vessel density (LVD), since false data arising from low specificity staining must be avoided. Although recent data demonstrated a large spectrum of candidate lymphatic markers for which antibodies are available (VEGFR-3, Lyve-1, Prox-1, podoplanin), their specificity may remain imprecise (85).

As mentioned earlier, VEGFR-3 is a tyrosine kinase that is predominantly expressed by LECs in adult tissues. However, VEGFR-3 expression was also been found in fenestrated capillaries of several organs and in endothelial cells of proliferating neovasculature in some cancers (86). Therefore, this marker is not reliable for discriminating between lymphatic and blood vascular endothelium.

LYVE-1 is an integral membrane glycoprotein that functions as a receptor for hyaluronan, a ubiquitous extracellular matrix glycosaminoglycan involved in cell migration and differentiation. LYVE-1 is expressed in cardinal vein endothelium during embryogenesis but its expression then persists into adulthood in most afferent vessels and lymphatic sinuses, but is absent from thoracic duct. LYVE-1 is also abundant in discontinuous endothelia including human liver and spleen sinusoids but is absent from the haemovasculature, thus demonstrating that LYVE-1 is indeed a reliable marker for distinguishing lymphatic vessels from blood vessels. Nevertheless, it can sometimes be downregulated in some tissues and can be absent in tumor-associated lymphatics (85). Furthermore, staining carried out on human LNs have shown poor specificity and positivity in some tumor-associated macrophages (87) (ref Swartz et al). Therefore, LYVE-1 should be use in combination with other lymphatic markers as podoplanin or Prox-1.

Another marker of the lymphatic endothelium is Prox-1, which is the master regulator of lymphatic vasculature development during embryogenesis. Prox-1 has also been found in other cell types in the lens, heart, liver, pancreas and nervous system (88). A recent study by Park *et al* has shown that Prox-1 is the only exclusive marker currently available for LECs within human LNs, capable of marking lymphatic sinuses and vessels in every zone of the LN (89). In contrast to Prox-1, expression of LYVE-1 was restricted to the paracortical and medullary sinuses in most LNs and was not expressed by Prox-1$^+$ LECs in the subcapsular and trabecular sinuses. These results highlighted that even LECs can have distinctive expression of markers and that different populations of LECs exist, at least in human LNs. Prox-1 has a nuclear localization and thus it is not an ideal marker for quantifying lymphatic vessels microscopically, but is a useful marker for multiplexed immunostainings.

Podoplanin is a surface glycoprotein that is expressed in several cell types other than lymphatic vessels such as osteoblastic cells, lung alveolar type I cells and kidney podocytes (90). Compared to LYVE-1 and Prox-1, podoplanin (D2-40 is a monoclonal antibody that specifically recognizes human podoplanin) is considered as one of the most reliable lymphatic markers (85). However, podoplanin has been shown to be present only in small lymphatic vessels and not in larger ones that have smooth-muscle cells (88).

A number of different methods have been developed to quantify lymphatic vessels in cancer tissues. These methods have already been reviewed and described (85, 90). Briefly, three important methods are frequently used while assessing lymphatic vessel numbers in human tissue slides. Firstly, the Weidner technique, the most widely used technique to count lymphatic vessels, involves quantifying the lymph vessels at “hot spots”, defined as areas of increased vessel density. Histological slides of the tumors are first examined at low power (x10) to identify hot spots and then at higher magnification (20x or 40x) to quantify the number of vessels in these hot spots. The second one is the Chalkley method (Figure 3), which is based on the use of a Chalkley eyepiece graticule with 25 randomly distributed points. This method is also based on hot spot selection but then the graticule is positioned until the largest possible number of points is located over the stained LECs. The score obtained is an indicator of the relative area occupied by lymphatic vessels, as the score does not count the number of vessels but rather the number of points of the graticule overlaying the vascular structures. This method is considered to be more objective and reproducible and should be used to assess lymphatic vessels. Finally, computerized counting systems have the best performance in terms of accuracy and reproducibility. However, their widespread applications are hampered by the need for costly specialized equipment to perform analyses and the automatic software may count non-specific staining on nonendothelial structures as lymphatic vasculature structures.

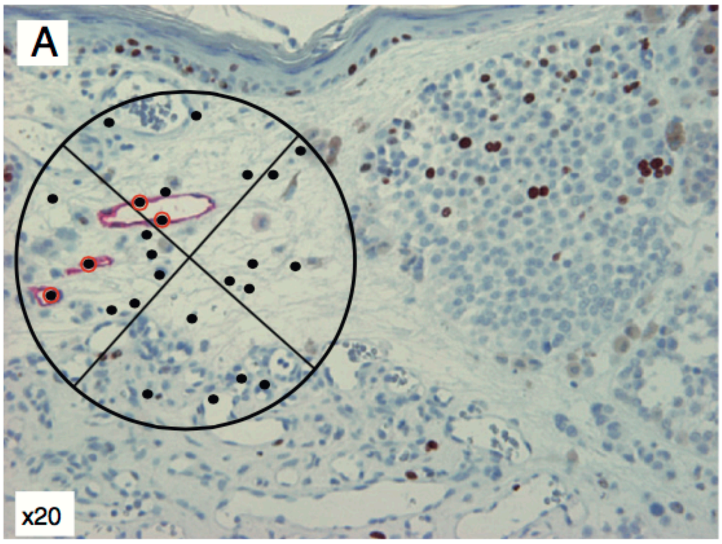

Figure 3 Representation of a Chalkley graticule on D2-40/Ki67 double stain of a melanoma metastatic lymph node. The points marked with red circles are considered positive (adapted from Pastushenko *et al,* 2015)

4.5 Lymphatic vessels in cancer

4.5.1 Tumor lymphangiogenesis

The expanding tumor mass can exploit the unique structural architecture and the microenvironment of the lymphatic vasculature. In most human cancers, the lymphatic vasculature serves as the primary route for the metastatic dissemination of tumor cells, which initially enter regional draining LNs prior to the establishment of metastases in distant organs. In fact, regional LN metastasis is often the most important prognostic factor for patients with malignancies and represents a major criterion for treatment choices. However, despite the importance associated with the presence of LN metastases in cancer progression the mechanisms of lymphatic metastasis formation remain poorly understood. Since the recent discovery of lymphatic vessel markers, new findings have been made regarding the particular role of the lymphatic system in tumor growth and progression.

Similar to tumor-associated angiogenesis, tumors also acquire the ability to form new lymphatic vessels. Our understanding of tumor-induced lymphangiogenesis and its clinical impact on tumor progression and metastasis has primarily relied on mouse models of cancer. In 2001, Skobe *et al,* using a mouse model of breast cancer, were the first to prove that overexpression of VEGF-C in tumor cells significantly increased lymphatic vessel growth within and around the tumor leading to increased metastatic spread to LNs and distant organs (91). Further studies followed and confirmed these results (92, 93). Moreover, blockade of VEGFR-3 in mouse reduced tumor lymphangiogenesis and LN metastasis (94). However, proliferation and activation of lymphatic vasculature is not only restricted to the primary tumor microenvironment as some studies detected LN lymphangiogenesis within SLNs (95, 96). Interestingly, B cells have been shown to be a major source of lymphangiogenic factors and promote lymphangiogenesis in tumor draining LNs by secreting VEGF-C (97). Importantly, draining LN lymphangiogenesis can even start prior to tumor metastasis, indicating the creation of a premetastatic niche by the primary tumor (97, 98). In addition, lymphangiogenic growth factors also act to enlarge and dilate lymphatic vessel size and lymphatic flow rate, facilitating the dissemination of tumor cells. Taken together, these murine tumor experimental systems have established that tumors can actively induce the growth of lymphatic vessels (mediated by prolymphangiogenic factors) and promote metastasis to LNs and possibly beyond to distal organs (94).

On the other hand, our knowledge of the role of lymphatic vessels in tumor metastasis and their impact on prognosis in human cancer came from retrospective IHC analysis of tumor tissue samples and correlation with clinical outcome. Expression of VEGF-C occurs in a variety of human tumors such as breast, colon, gastric, head and neck, lung, squamous cell carcinoma and melanoma (93). In melanoma, statistically significant positive correlations or at least trends have been observed between VEGF-C expression, LVD, LN metastasis and prognosis (99-102). However, in some other studies this correlation between elevated VEGF-C and either increased LVD, LN metastasis or survival was not observed (103-106), suggesting that the situation may be more complex and could vary depending on the cohort of patients studied. In line with this, increased intra and peritumoral lymphangiogenesis in the primary tumor as well as in the tumor-draining LNs have also been implicated in increasing LN metastasis, distant metastasis and poor prognosis in melanoma as well as in other types of cancer (e.g breast cancer, colon cancer, gastric cancer…) (107-111). Here again, exceptions exist and some studies did not identify lymphangiogenesis as an independent prognostic factor (105, 112). Patient cohorts studied, lymphatic markers selected and methods of quantification used are potential factors explaining this discrepancy. Furthermore, a higher density of lymphatic vessels in or around the tumor may be necessary but not sufficient for metastasis, as tumor cells may not have acquired the properties required for metastasis, such as invasiveness (103).

The chemokines CC chemokine ligand 19 (CCL19) and CC chemokine ligand 21 (CCL21) and their associate receptor CC chemokine receptor 7 (CCR7) are also involved in tumor dissemination via the lymphatic system. The CCR7/CCL21/CCL19 axis regulates several mechanisms involved in normal physiology and immunity. CCR7 is regarded as a LN homing receptor for lymphocytes and antigen-presenting cells and the CCR7/CCL21/CCL19 axis is also implicated in the organization of the thymic architecture, lymphoid neogenesis and the balance between immunity and peripheral tolerance (113). CCL19 and CCL21 are both expressed by LECs and FRCs. CCR7 expression within tumors correlates with metastasis to LNs in human malignancies (e.g. melanoma, colorectal cancer, gastric cancer…) (114-116) and mouse models have demonstrated the chemotactic migration of CCR7-positive tumor cells towards CCL21-producing LECs (117). Moreover, *in vivo* inhibition of LN metastases has been achieved using a soluble inhibitor of CCL21 (118).

Overall, these considerations highlight the fact that lymphangiogenic growth factors and chemokines can systematically induce alterations in tissue stroma not only within the primary tumor but also in the draining LNs, secondary lymphoid organs and other distant metastatic sites, which may promote tumor cell dissemination.

4.5.2 Immunoregulatory functions of tumor lymphangiogenesis

Traditionally, lymphatic vessels were considered to be passive channels allowing tumor cells entrance and transport (119). However, new evidence is emerging suggesting that the lymphatic vasculature plays a more active role in tumor metastases through its action on the recruitment of cancer cells (120), the maintenance of cancer stem cell-like properties (121), and the antitumor immune response (74, 122). This immune modulation seems to be driven notably by VEGF-C as it may directly influence the maturation, phenotype, activity and recruitment of immune cell subsets (123-126).

In line with this, Melody Swartz’s laboratory have proposed a novel hypothesis regarding the mechanism of lymphatic metastases, linking lymphangiogenic factors, tumor-associated lymphangiogenesis, and the induction of immune tolerance. Specifically, using a mouse melanoma model, she has suggested that cells of the lymphatic vasculature may play an active role in mediating tumor tolerance. First, her group demonstrated the importance of the crosstalk between VEGF-C and CCL21 in promoting lymphatic invasion. Tumor-secreted VEGF-C induces the expression of CCL21 in LECs, which attract CCR7-expressing tumor cells to the lymphatic vessels. In addition to sensing the gradient established by LECs, tumor cells may also set up autologous gradients via the secretion of CCL21 in the extracellular matrix (127). Furthermore, VEGF-C itself can promote proteolytic activity and motility of tumor cells, and, therefore, enhance tumor aggressiveness (128). Secondly, the up-regulation of CCL21 in the tumor stroma recruits lymphoid tissue inducer (LTi) cells, naïve T cells, Treg cells, and MDSCs. LTi cells direct the reorganization of local stroma into lymphoid tissue–like structures that support Treg cells and MDSCs and promote naïve T cell education leading to immune tolerance of the tumor (129).

Furthermore, under physiological conditions, LN associated-LECs play an important immunoregulatory role in preventing autoimmunity by scavenging antigens and cross-presenting them to T cells, which can lead to T cell anergy and deletion. In a cancer setting, the idea proposed is that lymphangiogenic tumors may hijack these mechanisms and cross-present tumor antigens, leading to CD8+ T cell deletion and immune tolerance (130, 131). Preliminary results in mice have shown that anti-lymphangiogenic therapy (such as anti-VEGFR3 antibody) can reverse the CCL21-induced lymphoid-like stroma and render an anti-tumor vaccine (OVA+CpG) more effective when used in combination (data not published). These interesting results suggest that lymphatic vessels may have a role on the outcome and efficiency of immunotherapy.

Taken together, these studies indicate that tumor-associated lymphatics and their respective draining LNs may promote tumor immune tolerance in murine models of melanoma and contribute to the generation of a TME that is permissive to malignant progression and metastases. However, it remains unknown whether similar mechanisms of lymphatic-mediated immune regulation exist in human melanoma.

5 Summary of the introduction

Cancer will become the first cause of mortality ahead of cardiovascular disease in the next few decades. The heterogeneity, unpredictable progression and resistance to treatment of this disease make it a health concern of paramount importance. Therefore, novel therapeutic strategies have to be explored and developed to improve curative responses in cancer. Given that patients can develop a spontaneous adaptive immune response to their cancer and that the quality and density of specific immune components within the TME can predict disease progression, immunotherapies that aim to induce an immune response are considered highly attractive approaches. Melanoma, in particular, has attracted the attention of tumor immunologists as its aggressiveness, immunogenic properties and the scarcity of potent therapeutic options have made it a promising model for developing immunotherapy. Indeed, multiple clinical trials have shown spectacular responses in melanoma patients to these therapies. However, complete regressions are infrequent and resistance to these therapies has been extensively described. Data from the literature strongly suggest that the TME modulates local and systemic immune responses to tumor and thereafter to therapies. In particular, lymphatic vessels have been shown to be active regulators of anti-tumor immune responses in tumor and draining LNs of mouse models of melanoma. Addressing this question in human melanoma by dissecting the link between lymphatics, immune cells and immune suppressive pathways both within the TME as well as systemically may reveal new knowledge of disease mechanisms and potentially identify targets for novel therapies.

OBJECTIVES

Various strategies (IHC, genetics,…) have been employed in an attempt to characterize and dissect tissue samples of cancer patients to improve diagnosis, prognostic evaluation and the design of combinatorial therapeutic approaches. Several recent publications pointed out the limited success of these different methods in assessing the complexity, heterogeneity and spatial relationships of the different cell types present in tumor tissue (18, 132).

Immunohistochemical techniques that characterize the morphology, spatial relationships and phenotype of tissue-infiltrating cells are probably the methods with the greatest potential for insight into the wealth of information contained within the tissue. However, until recently, IHC data has not been used to it’s full potential due to a lack of tools for systematic quantification and automated analysis. Indeed, a large part of the IHC staining analysis has typically been done by visual assessment on specifically selected fields and has been shown to be subjective with a very high level of inter-observer variability (133). The emergence of computer-based image analysis systems has overcome these limitations and offers the advantage of analyzing quality, high-resolution digital images via dedicated software to obtain precise and quantitative data from an entire tissue or from specific regions within the tumor. The results obtained with these methods are accurate, reproducible and can be shared and reviewed by external evaluators (e.g. pathologists) (134-136).

Overall, these facts underscore the need for a better understanding of the composition and spatial relationships between tumor cells and their microenvironment. The ultimate goal of this thesis was, thus, to obtain greater insight into the complexity and heterogeneity of the TME in human melanoma with the help of multiple recently developed IHC techniques. To achieve this, we established two main objectives: to precisely characterize the local and systemic immune modulation (i) in untreated melanoma patients and (ii) in patients undergoing vaccination or checkpoint blockade therapies.

Four studies have emerged from these two aims:

(1) The analysis of lymphatic vessels in relation to anti-tumor immune response in peptide-vaccinated patients through a combination of IHC techniques, whole slide scanning/analysis, and an automatic quantification system

(2) The description of an auto-immune adverse event in a peptide-vaccinated patient by IHC and ex-vivo peripheral blood mononuclear cells (PBMC) analysis

(3) The development of a new diagnostic tool for melanoma metastasis in LNs of peptide-vaccinated patients using Fourier Transform Infrared (FTIR) imaging

(4) The role of colony-stimulating factor-1 (CSF-1) in modulating the anti-tumor response in Ipilimumab-treated patients using IHC and *in vitro* co-culture assay

The data generated as part of this thesis are not routinely assessed but are nevertheless key aspects in deciphering mechanisms responsible for immune responses. Thus, they may improve future clinical biomarker implementation and patient management.

1 Analysis of lymphatic vessels in relation to anti-tumor immune response

This project originated from recent studies from the group of Melody Swartz, evaluating the role of the lymphatic system in anti-tumor immunity. They demonstrated that lymphatic vessels are directly involved in sculpting the TME and in shaping the anti-tumor immune response in mouse primary melanoma and melanoma-draining LNs (129, 130). Based on this, we set out to better understand the cellular and molecular interactions between lymphatics and immune cells in melanoma patients. Specifically, the goal of this study was to investigate correlations between lymphatic vessels, immune cells and immune suppressive molecules within human melanoma-associated tissues. We hypothesized that higher density of lymphatic vessels will be associated with higher expression of immune suppressive factors and an altered anti-tumor T cell response.

To test our hypotheses, we selected a cohort of vaccinated melanoma patients for whom formalin-fixed paraffin-embedded (FFPE) tissues were available (primary melanoma, metastatic LNs and non-metastatic LNs). We phenotypically characterized the lymphatic vessels, immune cell populations and immune suppressive molecules within these tissues by IHC and multiplex staining. We then developed a software-assisted image analysis protocol to precisely quantify staining within entire tissue sections. Finally, we compared our IHC results to clinico-pathological and prognosis factors for the cohort of patients.

Results from this objective are described in manuscript 1 on page 45 of this thesis.

2 An autoimmune adverse event following multiple cycles of vaccination

Recently, significant progress has been made in developing therapeutic cancer vaccines. Specifically, the use of potent adjuvants such as the TLR ligand, CpG, in ‘new generation’ vaccines has been shown to give rise to strong activation of cancer-specific T cells without inducing serious autoimmune adverse events in cancer patients. During one such vaccine clinical trial performed by our institute, a stage IV metastatic melanoma patient receiving repetitive vaccination with peptides and CpG developed a pulmonary sarcoid-like granulomatosis.

We hypothesized that the development of a strong and long lasting specific immune response to the vaccine may have led to the development of an autoimmune pulmonary AE. To explore this hypothesis, we analyzed *ex vivo* PBMC collected at different time points before and after vaccination by flow cytometry. We also evaluated the capacity of the tumor antigen-specific CD8$^+$ T cells to produce IFN-γ by ELISPOT assay. Finally, we collected the clinical data and the radiological images done during the course of his disease.

Results from this objective are described in manuscript 2 on page 107 of this thesis.

3 Development of a new diagnostic tool for identification of lymph node melanoma metastases

Early diagnosis of melanoma is essential to reduce mortality and select appropriate treatments. Currently, diagnosis of melanoma is mainly based on visual inspection of skin or LN sections with optical microscopy. Melanoma usually exhibits a wide spectrum of histological appearances and some pigmented lesions can mimic melanoma histologically. A high degree of inter-observer discrepancy has also been highlighted for micrometastasis detection in LNs. These various factors introduce the possibility for significant errors in the diagnosis of melanoma and stress the need to have a powerful and objective method to help in the diagnosis of this malignancy. We assessed the potential of a new technique based on infrared (IR) spectroscopy to identify melanoma cells and characterize lymphocytes in metastatic lymph nodes and in non-metastatic LNs of melanoma patients.

Results from this objective and my specific contributions are described in manuscript 3 on page 114 of this thesis.

4 The role of CSF-1 in modulating the anti-tumor immune response

CSF-1 and its receptor, CSF-1R, are known to regulate the migration, differentiation and survival of macrophages and their precursors (137). Furthermore, tumor-associated macrophages (TAMs) represent key orchestrators of various tumor-promoting processes and have been identified as an independent poor prognosis factor in several cancer types (138). Recent studies have shown that treatment with anti-CSF-1R antibody decreased pro-tumoral CSF-1R$^+$CD163$^+$TAMs in patients with various tumor types and altered T cell tumor microenvironment composition (139).

For this project, we postulated that CSF-1 is secreted by melanoma cells and investigated whether this occurs in response to specific attack by cytotoxic T lymphocytes (CTLs). To test this hypothesis, we first performed CSF-1 quantification in the plasma of Ipilimumab-treated patients before and after therapy. Next, CSF-1 protein expression was measured in the supernatant of untreated melanoma cells, cytokine-treated melanoma cells or melanoma cells that were co-cultured with melanoma-specific CTLs. To determine whether direct CTL-melanoma cell contact was necessary to induce CSF-1 induction, melanoma cells were treated with tumor necrosis factor-alpha (TNF-α) and interferon gamma (IFN-γ), two cytokines that are secreted by activated CTLs. We also compared levels of CSF-1 mRNA in untreated melanoma cell lines and melanoma cell lines cultured in the presence of melanoma-specific CTLs using a differential gene expression microarray and NanoString technology. Finally, we selected FFPE primary melanoma and cutaneous melanoma metastasis samples from the same patients and assessed CSF-1, CSF-1R and CD163 *in situ* expression in regions of high and low CD8+ T cell infiltration.

Results from this objective are described and my specific contributions in manuscript 4 on page 160 of this thesis.

RESULTS

Pursuing objectives 1-4 lead to four manuscripts presented here.

The four manuscripts are entitled:

1) Local and distant immune modulation associated with lymphangiogenesis in melanoma patients
2) Pulmonary sarcoid-like granulomatosis after multiple vaccinations of a long-term surviving metastatic melanoma patient
3) Identification of melanoma cells and lymphocyte subpopulation in lymph node metastases by FTIR imaging histopathology
4) Adaptive immune resistance via CSF-1 produced by melanoma cells

1 Local and systemic immune modulation associated with lymphangiogenesis in melanoma patients

In this study, we investigated correlations between lymphatic vessels, immune cells and immune suppressive molecules within human melanoma-associated tissues. We established that increased lymphatic vessel density was associated with high expression of immune suppressive molecules, low functionality of tumor-infiltrating CD8+ T cells and decreased cytokine production by tumor-antigen specific CD8+ T cells in the blood. These data revealed local and systemic roles of tumor-associated lymphatics in modulating T cell responses in human cancer. None of the results presented here are published and should therefore be considered as preliminary and confidential.

Local and distant immune modulation associated with lymphangiogenesis in melanoma patients

Bordry N.[1,4,5], Broggi MA.[4,5], De Jonge K.[1], Foukas PG.[2,3], Danenberg E.[2,3], Gannon PO.[2], Cagnon L.[2], Abed Maillard S.[2], Maby-El Hajjami H.[1], Letovanec I.[3], Yan P.[3], Romano E.[1], Swartz MA.[4,5,6] and Speiser DE.[1,2]

[1] Clinical Tumor Biology and Immunotherapy Group, Department of Oncology and Ludwig Cancer Research Center, University of Lausanne (UNIL), Lausanne, Switzerland

[2] Department of Oncology, Lausanne University Hospital Center (CHUV) and University of Lausanne, Lausanne, Switzerland

[3] Pathology department, CHUV, Lausanne, Switzerland

[4] Institute of Bioengineering, School of Life Sciences and School of Engineering, Ecole Polytechnique Fédérale de Lausanne (EPFL), Lausanne, Switzerland

[5] Swiss Institute for Experimental Cancer Research (ISREC), School of Life Sciences, EPFL, Lausanne, Switzerland

[6] Institute for Molecular Engineering, University of Chicago, Chicago, IL, USA

Abstract

Tumor induced lymphangiogenesis may precede metastasis, and is associated with poor patient survival. Furthermore, tumor-associated lymph vessels are known to impair host immune responses in mouse models, but this concept remains unexplored in humans. We hypothesized that the density of lymphatic vessels may impact on the quality of anti-tumor T cell responses in melanoma patients. Therefore, we characterized the tumor microenvironment (TME) in primary melanomas, metastatic lymph nodes (LNs) and non-metastatic LNs by immunohistochemistry (IHC) and quantitative image analysis. Lymphatic vessels (Prox-1, podoplanin), immune cells (CD8, CD4, FoxP3, CD19) and lymphangiogenic and immunosuppressive molecules (VEGF-C, IDO, INOS, Arg-1) were assessed in specific anatomical regions. Significant positive correlations between lymphatic vessels and VEGF-C, iNOS and IDO were observed in primary tumors and in LN metastases. Consistent with studies in mouse, lymphatic vessels were associated with locally enhanced infiltration of CD8^{+} T cells. Importantly, we show for the first time that low functionality of local CD8^{+} T cells, and decreased cytokine production by tumor-antigen specific CD8^{+} T cells in circulating blood were associated with increased lymph vessel density. Interestingly, lymphatic vessel-associated immune modulation was also evident in non-metastatic LNs adjacent to metastatic ones, emphasizing loco-regional effects and underscoring systemic immune suppression. Together, these data reveal a previously unrecognized local and systemic role of lymphangiogenesis in modulating T cell responses in human cancer.

Introduction

In the last decade, particular attention has been given to understanding the complex interactions between a developing tumor and the host immune system. It is known that the immune system can operate as a significant barrier to tumor formation and progression in humans (1). Tumor cells can express immunogenic antigens through mutation, and adaptive immune responses can be mounted in tumor-bearing hosts (2, 3). Furthermore, strong memory Th1/cytotoxic T cell responses correlate with favourable clinical outcomes in a large array of human malignancies, including melanoma (4-6).

In spite of the development of an immune response to tumors and the accumulation of highly differentiated tumor-specific T cells at the tumor site in cancer patients, immune responses are rarely capable of complete tumor eradication (2, 7). Tumors develop multiple strategies to inhibit effector T cells, including triggering of surface inhibitory molecules, attraction of immune suppressive cells (e.g. T regulatory cells (Tregs) and myeloid-derived suppressor cells (MDSCs)) and production of enzymes that deplete essential nutrients for T cell activation and proliferation such as indoleamine 2,3-dioxygenase (IDO), inducible nitric oxide synthase (iNOS) and arginase (8, 9). It is now recognized that these tumor immune escape mechanisms are initiated and maintained by specific interactions between tumor cells and their TME.

Lymphatic vessels have been shown to play important roles in malignant diseases. In human melanoma, expression of the lymphangiogenic vascular endothelial growth factor-C (VEGF-C) in the tumor promotes lymphangiogenesis, LN metastases and poor prognosis (10-14). The formation of a lymphatic network within the tumour and the tumour-draining LNs facilitates the migration of invasive tumor cells. More recent mouse studies demonstrate additional roles of lymphatics and their associated chemokines in promoting tumor progression and metastasis to the tumor-draining LNs (15-17). Indeed, lymphatic endothelial cells (LECs) can suppress immunity and promote tolerance in multiple ways such as (a) inhibiting the maturation of dendritic cells (DC), (b) producing molecules such as IDO, iNOS and transforming growth factor beta (TGF-β) and (c) impairing T cell activation through direct presentation of exogenous antigens and expression of inhibitory molecules (e.g. programmed cell death ligand 1 (PD-L1)) (18). Taken together, these findings support the emerging hypothesis that tumor-induced lymphangiogenesis may regulate host immunity and, thus, constitute a new target for cancer immunotherapy. However, to date the effects of tumor-associated lymphangiogenesis on host anti-tumor immunity in humans remain to be established.

The aim of this study was to determine whether tumor-associated lymphatic vessels are associated with modifications of the immune profile in selected anatomical compartments of melanoma patients. We characterized the TME of primary melanoma, metastatic LNs and non-metastatic LNs of melanoma patients by IHC and quantitative image analysis. We developed a novel method enabling quantitative assessment of unusually large tissue fields. To characterize lymphatic vessels, we used the markers Prox-1 and podoplanin, in combination with VEGF-C. Furthermore, we characterized the immunosuppressive molecules Arg-1, iNOS, and IDO, and various lymphocyte populations (CD8, CD4, FoxP3 and CD19). Finally, the results from tissue analyses were compared to numbers and functionality of tumor antigen specific CD8 T cells from peripheral blood.

Material and Methods

1. Patients

29 metastatic melanoma patients that had been included in phase I prospective vaccination trial (LUD 00-018 study, ClinicalTrials.gov Identifier NCT00112229) at the Ludwig Cancer Research Center (LICR, CHUV hospital, Lausanne, Switzerland) between 2003 and 2011 were the main subjects of our study and were therefore reviewed for formalin-fixed paraffin-embedded (FFPE) tissue specimen's availability (Table S1). These patients were recruited and vaccinated as described in (19, 20). Briefly, 29 HLA-A2$^+$ patients with histologically proven metastatic melanoma of the skin expressing Melan-A/MART-1 were included upon informed consent, and received 4 vaccinations subcutaneously in monthly intervals composed of Melan-A analog (ELA) or native (EAA) peptide ± Tyrosinase (YMD) peptide, CpG-7909 and Montanide ISA-51 adjuvants. The patients were evaluated for immune response (CD8$^+$ T cell response), treatment toxicity, tumor response and survival (Table S2). On the 29 patients included in the study, 25 were selected for analysis and 4 were excluded (one patient had uveal melanoma and three patients did not have any FFPE tissues available). 14 primary melanoma samples from 14 patients, 33 metastatic LNs from 14 patients (25 metastatic LNs were taken before the vaccination and 10 metastatic LNs were taken after the end of the vaccination trial) and 23 non-metastatic LNs from 20 patients (17 non-metastatic LNs were taken before the vaccination and 6 non-metastatic LNs were taken after the end of the vaccination trial) were obtained and were analysed for their immune cell types, lymphatic vessel and immunosuppressive molecule densities (Table S3, S4 and Fig. S1A-J). 14 non-metastatic LNs from 12 patients were from negative LN dissection and 9 non-metastatic LNs from 8 patients were from positive LN dissection.

2. Immunohistochemistry (IHC)

Chromogenic IHC staining

4-µm tick tissue sections were first deparaffinised in xylene and rehydrated by sequential incubation in EtOH/water solutions. Tissues were then treated with 3% H_2O_2 in distilled water for 5 minutes to quench endogenous peroxidase activity. Heat-induced antigen retrieval was performed in Tris-EDTA buffer (pH 9) for 1'30'' in a steamer. Subsequently, sections were incubated at room temperature with primary antibodies to CD8 (clone C8/144b, Dako, 1:30, 32 min), CD4 (clone 4B12, Novocastra, 1:10, 90 minutes), CD19 (clone BT51E, Novocastra, 1:50, 32 min), FoxP3 (clone 236a/E7, Abcam, 1:50, 60 min), Podoplanin (clone D2-40, Covance, 1/400, 60 min), Prox-1 (R&D, 1:100, 32 min), VEGF-C (Invitrogen, 1:20, 40 min), IDO (from Brussels, 1:500, 40 min), iNOS (Thermoscientific, 1:75, 40 min), Arg-1 (Mybiosource, 1:300, 40 min), Melan-A (clone A103, Dako, 1:50, 32 min), melanosome (clone HMB45, Dako, 1:50, 32 min) and S100 (Novocastra, 1:800, 40 min) followed by a secondary anti-mouse (K4001, Dako), anti-rabbit (DK4003, Dako) or anti-goat antibody (Histofine RTU-Biosciences) RTU/HRP ENVISION for 30 minutes. 3-amino-9 ethylcarbazole (AEC) was used as a red chromogen (K3464, Dako) for CD4, S100, Melan-A and melanosome and Diaminobenzidine (DAB, K3468, Dako) as a brown chromogen (K3468, Dako) for the rest of the antibodies. After rinsing with water, sections were counterstained with Hematoxylin Gill II (Merck 1.05175) and coverslipped with xylol*.* CD8, CD4, CD19, FoxP3, Podoplanin, Prox-1, Melan-A, S100 and Melanosome were done on Ventana BenchMark machine using Cell Conditioning 1 (CC1, 950-124, Ventana) as a buffer for heat-induced antigen retrieval with varied time for the different antibodies, other reagent and time was done as described above. iNOS, VEGF-C, Arg-1 and IDO were done manually with the above-mentioned protocol. Positive controls included tonsil, lung, liver and colon. Immunostaining with appropriate isotype control antibodies were used as negative controls.

Conventional immunofluorescence staining

As for chromogenic IHC staining, 4-µm tick tissue sections were first deparaffinised in xylene and rehydrated by sequential incubation in EtOH/water solutions. Antigen retrieval was performed using a 15 minutes incubation in boiling Tris-EDTA buffer (pH 9), following 30 minutes incubation in blocking solution (TBS+0.01% Triton X-100+2%BSA+2%total serum from host secondary antibody). Sections were incubated overnight at 4°C with primary antibodies to CD8 (clone C8/144b, Dako, 1:30), Podoplanin (clone D2-40, Covance, 1/200), Prox-1 (R&D, 1:100), iNOS (Thermoscientific, 1:75), Arg-1 (Mybiosource, 1:300), IDO (from Brussels, 1:500), CCL21 (Atlas antibodies, 1:200) and PD-L1 (Cell Signaling,1:200). Alexa Fluor 488-labeled donkey anti-mouse IgG (Invitrogen, 1:400), 568-labeled donkey anti-goat IgG (Invitrogen, 1:600) and 647-labeled donkey anti-rabbit IgG (Invitrogen, 1:800) antibodies were used as secondary antibodies and incubated for 1 hour at room temperature. After stringent washes, sections were counterstained with DAPI (Vector Laboratories, Burlingame, CA) for 5 minutes and coverslipped with mounting medium (Vectashield mounting media). Positive controls were done on tonsils, LNs and skin tissues. Negative slides used TBS instead of primary antibody, with other conditions constant. Images were obtained with confocal microscope ZEISS LSM 700 UPRIGHT.

Tyramide Signal Amplification (TSA) system

Multiplex stainings were done on the same slides described in part 1 using the automated Discovery ULTRA Staining Module (Ventana, Roche). Staining was done in consecutive rounds and each round consisted of: antigen retrieval, blocking, primary antibody, secondary antibody and TSA amplification as described before (21). Following primary antibodies were used: CD8 (clone SP16, Fischer Scientific AG, 1:1000), Granzyme B (Clone Grb-7, Monosan, 1:100) and PD-1 (Clone MRQ-22, BioSB, 1:1200). Polyclonal goat anti-mouse Immunoglobulins/HRP (P044701, DAKO) and polyclonal goat anti-rabbit Immunoglobulins/HRP (P044801, DAKO) were used as secondary HRP-labelled antibodies. This was followed by consecutive incubations with TSA reagents: TSA Cyanine 3

(NEL744B001KT, Perkin Elmer (PE)), TSA Cyanine 5 (NEL745B001KT, PE), TSA Cyanine 3.5 (NEL763B001KT, PE), TSA Fluorescein (NEL741B001KT, PE), TSA Cyanine 5.5 (NEL766B001KT, PE). Sections were counterstained with DAPI (422801, Lucerna Chem AG) and coverslipped with mounting medium (S3023, DAko fluorescence mounting media).

3. Staining quantification

Imagescope Aperio software

Whole slide digital images were obtained for each specimen stained with Chromogenic IHC staining using NanoZoomer 2-HT digital slide scanner (Hamamatsu). The resulting high-resolution digital images were analysed using the ImagescopeTM software, version 12.1 (Aperio Technologies, Vista, CA, USA) using the positive pixel cell algorithm 9.1 as previously described and validated (22). Briefly, this algorithm detects pixels that match input parameters set for the algorithm and generates four output values based on the pixel's color range: haematoxylin or negative signal (blue in mark-up image), weak positive (yellow in mark-up image), positive (orange in mark-up image) and strong positive (brown in mark-up image) (Fig. S2A). Using these parameters, the strong non-specific (brown) as well as the weak positive (yellow) signals were considered as debris background staining, whereas the positive value (orange) was considered as specific. Folds, debris, holes were also removed manually to be exclude from the staining quantification analysis. Quantification of the staining in the tissue selected was reported as a relative abundance ratio, which was based on the number of positive pixels (orange) divided by the total number of pixels (blue + yellow + orange + brown). The relative abundance ratio was reported in % and represented the percentage of density per tissue area for the quantified staining. Results obtained were controlled to match with visual inspection.

The positive pixel cell algorithm has been applied in the total tissue of the non-metastatic LNs whereas metastatic LNs and primary tumors have first been divided into relevant histological regions. For metastatic LNs, we selected 6 different zones. 1) tumor cells, 2) stroma, 3) residual LN, 4) reactive connective tissue, 5) capsule, 6) total tissue. For the primary melanoma tumor, we selected 4 different regions: 1) Invasive Margin (IM), 2) Center of the tumor (CT), 3) Peritumoral region and 4) Normal skin. Finally, a trained pathologist confirmed the quality of all the zone and analyses.

Vectra multispectral analysis system (Perkin Elmer)

Fluorescence slides stained with TSA system were scanned in a batch format by using the Vectra multispectral imaging system (Perkin-Elmer). Tissue finder algorithm was first applied to scan the entire tissue in low power field and then 15 20x multispectral images were randomly acquired from the collected areas. Images were processed by using inForm tissue finder software (PerkinElmer). For unmixing of the images and analysis, the spectral libraries of DAPI as well as of all the fluorochroms were generated. The percentages of Granzyme B and PD-1 that colocalized with CD8 within the tumor areas were calculated through a thresholded colocalization analysis (Fig. S2B). Thresholds used to determine the cutoff for all three antibodies stains were set visually.

4. Statistical analysis

The non-parametric Mann–Whitney U test was used to assess statistical significance of differences between two data sets. Correlation coefficients were computed using Spearman's non-parametric test. To compare categorical data, One-Way ANOVA Kruskal-Wallis unparametric test was applied with post-hoc test Dunn correction. A *p value* of less than 0.05 was considered to indicate significance. Analyses were performed with GraphPad Prism, version 6.0b.

Results

Method for quantitative IHC assessment in specific tissue zones of tumors from melanoma patients

Frequently, IHC staining is quantified by visual assessment (HSCORE). This method can be subjective and can lead to variability depending on the observer, especially when evaluating the expression of novel markers. Recently, the emergence of automated IHC measurement using computer-based analysis systems began to overcome these limitations. To date our knowledge of lymphatic vessel density and the distribution and infiltration of immune cells in melanoma samples comes from visual and/or computer-based quantification of specific regions (i.e. hot spots) or from small core biopsies containing representative areas of tumor or stroma tissue. For our analyses, we used a 'whole-slide' imaging software (Aperio Technologies, Vista, CA, USA) to quantify staining upon distinctly defined tissue zones.

For our IHC quantification strategy, we selected four zones in each of the 14 primary melanomas selected (Fig. 1A): 1) Invasive Margin (IM), 2) Center of the tumor (CT), 3) Peritumoral region and 4) Normal skin. Tumor cells were identified based on Melan-A, Melanosome (HMB45) and S100 positive staining or morphological criteria (large atypical and pleomorphic cells with abundant eosinophilic cytoplasm, visible nucleoli and mitosis) when these markers were negative. The invasive margin (IM) was defined as a tumor region of 400-μm width between the tumor and the reticular dermis. The remaining tumor was defined as center of the tumor (CT). The peritumoral region was defined as a region of 400-μm width in the dermis surrounding the invasive margin. Finally, normal skin was determined as a region of 200-μm width separated by at least 1mm from tumor cells. Normal skin was identifiable on 9 primary tumor samples (64%).

For the analysis of lymph node metastases, we pre-selected 33 metastatic LNs from 14 melanoma patients. 10 metastatic LNs were excluded from the analysis because of the presence of large regions of tumor necrosis (2/10), presence of excessive melanin pigments rendering analysis impossible (5/10), tumor metastasis less than 1mm^2 (1/10) or tumor metastasis size more than 98% of the entire LN (2/10). In the 23 remaining metastatic LNs, we defined six different zones corresponding to the different micro-anatomical regions (Fig. 1B): 1) tumor cells, 2) stroma, 3) residual LN, 4) reactive connective tissue, 5) capsule, 6) total tissue. The tumor cell zones were determined as previously described for primary tumors. Stroma was defined as connective tissue surrounding the tumor cells (present in 14 (61%) metastatic LNs). Regions of the LN that did not match the tumor or stroma criteria were considered as “residual LN” (these zones were similar to non-metastatic LN regions) in 19 metastatic LNs (83%). A dense and inflammatory irregular connective tissue was present around the LN and was described as reactive connective tissue (present in 13 (56%) metastatic LNs). Finally, the capsule was composed of thin dense irregular connective tissue surrounding the LN and was present in 16 (69%) metastatic LNs.

Importantly, we also studied non-metastatic LNs that had been obtained through lymph node dissection surgery. We analyzed the total area without defining specific zones in these 23 non-metastatic LNs.

Enhancement of lymphatic vessels in melanoma tissues

LECs are commonly described as being positive for Prox-1 (in the nucleus) and podoplanin and/or Lyve-1 (on the membrane). But depending on the tissue types investigated and the heterogeneity of tumor-associated lymphatic endothelium, their specificity can be variable (23). To optimize the characterization of tumor-associated lymphatics, we first stained primary melanoma tumors, metastatic LNs and non-metastatic LNs for Prox-1 and podoplanin by IHC. Interestingly, we found expression of Prox-1 and podoplanin in the analysed tissues (Fig. 2A – F). Melanoma cells in primary tumor and in metastatic LNs expressed Prox-1 in the cytoplasm (Fig. 2B, 2D) in combination with other melanoma cell markers such as Melan-A (Fig. S3A). As expected, lymphatic vessels in the primary tumor

(Fig. 2A) and in the tumor region of metastatic LNs (Fig. 2C) expressed podoplanin and nuclear Prox-1. In the stromal region of metastatic and in non-metastatic LNs Prox-1 better identified LECs since, in some tissue sections, other cells also expressed podoplanin such as follicular dendritic cells (FDCs) in germinal centres (Fig 2C, 2E). However, alpha-sma staining did not colocalize with podoplanin in the three different tissues tested (Fig. S3B). Given these results we decided to optimize our lymphatic vessel quantification strategy using podoplanin in the primary tumor and in the tumor region of the LNs and Prox-1 in the stroma of metastatic and non-metastatic LNs as LEC-specific. Immunofluorescence imaging confirmed the co-expression of podoplanin and nuclear Prox-1 as being the best combination to identify lymphatic vessels in all tissues analysed (Fig. S3C).

Demonstration of lymphangiogenesis in primary tumors

Lymphatic vessels are found in prominent hot spots both within and around primary cutaneous malignant melanoma (24). Moreover, melanoma lesions have been shown to have higher intratumoral lymphatic vessels density (LVD) compared to benign melanocytic lesions, likely due pro-lymphangiogeneic factors such as VEGF-C secreted by tumor cells (25). Indeed, in our study, lymphatic vessel staining quantification of the primary tumor (IM, CT and peritumoral areas) and the adjacent normal skin revealed increased Prox-1 and podoplanin-expressing lymphatics in the IM and peritumoral areas compared to the adjacent normal skin (Fig. 3A, 3B). A positive correlation was observed between podoplanin and Prox-1 in the IM (Spearman correlation, rho = 0.57, p = 0.08) and in the peritumoral area (rho = 0.5, p = 0.12), validating the fact that lymphangiogenesis occurs primarily in these zones (Fig. 3C). VEGF-C is a growth factor produced by tumor cells and tumor-associated macrophages (TAM) that promotes lymphangiogenesis. To assess potential pro-lymphangiogenic roles of VEGF-C, we compared VEGF-C expression in the different regions of the primary tumor and correlated VEGF-C with the two lymphatic markers. In comparison with podoplanin and Prox-1, we did not observe a statistically significant difference in VEGF-

C expression throughout the tumor regions and the adjacent normal skin (Fig. 3D). However, VEGF-C correlated positively with Prox-1 in the peritumoral area (rho = 0.63, *p* = 0.04) (Fig. 2E) whereas only a trend was seen for podoplanin in the peritumoral area (rho = 0.5, *p* = 0.09) (Fig. 2F).

Association of lymphatic vessels with immune suppressive molecules and immune cells in primary tumors

Next, we assessed associations between lymphatic vessels and immune suppressive molecules. Interestingly, there was a highly significant positive correlation between lymphatics and iNOS expression in IM of the primary tumor (rho = 0.74, *p* = 0.004*)* but not in the CT (rho = 0.32, *p* = 0.29) or in the peritumoral region (rho = -0.11, *p* = 0.72) (Fig. 4A). iNOS was mainly produced by melanoma cells and lymphatic vessels did not display cytoplasmic expression of iNOS (Fig. 4D). In contrast, lymphatics correlated positively with IDO expression in the CT of the primary tumor (rho = 0.58, *p* = 0.04) (Fig. 4B) but neither iNOS nor IDO were expressed by lymphatic vessels (Fig. 4E). Finally, there were no statistically significant correlations among lymphatic vessels and Arg-1 expression in the three different regions (Fig. 4C, 4F).

A major aim of our study was to evaluate and quantify the density of infiltrating lymphocytes in primary tumors using CD8, CD4, CD19 and FoxP3 markers and to investigate potential associations with lymphatic vessels. While correlating these markers with podoplanin, we found highly significant associations between lymphatic vessels and $CD8^+$ cells in the three different regions of the primary tumor (CT: rho = 0.69, *p* = 0.01; IM: rho = 0.66, *p* = 0.01 and Peritumoral: rho = 0.78, *p* = 0.003) (Fig. 5A, 5E). Interestingly, we saw that these associations held true not only between different patients but also in different regions of a particular patient's tumor, implicating that regions with a greater density of lymphatics have higher $CD8^+$ infiltration compared to regions with lower density of lymphatics. Analysis of $CD4^+$ and $CD19^+$ cells in relation to lymphatics showed positive trends for CD4 only in the IM

(IM: rho = 0.3, *p* = 0.07) (Fig. 5B) and for CD19 in the three regions of the tumor samples (CT: rho = 0.37, *p* = 0.12; IM: rho = 0.51, *p* = 0.16 and Peritumoral: rho = 0.26, *p* = 0.13) (Fig. 5C). No significant correlations were seen for FoxP3$^+$ infiltrating cells (CT: rho = 0.31, *p* = 0.35; IM: rho = 0.3, *p* = 0.34 and Peritumoral: rho = 0.19, *p* = 0.54) (Fig. 5D). In order to better assess the phenotype of CD8$^+$ infiltrating cells, we performed multiplex staining for CD8, PD-1, and Granzyme B on 10 primary melanoma samples. Importantly, CD8$^+$ cells in the tumor were found to be mostly Granzyme B$^-$ than Granzyme B$^+$ (Mann-Whitney, *p* = 0.0003) (Fig. 5F) and mostly PD-1$^-$ than PD-1$^+$ (*p* = 0.004) (Fig 5G). No statistically significant association was observed between lymphatic vessels in the tumor and infiltration of CD8$^+$GranzymeB$^-$ (rho = 0.31, *p* = 0.42), CD8$^+$GranzymeB$^+$ (rho = 0.32, *p* = 0.49), CD8$^+$PD-1$^-$ (rho = 0.05, *p* = 0.91) or CD8$^+$PD-1$^+$ (rho = 0.26, *p* = 0.49) (Fig. 5H).

Correlations between anti-tumoral T cell responses and vaccination

Patients in this cohort had been included in a cancer vaccine trial in which they received monthly subcutaneous (s.c) injections of Melan-A/MART-1$_{26-35}$ peptide and CpG-B 7909, emulsified in incomplete Freund's adjuvant (IFA). The phenotype and the functionality of specific CD8 T cells in the blood of these patients had been assessed previously (20, 26). Briefly, peripheral blood mononuclear cells (PBMC) were collected at different time points during the course of vaccination and direct *ex vivo* tetramer analysis of Melan-A-specific CD8$^+$ T cells and Enzyme-Linked ImmunoSpot (ELISPOT) analysis of total PMBC for IFN-γ production after 24 hours incubation with Melan-A were performed. The peak value of Melan-A-specific CD8$^+$ T cells and IFN-γ producing Melan-A specific CD8$^+$ T cells reached during the study was used to assess the response to vaccination. Since we observed that lymphatic vessel density correlated with both higher iNOS expression and higher T cell infiltration in the tumor, we evaluated lymphatic vessel density in the primary tumor together with the T cell response to vaccination. No correlation was found between lymphatics in the primary tumor and peak frequencies of Melan-A specific CD8$^+$ T cells in the blood reached during the study

(Fig. 6A). Remarkably, more lymphatic vessels in the IM were associated with less IFN-γ production by Melan-A specific CD8$^+$ T cells present in the blood of patients during the vaccination study (IM: rho = -0.8, *p* = 0.01). In contrast, lymphatics present in the CT and the peritumoral area did not correlate negatively with frequency of IFN-γ-producing Melan-A specific CD8$^+$ T cells in the blood (CT: rho = -0.4, *p* = 0.19; Peritumoral: rho = 0.02, *p* = 0.93) (Fig. 6B). The same association between lymphatics and IFN-γ-producing Melan-A specific CD8$^+$ T cells was also observed for iNOS (Fig. 6C, 6D), suggesting that iNOS expressing cells attracted by lymphatic vessels in IM impair the functionality of Melan-A specific CD8$^+$ T cells responding to the vaccine. Moreover, we also found a positive correlation between Melan-A expression in the IM and the frequency and functionality of Melan-A specific CD8 T cells in the blood of vaccinated patients (Fig. 6E, 6F).

Associations between lymphatic vessels, infiltrating immune cells and immune suppressive molecules in metastatic LNs

Regional LN metastases are important for prognosis and treatment decisions. LNs are the primary sites of adaptive immune responses. Since we found that the density and the phenotype of lymphatic vessels in the IM of primary tumors correlated with the quality of the anti-tumoral T cell response, we hypothesized that similar associations may be seen in metastatic LNs of these patients. Indeed, in metastatic LNs we found that greater lymphatic vessel density in the tumor region correlated positively with higher CD8$^+$ cell infiltration in the tumor areas of metastatic LNs (rho = 0.6, *p* = 0.002) (Fig. 7A, 7E). Here again, no correlation was detected between lymphatic vessels and CD4$^+$ cell infiltration in the tumor (rho = 0.27, *p* = 0.22) (Fig. 7B). Strikingly, as opposed to primary tumors, positive associations between lymphatic vessel density were found for CD19$^+$ (rho = 0.68, *p* = 0.0007) (Fig. 7C) and FoxP3$^+$ (rho = 0.44, *p* = 0.03) (Fig. 7D) infiltrating cells, as observed in the tumor region of metastatic LNs, suggesting potentially immune suppressive roles of lymphatic vessels. IHC quantification of Granzyme B and PD-1 expression in tumor-infiltrating CD8+ cells in primary tumor highlighted greater infiltration of $CD8^+GranzymeB^-$ ($p < 0.0001$) (Fig. 7F, left panel) and $CD8^+PD\text{-}1^-$ ($p = 0.0003$) (Fig. 7F, right panel) in the tumor region. However, we did not find a positive correlation between tumor-associated lymphatic vessels and infiltration of $CD8^+GranzymeB^-$ (rho = -0.66, $p = 0.88$), $CD8^+GranzymeB^+$ (rho = 0.07, $p = 0.88$), $CD8^+PD\text{-}1^-$ (rho = 0.02, $p = 0.98$) and $CD8^+PD\text{-}1^+$ (rho = 0.26, $p = 0.49$) (Fig. 7G). Similar to the IM of primary tumors, iNOS expression in the tumor region of metastatic LNs was found to correlate with tumor-associated lymphatic vessels (rho = 0.47, $p = 0.02$) (Fig. 7H). Interestingly, compared to primary tumors, some tumor-associated lymphatic vessels demonstrated direct expression of iNOS in the cytoplasm (Fig. 7J), thus suggesting direct and active modulation of TME by tumor-associated lymphatics. Even if positive associations were observed between lymphatic vessels and IDO^+ expressing cells (rho = 0.49, $p = 0.02$) (Fig. 7I), direct expression of IDO in LECs was not observed (Fig. 7K). Arg-1 was not associated with lymphatic vessels density and was not expressed by LECs (data not shown). Finally, these different positive associations between lymphatic vessels, immune cells and immune suppressive molecules did not hold true in stroma regions of metastatic LNs (data not shown).

Mouse melanoma tumors have been reported to pre-condition future sites of metastasis in the lymph node by enhancing lymphangiogenesis, inducing an immunotolerant microenvironment and thus impairing the development of anti-tumor immunity (27, 28). This mechanism has been shown to be driven by secretion of VEGF-C and CCL21 by tumors (16, 17). To address the potential role of VEGF-C in modulating host antitumor immunity in human melanoma, we looked at associations between VEGF-C and tumor infiltrating immune cells and immune suppressive molecules in metastatic LNs. We observed a strong positive correlation between VEGF-C expression in the tumor region of metastatic LNs with iNOS (rho = 0.47, $p = 0.0002$) (Fig. 8A, 8E) and IDO (rho = 0.69, $p = 0.021$) (Fig. 8B, 8E) in the same region. Furthermore, a positive trend was also seen with CD8 (rho = 0.29, $p = 0.17$) (Fig. 8C, 8E) and FoxP3 (rho = 0.34, $p = 0.11$) (Fig. 8D, 8E) but not with CD4 (rho = -0.14, p

= 0.51) or CD19 (rho = 0.17, *p* = 0.44) (data not shown). We found similar trends in the stroma regions of metastatic LNs, although the results were not statistically significant due to the limited number of samples containing a region of stroma (data not shown).

Recent studies have suggested that larger size melanoma metastases in lymph nodes correlate with shorter progression-free survival (29). We therefore postulated that the degree of tumor-infiltration may have an impact on tumor-associated lymphatic vessels by inducing them to promote a more immune suppressive TME. Tumor size was calculated by taking the mean of the total number of positive and negative pixels (= total tumor density) in Melan-A, HMB45 and S100 stained slides divided by the total number of pixels of the entire LN (= LN size). Metastatic LNs were ordered by tumor size and divided into two groups. (Fig. 9A, left panel). Metastatic LN tumor sizes below the median were considered as “low tumor-infiltrated LNs” and those above the median as “high tumor-infiltrated LNs” (Fig. 9A, right panel). Remarkably, lymphatic vessels present in the tumor regions of high-tumor infiltrated LNs were associated with higher infiltration of CD8$^+$ cells (rho = 0.79, *p* = 0.0008) (Fig. 9B), CD19$^+$ cells (rho = 0.64, *p* = 0.04) (Fig. 9D) and FoxP3$^+$ (rho = 0.71, *p* = 0.02) (Fig. 9E) but not CD4$^+$ cells (rho = 0.06, *p* = 0.86) (Fig. 9C) compared to lymphatics present in the tumor of low-tumor infiltrated LNs. Furthermore, these lymphatic vessels were also associated with higher iNOS$^+$ cells (rho = 0.66, *p* = 0.04) (Fig. 9F) and (rho = 0.87, *p* = 0.001) VEGF-C$^+$ cells (Fig. 9H) as well as higher iNOS expression in their cytoplasm compared to those of low-tumor infiltrated LNs (Fig. 9G).

Lymphatic vessels, immune cells and immune suppressive molecules in non-metastatic LNs

In parallel, we also analyzed 23 non-metastatic LNs from the same patients. A positive trend was observed between lymphatic vessels and CD8$^+$ (rho = 0.31, *p* = 0.15) (Fig. 10A) cell infiltration. No correlation was found with CD4$^+$ (rho = -0.002, *p* = 0.98) (Fig. 10B), CD19$^+$ (rho = -0.14, *p* = 0.54) (Fig. 10C) or FoxP3$^+$ (rho = 0.34, *p* = 0.19) (Fig. 10D) infiltrating cells.

In line with what we saw for the primary tumor and metastatic LNs, we saw more CD8$^+$Granzyme B$^-$ cells than CD8$^+$Granzyme B$^+$ in the total area of non-metastatic LNs ($p < 0.0001$) (Fig. 10E). However, no statistically significant difference was observed between the number of CD8$^+$PD-1$^-$ and CD8$^+$PD-1$^+$ cells in the total area of non-metastatic LNs ($p = 0.37$) (Fig. 10F). Interestingly, we found a positive trend between lymphatic vessels and CD8$^+$PD-1$^-$ (rho = 0.47, $p = 0.12$) and CD8$^+$PD-1$^+$ (rho = 0.45, $p = 0.14$) but not with CD8$^+$GranzymeB$^-$ (rho = 0.26, $p = 0.39$) or CD8$^+$GranzymeB$^+$ (rho = 0.07, $p = 0.88$) (Fig. 10G). As in primary tumor and metastatic LNs, lymphatic vessels were strongly positively associated with iNOS (rho = 0.67, $p = 0.0004$) (Fig. 10H) but in contrast they were not associated with IDO (rho = 0.12, $p = 0.61$) (data not shown) or VEGF-C (rho = 0.23, $p = 0.32$) (data not shown). Consistent with all melanoma tissues analyzed in this study, no correlation was observed between lymphatic vessels and Arg-1 expression (rho = 0.24, $p = 0.25$) (data not shown). As seen in metastatic LNs, some lymphatic vessels in non-metastatic LNs were also seen to express iNOS in their cytoplasm. Finally, also similar to metastatic LNs, VEGF-C correlated positively with iNOS (rho = 0.63, $p = 0.002$) and IDO (rho = 0.47, $p = 0.02$) (data not shown).

Several studies have examined immune parameters in regional lymph nodes of melanoma patients, and have shown that LNs close to the primary melanoma or nodal metastases were less immunologically reactive than were more remote nodes as assessed by indices including the area occupied by the density of paracortical dendritic cells (DC) and T cells, capacity of T cells to inhibit or enhance melanoma cell growth *in vitro*, and the frequency of high endothelial venules (HEV) (30). These data suggest that the proximity of tumor-draining LNs to tumor cells can have an impact on anti-tumor immunity. As such, we analyzed non-metastatic LNs with regard to the positivity of the total LN dissection from which they were derived. Of 23 non-metastatic LNs, 14 were from LN dissections where at least one LN was found to be positive for melanoma metastasis (“positive LN dissection” or “LN diss. +”). The remaining nine non-metastatic LNs were from LN dissections where no melanoma metastasis was found in any of the LNs removed (“negative LN dissection” or “LN diss. -”).

Interestingly, non-metastatic LNs from positive LN dissections had higher $CD8^+$ and $CD4^+$ ($p = 0.04$) cells compared to LNs from negative LN dissections (Fig. 11A, right and left panel). Statistical significance was not reached for $FoxP3^+$ cells ($p = 0.06$, data not shown) and no difference was observed for $CD19^+$ cells ($p = 0.91$, data not shown). A greater number of $podoplanin^+$ ($p = 0.005$) and Prox-1^+ ($p = 0.02$) lymphatic vessels were seen in LNs from positive LN dissections compared to negative LN dissections (Fig. 11B, right and left panel). In line with this, the non-metastatic LNs from positive LN dissections showed more iNOS ($p = 0.03$) and Arg-1 ($p = 0.02$) but not more IDO ($p = 0.12$) or VEGF-C ($p = 0.17$) expression than LNs from negative LN dissections (Fig 11C). However, we did not find differences between the two groups for Granzyme B and PD-1 expression in $CD8^+$ cells (Fig. 11D). Finally, lymphatic vessels in non-metastatic LNs from positive LN dissections showed a positive trend with $CD8^+$ (rho = 0.4, $p = 0.15$) (Fig. 11E) cells but were negatively correlated with $CD4^+$ (rho = -0.55, $p = 0.04$) (Fig. 11F) cells compared to LNs from negative LN dissection. No difference was observed for $CD19^+$ (rho = -0.13, $p = 0.66$) and $FoxP3^+$ cells (rho = 0.16, $p = 0.57$) (data not shown). iNOS (rho = 0.52, $p = 0.04$) expression correlated with lymphatic vessels within LNs from positive LN dissections compared to those from negative LN dissections (Fig. 11G). However, there was no correlation with Arg-1 (rho = -0.12, $p = 0.65$), IDO (rho = -0.14, $p = 0.62$) or VEGF-C (rho = 0.32, $p = 0.27$) in LNs from positive LN dissections (data not shown). Importantly, higher iNOS expression in LEC was found in LNs from positive LN dissections as compared to those from negative LN dissections (Fig. 11H, upper and lower panel)

Discussion

Although researchers have long appreciated the clinical relevance of lymphangiogenesis in the TME (31) and the involvement of the lymphatic system in malignant spread, the underlying mechanisms remain poorly understood. Mouse melanoma models have recently demonstrated immune-modulatory effects of lymphangiogenesis in primary tumors and draining LNs (16, 17, 32), thus proposing a link between lymphangiogenesis and poor clinical outcome of cancer patients (13, 24, 33). However, corresponding human data was still missing. In the present study, we assessed for the first time human lymphatic vessels as an active modulator of anti-tumor immunity and identified new associations between lymphatic vessels, immune cells and immune suppressive molecules in human melanoma tissues (Table 1). These findings improve our understanding of lymphangiogenesis as a tumor metastasis promoter, by linking it to the sculpting of host immunity, considered critical to tumor progression.

The methodology of lymphangiogenesis quantification is predominantly based on the assumption that functional increases in lymphatic vessels during tumor growth occur in “hot spots” (i.e. areas of particularly high density of lymphatic vessels) (23). In recent decades, the majority of studies that investigated links between lymphangiogenesis and clinical outcome in human melanoma tissues have used staining quantification methods based on visual inspection and selection of hot spots (e.g. Weidner and Chalkley method) (25, 34, 35). Despite the recent emergence of computer-assisted image analysis that reduces the variability and subjectivity in quantifying lymphatic vessels, studies were still based on either selected hot spot regions or randomly selected fields (10, 36). In line with this, Balsat *et al* recently questioned the relevance of counting lymphatic vessels in hot spots by comparing intra- and peritumoral lymphatic vessel density using the hot spot technique with that determined by a computerized method on early cervical cancer tissues (37). While comparing the two groups they found that inter-observer variability obtained after quantifications within hot spot regions reached 33.8% and 23.6% of intra- and peritumoral LVD respectively. The same was even true for intra-observer variability, whereas this variability did not exceed 5% with the whole slide analysis using the computer–assisted technique. Furthermore, few studies have investigated and compared LVD in different involved and non-involved melanoma tissues (38).

We analysed specific regions as well as entire tissue sections of different melanoma-associated tissues with dedicated analysis software. Our quantification of lymphatic vasculature and further markers covers unusually large tissue areas in a reproducible manner. However, this zone-defined method is time consuming and not well suited to analysis of large numbers of cases. In our study, we used the pixel count algorithm (ImageScope^{TM}, Aperio) to quantify lymphatic vessels, immune cells and immune suppressive molecules. This algorithm presents several advantages as well as disadvantages. Pixel based analysis has been shown to be more precise than cell-counting algorithms, especially in the setting of dense cell concentrations such as in LNs (data not published). Pixel based analysis has been validated as an accurate strategy by which to assess the relative density of positively stained cells in tissue sections (22). However, pixel counts may not be precise in the setting of high heterogeneity in the cell size, and did not represent the numbers of distinct lymphatic vessel structures or cells per tissue area. Moreover, such algorithms are imprecise in capturing the area and circumference of vessel lumens, and in the evaluation of potentially important structural and morphological features of lymphatic vessels and other cells (39).

As recommended recently, we used podoplanin in combination with the nuclear marker Prox-1 to specifically quantify lymphatic vessels (23). However, recent studies pointed out that podoplanin can also be expressed by melanoma cells, cancer-associated fibroblasts (CAFs) (40), fibroblastic reticular cells (FRCs) (41) and FDCs (42) in lymphoid organs. We did not find podoplanin staining in melanoma cells when considering either primary melanoma or metastatic LNs. These data agree with Jokinen *et al* who showed absence of podoplanin expression in cutaneous melanoma devoid of spindle cell morphologic features (43). Co-staining of alpha-sma and podoplanin did not reveal any colocalization between the two markers in any of the tissues analysed, suggesting that podoplanin expression does not correlate with alpha-sma positive CAFs and FRCs. Podoplanin expression in CAFs in human primary melanoma was described in only one IHC study, however in absence of co-staining with alpha-sma, CD10, CD34, desmin, or similar markers (40). In addition, a recent comprehensive study by Kitano *et al* showed that stromal CAFs express podoplanin in only some but not all types of cancers (44). Melanoma was not considered in this study. The heterogeneity of CAFs and the lack of specific markers to identify them could explain these discrepancies and underscore the need for further studies on podoplanin expression in human melanoma tissue samples. Nevertheless, we observed podoplanin staining in the germinal centers of non-metastatic LNs suggesting positive FDCs, but we did not confirm this finding with antibodies specific for FDCs.

Surprisingly, we found Prox-1 staining in the cytoplasm of melanoma cells. Prox-1 is a forkhead-box-transcription factor widely known to have an IHC nuclear expression pattern, notably in LECs but also in tumor cells, as previously described in colon cancer (45). However, recent evidence suggests that cytoplasmic Prox-1 IHC staining is not a false-positive expression, though this needs to be validated through more in-depth techniques like *in situ* hybridization (46). One possible explanation is that Prox-1 is enriched and activated in the cytoplasm before being translocated to the nucleus to become functionally active (47). Of note, other studies have also investigated the expression of Prox-1 and validated its cytoplasmic expression by reverse transcription polymeras chain reaction (RT-PCR), PCR or western blot (48, 49). Nevertheless, further investigation is required to understand the potential role of cytoplasmic expression of Prox-1 in tumor pathogenesis and cancer invasion.

It has been reported that LVD is higher in and around primary melanomas compared to melanocytic nevi and normal dermis (25, 50, 51), thus supporting the data described here. The comparison of melanoma with normal skin suggests that lymphangiogenesis into the tumour must have occurred, even if we did not assess proliferation of LEC as now recommended by an international consensus on lymphangiogenesis quantification (23). In contrast, we did not find statistically significant differences between intra- (neither CT nor IM) or peri-tumoral lymphatic vessel density as described by others (34, 52). However, other studies have also not found significant differences, or even contradictory results (36, 53). The major difference between our findings and those of Straume *et al* and Toader *et al* is that we have determined the relative density of lymphatic vessels within and around the entire melanoma and not by hot spot selection. Moreover, our quantification method relies on the analysis of two distinct regions within the primary melanoma, namely the IM and CT, which are not generally distinguished in other studies.

Many reports have now established the role of VEGF-C in promoting lymphangiogenesis and lymph node metastases in mouse models of cancer as well as in human tumors (31). Nonetheless, a direct relationship between high immunohistochemical VEGF-C expression and high LVD has not always been found in cutaneous melanoma (34). This observation suggests the existence of additional mechanisms of action of VEGF-C on lymphatic vessels and tumor metastasis, such as promoting dilation of collecting lymph vessels and increasing lymph fluid drainage (54). Likely due to the limited number of patients analyzed in this study, we only found a positive trend between VEGF-C expression and lymphatic vessels in the peritumoral region of primary melanoma. It may well be that VEGF-C expression by cells other than tumor cells has a stronger impact on intratumoral lymphangiogenesis. In support of this interpretation, Boon *et al* found higher percentages and intensities of VEGF-C staining in TAMs compared to tumor cells, in their study on 113 primary melanomas (55). Furthermore, Gallego et *al* showed that VEGF-C expression by peritumoral dermal fibroblasts in primary melanoma was associated with the presence of metastases in regional lymph nodes, whereas this association was not seen with VEGF-C expression by tumor cells (56).

Taken together, our results suggest that VEGF-C promotes tumor lymphangiogeneis in primary tumors, particularly in and around the invasive margin. In line with this, several studies have concluded that the extent of invasive margin and peritumoral lymphangiogenesis was the most important prognostic factor for melanoma metastases (57, 58).

The role of VEGF-C and lymphangiogenesis, which enables and enhances communication between tumors and draining lymph nodes, in modulating anti-tumor immune responses has not yet been explored in human cancer. Here, we report for the first time a positive association between lymphatic vessels and $CD8^+$ T cell infiltration in primary cutaneous melanoma. In contrast to $CD8^+$ T cells, only a positive trend was seen for $CD4^+$ T cells and $CD19^+$ B cells. Interestingly, these associations were found in the three different zones delimited in the primary tissue sections, suggesting that lymphatic vessels may promote accumulation of $CD8^+$ T cells not only around but also within the tumor mass.

Although controversy has prevailed on the presence and functionality of intratumoral lymphatic vessels (with regard to fluid drainage or transport of tumor cells) in mouse models of human fibrosarcoma, melanoma and prostate cancer (57, 59), intratumoral lymphatics have been observed in human melanoma and were found more frequently in patients with LN metastases (24). In this regard, Ondondo *et al* have recently shown that naïve T cells can accumulate within tumors through lymphatic vessels in a fibrosarcoma mouse model, suggesting that tumor-associated lymphatics not only drain lymph to the tumor-draining LNs but can also deliver lymph directly to the tumor, thus potentially attracting immune cells (60). Furthermore, Shields *et al* reported that CCL21-secreting mouse melanoma tumors induced the formation of lymphoid-like reticular stroma networks and enhanced the recruitment of T cells, specifically regulatory T cells, within the tumor mass, therefore creating an immune suppressive microenvironment (17). In contrast, we did not find significant associations between lymphatic vessels and $FoxP3^+$ cells. Nevertheless, CD8 T cells in the TME were found to be preferentially Granzyme B negative and PD-1 negative. These findings are compatible with the notion that CD8 T cells were not highly differentiated (Granzyme low) or activated (PD-1 low). However, this interpretation is not definitive and alternative explanations are possible.

Further ex-vivo analysis will be needed to better characterize the phenotype and the functionality of the immune cells present in primary tumor with high LVD compared to those with low LVD. This knowledge will be important to assess the contribution of these cells to the antitumor immune response and their involvement in shaping the progression of the tumor. Finally, in-depth analysis of the expression of chemokine and homing receptors on immune cells and lymphatic vessels, as well as mechanistic studies, will be required in order to understand which cells are attracted by lymphatic vessels, potentially explaining the differences seen in correlations of lymphatic vessels and immune cells in this study. Nevertheless, our data suggest that LECs not only express trafficking molecules that affect migration of immune cells, but also play several other roles in modulating immune responses.

Although the presence of HEVs have been described in primary melanoma and have been linked to a good clinical outcome (61, 62), conflicting results exist in regard to the presence of tertiary lymphoid structures (TLSs) in primary melanoma, in spite of the fact that the latter frequently contain HEVs (63, 64). While we found a positive association between lymphatics and CD19$^+$ B cells in the primary tumor, we did not detect B cell clusters in the tumor samples examined here. However, this increased infiltration of B cells in association with lymphatic vessels in primary melanoma underlines the probable involvement of lymphatics in shaping the humoral immune response. There is still a paucity of information on the interactions between lymphatics and B cells and this needs to be further delineated to better understand the role of humoral immunity in cancer.

It has been shown recently that LECs not only express trafficking molecules that affect the migration of immune cells, but also possess the appropriate machinery to modulate T cell function. Indeed, studies have reported that LECs could directly induce T cell tolerance as well as suppress DC-mediated T cell activation by secreting a variety of immune suppressive factors such as TGF-β, IDO and iNOS (18). In one study, Kornek *et al* reported that mouse *in vitro*-expanded LECs mediated direct suppression of T cell proliferation and that IFN-γ derived from activated T cells was essential for this suppressive mechanism (65). A subsequent report from Nörder *et al* demonstrated that human *in vitro* IFN-γ-activated LECs produce IDO that suppresses T cell activation (66). However, these findings stemmed from *in vitro* studies of normal mouse and human LN derived-LECs. To date, these possible mechanisms of direct modulation of T cell function by LECs have not been shown in the cancer setting. Here, we observed significant associations between lymphatic vessels and iNOS expression at the invasive front and IDO expression in the CT. However, we observed neither iNOS nor IDO expression in tumor-associated lymphatics. It is of note that lymphatic vessels and iNOS expression in the IM of primary tumors was associated with an impaired functionality of Melan-A specific T cells in the blood following vaccination, suggesting that LECs are indeed active immune regulators and suppress T cell function in human melanoma patients. The reason that these findings were only found in the IM and not in the other zones defined in the primary tumor is still obscure and will require further investigation. Nevertheless, it is reasonable to assume that immune suppressive capacity is preferentially found in aggressive parts of tumors such as in the IM. Our study was only focused on possible associations between lymphatics and immune suppressive factors, therefore further mechanistic studies will be needed to address the role of LECs on the modulation of the anti-tumor immune response.

It is now well-established that tumor cells generate and secrete factors that can suppress immune responses in tumor-draining LNs (30, 67, 68). Since we found the same associations between lymphatic vessels, immune cells and immune suppressive molecules in metastatic LNs as in primary tumors from the same patients, our study identifies tumor-draining LNs as a tissue for immunosuppression and suggests that the mechanisms operating there may be similar to those in primary tumors (69). These changes are consistent with earlier reports that the tumor-promoting roles of lymphatics also occur in tumor-draining LNs in mouse models of melanoma (16). Furthermore, these positive associations between lymphatics, immune cells and immune suppressive factors such as iNOS and IDO held true in metastatic LNs with bigger tumor size. Interestingly, iNOS expression was found in the cytoplasm of tumor-associated lymphatics in these LNs, a finding that was not evident in the primary tumor. These data indicate that the degree of tumor-infiltration impacts on tumor-associated lymphatic vessels by inducing them to promote a more tolerogenic TME. We are currently continuing our analyses to determine whether lymphatic vessel phenotypes and functions differ between high and low tumor-infiltrated LNs.

In contrast to primary tumors, we found a significant correlation between lymphatic vessels and FoxP3$^+$ lymphocytes. The question of whether regulatory T cells play an important role in melanoma progression and metastasis formation is still unanswered, and conflicting data have been reported with regard to clinical impact (6). Notably, although still recognized as the most specific marker for regulatory T cells, Foxp3 can also be expressed by activated human T lymphocytes (70). It is, therefore, difficult to draw conclusions on the phenotype of Foxp3$^+$ lymphocytes in immunohistochemical studies. Further, more detailed studies on the relationship between Foxp3$^+$ regulatory T cells and lymphatic vessels are warranted.

Evidence from mouse models suggests that secretion of VEGF-C by tumor cells or other cells (e.g. B cells) induces LN lymphangiogenesis, fosters tumor metastases and suppresses anti-tumor immunity (16, 27, 28, 71). Although these mechanisms have been appreciated, the importance of the communication between the tumor and the draining LNs in suppressing anti-tumor immune responses (3), as well as the roles of tumor VEGF-C and lymphangiogenesis in modulating tumor immunity remained largely unexplored. Here, we provided the first evidence that VEGF-C is associated with iNOS and IDO expression in the tumor of metastatic LNs of melanoma patients, thus suggesting the induction of a tolerogenic

TME. Interestingly, VEGF-C correlated positively with CD8$^+$ T cells and FoxP3$^+$ lymphocytes. As recent data have shown that elements of the immune, inflammatory and angiogenic tumor microenvironment can have a strong impact on the prognostic value of CD8+ T cells (69), analysis of the overall inflammatory components of the TME and phenotype and functionality of immune cells will undoubtedly reveal information on the global immune contexture induced by VEGF-C in tumor-draining LNs of melanoma patients.

Many studies have identified alterations in both local and regional immune functions of metastatic tumor-draining LNs that may contribute to expansion and metastasis formation (30). However, only limited data exists on the differences between LNs from node positive patients and node negative patients with regard to their immune function. Zuckerman *et al* examined differences in immune cell signatures between tumor-free LNs of node negative breast cancer patients and tumor-invaded sentinel lymph nodes (SLNs), tumor-free SLNs or tumor-free non-sentinel lymph nodes (NSLNs) of node positive breast cancer patients (38). This study provided the first report that immune-related gene expression (e.g. antigen presentation, cell cycle…) was down-regulated in node positive patients compared to those in node negative patients not only locally, but also systemically in circulating immune cells of these patients.

In line with this, we investigated the immunological differences between non-metastatic LNs from patients with positive versus negative LN dissection surgery samples. We notably demonstrated that non-metastatic LNs from positive LN dissections were characterized by higher relative density of T lymphocytes, lymphatic vessels and immune suppressive molecules such as iNOS and Arg-1, as compared to those from negative LN dissections. However, we did not find a significant difference with regard to Granzyme B and PD-1 expression on CD8$^+$ T cells. Strikingly, lymphatic vessels correlated positively with iNOS but negatively with CD4+ T cells in non-metastatic LNs from positive LN dissections, as compared to those from negative LN dissections. These results suggest that lymphatic vessels may induce immune dysfunction and alteration in non-metastatic LNs of positive LN dissection patients, thus implying that immune modulator functions of lymphatic vessels could be systemic and occur beyond the TME, prior to metastasis formation. Further detailed evaluation of immune functions in relation to lymphatics in non-metastatic LNs of both positive and negative LN dissection patients might provide important clues regarding the events leading to the development of melanoma LN metastasis.

Mouse melanoma models have demonstrated the tumor-promoting role of lymphatics in the tumor and draining LNs. Here we describe novel associations between lymphatic vessels, immune cells and immune suppressive molecules within different tissues of melanoma patients. Lymphatic vessels were positively associated with iNOS and IDO as well as with locally enhanced $CD8^+$ T cell infiltration within primary melanoma tissues and in metastatic LNs. Interestingly, non-metastatic LNs showed similar associations, albeit less pronounced. Nonetheless, these associations were predominantly seen in non-metastatic LNs from positive LN dissection patients. It is of note that tumor-associated lymphatic vessels were associated with systemically altered CD8 T cell responses. Taken together, these results strongly suggest that lymphatic endothelium is an active modulator of antitumor immune responses locally within different human melanoma tissues and systematically throughout large parts of the immune system. Due to the relatively small size of our patient cohort, these results should be validated in a larger independent cohort. Furthermore, since these findings are based on correlations found between different IHC markers, it would be particularly interesting to further investigate the underlying mechanisms with in-depth studies on both the function and phenotype of immune cell subsets by ex-vivo functional analysis as well as gene expression profiling and further systems biology analyses. A major aim in the development of cancer immunotherapies is to overcome suppression of anti-tumor T cell responses. Our study provides evidence that lymphatic endothelium is implicated in this suppression in melanoma patients, thus providing a rationale to launch clinical trials associating treatments that target lymphatic vessels, combined with established and future immunotherapies (such as anti-PD-1 or anti-CTLA-4 antibodies, adoptive T cell therapy or vaccination), thereby improving treatment efficacy for cancer patients.

Acknowledgments

The authors gratefully acknowledge Susana Leubat, Véronique Noguet, Solange Gros, Isabelle Surchet for tissue processing and staining, Alain Michel for slide scanning and the pathology department of Geneva, Neuchâtel, Sion, UNILBAS, Meditest, Promed and Synlabs for providing tissues.

Grant support

This research has been supported by ISREC Foundation (Switzerland), the Cancer Research Institute, Ludwig Cancer Research (USA), SwissTransMed (KIP 18), Gabriela and Theodor Kümmer foundation (Switzerland), Erna Hamburger foundation (Switzerand) and Société Académique Vaudoise (Swizerland),

Figure legends

Figure 1. Histological zones defined in primary melanoma and metastatic LNs. A) Representation of the different histological zones in one primary melanoma stained with Melan-A: center of the tumor (green), Invasive margin (red), peritumoral region (pink) and normal skin (light blue). **B)** Representation of the different histological zones in one metastatic LN stained with Melan-A: tumoral zone (green), stromal zone (red), residual LN (light blue), reactive connective tissue (dark blue), capsular and subcapsular zone (yellow) and total zone (pink).

Figure 2. Podoplanin as a specific lymphatic vessel marker in tumor areas of primary tumors and metastatic LNs, and Prox-1 as a specific lymphatic vessel marker in stromal areas of LNs. Representative images of **(A)** podoplanin and **(B)** Prox-1 staining in the **(i)** IM, **(ii)** CT and **(iii)** peritumoral area. **(C)** Podoplanin and **(D)** Prox-1 staining in the **(i)**

tumor and **(ii)** stroma region of metastatic LNs. **(E)** Podoplanin and **(F)** Prox-1 staining **(i)** in non-metastatic LN. Scale bar, 100 μm.

Figure 3. Lymphangiogenesis primarily occurs in the invasive margin (IM) and peritumoral area of primary tumors and correlates with VEGF-C expression in peritumoral areas. The density and the individual data points of **(A)** Prox-1 and **(B)** podoplanin expression in the different histological zones of primary melanoma tissues. Error bars indicate mean ± SEM (one-way ANOVA Kruskal-Wallis unparametric test with post-hoc test Dunn correction). **C)** Spearman correlation of Prox-1 positive lymphatic vessels in the CT, IM and peritumoral area of primary tumors in relation to podoplanin positive lymphatic vessels in the same areas. **D)** The density and the individual data points of VEGF-C expression in the different histological zones of primary melanoma tissues (one-way ANOVA Kruskal-Wallis unparametric test with post-hoc test Dunn correction). Spearman correlation of **(E)** Prox-1 and **(F)** podoplanin positive lymphatic vessels in the CT, IM and peritumoral area of primary tumors in relation to VEGF-C density in the same areas. Statistically significant differences are highlighted in bold, when *p* values were < 0.05. (CT): center of tumor; (IM): invasive margin; (Peri.): peritumoral area and (N. skin): normal skin.

Figure 4. Lymphatic vessels in the IM of primary tumors correlate with iNOS expression but not IDO or Arg-1. Spearman correlations of podoplanin positive lymphatic vessels in the CT, IM and peritumoral area of primary tumors in relation with **(A)** iNOS, **(B)** IDO and **(C)** Arg-1 density in the same areas. Immunofluorescence staining showing Prox-1 and podoplanin positive lymphatic vessels with **(D)** iNOS, **(E)** IDO and **(F)** Arg-1 staining in the IM of primary tumor tissues. Scale bar, 50 μm. Statistically significant differences are highlighted in bold, when *p* values were < 0.05. (CT): center of tumor; (IM): invasive margin; (Peri.): peritumoral area; (podo): podoplanin.

Figure 5. Tumor-associated lymphatic vessels correlate with increased tumor-infiltrating CD8$^+$ cells. Spearman correlation of podoplanin positive lymphatic vessels in the

CT, IM and peritumoral area of primary tumors in relation to **(A)** CD8, **(B)** CD4, **(C)** CD19 and **(D)** FoxP3 density in the same areas. **E)** Immunofluorescence staining of Prox-1 and podoplanin positive lymphatic vessels with CD8 in a primary tumor with low lymphatic vessel density (left panel) and one with high lymphatic vessel density (right panel). Scale bar, 50 μm. Quantitative IHC analysis of tumor-infiltrating **(F)** $CD8^+GranzymeB^-$ and $CD8^+GranzymeB^+$ $cells/mm^2$ and **(G)** $CD8^+PD\text{-}1^-$ and $CD8^+PD\text{-}1^+$ $cells/mm^2$ in 10 primary melanomas. Error bars indicate mean ± SEM (nonparametric unpaired Mann-Whitney *t* test). **H)** Spearman correlation of podoplanin positive lymphatic vessels in the primary tumor in relation to $CD8^+GranzymeB^-$, $CD8^+GranzymeB^+$; $CD8^+PD\text{-}1^-$ and $CD8^+PD\text{-}1^+$ tumor-infiltrating $cells/mm^2$. Statistically significant differences are highlighted in bold, when *p* values were < 0.05. (CT): center of tumor; (IM): invasive margin; (Peri.): peritumoral area and (Prim. Tum.): primary tumor

Figure 6. Patients with increased lymphatic vessel density and iNOS expression in the IM of the primary tumor show impaired anti-tumoral T cell responses to vaccination. Spearman correlations of podoplanin, iNOS and Melan-A density in the CT, IM and peritumoral area of primary tumor tissues in relation to percentages of circulating **(A, C and E)** Melan-A specific $CD8^+$ T cells and **(B, D and F)** IFN-γ producing circulating Melan-A specific $CD8^+$ T cells respectively, reached during the vaccination. The data show peak values, i.e. the maximum value reached during the vaccination study for each patient. Percentages of Melan-A specific $CD8^+$ T cells were determined by direct *ex-vivo* tetramer staining, and percentages of IFN-γ producing Melan-A specific $CD8^+$ T cells were determined by direct *ex-vivo* ELISPOT analysis, following overnight incubation with Melan-A peptide. Statistically significant differences are highlighted in bold, when *p* values were < 0.05. (CT): center of tumor; (IM): invasive margin and (Peri.): peritumoral area

Figure 7. Tumor-associated lymphatics in metastatic LNs are associated with infiltration of CD8$^+$, CD19$^+$ and FoxP3$^+$ cells, and with expression of iNOS. Spearman correlations of podoplanin positive lymphatic vessels in the tumor region of metastatic LNs in relation to **(A)** CD8, **(B)** CD4, **(C)** CD19 and **(D)** FoxP3 density in the same area. **E)** Immunofluorescence staining of Prox-1 and podoplanin positive lymphatic vessels with CD8 in the tumor region of a metastatic LN with low lymphatic vessel density (left panel) and one with high lymphatic vessel density (right panel). **F)** Quantitative IHC analysis of tumor-infiltrating CD8$^+$GranzymeB$^-$ and CD8$^+$GranzymeB$^+$ cells/mm^2 (left panel) and CD8$^+$PD-1$^-$ and CD8$^+$PD-1$^+$ cells/mm^2 (right panel) in 12 metastatic LNs. Errors bars indicate mean ± SEM (nonparametric unpaired Mann-Whitney *t* test). **G)** Spearman correlation of podoplanin positive lymphatic vessels in the tumor region of metastatic LN in relation to CD8$^+$GranzymeB$^-$, CD8$^+$GranzymeB$^+$; CD8$^+$PD-1$^-$ and CD8$^+$PD-1$^+$ tumor-infiltrating cells per mm^2. Spearman correlation of podoplanin positive lymphatic vessels in the tumor region of metastatic LNs in relation to **(H)** iNOS and **(I)** IDO density in the same areas. Immunofluorescence staining showing Prox-1 and podoplanin positive lymphatic vessels with **(J)** iNOS and **(K)** IDO in the tumor region of a metastatic LN. Scale bar, 50 μm. Statistically significant differences are highlighted in bold, when *p* values were < 0.05. (Podo): podoplanin.

Figure 8. Tumor expression of VEGF-C is associated with IDO and iNOS expression in metastatic LNs. Spearman correlations of VEGF-C density in the tumor region of metastatic LNs in relation to **(A)** iNOS, **(B)** IDO, **(C)** CD8 and **(D)** FoxP3 density in the same area. **E)** Representative images of VEGF-C, iNOS, IDO and FoxP3 in tumor region of metastatic LNs with high VEGF-C density (upper panel) and low VEGF-C density (lower panel). Scale bar, 100 μm. Statistically significant differences are highlighted in bold, when *p* values were < 0.05.

Figure 9. Tumor-associated lymphatics in high-tumor infiltrated LNs are associated with higher infiltration of CD8$^+$, CD19$^+$, FoxP3$^+$ and VEGF-C$^+$ cells and with higher expression of iNOS. A) (Left panel): The different metastatic LNs in relation to the percentage of the tumor size in the entire LN. (Right panel) Representative image of tumor and stroma histological zones in a low and a high tumor-infiltrated LNs. Spearman correlation of podoplanin positive lymphatic vessels in the tumor of low tumor-infiltrated LNs and high-tumor infiltrated LNs in relation with **(B)** CD8, **(C)** CD4, **(D)** CD19**, (E)** FoxP3 **(F)** iNOS and **(H)** VEGF-C density in the same area. **G)** Immunofluorescence staining showing Prox-1 and podoplanin positive lymphatic vessels with iNOS in a low tumor-infiltrated LN and a high-tumor infiltrated LN. Scale bar, 50 μm. Statistically significant differences are highlighted in bold, when *p* values were < 0.05. (Low Tum LNs): low tumor-infiltrated LNs; (High Tum LNs): high tumor-infiltrated LNs**.**

Figure 10. Tumor-associated lymphatics in non-metastatic LNs are not associated with infiltration of CD8$^+$ T cells or IDO but express iNOS. Spearman correlation of podoplanin positive lymphatic vessels in the total area of non-metastatic LNs in relation to **(A)** CD8, **(B)** CD4, **(C)** CD19 and **(D)** FoxP3 density in the same areas. Quantitative IHC analysis of **(E)** CD8$^+$GranzymeB$^-$ and CD8$^+$GranzymeB$^+$ cells/mm^2 and CD8$^+$PD-1$^-$ and **(F)** CD8$^+$PD-1$^+$ cells/mm^2 in 12 non metastatic LNs. Error bars indicate mean ± SEM (nonparametric unpaired Mann-Whitney *t* test). **G)** Spearman correlation of podoplanin positive lymphatic vessels in non-metastatic LNs in relation to CD8$^+$GranzymeB$^-$; CD8$^+$PD-1$^-$ and CD8$^+$PD-1$^+$ tumor-infiltrating cells per mm^2. **H)** Spearman correlation of podoplanin positive lymphatic vessels in the total area of non-metastatic LNs in relation to iNOS. Statistically significant differences are highlighted in bold, when *p* values were < 0.05.

Figure 11. Non-metastatic LNs from positive LN dissections have higher infiltrating immune cells, lymphatic vessels, iNOS and Arg-1 than non-metastatic LNs from negative LN dissections. The density of **(A)** (left panel) CD8, **(A)** (right panel) CD4, **(B)** (left

panel) podoplanin, **(B)** (right panel) Prox-1, **(C)** (left panel) iNOS, **(C)** (middle left panel) IDO, **(C)** (middle right panel) Arg-1 and **(C)** (right panel) VEGF-C in non-metastatic LNs from negative LN dissection and in non-metastatic LNs from positive LN dissection. Error bars indicate mean ± SEM (nonparametric unpaired Mann-Whitney *t* test). **D)** Quantitative IHC analysis of $CD8^{+}GranzymeB^{-}$, $CD8^{+}GranzymeB^{+}$, $CD8^{+}PD\text{-}1^{-}$ and $CD8^{+}PD\text{-}1^{+}$ cells mm^{2} in 5 non-metastatic LNs from negative LN dissection and 7 non-metastatic LNs from positive LN dissection, respectively. Error bars indicate mean ± SEM (one-way ANOVA Kruskal-Wallis unparametric test with post-hoc test Dunn correction). Spearman correlation of podoplanin positive lymphatic vessels in non-metastatic LNs from negative and positive LN dissection in relation to **(E)** CD8, **(F)** CD4 and **(G)** iNOS density. **H)** Immunofluorescence staining showing Prox-1 and podoplanin positive lymphatic vessels with iNOS in a non-metastatic LN from a negative LN dissection patient (upper panel) and in a non-metastatic LN from a positive LN dissection patient (lower panel). Scale bar, 50 μm. Statistically significant differences are highlighted in bold, when *p* values were < 0.05. (LN diss. $^{-}$): non-metastatic LNs from negative LN dissection, and (LN diss. $^{+}$): non-metastatic LNs from positive LN dissection.

Supplementary Figure 1. Representative images of immunohistochemical staining of formalin-fixed paraffin embedded non-metastatic LNs tissue sections for each antibody. Representative images of staining for **(A)** CD8, **(B)** CD4, **(C)** CD19, **(D)** FoxP3, **(E)** podoplanin **(F)** Prox-1 **(G)** VEGF-C **(H)** iNOS **(I)** IDO and **(J)** Arg-1.

Supplementary Figure 2. Image analysis with the pixel-count algorithm (ImageScope, Aperio) and with thresholded colocalization algorithm (Inform, Perkin-Elmer). Representative images of various densities of CD4+ T lymphocytes in metastatic LN demonstrating that the image-analysis output from ImageScope matches visual evaluation. **A)** (Upper panel) Example of a metastatic LN stained with anti-CD4 antibody. (Lower panel) Pseudo-colored image of upper panel illustrating the four output values of the pixel-count algorithm: haematoxylin or negative signal (blue), weak positive (yellow), positive (orange) and strong non-specific (brown) and the respective relative units obtained. **B)** (Left panel) Fluorescence multiplex IHC of primary tumor stained with anti-CD8 (magenta), anti-PD-1 (red) and anti-Granzyme B (green). (Right panel) Score segmentation image of left panel illustrating use of the InForm analysis software.

Supplementary Figure 3. Prox-1 is expressed in the cytoplasm of melanoma cells and alpha-sma positive cells do not express podoplanin. A) Immunofluorescence staining showing Prox-1 with Melan-A in primary tumor. **B)** Immunofluorescence staining showing Prox-1 and podoplanin positive lymphatic vessels with alpha-sma in primary tumor (left panel), metastatic LN (middle panel) and non-metastatic LN (right panel). **C)** Immunofluorescence staining showing Prox-1 and podoplanin positive lymphatic vessels. Scale bar, 50 μm.

References

1. Dunn, G. P., A. T. Bruce, H. Ikeda, L. J. Old, and R. D. Schreiber. 2002. Cancer immunoediting: from immunosurveillance to tumor escape. *Nat. Immunol.* 3: 991–998.

2. Baitsch, L., P. Baumgaertner, E. Devevre, S. K. Raghav, A. Legat, L. Barba, S. Wieckowski, H. Bouzourene, B. Deplancke, P. Romero, N. Rufer, and D. E. Speiser. 2011. Exhaustion of tumor-specific CD8$^+$ T cells in metastases from melanoma patients. *J. Clin. Invest.* 121: 2350–2360.

3. Munn, D. H., and A. L. Mellor. 2006. The tumor-draining lymph node as an immune-privileged site. *Immunol. Rev.* 213: 146–158.

4. Erdag, G., J. T. Schaefer, M. E. Smolkin, D. H. Deacon, S. M. Shea, L. T. Dengel, J. W. Patterson, and C. L. Slingluff. 2012. Immunotype and immunohistologic characteristics of tumor-infiltrating immune cells are associated with clinical outcome in metastatic melanoma. *Cancer Res.* 72: 1070–1080.

5. Galon, J., F. Pagès, F. M. Marincola, M. Thurin, G. Trinchieri, B. A. Fox, T. F. Gajewski, and P. A. Ascierto. 2012. The immune score as a new possible approach for the classification of cancer. *Journal of Translational Medicine* 10: 1.

6. Fridman, W.-H., F. Pagès, C. Sautès-Fridman, and J. Galon. 2012. The immune contexture in human tumours: impact on clinical outcome. *Nat. Rev. Cancer* 12: 298–306.

7. Zippelius, A., P. Batard, V. Rubio-Godoy, G. Bioley, D. Liénard, F. Lejeune, D. Rimoldi, P. Guillaume, N. Meidenbauer, A. Mackensen, N. Rufer, N. Lubenow, D. Speiser, J.-C. Cerottini, P. Romero, and M. J. Pittet. 2004. Effector function of human tumor-specific CD8 T cells in melanoma lesions: a state of local functional tolerance. *Cancer Res.* 64: 2865–2873.

8. Marincola, F. M., E. Wang, M. Herlyn, B. Seliger, and S. Ferrone. 2003. Tumors as elusive targets of T-cell-based active immunotherapy. *Trends Immunol.* 24: 335–342.

9. Cham, C. M., and T. F. Gajewski. 2005. Metabolic mechanisms of tumor resistance to T cell effector function. *Immunol. Res.* 31: 107–118.

10. Dadras, S. S., T. Paul, J. Bertoncini, L. F. Brown, A. Muzikansky, D. G. Jackson, U. Ellwanger, C. Garbe, M. C. Mihm, and M. Detmar. 2003. Tumor lymphangiogenesis: a novel prognostic indicator for cutaneous melanoma metastasis and survival. *Am. J. Pathol.* 162: 1951–1960.

11. Schietroma, C., F. Cianfarani, P. M. Lacal, and T. Odorisio. 2003. Vascular endothelial growth factor-C expression correlates with lymph node localization of human melanoma metastases - Schietroma - 2003 - Cancer - Wiley Online Library. *Cancer.*

12. Mandriota, S. J. 2001. Vascular endothelial growth factor-C-mediated lymphangiogenesis promotes tumour metastasis. *EMBO J.* 20: 672–682.

13. Rinderknecht, M., and M. Detmar. 2008. Tumor lymphangiogenesis and melanoma metastasis. *J. Cell. Physiol.* 216: 347–354.

14. Christiansen, A., and M. Detmar. 2011. Lymphangiogenesis and Cancer. *Genes & cancer.*

15. Issa, A., T. X. Le, A. N. Shoushtari, J. D. Shields, and M. A. Swartz. 2009. Vascular endothelial growth factor-C and C-C chemokine receptor 7 in tumor cell-lymphatic cross-talk promote invasive phenotype. *Cancer Res.* 69: 349–357.

16. Lund, A. W., F. V. Duraes, S. Hirosue, V. R. Raghavan, C. Nembrini, S. N. Thomas, A. Issa, S. Hugues, and M. A. Swartz. 2012. VEGF-C promotes immune tolerance in B16 melanomas and cross-presentation of tumor antigen by lymph node lymphatics. *Cell Rep* 1: 191–199.

17. Shields, J. D., I. C. Kourtis, A. A. Tomei, J. M. Roberts, and M. A. Swartz. 2010. Induction of lymphoidlike stroma and immune escape by tumors that express the chemokine CCL21. *Science* 328: 749–752.

18. Card, C. M., S. S. Yu, and M. A. Swartz. 2014. Emerging roles of lymphatic endothelium in regulating adaptive immunity. *J. Clin. Invest.* 124: 943–952.

19. Speiser, D. E., D. Liénard, N. Rufer, V. Rubio-Godoy, D. Rimoldi, F. Lejeune, A. M. Krieg, J.-C. Cerottini, and P. Romero. 2005. Rapid and strong human CD8+ T cell responses to vaccination with peptide, IFA, and CpG oligodeoxynucleotide 7909. *J. Clin. Invest.* 115: 739–746.

20. Baumgaertner, P., C. Jandus, J.-P. Rivals, L. Derré, T. Lövgren, L. Baitsch, P. Guillaume, I. F. Luescher, G. Berthod, M. Matter, N. Rufer, O. Michielin, and D. E. Speiser. 2012. Vaccination-induced functional competence of circulating human tumor-specific CD8 T-cells. *Int. J. Cancer* 130: 2607–2617.

21. Stack, E. C., C. Wang, K. A. Roman, and C. C. Hoyt. 2014. Multiplexed immunohistochemistry, imaging, and quantitation: A review, with an assessment of Tyramide signal amplification, multispectral imaging and multiplex analysis. *Methods* 70: 46–58.

22. Gannon, P. O., A. O. Poisson, N. Delvoye, R. Lapointe, A.-M. Mes-Masson, and F. Saad. 2009. Characterization of the intra-prostatic immune cell infiltration in androgen-deprived prostate cancer patients. *J. Immunol. Methods* 348: 9–17.

23. Van der Auwera, I., Y. Cao, J. C. Tille, M. S. Pepper, D. G. Jackson, S. B. Fox, A. L. Harris, L. Y. Dirix, and P. B. Vermeulen. 2006. First international consensus on the methodology of lymphangiogenesis quantification in solid human tumours. In vol. 95. 1611–1625.

24. Dadras, S. S., B. Lange-Asschenfeldt, P. Velasco, L. Nguyen, A. Vora, A. Muzikansky, K. Jahnke, A. Hauschild, S. Hirakawa, M. C. Mihm, and M. Detmar. 2005. Tumor lymphangiogenesis predicts melanoma metastasis to sentinel lymph nodes. *Mod. Pathol.* 18: 1232–1242.

25. Giorgadze, T. A., P. J. Zhang, T. Pasha, P. S. Coogan, G. Acs, D. E. Elder, and X. Xu. 2004. Lymphatic vessel density is significantly increased in melanoma. *J. Cutan. Pathol.* 31: 672–677.

26. Speiser, D. E., P. Baumgaertner, V. Voelter, E. Devevre, C. Barbey, N. Rufer, and P. Romero. 2008. Unmodified self antigen triggers human CD8 T cells with stronger tumor reactivity than altered antigen. *Proc. Natl. Acad. Sci. U.S.A.* 105: 3849–3854.

27. Hirakawa, S., L. F. Brown, S. Kodama, K. Paavonen, K. Alitalo, and M. Detmar. 2007. VEGF-C-induced lymphangiogenesis in sentinel lymph nodes promotes tumor metastasis to

distant sites. *Blood* 109: 1010–1017.

28. Harrell, M. I., B. M. Iritani, and A. Ruddell. 2007. Tumor-induced sentinel lymph node lymphangiogenesis and increased lymph flow precede melanoma metastasis. *Am. J. Pathol.* 170: 774–786.

29. Leong, S. P. L., E. K. Nakakura, R. Pollock, M. A. Choti, D. L. Morton, W. D. Henner, A. Lal, R. Pillai, O. H. Clark, and B. Cady. 2011. Unique patterns of metastases in common and rare types of malignancy. *J Surg Oncol* 103: 607–614.

30. Cochran, A. J., R.-R. Huang, J. Lee, E. Itakura, S. P. L. Leong, and R. Essner. 2006. Tumour-induced immune modulation of sentinel lymph nodes. *Nat. Rev. Immunol.* 6: 659–670.

31. Tammela, T., and K. Alitalo. 2010. Lymphangiogenesis: Molecular mechanisms and future promise. *Cell* 140: 460–476.

32. Tewalt, E. F., J. N. Cohen, S. J. Rouhani, C. J. Guidi, H. Qiao, S. P. Fahl, M. R. Conaway, T. P. Bender, K. S. Tung, A. T. Vella, A. J. Adler, L. Chen, and V. H. Engelhard. 2012. Lymphatic endothelial cells induce tolerance via PD-L1 and lack of costimulation leading to high-level PD-1 expression on CD8 T cells. *Blood*.

33. Pastushenko, I., P. B. Vermeulen, F. J. Carapeto, G. Van den Eynden, A. Rutten, M. Ara, L. Y. Dirix, and S. Van Laere. 2014. Blood microvessel density, lymphatic microvessel density and lymphatic invasion in predicting melanoma metastases: systematic review and meta-analysis. *Br. J. Dermatol.* 170: 66–77.

34. Straume, O., D. G. Jackson, and L. A. Akslen. 2003. Independent prognostic impact of lymphatic vessel density and presence of low-grade lymphangiogenesis in cutaneous melanoma. *Clin. Cancer Res.* 9: 250–256.

35. Valencak, J., E. Heere-Ress, T. Kopp, S. F. Schoppmann, H. Kittler, and H. Pehamberger. 2004. Selective immunohistochemical staining shows significant prognostic influence of lymphatic and blood vessels in patients with malignant melanoma. *Eur. J. Cancer* 40: 358–364.

36. Massi, D. 2006. Tumour lymphangiogenesis is a possible predictor of sentinel lymph node status in cutaneous melanoma: a case-control study. *Journal of Clinical Pathology* 59: 166–173.

37. Balsat, C., N. Signolle, F. Goffin, K. Delbecque, B. Plancoulaine, P. Sauthier, V. Samouëlian, A. Béliard, C. Munaut, J.-M. Foidart, S. Blacher, A. Noël, and F. Kridelka. 2014. Improved computer-assisted analysis of the global lymphatic network in human cervical tissues. *Mod. Pathol.* 27: 887–898.

38. Zuckerman, N. S., H. Yu, D. L. Simons, N. Bhattacharya, V. Carcamo-Cavazos, N. Yan, F. M. Dirbas, D. L. Johnson, E. J. Schwartz, and P. P. Lee. 2013. Altered local and systemic immune profiles underlie lymph node metastasis in breast cancer patients. *Int. J. Cancer* 132: 2537–2547.

39. Pastushenko, I., C. Conejero, and F. J. Carapeto. 2015. Lymphangiogenesis: Implications for Diagnosis, Treatment, and Prognosis in Patients With Melanoma. *Actas Dermo-Sifiliográficas (English Edition)* 106: 7–16.

40. Kan, S., E. Konishi, T. Arita, C. Ikemoto, H. Takenaka, A. Yanagisawa, N. Katoh, and J. Asai. 2014. Podoplanin expression in cancer-associated fibroblasts predicts aggressive behavior in melanoma. *J. Cutan. Pathol.* 41: 561–567.

41. Astarita, J. L., S. E. Acton, and S. J. Turley. 2012. Podoplanin: emerging functions in development, the immune system, and cancer. *Front Immunol* 3: 283.

42. Xie, Q., L. Chen, K. Fu, J. Harter, K. H. Young, J. Sunkara, D. Novak, E. Villanueva-Siles, and H. Ratech. 2008. Podoplanin (d2-40): a new immunohistochemical marker for reactive follicular dendritic cells and follicular dendritic cell sarcomas. *Int J Clin Exp Pathol* 1: 276–284.

43. Jokinen, C. H., S. S. Dadras, J. R. Goldblum, M. van de Rijn, R. B. West, and B. P. Rubin. 2008. Diagnostic implications of podoplanin expression in peripheral nerve sheath neoplasms. *Am. J. Clin. Pathol.* 129: 886–893.

44. Kitano, H., S.-I. Kageyama, S. M. Hewitt, R. Hayashi, Y. Doki, Y. Ozaki, S. Fujino, M. Takikita, H. Kubo, and J. Fukuoka. 2010. Podoplanin expression in cancerous stroma induces lymphangiogenesis and predicts lymphatic spread and patient survival. *Arch. Pathol. Lab. Med.* 134: 1520–1527.

45. Skog, M., P. Bono, M. Lundin, J. Lundin, J. Louhimo, N. Linder, T. V. Petrova, L. C. Andersson, H. Joensuu, K. Alitalo, and C. H. Haglund. 2011. Expression and prognostic value of transcription factor PROX1 in colorectal cancer. *Br. J. Cancer* 105: 1346–1351.

46. TABAN, O., A. M. CIMPEAN, M. RAICA, and S. OLARIU. 2014. PROX1 expression in gastric cancer: from hypothesis to evidence. *Anticancer Res.* 34: 3439–3446.

47. Petrova, T. V., A. Nykänen, C. Norrmén, K. I. Ivanov, L. C. Andersson, C. Haglund, P. Puolakkainen, F. Wempe, H. von Melchner, G. Gradwohl, S. Vanharanta, L. A. Aaltonen, J. Saharinen, M. Gentile, A. Clarke, J. Taipale, G. Oliver, and K. Alitalo. 2008. Transcription factor PROX1 induces colon cancer progression by promoting the transition from benign to highly dysplastic phenotype. *Cancer Cell* 13: 407–419.

48. Duncan, M. K., W. Cui, D.-J. Oh, and S. I. Tomarev. 2002. Prox1 is differentially localized during lens development. *Mech. Dev.* 112: 195–198.

49. Xu, S.-Z. 2010. Prox1 Facilitates Transfected CHO Cell Proliferation through Activation of the AKT Signaling Pathway. *Int J Biomed Sci* 6: 49–59.

50. Massi, D., M. C. De Nisi, A. Franchi, V. Mourmouras, G. Baroni, J. Panelos, M. Santucci, and C. Miracco. 2009. Inducible nitric oxide synthase expression in melanoma: implications in lymphangiogenesis. *Mod. Pathol.* 22: 21–30.

51. Shields, J. D., M. Borsetti, H. Rigby, S. J. Harper, P. S. Mortimer, J. R. Levick, A. Orlando, and D. O. Bates. 2004. Lymphatic density and metastatic spread in human malignant melanoma. *Br. J. Cancer* 90: 693–700.

52. Toader, M. P., T. Ţăranu, Ş. Toader, A. Chirana, and T. Ţăranu. 2014. Correlation between lymphatic vessel density and microvessel density in cutaneous malignant melanoma. *Rom J Morphol Embryol* 55: 141–145.

53. Sahni, D., A. Robson, G. Orchard, R. Szydlo, A. V. Evans, and R. Russell-Jones. 2005. The use of LYVE-1 antibody for detecting lymphatic involvement in patients with malignant

melanoma of known sentinel node status. *Journal of Clinical Pathology* 58: 715–721.

54. He, Y., I. Rajantie, K. Pajusola, M. Jeltsch, T. Holopainen, S. Ylä-Herttuala, T. Harding, K. Jooss, T. Takahashi, and K. Alitalo. 2005. Vascular endothelial cell growth factor receptor 3-mediated activation of lymphatic endothelium is crucial for tumor cell entry and spread via lymphatic vessels. *Cancer Res.* 65: 4739–4746.

55. Boone, B., W. Blokx, D. De Bacquer, J. Lambert, D. Ruiter, and L. Brochez. 2008. The role of VEGF-C staining in predicting regional metastasis in melanoma. *Virchows Arch.* 453: 257–265.

56. Gallego, E., L. Vicioso, M. Alvarez, I. Hierro, L. Pérez-Villa, A. Blanes, and A. Matilla. 2011. Stromal expression of vascular endothelial growth factor C is relevant to predict sentinel lymph node status in melanomas. *Virchows Arch.* 458: 621–630.

57. Wong, S. Y., H. Haack, D. Crowley, M. Barry, R. T. Bronson, and R. O. Hynes. 2005. Tumor-secreted vascular endothelial growth factor-C is necessary for prostate cancer lymphangiogenesis, but lymphangiogenesis is unnecessary for lymph node metastasis. *Cancer Res.* 65: 9789–9798.

58. Alitalo, A., and M. Detmar. 2012. Interaction of tumor cells and lymphatic vessels in cancer progression. *Oncogene* 31: 4499–4508.

59. Padera, T. P., A. Kadambi, E. di Tomaso, and C. M. Carreira. 2002. Lymphatic Metastasis in the Absence of Functional Intratumor Lymphatics. *Science*.

60. Ondondo, B., E. Jones, J. Hindley, S. Cutting, K. Smart, H. Bridgeman, K. K. Matthews, K. Ladell, D. A. Price, D. G. Jackson, A. Godkin, A. Ager, and A. Gallimore. 2013. Progression of carcinogen-induced fibrosarcomas is associated with the accumulation of naïve CD4+ T cells viablood vessels and lymphatics. *Int. J. Cancer* 134: 2156–2167.

61. Avram, G., B. Sánchez-Sendra, J. M. Martín, L. Terrádez, D. Ramos, and C. Monteagudo. 2013. The density and type of MECA-79-positive high endothelial venules correlate with lymphocytic infiltration and tumour regression in primary cutaneous melanoma. *Histopathology* 63: 852–861.

62. Martinet, L., S. Le Guellec, T. Filleron, L. Lamant, N. Meyer, P. Rochaix, I. Garrido, and J.-P. Girard. 2012. High endothelial venules (HEVs) in human melanoma lesions: Major gateways for tumor-infiltrating lymphocytes. *oncoimmunology* 1: 829–839.

63. van Baren, N., J.-F. Baurain, and P. G. Coulie. 2013. Lymphoid neogenesis in melanoma. *oncoimmunology*.

64. Ladányi, A., T. Sebestyén, A. Mohos, G. Liszkay, B. Somlai, E. Tóth, and J. Timar. 2014. Ectopic lymphoid structures in primary cutaneous melanoma. *Pathol. Oncol. Res.* 20: 981–985.

65. Lukacs-Kornek, V., D. Malhotra, A. L. Fletcher, S. E. Acton, K. G. Elpek, P. Tayalia, A.-R. Collier, and S. J. Turley. 2011. Regulated release of nitric oxide by nonhematopoietic stroma controls expansion of the activated T cell pool in lymph nodes. *Nat. Immunol.* 12: 1096–1104.

66. Nörder, M., M. G. Gutierrez, S. Zicari, E. Cervi, A. Caruso, and C. A. Guzmán. 2012. Lymph node-derived lymphatic endothelial cells express functional costimulatory molecules

and impair dendritic cell-induced allogenic T-cell proliferation. *FASEB J.* 26: 2835–2846.

67. Lee, E., N. B. Pandey, and A. S. Popel. 2015. Crosstalk between cancer cells and blood endothelial and lymphatic endothelial cells in tumour and organ microenvironment. *Expert Rev Mol Med* 17: e3.

68. Ferguson, A. R., L. A. Nichols, A. L. Zarling, E. D. Thompson, C. C. Brinkman, K. M. Hargadon, T. N. Bullock, and V. H. Engelhard. 2008. Strategies and challenges in eliciting immunity to melanoma. *Immunol. Rev.* 222: 28–42.

69. Fridman, W.-H., R. Remark, J. Goc, N. A. Giraldo, E. Becht, S. A. Hammond, D. Damotte, M.-C. Dieu-Nosjean, and C. Sautès-Fridman. 2014. The immune microenvironment: a major player in human cancers. *Int. Arch. Allergy Immunol.* 164: 13–26.

70. Shevach, E. M. 2006. From vanilla to 28 flavors: multiple varieties of T regulatory cells. *Immunity* 25: 195–201.

71. Ruddell, A., M. I. Harrell, M. Furuya, S. B. Kirschbaum, and B. M. Iritani. 2011. B lymphocytes promote lymphogenous metastasis of lymphoma and melanoma. *Neoplasia* 13: 748–757.

Figure 1

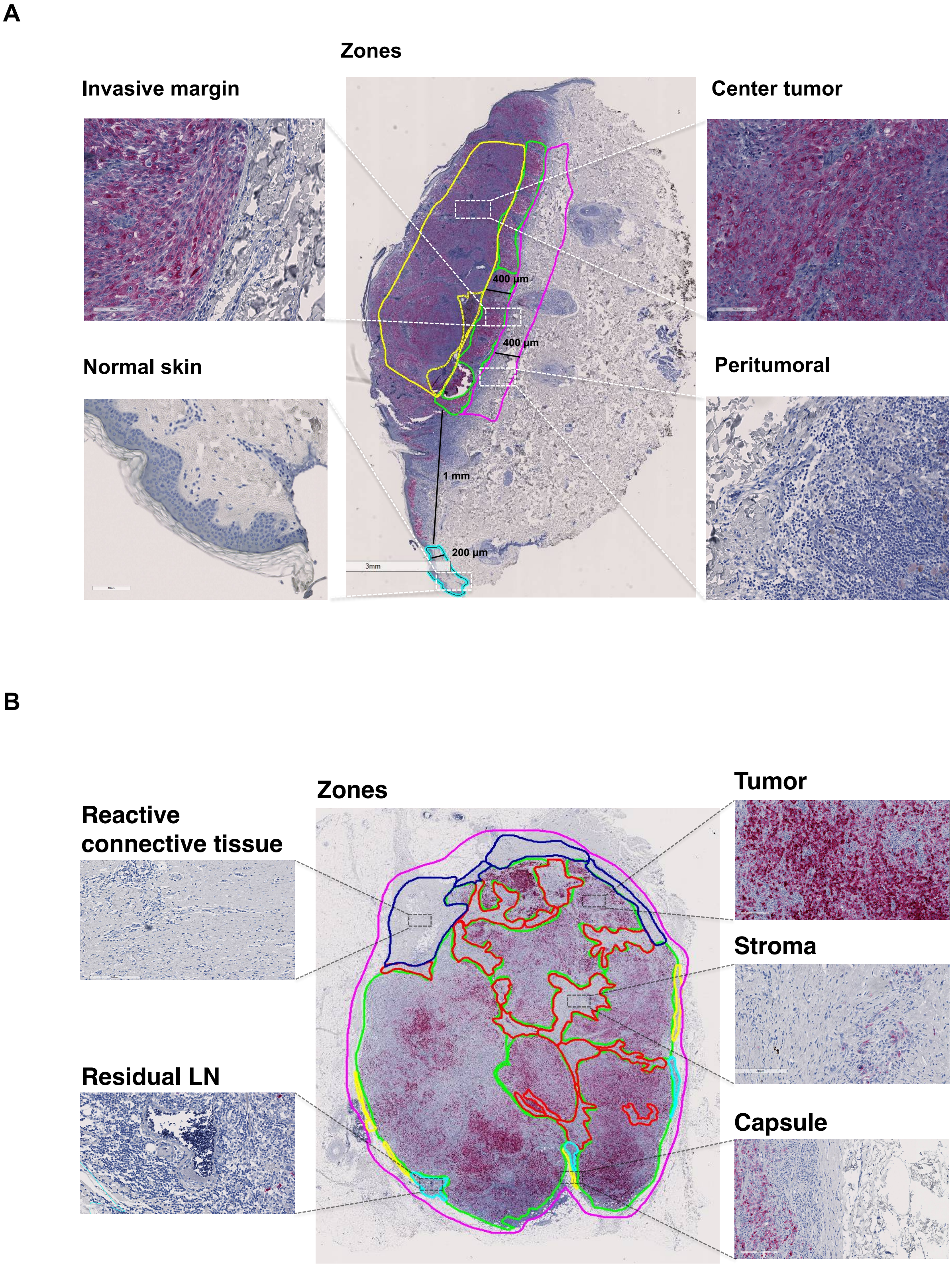
A
Zones
Invasive margin
Center tumor
400 µm
400 µm
Normal skin
Peritumoral
1 mm
200 µm
3mm
B
Zones
Tumor
Reactive connective tissue
Stroma
Residual LN
Capsule

Figure 2

Primary melanoma

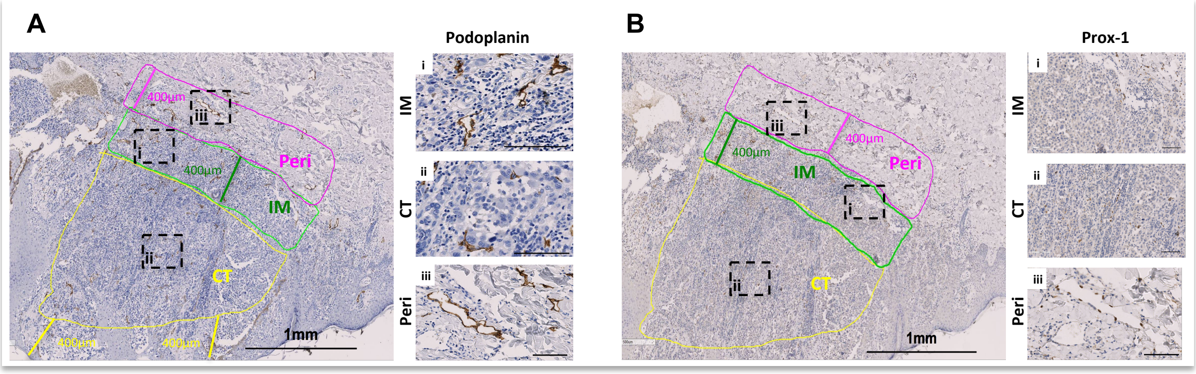

Metastatic LN

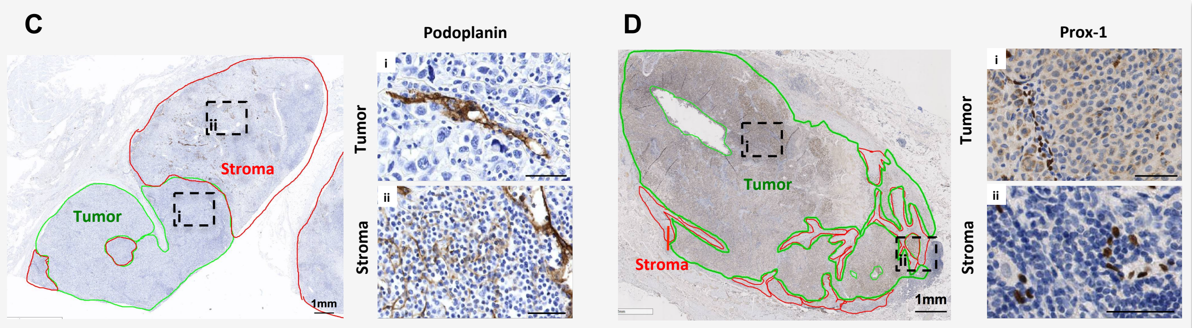

Non-metastatic LN

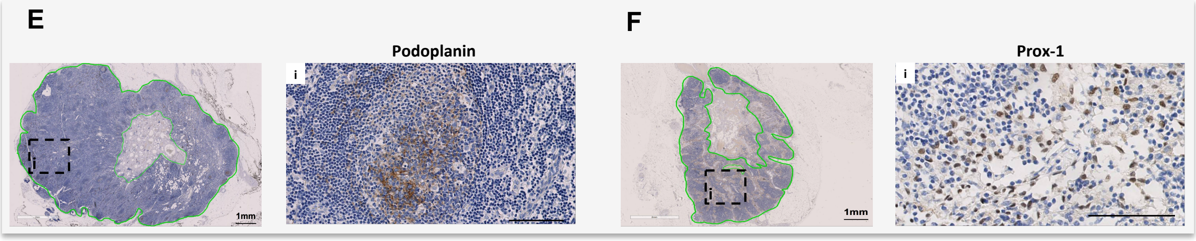

Figure 3

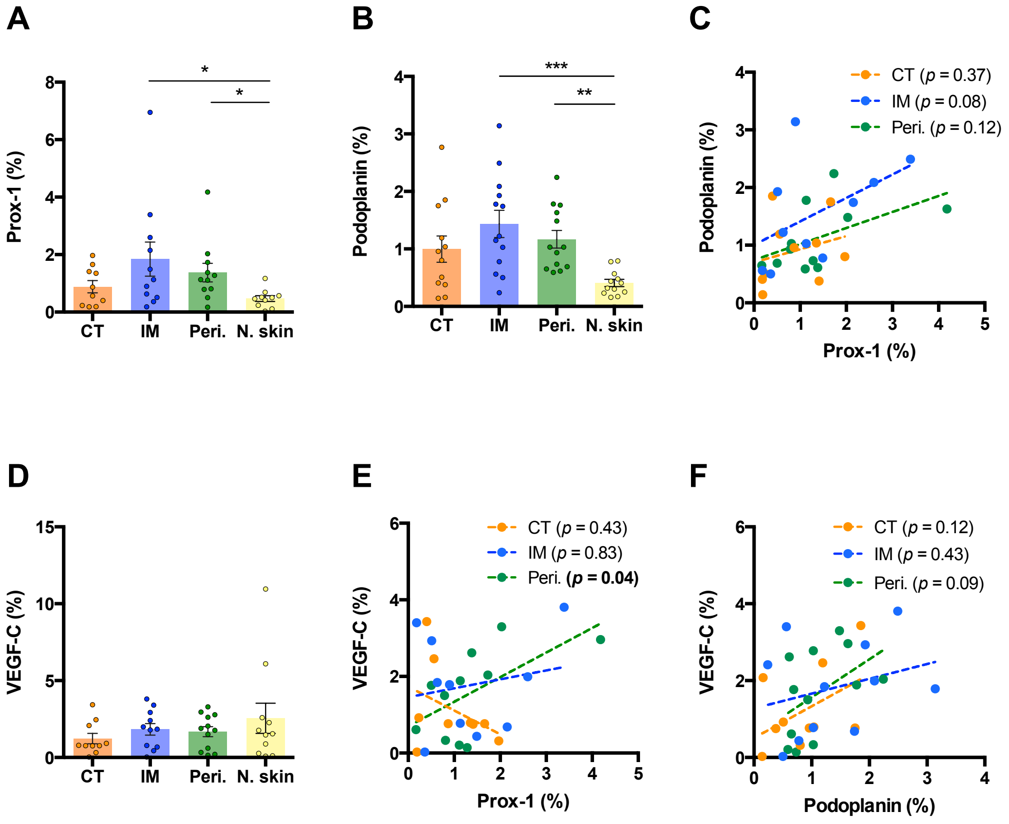
A
Prox-1 (%)
8
6
4
2
0
*
*
CT
IM
Peri.
N. skin
B
Podoplanin (%)
4
3
2
1
0
***
**
CT
IM
Peri.
N. skin
C
CT (p = 0.37)
IM (p = 0.08)
Peri. (p = 0.12)
Podoplanin (%)
Prox-1 (%)
0
1
2
3
4
5
D
VEGF-C (%)
15
10
5
0
CT
IM
Peri.
N. skin
E
CT (p = 0.43)
IM (p = 0.83)
Peri. (p = 0.04)
VEGF-C (%)
6
4
2
0
Prox-1 (%)
F
CT (p = 0.12)
IM (p = 0.43)
Peri. (p = 0.09)
VEGF-C (%)
Podoplanin (%)

Figure 4

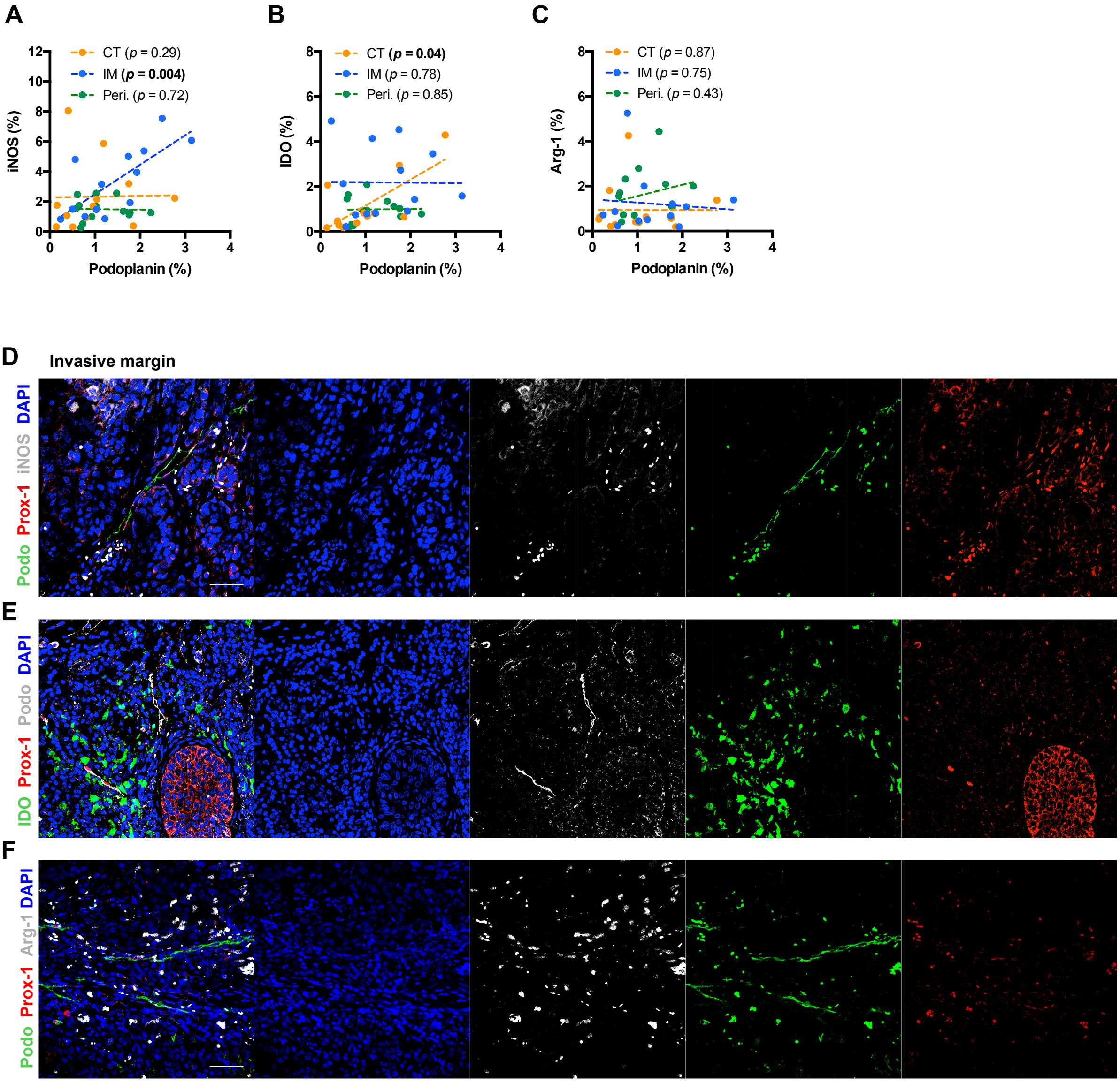
A
12
10
8
6
4
2
0
iNOS (%)
CT (p = 0.29)
IM (p = 0.004)
Peri. (p = 0.72)
0
1
2
3
4
Podoplanin (%)
B
8
6
4
2
0
IDO (%)
CT (p = 0.04)
IM (p = 0.78)
Peri. (p = 0.85)
0
1
2
3
4
Podoplanin (%)
C
8
6
4
2
0
Arg-1 (%)
CT (p = 0.87)
IM (p = 0.75)
Peri. (p = 0.43)
0
1
2
3
4
Podoplanin (%)
D
Invasive margin
Podo Prox-1 iNOS DAPI
E
IDO Prox-1 Podo DAPI
F
Podo Prox-1 Arg-1 DAPI

Figure 5

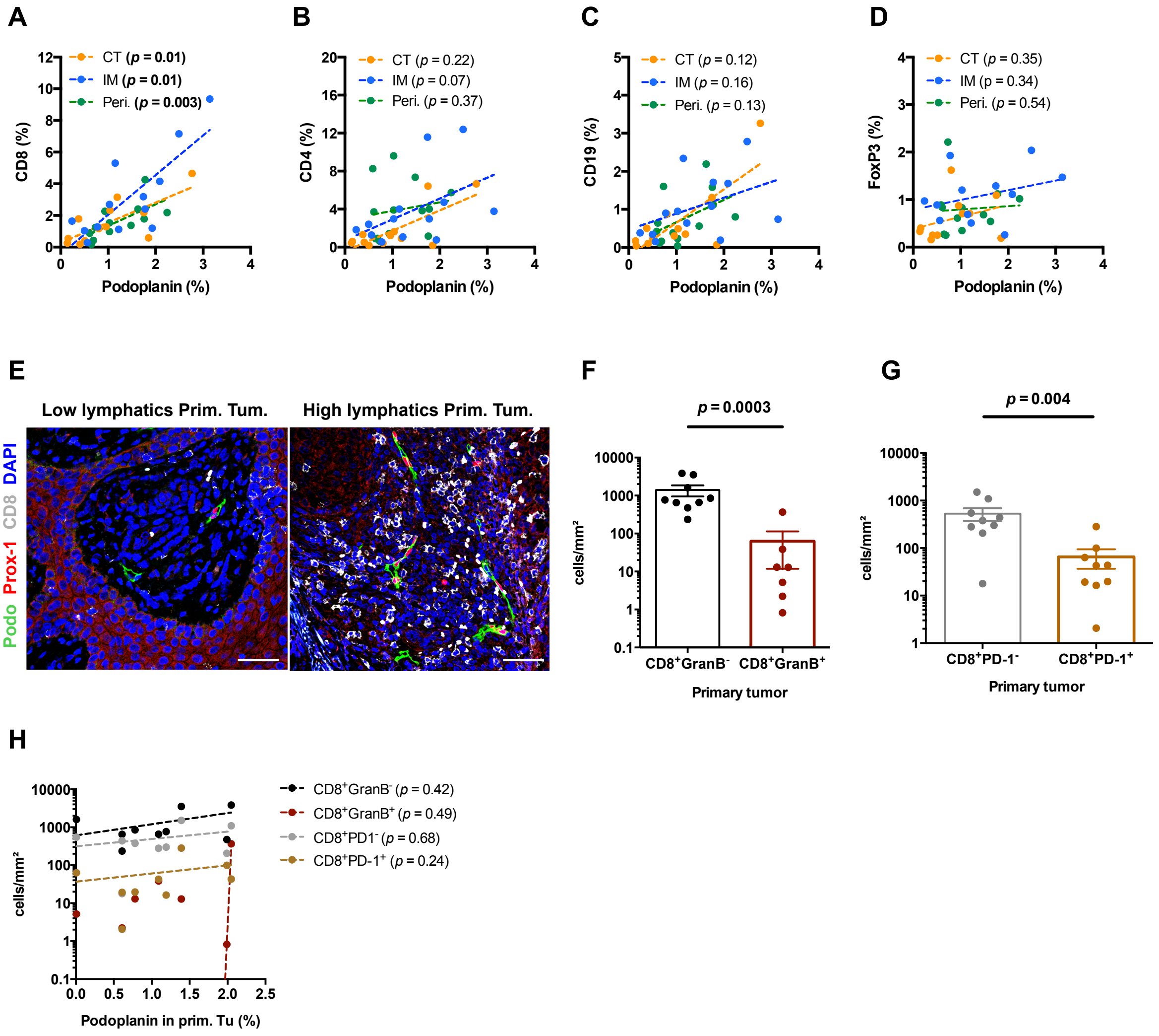
A
CT (p = 0.01)
IM (p = 0.01)
Peri. (p = 0.003)
CD8 (%)
Podoplanin (%)
B
CT (p = 0.22)
IM (p = 0.07)
Peri. (p = 0.37)
CD4 (%)
Podoplanin (%)
C
CT (p = 0.12)
IM (p = 0.16)
Peri. (p = 0.13)
CD19 (%)
Podoplanin (%)
D
CT (p = 0.35)
IM (p = 0.34)
Peri. (p = 0.54)
FoxP3 (%)
Podoplanin (%)
E
Low lymphatics Prim. Tum.
High lymphatics Prim. Tum.
Podo Prox-1 CD8 DAPI
F
p = 0.0003
cells/mm²
CD8+GranB-
CD8+GranB+
Primary tumor
G
p = 0.004
cells/mm²
CD8+PD-1-
CD8+PD-1+
Primary tumor
H
CD8+GranB- (p = 0.42)
CD8+GranB+ (p = 0.49)
CD8+PD1- (p = 0.68)
CD8+PD-1+ (p = 0.24)
cells/mm²
Podoplanin in prim. Tu (%)

Figure 6

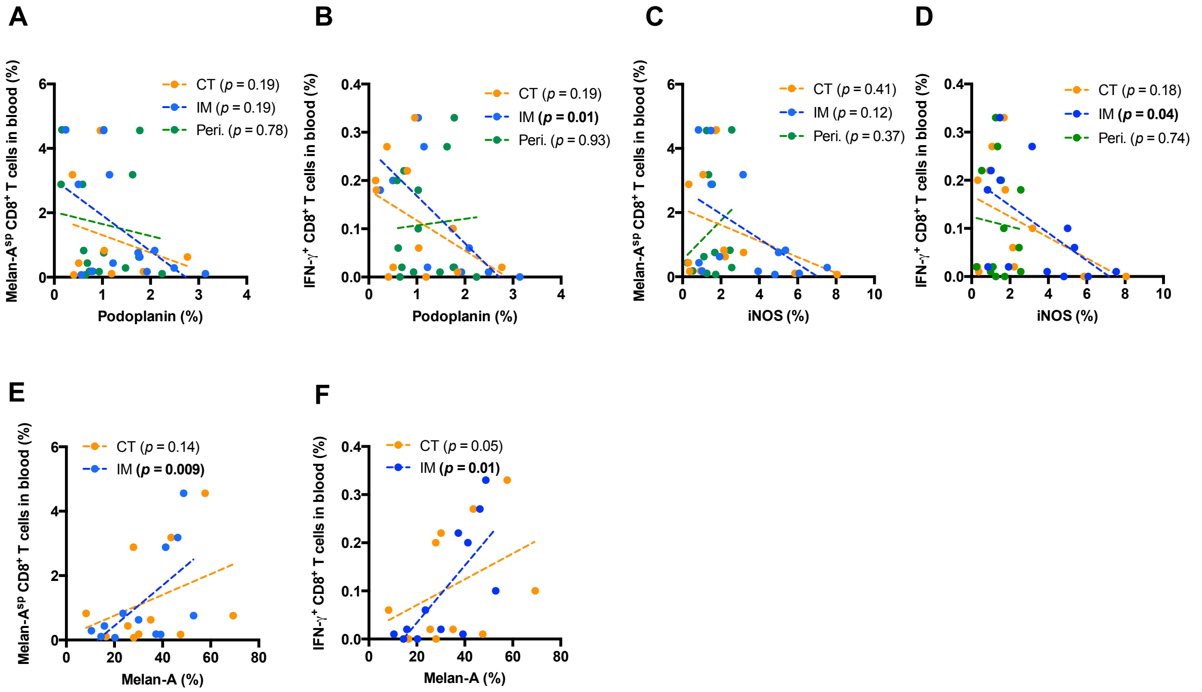

A
Melan-A^{SP} CD8$^+$ T cells in blood (%)
Podoplanin (%)
CT (p = 0.19)
IM (p = 0.19)
Peri. (p = 0.78)
B
IFN-γ$^+$ CD8$^+$ T cells in blood (%)
Podoplanin (%)
CT (p = 0.19)
IM **(p = 0.01)**
Peri. (p = 0.93)
C
Melan-A^{SP} CD8$^+$ T cells in blood (%)
iNOS (%)
CT (p = 0.41)
IM (p = 0.12)
Peri. (p = 0.37)
D
IFN-γ$^+$ CD8$^+$ T cells in blood (%)
iNOS (%)
CT (p = 0.18)
IM **(p = 0.04)**
Peri. (p = 0.74)
E
Melan-A^{SP} CD8$^+$ T cells in blood (%)
Melan-A (%)
CT (p = 0.14)
IM **(p = 0.009)**
F
IFN-γ$^+$ CD8$^+$ T cells in blood (%)
Melan-A (%)
CT (p = 0.05)
IM **(p = 0.01)**

Figure 7

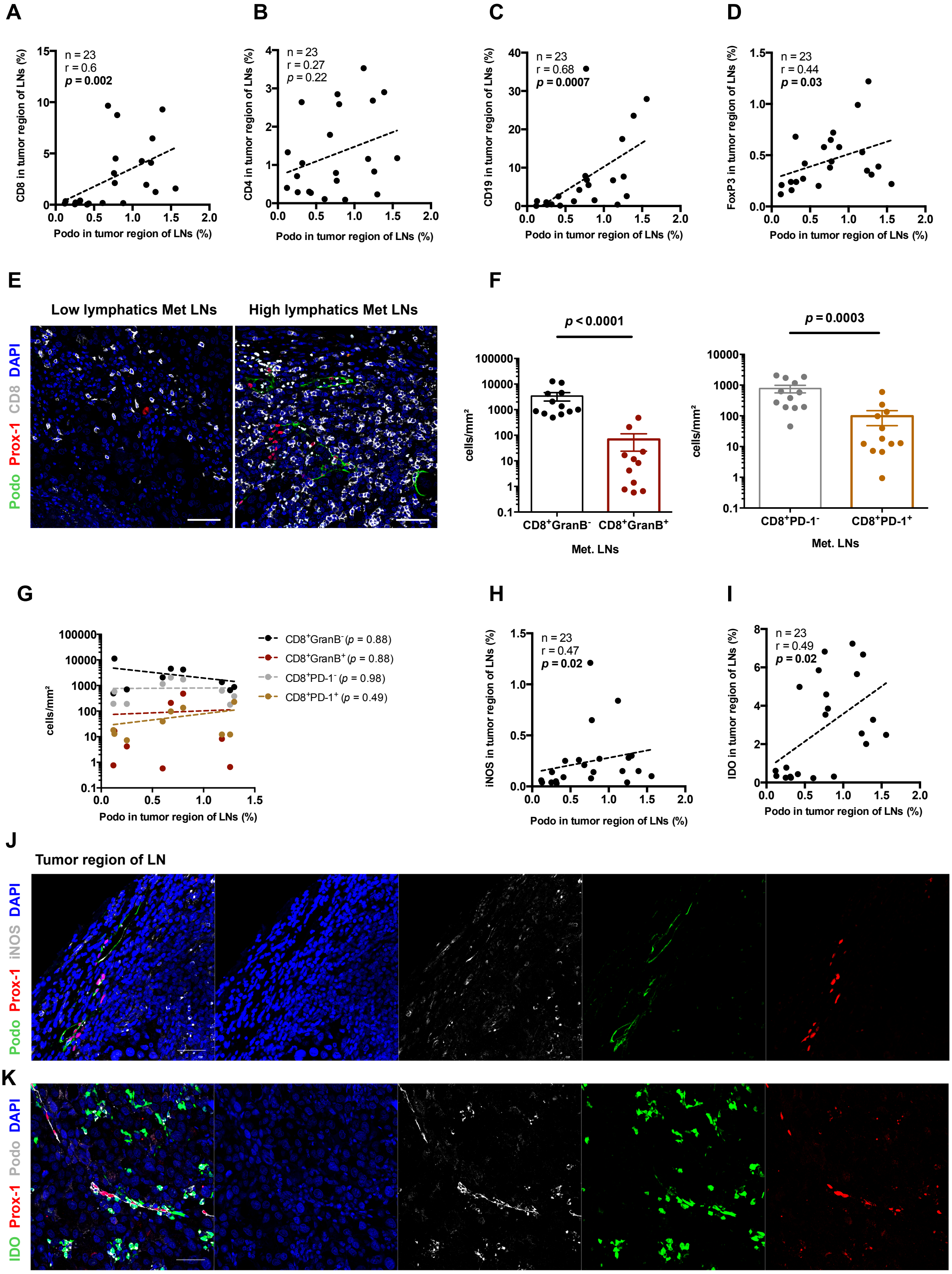
A
n = 23
r = 0.6
p = 0.002
CD8 in tumor region of LNs (%)
Podo in tumor region of LNs (%)
B
n = 23
r = 0.27
p = 0.22
CD4 in tumor region of LNs (%)
Podo in tumor region of LNs (%)
C
n = 23
r = 0.68
p = 0.0007
CD19 in tumor region of LNs (%)
Podo in tumor region of LNs (%)
D
n = 23
r = 0.44
p = 0.03
FoxP3 in tumor region of LNs (%)
Podo in tumor region of LNs (%)
E
Low lymphatics Met LNs
High lymphatics Met LNs
Podo Prox-1 CD8 DAPI
F
p < 0.0001
cells/mm²
$CD8^+GranB^-$
$CD8^+GranB^+$
Met. LNs
p = 0.0003
cells/mm²
$CD8^+PD\text{-}1^-$
$CD8^+PD\text{-}1^+$
Met. LNs
G
cells/mm²
$CD8^+GranB^-$ (p = 0.88)
$CD8^+GranB^+$ (p = 0.88)
$CD8^+PD\text{-}1^-$ (p = 0.98)
$CD8^+PD\text{-}1^+$ (p = 0.49)
Podo in tumor region of LNs (%)
H
n = 23
r = 0.47
p = 0.02
iNOS in tumor region of LNs (%)
Podo in tumor region of LNs (%)
I
n = 23
r = 0.49
p = 0.02
IDO in tumor region of LNs (%)
Podo in tumor region of LNs (%)
J
Tumor region of LN
Podo Prox-1 iNOS DAPI
K
IDO Prox-1 Podo DAPI

Figure 8

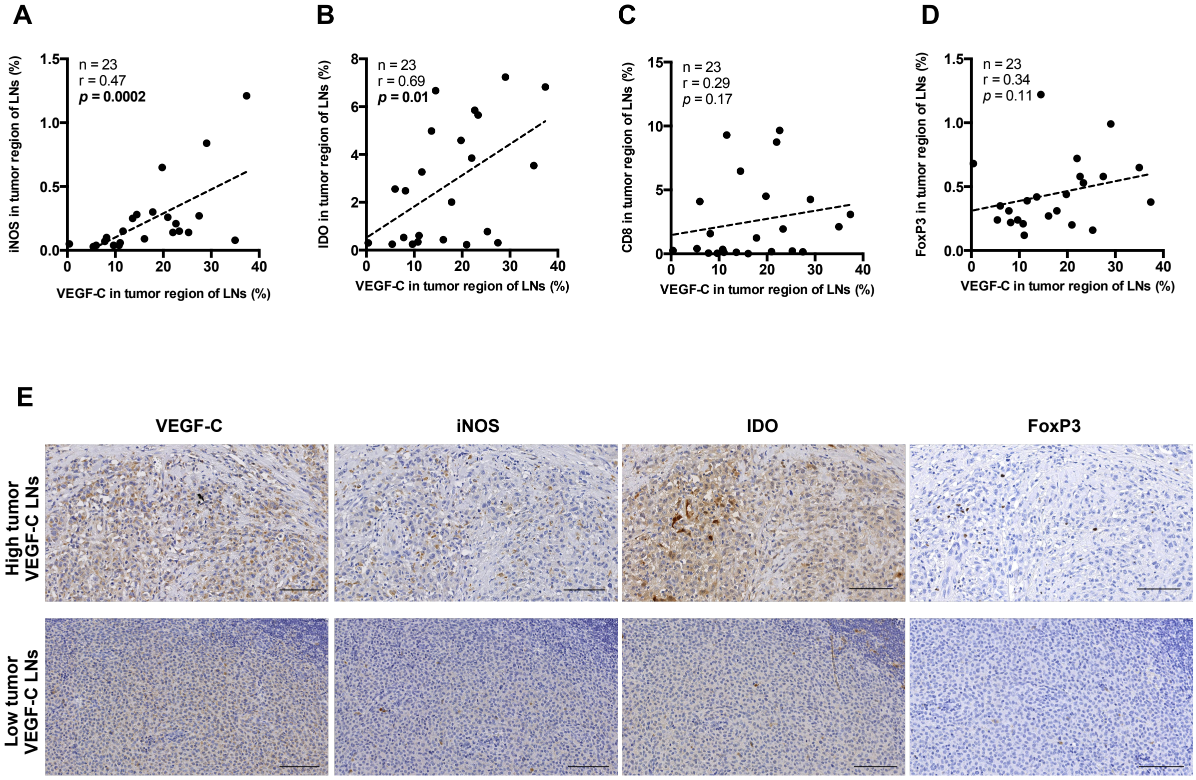
A
n = 23
r = 0.47
p = 0.0002
iNOS in tumor region of LNs (%)
VEGF-C in tumor region of LNs (%)
B
n = 23
r = 0.69
p = 0.01
IDO in tumor region of LNs (%)
VEGF-C in tumor region of LNs (%)
C
n = 23
r = 0.29
p = 0.17
CD8 in tumor region of LNs (%)
VEGF-C in tumor region of LNs (%)
D
n = 23
r = 0.34
p = 0.11
FoxP3 in tumor region of LNs (%)
VEGF-C in tumor region of LNs (%)
E
VEGF-C
iNOS
IDO
FoxP3
High tumor VEGF-C LNs
Low tumor VEGF-C LNs

Figure 9

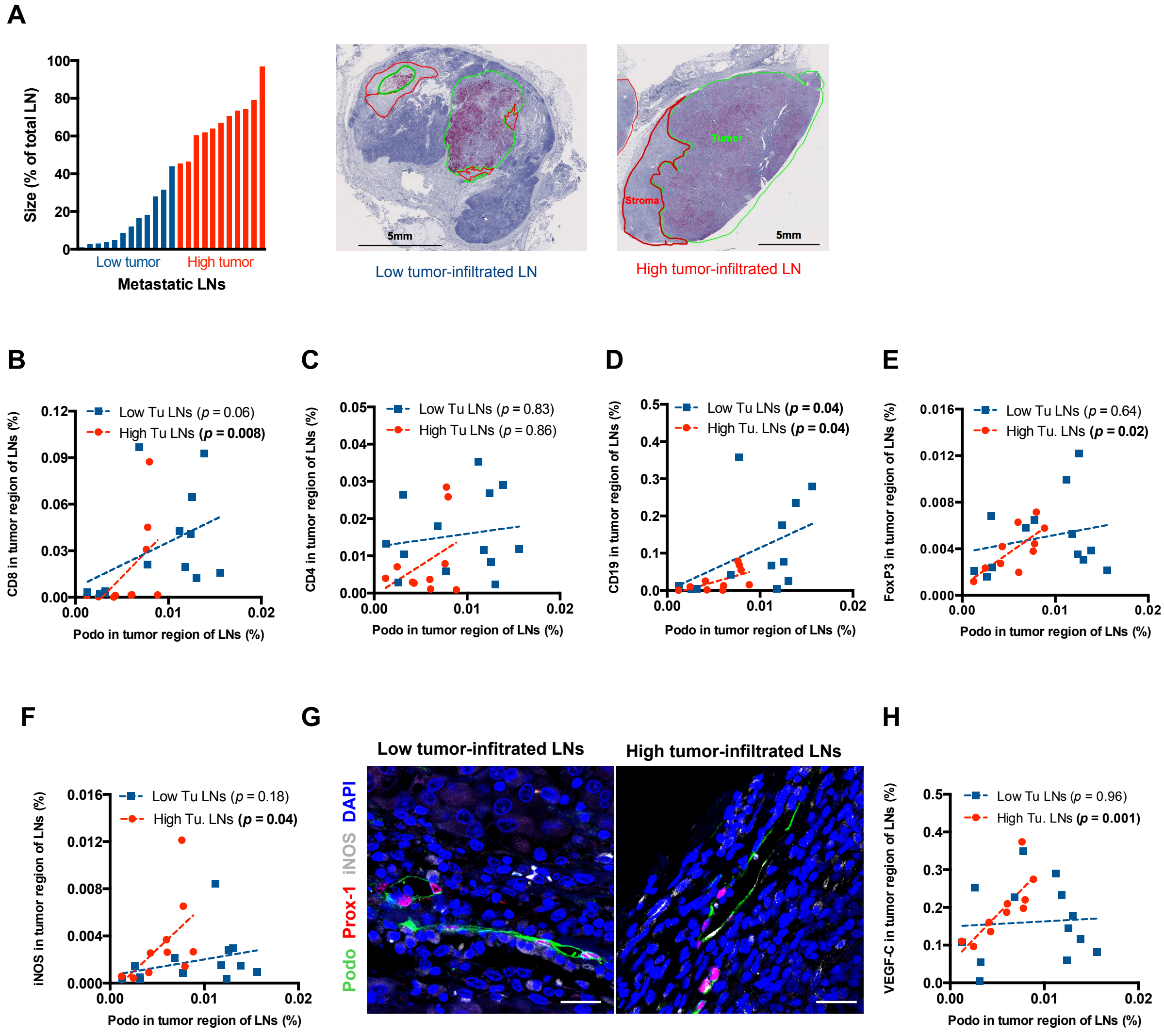
A
Size (% of total LN)
100
80
60
40
20
0
Low tumor
High tumor
Metastatic LNs
5mm
Tumor
Stroma
5mm
Low tumor-infiltrated LN
High tumor-infiltrated LN
B
CD8 in tumor region of LNs (%)
Low Tu LNs (p = 0.06)
High Tu LNs (p = 0.008)
0.12
0.09
0.06
0.03
0.00
0.00
0.01
0.02
Podo in tumor region of LNs (%)
C
CD4 in tumor region of LNs (%)
Low Tu LNs (p = 0.83)
High Tu LNs (p = 0.86)
0.05
0.04
0.03
0.02
0.01
0.00
0.00
0.01
0.02
Podo in tumor region of LNs (%)
D
CD19 in tumor region of LNs (%)
Low Tu LNs (p = 0.04)
High Tu. LNs (p = 0.04)
0.5
0.4
0.3
0.2
0.1
0.0
0.00
0.01
0.02
Podo in tumor region of LNs (%)
E
FoxP3 in tumor region of LNs (%)
Low Tu LNs (p = 0.64)
High Tu. LNs (p = 0.02)
0.016
0.012
0.008
0.004
0.000
0.00
0.01
0.02
Podo in tumor region of LNs (%)
F
iNOS in tumor region of LNs (%)
Low Tu LNs (p = 0.18)
High Tu. LNs (p = 0.04)
0.016
0.012
0.008
0.004
0.000
0.00
0.01
0.02
Podo in tumor region of LNs (%)
G
Low tumor-infitrated LNs
High tumor-infiltrated LNs
Podo Prox-1 iNOS DAPI
H
VEGF-C in tumor region of LNs (%)
Low Tu LNs (p = 0.96)
High Tu. LNs (p = 0.001)
0.5
0.4
0.3
0.2
0.1
0.0
0.00
0.01
0.02
Podo in tumor region of LNs (%)

Figure 10

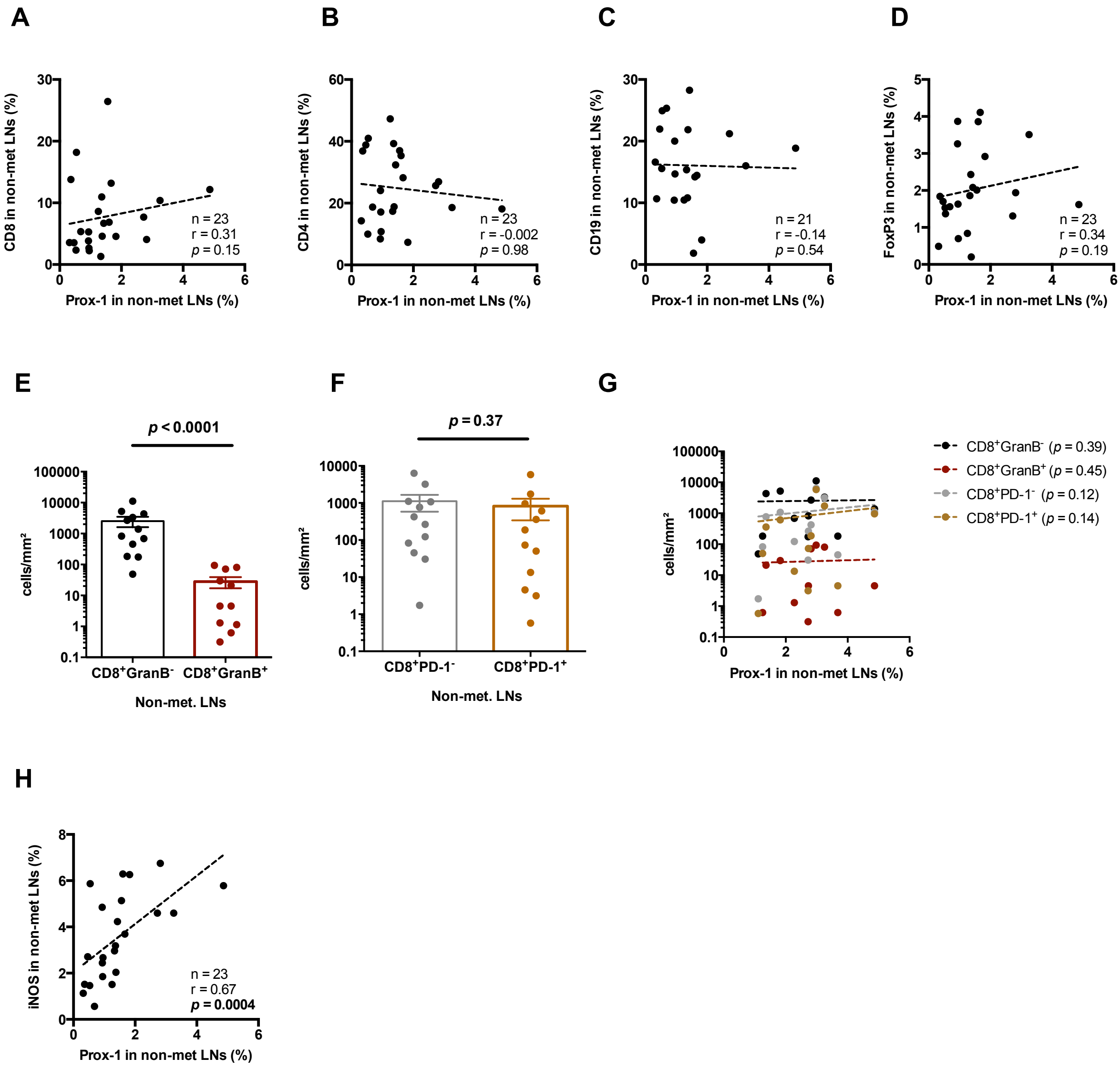
A
CD8 in non-met LNs (%)
Prox-1 in non-met LNs (%)
n = 23
r = 0.31
p = 0.15
B
CD4 in non-met LNs (%)
Prox-1 in non-met LNs (%)
n = 23
r = -0.002
p = 0.98
C
CD19 in non-met LNs (%)
Prox-1 in non-met LNs (%)
n = 21
r = -0.14
p = 0.54
D
FoxP3 in non-met LNs (%)
Prox-1 in non-met LNs (%)
n = 23
r = 0.34
p = 0.19
E
p < 0.0001
cells/mm²
CD8⁺GranB⁻
CD8⁺GranB⁺
Non-met. LNs
F
p = 0.37
cells/mm²
CD8⁺PD-1⁻
CD8⁺PD-1⁺
Non-met. LNs
G
cells/mm²
Prox-1 in non-met LNs (%)
CD8⁺GranB⁻ (p = 0.39)
CD8⁺GranB⁺ (p = 0.45)
CD8⁺PD-1⁻ (p = 0.12)
CD8⁺PD-1⁺ (p = 0.14)
H
iNOS in non-met LNs (%)
Prox-1 in non-met LNs (%)
n = 23
r = 0.67
p = 0.0004

Figure 11

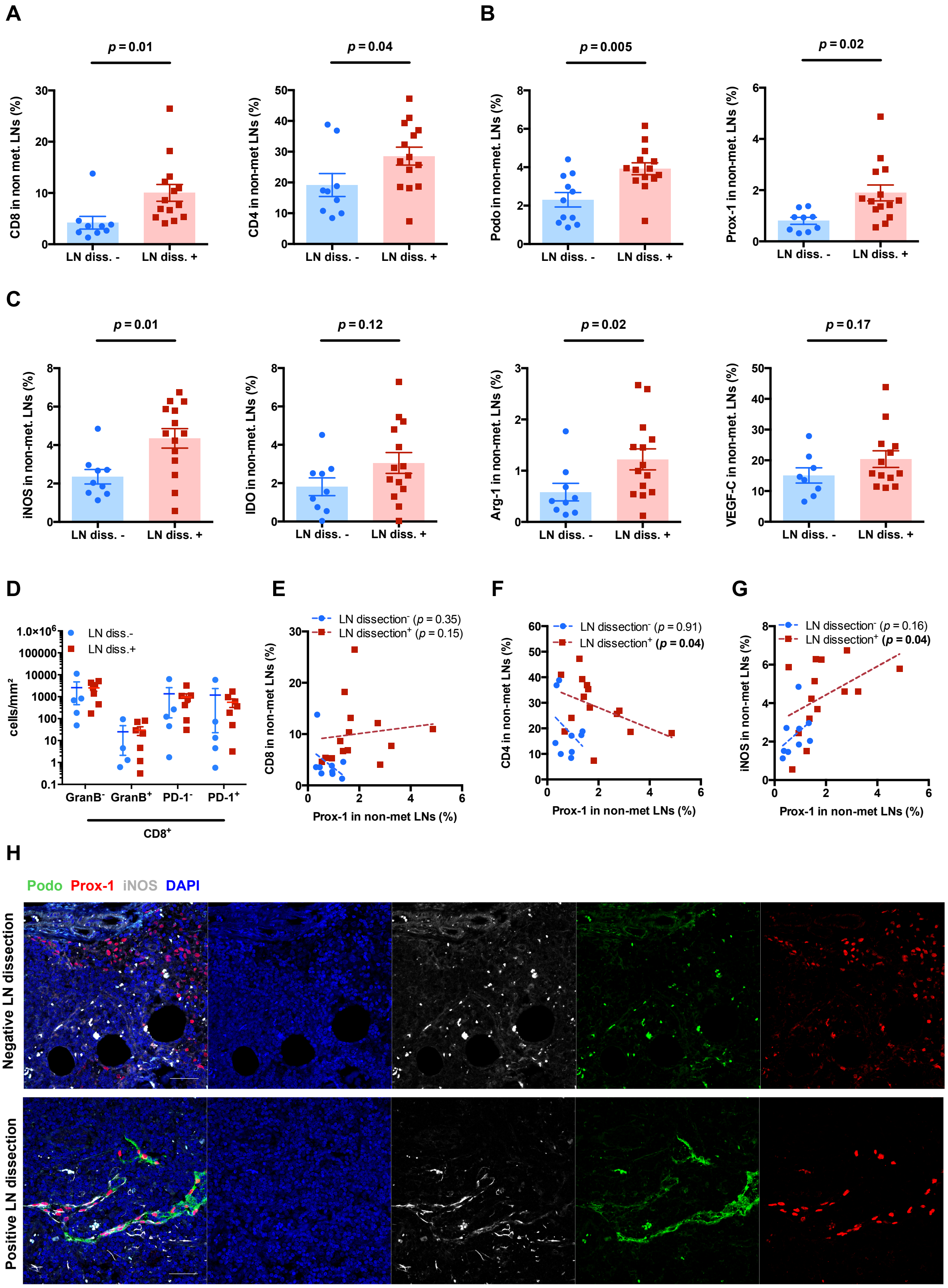
A
p = 0.01
CD8 in non met. LNs (%)
30
20
10
0
LN diss. -
LN diss. +
p = 0.04
CD4 in non-met LNs (%)
50
40
30
20
10
0
LN diss. -
LN diss. +
B
p = 0.005
Podo in non-met. LNs (%)
8
6
4
2
0
LN diss. -
LN diss. +
p = 0.02
Prox-1 in non-met. LNs (%)
6
4
2
0
LN diss. -
LN diss. +
C
p = 0.01
iNOS in non-met. LNs (%)
p = 0.12
IDO in non-met. LNs (%)
p = 0.02
Arg-1 in non-met. LNs (%)
p = 0.17
VEGF-C in non-met. LNs (%)
LN diss. -
LN diss. +
D
1.0×10^6
100000
10000
1000
100
10
1
0.1
cells/mm²
LN diss.-
LN diss.+
GranB⁻
GranB⁺
PD-1⁻
PD-1⁺
CD8⁺
E
LN dissection⁻ (p = 0.35)
LN dissection⁺ (p = 0.15)
CD8 in non-met LNs (%)
Prox-1 in non-met LNs (%)
F
LN dissection⁻ (p = 0.91)
LN dissection⁺ (p = 0.04)
CD4 in non-met LNs (%)
Prox-1 in non-met LNs (%)
G
LN dissection⁻ (p = 0.16)
LN dissection⁺ (p = 0.04)
iNOS in non-met LNs (%)
Prox-1 in non-met LNs (%)
H
Podo Prox-1 iNOS DAPI
Negative LN dissection
Positive LN dissection

Table 1

Table 1. Summary of spearman correlation of lymphatic vessels in relation with the different markers in primary melanoma and tumor-assocatied tissues

Lymphatics markers	Tissue markers												Blood markers	
	CD8	$CD8^+GranzB^-$	$CD8^+GranzB^+$	$CD8^+PD\text{-}1^-$	$CD8^+PD\text{-}1^+$	CD4	CD19	FoxP3	VEGF-C	iNOS	IDO	Arg-1	Melan-A^{sp} $CD8^+$ T cells (%)	IFN-γ^+ Melan-A^{sp} $CD8^+$ T cells (%)
Primary tumor														
Podoplanin CT	+	/	/	/	/	/	T+	/	T+	/	+	/	T-	T-
Podoplanin IM	+	/	/	/	/	T+	T+	/	/	+	/	/	T-	-
Podoplanin Peri.	+	/	/	/	/	/	T+	/	T+	/	/	/	/	/
Metastatic LNs														
Podoplanin tumor	+	/	/	/	/	/	+	+	/	+	+	/	NA	NA
in low tumor LNs	/	NA	NA	NA	NA	/	+	/	/	/	/	/	NA	NA
in high tumor LNs	+	NA	NA	NA	NA	/	+	+	+	+	/	/	NA	NA
Non-metastatic LNs														
Prox-1 total	T+	/	/	T+	/	/	/	/	/	+	/	/	NA	NA
in neg. LN dissection	/	NA	NA	NA	NA	/	/	/	/	/	/	/	NA	NA
in pos. LN dissection	T+	NA	NA	NA	NA	T-	/	/	/	+	/	/	NA	NA

+ positive significant correlation ($p < 0.05$)

- negative significant correlation ($p < 0.05$)

T+ positive correlation trend ($0.05 < p < 0.15$)

T- negative correlation trend ($0.05 < p < 0.15$)

/ no correlation

NA non applicable

Supplementary Table 1

Suplemtary Table 1. Patients characteristics

	Stage III (n = 21)	Stage IV (n = 8)
Age		
Median	60.1	37.9
Range	27.7 – 75.1	24.5 – 71.8
Sex		
Male	13 (62%)	5 (63%)
Female	8 (38%)	3 (38%)
Primary melanoma type		
SSM	9 (43%)	5 (63%)
NM	6 (29%)	2 (25%)
ALM	1 (5%)	0 (0%)
Ocular	1 (5%)	0 (0%)
Unknown	4 (19%)	1 (13%)
At the start of the study		
N Stage (2009 staging system)		
N0	1 (5%)	3 (38%)
N1	3 (14%)	1 (13%)
N2 and N3	17 (81%)	4 (50%)
Evidence of disease		
ED	4 (19%)	5 (63%)
NED	17 (81%)	3 (38%)
Number of metastatic LN		
0	5 (24%)	2 (25%)
1	5 (24%)	3 (38%)
≥ 2	10 (48%)	2 (25%)
Unknown	1 (5%)	1 (13%)
In-transit metastases	9 (43%)	4 (50%)
Sites of distant metastases		
Distant LN and distant skin	-	6 (75%)
Lung	-	3 (38%)
Visceral and other	-	3 (38%)
Previous therapy		
Radiotherapy	3 (14%)	2 (25%)
Chemotherapy	4 (19%)	1 (13%)
IFN and/or TNF	5 (24%)	2 (25%)
Vaccination with Melan-A peptide	5 (24%)	4 (50%)
During the study		
Metastatic LN	8 (38%)	4 (50%)
In-transit or satellite metastases	8 (38%)	1 (13%)
Distant metastases	6 (29%)	5 (63%)
Survival and Follow-up		
Relapse during study	14 (67%)	4 (50%)
Progression during study	3 (14%)	3 (37%)
Mortality	11 (52%)	6 (75%)
Disease free survival (months)		
Mean ± std.dev	28.01 ± 39.5	30.7 ± 41.9
Overall survival (months)		
Mean ± std.dev	51.7 ± 44.2	51.5 ± 47.2

(SSM) superfical spreading melanoma; (NM) nodular melanoma;
(ALM) acral lentiginous melanoma; (ED) evidence of disease; (NED) no evidence of disease

Supplementary Table 2

Supplementary Table 2. Clinical characteristics and immune responses of LUD 00-018 cohort

		Diagnosis						Disease at study entry				Immune response		Outcome					
Patient	**Vaccine**	**Sex**	**Age**	**TNM**	**Stage**	**Breslow**	**Clark**	**Age**	**TNM**	**Stage**	**Status**	**Melan-A^{sp} CD8^{+} T cells (%)§**	**IFN-γ^{+} Melan-A^{sp} CD8^{+} T cells (%)$^{\sharp}$**	**Progression***	**Relapse***	**Death**	**PFS***	**DFS***	**OS***
LAU 818	ELA	M	55	pT3bN0M0	IIB	2.44	III	58	pT3bN2bM0	IIIB	NED	0.76	0.10	NA	yes	no	NA	7.3	61.2
LAU 627	ELA	M	49	pT3bN1aM0	IIIB	2.23	IV	51	pT3bN2bM1b	IV	ED	1.55	0.09	yes	NA	yes	3.4	NA	15.2
LAU 618	ELA	F	69	pT4N0M0	IIC	8.00	V	74	pT4N2cM0	IIIB	ED	1.33	0.25	yes	NA	no	3.3	NA	30.4
LAU 321	ELA	M	60	pT3aN0M0	IIA	1.50	III	69	pT3aN3M1b	IV	ED	0.83	0.06	yes	NA	no	3.2	NA	75.5
LAU 371	ELA	M	29	pT3aN1M0	III	2.38	IV	33	pT3aN1M1	IV	ED	2.08	0.11	yes	NA	yes	3.6	NA	11.9
LAU 444	ELA	F	27	pT3aN0M0	IIA	1.90	IV	33	pT3aN2cM1c	IV	ED	3.42	0.69	yes	NA	yes	15.2	NA	30.8
LAU 701	ELA	F	70	pT3bN0M0	IIB	2.50	IV	71	pT3bN3M0	IIIC	NED	0.07	0.01	NA	yes	no	NA	2.9	140.6
LAU 672	ELA	M	34	pT1N0M0	IA	0.70	III	38	pT1N3M0	IIIC	ED	0.59	0.25	yes	NA	yes	3.2	NA	45.5
LAU 944	ELA	F	20	pT1aN0M0	IA	6.80	uk	28	pT1aN1M0	IIIA	NED	1.65	0.09	NA	yes	no	NA	23.8	136.7
LAU 660	EAA	F	22	pT2bN0M0	IIA	1.72	IV	25	pT2bN0M1	IV	NED	0.27	0.01	NA	yes	yes	NA	2.1	14.8
LAU 972	EAA	F	60	pT2bN1aM0	IIIB	1.60	III	60	pT2bN1aM0	IIIB	NED	4.56	0.33	NA	no	no	NA	129.3	129.3
LAU 1022	EAA	M	69	pT2bN2aM0	IIIB	1.49	IV	69	pT2bN2aM0	IIIB	NED	0.07	0.00	NA	yes	yes	NA	8.8	19.8
LAU 1034	EAA	M	47	pT2aN2aM0	IIIA	1.35	III-IV	47	pT2aN2aM0	IIIA	NED	0.01	0.00	NA	yes	no	NA	51.8	117.2
LAU 1090	EAA	M	68	pT3aN2bM0	IIIB	3.10	IV	69	pT3aN2bM0	IIIB	ED	0.07	0.00	yes	NA	yes	3.8	NA	21.0
LAU 1106	EAA	M	36	pT2aN1aM0	IIIA	1.35	IV	36	pT2aN1aM0	IIIA	NED	4.66	0.67	NA	no	no	NA	106.8	106.8
LAU 392	EAA + YMD	F	29	pT3aN0M0	IIA	2.50	IV	37	pT3aN2cM0	IIIB	ED	0.44	0.02	yes	NA	yes	2.5	NA	11.8
LAU 648	EAA + YMD	M	64	pT2aN0M0	IB	1.60	IV	70	pT2N2M0	III	NED	0.17	0.01	NA	no	no	NA	126.2	126.2
LAU 706	EAA + YMD	F	64	pTxNoM0	uk	uk	uk	67	pTxN3M0	III	ED	0.16	0.01	yes	NA	yes	3.8	NA	44.1
LAU 1015	EAA + YMD	M	75	pT2aN0M1a	IV	1.20	III	75	pT2aN0M1a	IV	NED	0.98	0.72	NA	yes	yes	NA	14.3	50.7
LAU 975	EAA + YMD	M	51	pT4N1bM0	IIIB	12.00	IV	52	pT4N1bM0	IIIB	NED	0.63	0.02	NA	yes	yes	NA	4.2	7.5
LAU 1013	EAA + YMD	M	55	pT3bN3M0	IIIC	3.00	IV	56	pT3bN3M0	IIIC	NED	3.18	0.27	NA	yes	yes	NA	8.8	25.1
LAU 1017	EAA + YMD	F	28	pT3N2bM0	IIIB	3.80	IV	28	pT3N2bM0	IIIB	NED	0.11	0.00	NA	yes	yes	NA	1.4	22.0
LAU 205	ELA + YMD	M	24	pT2aN1M0	IIIB	1.40	IV	33	pT2aN2cM0	IIIB	NED	1.92	0.19	NA	yes	yes	NA	25.2	50.6
LAU 936	ELA + YMD	F	52	pT3aN0M0	IIA	2.70	IV	54	pT3aN2bM0	IIIB	NED	0.56	0.01	NA	yes	yes	NA	7.1	3.1
LAU 1129	ELA + YMD	M	52	pT3N0M0	II	2.50	IV	66	pT3N3Mo	IIIC	NED	0.29	0.01	NA	yes	yes	NA	9.4	17.0
LAU 1144	ELA + YMD	M	68	pT3aN0M0	IIA	0.60	IV	72	pT3aN0M1b	IV	NED	4.58	0.18	NA	yes	yes	NA	8.9	29.4
LAU 1164	ELA + YMD	M	52	pTxNxM1a	IV	uk	uk	53	pTxNxM1a	IV	NED	8.10	0.32	NA	no	no	NA	56.6	56.6
LAU 1189	ELA + YMD	F	68	pT3bN2M0	IIIB	4.00	IV	68	pT3bN2M0	IIIB	NED	0.18	0.22	NA	no	no	NA	7.9	7.9
LAU 1264	ELA + YMD	M	46	pT3bN0M0	IIB	4.00	IV	49	pT3bN1bM0	IIIC	NED	2.88	0.20	NA	yes	no	NA	15.8	90.8

(ELA) Melan-A analog peptide; (EAA) Melan-A native peptide; (YMD) tyrosinase peptide; (NED) No evidence of disease; (ED) Evidence of disease; (uk) unknown; (NA) not applicable

[§] % of total CD8^{+} T cells in the blood, maximum reached during the study

[♯] % of Melan-A specific CD8^{+} T cells in the blood, maximum reached during the study

[*] Progression-free survival (PFS) was measured in the ED patients, who were tumor-bearing at the study entry and had a progressive disease; whereas disease-free survival (DFS) was calculated in the NED patients, who were tumor-free at the study entry and experienced a disease relapse or survived without any sign of disease after the study's maximum follow-up. The overall survival (OS), PFS and DFS are the time from the start of vaccination protocol to event (in months) which is the death, the progression and the relapse or the last date without disease, respectivelyInterval from the start of vaccination protocol to event (in months)

Supplementary Table 3

Supplemtary Table 3. Patient tissues selected from the LUD 00-018 study

Patient	Surgery	Pathological samples				
		Pre-vaccination			Post-vaccination	
		Primary Tumor	Non-met LN	Met LN	Non-met LN	Met LN
LAU 818	26.Apr.00	1	-	-	-	-
	16.Dec.02	-	1(1)	3(3)	-	-
	30.Jan.04	-	-	-	(3)	1(1)
	19.Apr.05	-	-	-	1(1)	1(1)
	12.Jul.06	-	-	-	(4)	1(3)
LAU 627	19.Jul.01	1	-	-	-	-
	19.Sep.01	-	1(28)	-	-	-
LAU 618	10.Jul.98	1	-	-	-	-
	8.Aug.01	-	1(5)	-	-	-
LAU 321	1.Aug.93	1	-	-	-	-
	23.Jun.99	-	(7)	-	-	-
	5.Feb.03	-	1(8)	1(2)	-	-
	18.Feb.04	-	-	-	1(1)	-
LAU 371	29.Sep.99	/	-	-	-	-
	15.Dec.99	-	(8)	-	-	-
	30.Mar.04	-	-	-	1(3)	2(2)
LAU 444	14.Jan.98	1	-	-	-	-
	7.Jun.00	-	1(13)	1(1)	-	-
	27.Jun.03	-	(9)	-	-	-
	20.Aug.03	-	(1)	-	-	-
LAU 701	11.Mar.02	1	-	-	-	-
	15.Nov.06	-	-	-	1(13)	-
LAU 672	29.Sep.99	/	-	-	-	-
	6.Feb.02	-	1(12)	1(7)	-	-
	11.Dec.03	-	-	-	-	/
	7.Jun.05	-	-	-	-	1(1)
LAU 972	15.Mar.04	1	-	-	-	-
	2.Jun.04	-	1(25)	-	-	-
LAU 1022	7.Mar.05	/	-	-	-	-
	1.Jun.05	-	1(29)	1(1)	-	-
LAU 1034	21.Mar.05	1	-	-	-	-
	15.Jun.05	-	1(20)	-	-	-
LAU 1090	7.Oct.05	1	-	-	-	-
	11.Jan.06	-	1(17)	-	-	-
LAU 392	18.Apr.96	1	-	-	-	-
	3.Feb.00	-	-	1(1)	-	-
	1.Mar.00	-	1(8)	4(8)	-	-
	20.Dec.01	-	-	3(3)	-	-
LAU 648	20.Jul.98	1	-	-	-	-
	21.Nov.01	-	1(40)	3(14)	-	-
	19.Nov.08	-	-	-	1(3)	-
LAU 706	1.Jan.94	/	-	-	-	-
	5.Nov.03	-	1(6)	-	-	-
LAU 1015	25.Nov.04	1	-	-	-	-
	12.May.06	-	-	-	1(7)	1(1)
LAU 975	3.Mar.04	1	-	-	-	-
	26.May.04	-	1(17)	-	-	-
	9.Mar.05	-	1(7)	-	-	-
LAU 1013	25.Jan.05	1	-	-	-	-
	3.Mar.05	-	1(36)	/	-	-
LAU 1017	20.Dec.04	1	-	-	-	-
	16.Mar.05	-	(8)	/	-	-
	8.Jun.05	-	-	-	1(20)	1(1)
LAU 205	22.May.96	1	-	-	-	-
	10.Jun.96	-	-	2(2)	-	-
	26.Jun.96	-	(14)	-	-	-
LAU 936	13.Oct.03	/	-	-	-	-
	7.Dec.04	-	1(12)	1(1)	-	-
LAU 1129	2.Sep.92	1	-	-	-	-
	6.Apr.06	-	-	2(2)	-	-
	24.Apr.07	-	-	-	-	2(2)
LAU 1144	21.Nov.95	1	-	-	-	-
	2.Aug.06	-	1(2)	-	-	-
LAU 1189	8.Jan.07	1	-	-	-	-
	27.Apr.07	-	1(7)	-	-	-
LAU 1264	22.Apr.05	1	-	-	-	-
	14.Aug.07	-	-	-	/	/

(LN) lymph nodes; (non met LN) non-metastatic lymph nodes; (met LN) metastatic lymph nodes
The numbers represent the samples collected from pathology department and analysed in this study
(n) number of total individual LN collected per surgery
/ tissues not found
− no tissue

Supplementary Table 4

Supplementary Table 4. Markers selection for IHC on LUD 00-018 study patient tissues

Antigens	Antibodies	Staining localisation	Physiological functions	Physiological expression
CD8	Clone C8/144B (DakoCytomatio)	Cytoplasmic/membranous	Transmembrane glycoprotein that serves as a coreceptor of TCR. Binds to MHC I. The protein functions to initiate or augment the early phase of T-cell activation	Cytotoxic T cells
CD4	Clone 4B12 (Novocastra)	Cytoplasmic/membranous	Transmembrane glycoprotein that serves as a coreceptor of TCR. Binds to MHC II. The protein functions to initiate or augment the early phase of T-cell activation	T helper cells, macrophages, B cells, granulocytes and DC
FoxP3	clone 236a/E7 (Abcam)	Nuclear	FoxP3 is a member of the forkhead/winged-helix family of transcriptional regulator. It is a master regulator in the development and function of regulatory T cells	T regs
CD19	Clone BT51E (Novocastra)	Cytoplasmic/membranous	CD19 is a surface molecules which assembles with the antigen receptor of B lymphocytes in order to decrease the threshold for antigen receptor-dependent stimulation	B cells
Prox-1	Prox-1 (R&D systems)	Nuclear	Prox-1 is a transcription factor that plays a major role during embryonic lymphangiogenesis and in the development of the central nervous system, heart, liver, pancreas, and in lens elongatio.	Embryonic and adult LECs and hepatocytes. Also expressed in heart, CNS, lens, pancreas and retina
Podoplanin	Clone D2-40 (Covance)	Membranous	LEC adhesion and migration, formation of connecting lymphatics between superficial and deep lymphatic plexuses.	Embryonic and adult LECs, kidney podocytes, osteoblasts, alveolar cells, epithelial cells of the choroid plexus
VEGF-C	VEGF-C (Invitrogen)	Cytoplasmic	VEGF-C is a member of the platelet-derived growth factor/vascular endothelial growth factor (PDGF/VEGF) family, is active in angiogenesis, lymphangiogenesis (budding and survival of LECs) and endothelial cell growth and survival, and can also affect the permeability of blood vessels. Can bind to VEGFR3 and VEGFR2	Mesenchymal cells around embryonic veins, macrophages, LECs. Weak expression in the spinal cord,placenta, prostate, liver, lymph nodes, heart, lung, kidney, placenta, skeletal muscle and ovary
IDO	IDO (From Bruxelles)	Cytoplasmic	IDO degrades the tryptophan, serotonin and melatonin. It is up-regulated in response to infection and tissue inflammation. Affects T-cell proliferation and survival	Macrophages, monocytes, MDSC, DC. Also expressed at basal level in epididymis, thymus, gut gallblader, liver, lung, and the maternal-fetal interface during gestation
iNOS	iNOS (Thermo scientific)	Cytoplasmic	NOS are a family of enzymes that catalyze the production of nitric oxide (NO) from L-arginine. INOS is induced in marcophages by inflammation and infection (IFN-β) and produced a large amount of NO as a defense mechanism	MDSC and macrophages
Arg-1	Arg-1 (Mybiosource)	Cytoplasmic	Arg-1 is a cytosolic enzyme constitutively expressed in the liver where it functions in nitrogen elimination by catalyzing arginine hydrolysis to urea and ornithine. Arg-1 is also expressed in macrophages in response to Th2 cytokines IL-4 and IL-13	MDSC and macrophages

(Arg-1) arginase-1; (CNS) central nervous system; (DC) dendritic cells; (FoxP3) forkhead box P3; (IDO) indoleamine 2,3-dioxygenase; (iNOS) inducible NOS; (LECs) lymphatic endothelial cells; (MDSC) myeloid-derived suppressor cells; (MHC) major histocompatibility complex; (NO) nitric oxyde; (NOS) nitric oxide synthase; (Prox-1) prospero-related homebox 1; (TCR) T-cell receptor; (TLRs) Toll-like receptors; (VEGF-C) vascular endothelial growth facror-C

Supplementary Figure 1

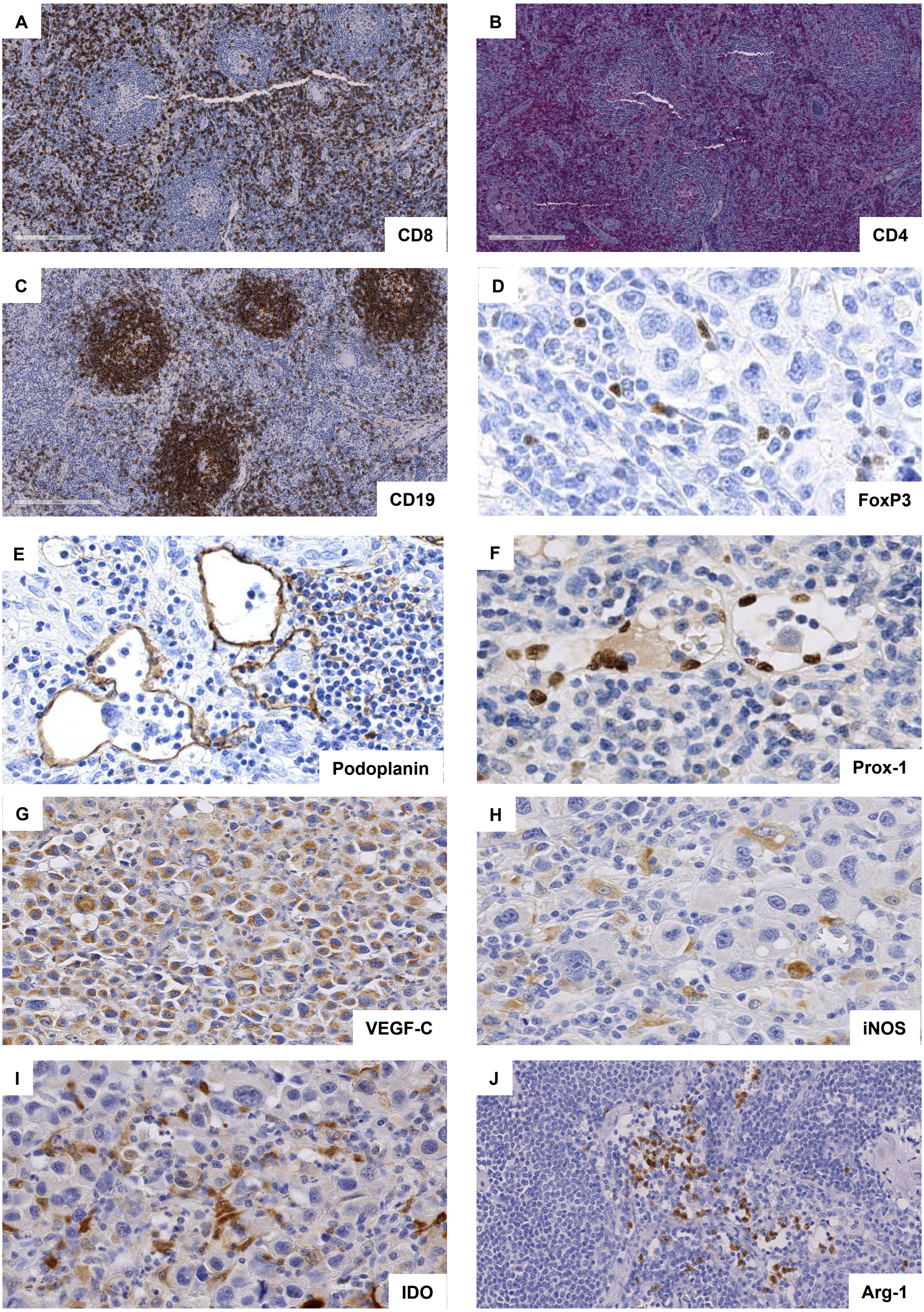

Supplementary Figure 2

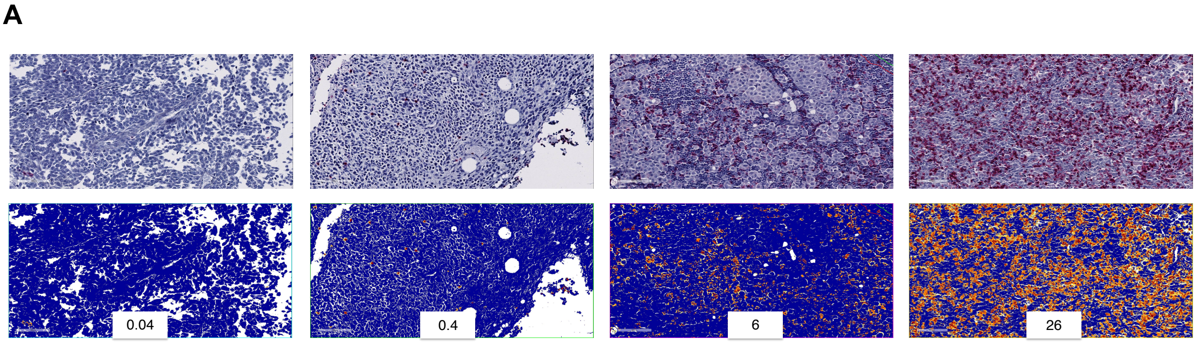

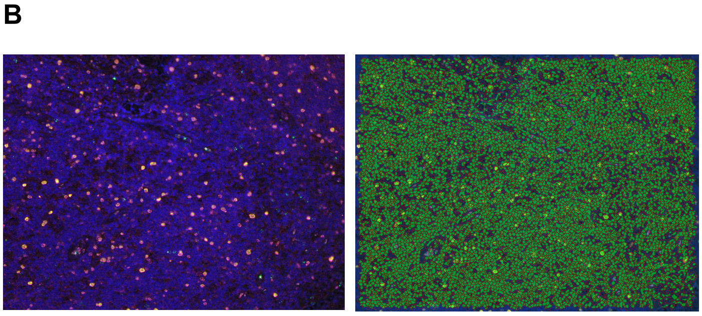

Supplementary Figure 3

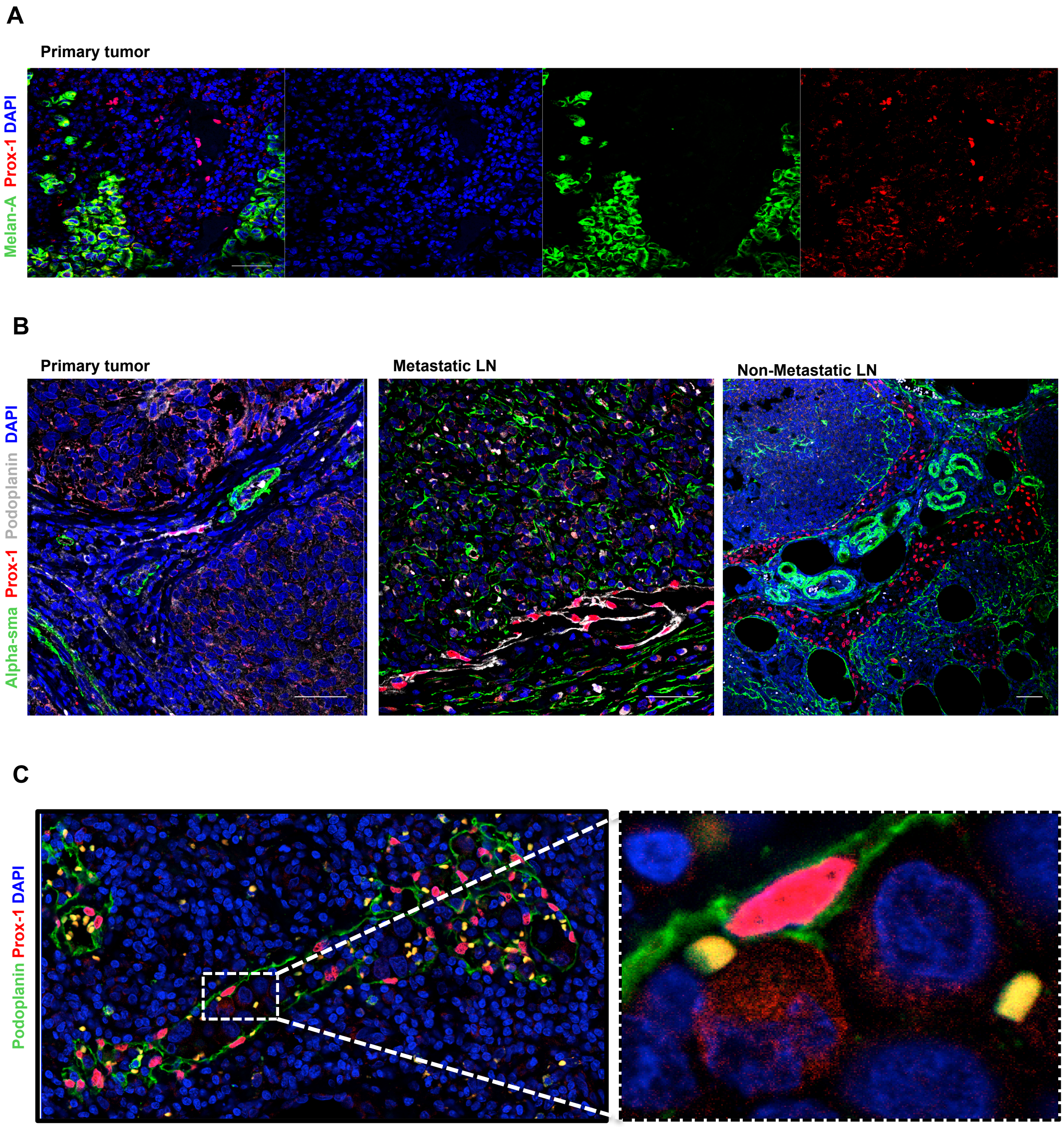

2 Pulmonary sarcoid-like granulomatosis after multiple vaccinations of a long-term surviving metastatic melanoma patient

In this study, we report the case of a long-term surviving metastatic melanoma patient (stage IV) who exhibited pulmonary sarcoid-like granulomatosis following the development of a strong T-cell response to repetitive cycles of vaccination with peptides and CpG. This paper is the first report describing an autoimmune pulmonary adverse event related to a cancer vaccine. It was published in the December 2014 edition of *Cancer Immunology Research.*

Cancer Immunology Research

Cancer Immunology Miniatures

Pulmonary Sarcoid–like Granulomatosis after Multiple Vaccinations of a Long-term Surviving Patient with Metastatic Melanoma

Natacha Bordry[1], Carla-Marisa Costa-Nunes[1], Laurène Cagnon[1], Philippe O. Gannon[1], Samia Abed-Maillard[1], Petra Baumgaertner[1], Timothy Murray[1], Igor Letovanec[2], Romain Lazor[3], Hasna Bouchaab[4], Nathalie Rufer[1], Emanuela Romano[4], Olivier Michielin[4], and Daniel E. Speiser[1]

Abstract

Autoimmune side effects are frequent in patients with cancer treated with immune checkpoint–targeting antibodies, but are rare with cancer vaccines. Here, we present a case report on a patient with metastatic melanoma who developed pulmonary sarcoid–like granulomatosis following repetitive vaccinations with peptides and CpG. Despite multiple metastases, including one lesion in the brain, the patient is alive and well more than 13 years after the diagnosis of metastatic disease. The strongly activated tumor-specific CD8$^+$ T cells showed robust long-term memory and effector functions. It is possible that long-term survival and adverse autoimmune events may become more common for vaccines inducing robust anticancer immune responses as were present in this patient. *Cancer Immunol Res; 2(12); 1148–53. ©2014 AACR.*

Introduction

Metastatic melanomas are aggressive tumors, accounting for approximately 80% of skin cancer–related deaths. The prognosis is particularly dismal for patients with brain metastases as they face a median overall survival of only 4 months (1). Moreover, failure of treatment is frequent despite considerable recent progress.

Immunotherapy, aiming at the induction of tumor-specific immune responses, has emerged as a promising clinical weapon against cancer. During the past decade, several novel immunologic approaches, such as adoptive cell therapy and immune checkpoint blockade (targeting CTLA-4 or PD-1/PD-L1), have shown substantial clinical benefits in patients with advanced disease (2). However, because of their capacity to break immune tolerance, their toxicity profiles are usually high, resulting in autoimmune adverse events (AE; refs. 3, 4).

Significant progress has also been achieved with therapeutic cancer vaccines. Vaccines have the potential benefits of being highly selective, stable, and relatively easy to produce (5, 6). Furthermore, their low-toxicity profiles suggest that they can be attractive options for patients with cancer. Until recently, however, the majority of cancer vaccines have shown only limited immunogenicity and clinical responses (7, 8). In contrast, new-generation vaccines can give rise to strong responses of cancer-specific T cells (9). This is the case with the use of potent adjuvants, such as the Toll-like receptor ligand CpG (10). It is likely that further progress in vaccination will lead to strong and long-term immune responses with a broad spectrum of tumor antigen specificities (11).

Here, we present a case report on a patient with melanoma, who has one metastatic lesion in the brain and multiple peripheral metastases, and who experienced complete remission and long-term survival after treatment with vaccines. During the past 13 years, the patient progressively developed strong T-cell responses following repetitive vaccinations with Melan-A, NY-ESO-1, and MAGE-A10 peptides. The vaccine regimen comprised multiple peptides of melanoma-associated antigens augmented with CpG as adjuvant and was administered in a total of 49 injections. The peptide vaccines were the only systemic antitumor treatments that the patient received. The patient developed an autoimmune disease in the form of pulmonary sarcoid–like granulomatosis without clinical complications. To our knowledge, this is the first description of an autoimmune pulmonary AE related to a cancer vaccine.

Case Report

A 42-year-old man was diagnosed in 2001 with a left paralumbar ulcerated superficial spreading melanoma (Breslow 2.5 mm, Clark III, pT3pN1bM0). A wide local excision of the primary lesion and of the right inguinal sentinel lymph node was performed. He underwent right iliac obturator and inguinal radical lymph node dissection (none of the 10 iliac obturator lymph nodes or the four right inguinal lymph nodes were

---

[1]Clinical and Tumor Biology and Immunotherapy Unit, Department of Oncology and Ludwig Cancer Research Center, University of Lausanne (UNIL), Lausanne, Switzerland. [2]Department of Pathology, Lausanne University Hospital Center (CHUV), Lausanne, Switzerland. [3]Department of Respiratory Medicine, CHUV, Lausanne, Switzerland. [4]Department of Oncology, CHUV and UNIL, Lausanne, Switzerland.

Corresponding Author: Daniel E. Speiser, Ludwig Center for Cancer Research, University of Lausanne, Rue Pierre-Decker 4, Lausanne, CH 1011, Switzerland. Phone: 0041-21-314-0182; Fax: 0041-21-314-7477; E-mail: doc@dspeiser.ch

doi: 10.1158/2326-6066.CIR-14-0143

metastatic). Subsequently, the patient received six vaccines composed of MAGE-A10 (GLYDGMEHL) and Melan-A (ELAGIGILTV) peptides with or without SB-AS2 adjuvant (a mixture of MPL and QS-21 in an oil-in-water emulsion) at 3-week intervals for a period of 3 months (ClinicalTrials.gov identifier NCT00112216). The adjuvant was used for every second vaccine (vaccine nos. 1, 3, and 5), injected intramuscularly (i.m.) according to the manufacturer's instructions, whereas the vaccines (peptides) without adjuvant were injected intradermally (i.d.; vaccines no. 2, 4, and 6) to optimally target the skin and its vaccine site skin-draining lymph nodes.

The patient remained disease free until 2005, when he developed a para-pubic subcutaneous (s.c.) nodule, 1.3 cm in diameter, on the right side. The mass was resected with histologic confirmation of melanoma metastasis. The patient then received seven monthly s.c. vaccinations with MAGE-A10 (GLYDGMEHL), Melan-A (ELAGIGILTV), and NY-ESO-1 (SLLMWITQA) peptides and montanide ISA-51 as adjuvant over a period of 7 months (NCT00112242).

In May 2006, cytopunction revealed a new subpubic subcutaneous metastasis of 8 mm in diameter, again on the right side. In addition, right and left pelvis dissection showed nine right pubic cutaneous metastases, four left inguinal metastatic lymph nodes, and four left iliac obturator metastatic lymph nodes. Subsequently, the patient received monthly vaccinations with the same peptides and montanide, this time including CpG 7909 as adjuvant (NCT00112242). After three monthly vaccinations, the patient developed very strong subcutaneous reactions at injection sites. Therefore, the next 33 vaccinations included only CpG as adjuvant and without montanide. The patient had no other clinically significant treatment-related toxicity and remained disease free for 1 year.

November 2007 was marked by a third relapse of metastatic disease with a positive biopsy for a right inguinal cutaneous metastatic nodule (3 mm in diameter). A CT scan in February 2008 showed a single cerebral left frontal metastasis in the precentral gyrus (16 mm in diameter; Fig. 1A). Stereotactic radiosurgery (20 Gy) was performed and led to a 34% reduction in tumor size (Fig. 1B). However, the lesion enlarged progressively (Fig. 1C). Brain metastasis resection was performed, and the pathology findings confirmed the melanocytic origin of the lesion. The cerebral MRI showed a reduction of the lesion size after resection (Fig. 1D). Remarkably, the lesion has disappeared 5 years after the surgery (Fig. 1E).

Although the patient continued to receive vaccinations with peptides and CpG, a CT scan in June 2011 revealed the apparition of new infracentimetric mediastinal lymphadenopathies (pretracheal and right paratracheal; Fig. 1I), bilateral hilar lymphandenopathies (Fig. 1J and K), multiple pulmonary micronodular opacities, and centrilobular ground-glass infiltrate (not shown) that were not present on the control CT scan in December 2005 (Fig. 1F, G, and H). In June 2012, imaging disclosed a new left axillary lymphadenopathy (23.8 × 19.33 mm) and a subcutaneous nodule (6 mm in diameter) in the left anterior thoracic wall. The PET-CT imaging showed hypermetabolic axillar, multiple mediastinal, and bilateral hilar lymphadenopathy and a subcutaneous nodule in the left anterior thoracic wall (Fig. 1O). The lesions were suspected to be multiple melanoma metastases. An endobronchial ultrasound with multiple cytopunctions in the right paratracheal and subcarinar lymph nodes were, however, negative for tumor cells.

After terminating vaccination in April 2012, the PET-CT performed in September 2012 (Fig. 1P) indicated an increased size and radiotracer uptake of the left axillary lymphadenopathy and the subcutaneous thoracic nodule, and an increased radiotracer uptake of bilateral hilar and mediastinal lymphadenopathies. Axillary lymph node dissection and resection of the subcutaneous nodule confirmed a fourth relapse of the disease with one left metastatic axillary lymph node and one metastasis in the left anterior thoracic wall. Biopsies of the right paratracheal and pretracheal lymph nodes from a mediastinoscopy were not positive for tumor cells but showed numerous well-formed giant-cell granulomas. These were characterized by macrophages ($CD68^+$; Fig. 2A) surrounded by an inflammatory ring with predominant $CD4^+$ (Fig. 2B) over $CD8^+$ T lymphocytes (Fig. 2C), large numbers of activated lymphocytes ($CD45RO^+$; Fig. 2D), and few regulatory T cells ($FoxP3^+$ and $CD25^+$; Fig. 2E and F). Ziehl–Neelsen stain was negative and no malignant cells, mast cells, or eosinophils were observed. These histopathologic features, along with the presence of multiple micronodular opacities, bilateral hilar and right paratracheal lymphadenopathies, and ground-glass infiltrate in the CT scan, were characteristics for sarcoidosis. However, the patient did not develop any sarcoidosis symptoms, and the clinical examination was normal. The control CT scan done 10 months later showed a stabilization of the mediastinal lymphadenopathies with no new lesion (Fig 1L, 1M, and 1N). Until today, he remains relapse free and enjoys a good quality of life.

Tumor antigen expression and immune response

Homogenously strong positive expression of Melan-A and MAGE-A10 was confirmed by reverse transcription PCR assay (RT-PCR) or IHC on various samples (Fig. 1: lymph nodes 1, 2, and 3 and subcutaneous melanoma metastases 1, 2, and 3). The cerebral metastasis was too necrotic to be analyzed by either IHC or RT-PCR. NY-ESO-1 was not expressed.

Peripheral blood mononuclear cells (PBMC) collected at different time points before and after vaccinations were analyzed directly *ex vivo* by flow cytometry. The percentages of CD3, CD4, and CD8 cells were stable (Fig. 3B). In contrast, the frequency of Melan-A–, MAGE-A10–, and NY-ESO-1–specific T cells changed substantially according to the antigens used in the vaccination. The SB-AS-2 adjuvant administered in conjunction with Melan-A and MAGE-A10 peptides had a moderate impact on the frequencies of MAGE-A10–specific T cells (maximum of 0.04%; Fig. 3H) and Melan-A–specific T cells (maximum of 0.02%; Fig. 3D), whereas the NY-ESO-1–specific T cells remained unchanged (Fig. 3F). The subsequent vaccines with montanide induced a moderate increase, reaching 0.04% for Melan-A–specific, 0.05% for NY-ESO-1–specific, and 0.03% for MAGE-A10–specific $CD8^+$ T cells (Fig 3D, F, H). However, the addition of CpG to the vaccine formulation resulted in strong expansions of Melan-A–specific T cells (maximum of 9.94%; Fig. 3A, left and D), NY-ESO-1–specific T cells (maximum of 1.58%; Fig. 3A, middle and F), and MAGE-A10–specific

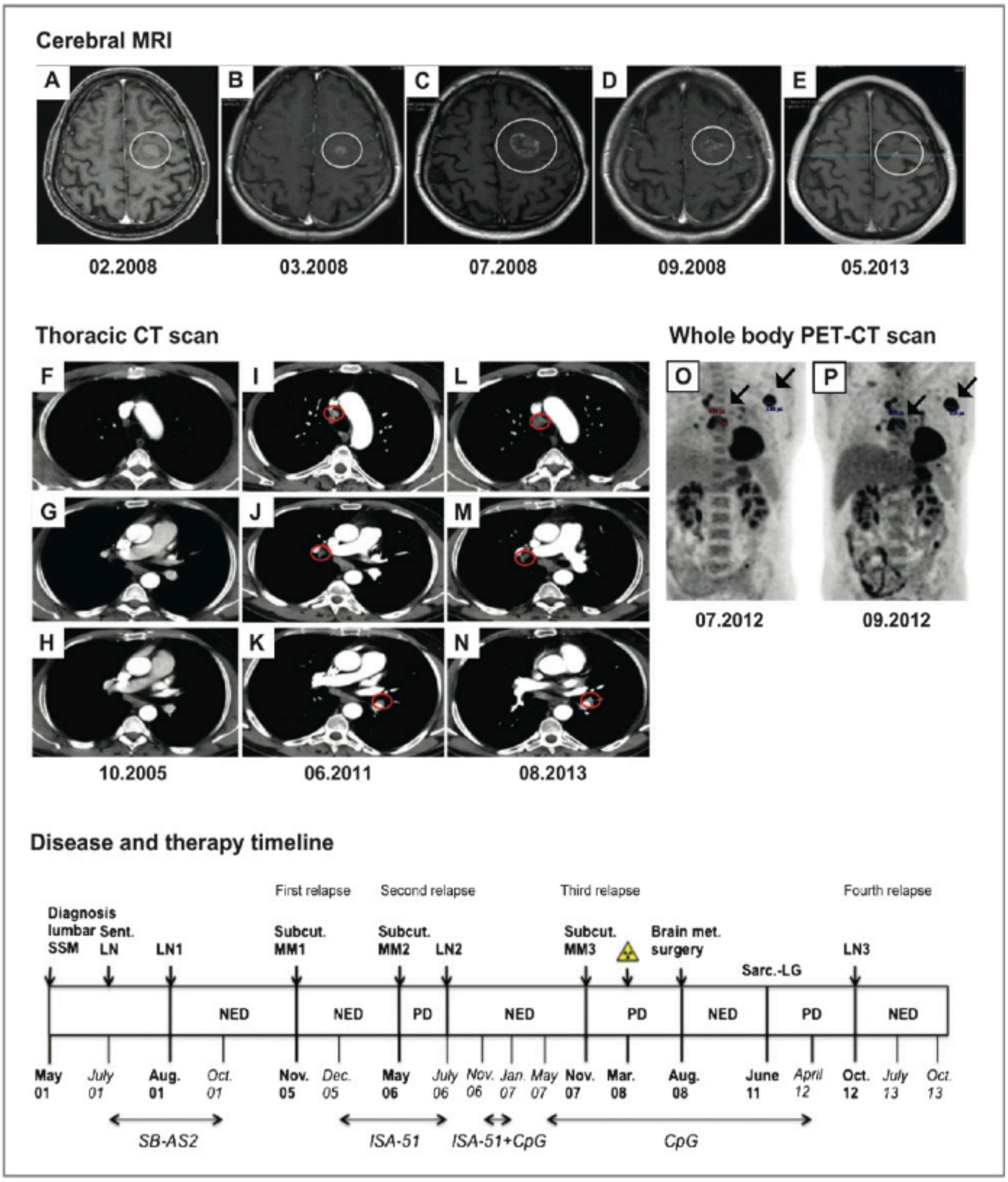

Figure 1. Radiologic images and disease course. A to E, cerebral MRI. White circles, brain metastasis. F to N, thoracic CT scan. Red circles, right paratracheal lymphadenopathies (I and L), right (J and M), and left hilar lymphadenopathies (K and N). F, G, and H, no lymphadenopathies. O to P, whole body PET-CT scan. Black arrows, left axillary lymphadenopathy and left anterior chest wall nodule. Bottom, timeline showing therapy and disease status. Sentinel lymph node procedure (Sent. LN). Lymph node metastasis surgery 1 (LN1), right iliac obdurator and inguinal radical lymph node dissection. LN2, right and left pelvic lymph node dissection. LN3, left axillary lymph node dissection + mediastinoscopy + left anterior chest wall nodule resection. Subcutaneous melanoma metastasis resection 1 (Subcut. MM1), right parapubic subcutaneous nodule resection. Subcut. MM2, right subpubic subcutaneous nodule resection. Subcut. MM3, right inguinal subcutaneous nodule resection. Sarcoid-like granulomatosis (Sarc-.LG). SB-AS2: i.d. vaccines 1, 3, and 5 of Melan-A + MAGE-A10; i.m. vaccines 2, 4 and 6 of Melan-A + MAGE-A10 + SB-AS2. ISA-51: s.c vaccines of Melan-A + MAGE-A10 + NY-ESO-1 + Montanide. ISA-51 + CpG, s. c. vaccines of Melan-A + MAGE-A10 + NY-ESO-1 + Montanide+ CpG. CpG, s.c. vaccines of Melan-A + MAGE-A10 + NY-ESO-1 + CpG; MM, melanoma metastasis; NED, no evidence of disease. PD, progressive disease; vertical arrows, surgeries; irradiation symbol + vertical arrow, radiosurgery.

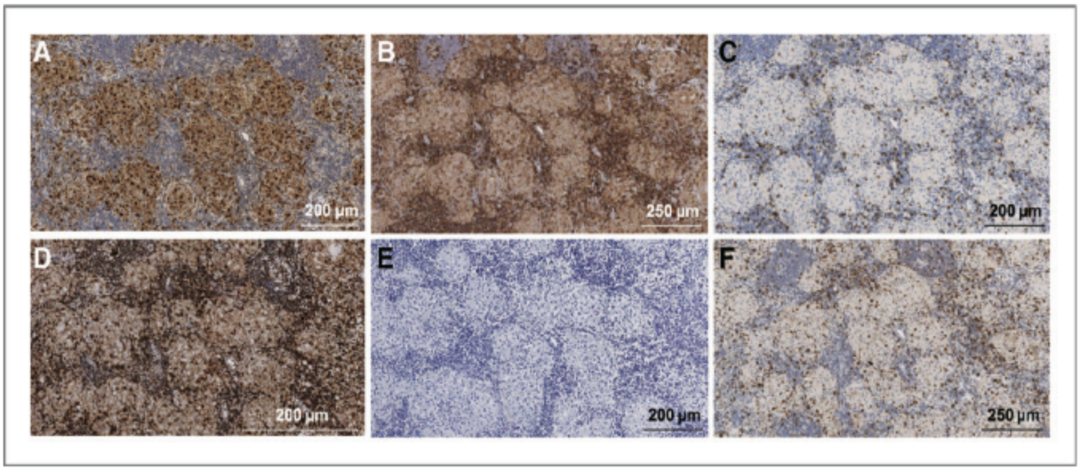

Figure 2. Immunohistochemical analysis of immune cells in paraffin-embedded right paratracheal lymph nodes. A, CD68$^+$ macrophages. B, CD4$^+$ T lymphocytes. C, CD8$^+$ T lymphocytes. D, CD45RO$^+$ lymphocytes. E, FoxP3$^+$ lymphocytes. F, CD25$^+$ lymphocytes. All images were taken from the same tissue section. IHC with isotype control antibodies were negative (not shown).

T cells (maximum of 0.08%; Fig. 3A, right and H). Despite these strong expansions of tumor antigen–specific T cells, the total leukocyte counts (absolute numbers) remained in the normal range, between 1.5 and 4 G/L (data not shown).

The three antigen-specific CD8$^+$ T-cell populations showed different kinetics, particularly after the introduction of CpG as vaccine adjuvant (Fig. 3D, F, and H). Furthermore, for all three antigen specificities, we observed significant T-cell differentiation to effector memory cells (CD45RA$^-$CCR7$^-$CD28$^-$) and terminally differentiated effector "EMRA" cells (CD45RA$^+$CCR7$^-$CD28$^-$; Fig. 3E, G, and I).

Finally, we also evaluated the capacity of the tumor antigen–specific CD8$^+$ T cells to produce IFNγ. The frequency of Melan-A–specific IFNγ-producing CD8$^+$ T cells increased 352-fold after vaccination in conjunction with CpG. IFNγ$^+$ NY-ESO-1– and MAGE-A10–specific CD8$^+$ T cells increased a maximum of 79-fold and 33-fold, respectively, compared with the values before vaccination (Fig. 3C).

Discussion

Therapeutic cancer vaccines are known to be well tolerated and only rarely are associated with severe AEs (12, 13). In fact, very few trials have documented detrimental effects that would raise safety concerns (14). The most common AEs are local induration, pain, and erythema at injection sites. Yoshida and colleagues (15) investigated the severe AEs (grade $\geq$3) after therapeutic peptide vaccinations in >500 patients with advanced cancer. They found that 20.4% of patients presented at least one AE during the vaccine trial, with 5.9% of the AEs being vaccine related and consisting of skin reactions at the injection site, edemas of the head and neck regions, colitis, and rectal bleeding. Similar findings were made in another phase III trial with 440 patients (16). In a first randomized phase II trial conducted by Slingluff and colleagues (17) of vaccination using four melanoma peptides (either with granulocyte-macrophage colony-stimulating factor and montanide or pulsed on monocyte-derived dendritic cells) with systemic low-dose IL2 infusion, grade 3 toxicities occurred in 35% of patients as diarrhea, rash, and pain. In a second randomized phase II trial of two multipeptide vaccines (8), 38% of patients experienced grade 3 toxicities, and local vaccine reaction was the most frequent grade 3 toxicity (15%–32%). Notably, no lung toxicity was reported in these clinical trials.

Sarcoidosis is a multisystem granulomatous disorder of unknown etiology with both pulmonary and extrapulmonary manifestations. Many patients with sarcoidosis do not require therapy, and two thirds experience a remission within a decade after diagnosis with few or no consequences. The presence of granulomatous inflammation is thought to result from an exaggerated cell-mediated immune response to unidentified antigens (18). Although its exact immunopathogenesis is not clearly understood, this disorder is characterized by a T-helper 1 (Th1) cell response. The release of IFNγ and IL2 by Th1 cells promotes macrophage accumulation and activation, as well as aggregation with fibroblasts and T cells, resulting in the development of granulomatous inflammation.

Our patient presented radiologic and histologic alterations characteristic of sarcoidosis (19, 20), while he was treated with cancer vaccines. He developed and maintained particularly high frequencies of cancer antigen-specific T cells, reaching a maximum of almost 10% of his circulating CD8$^+$ T cells, induced by multiple injections of highly immunogenic vaccines. Even though such strong T-cell responses are rarely seen after vaccination, we (10) and others have described this phenomenon previously for single-peptide vaccines. However, to our knowledge, such high T-cell frequencies were not yet described after vaccination with multiple peptides. Therefore, it seems possible that vaccination with multiple antigens and high CD8$^+$ T-cell frequencies may be associated with autoimmunity.

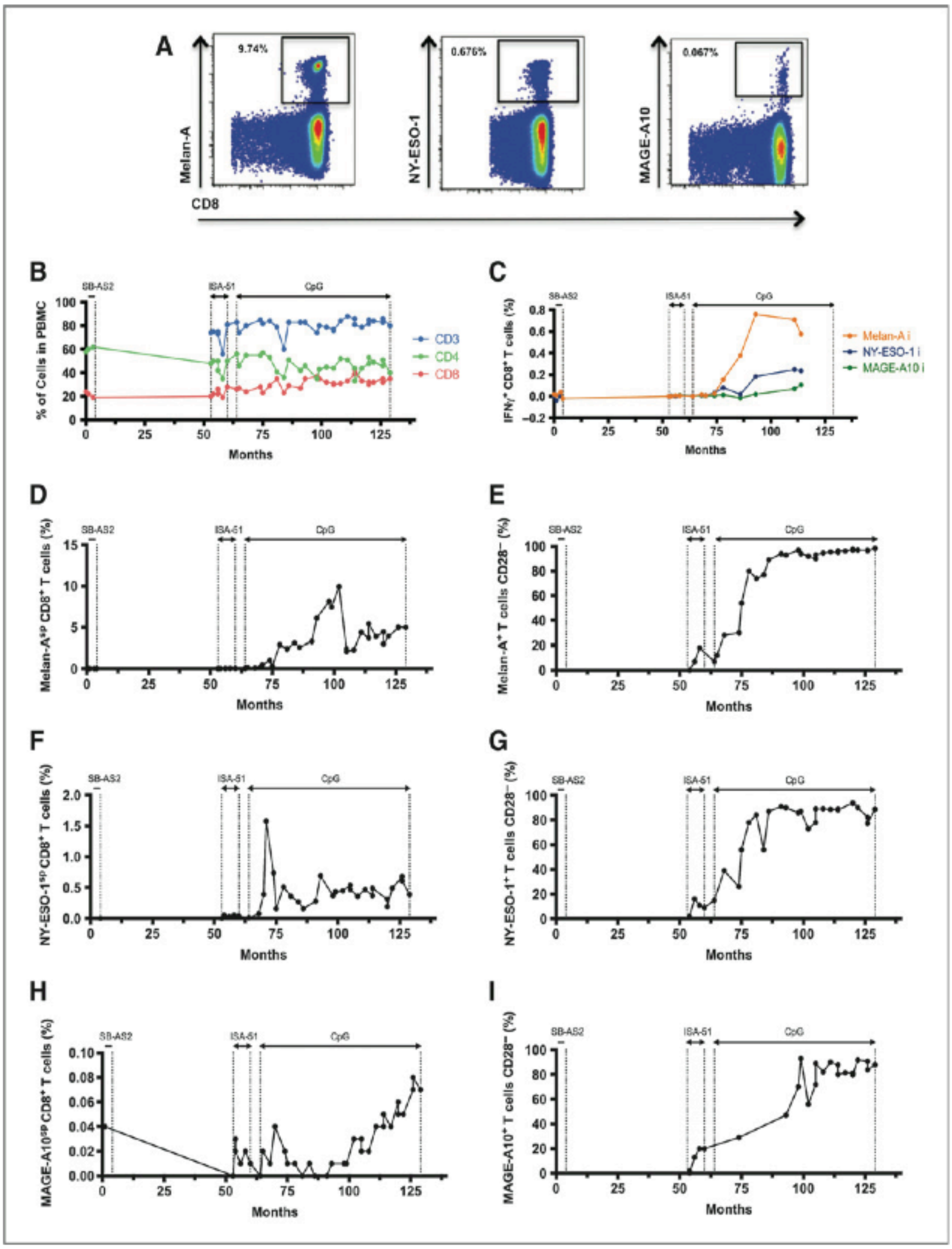

Figure 3. T-cell responses. A, representative example dot plots from PBMCs, showing Melan-A–specific cells (left), of NY-ESO-1–specific cells (middle), and MAGE-A10–specific cells (right) among CD8$^+$ T cells. B, percentages of CD3$^+$, CD4$^+$, and CD8$^+$ T cells in PBMCs. C, direct *ex vivo* ELISPOT analysis of total PBMCs, IFNγ production after 24 hours incubation with specific peptides (Melan-A, NY-ESO-1, and MAGE-A10). *Ex vivo* tetramer analysis of Melan-A– (D), NY-ESO-1– (F), and MAGE-A10 (H)–specific CD8$^+$ T cells after the different vaccinations. Percentages of CD28$^-$ cells among the Melan-A–specific (E), NY-ESO-1–specific (G), and MAGE-A10–specific (I) CD8$^+$ T cells.

This AE was classified as grade 1 according to Common Terminology Criteria for Adverse Events (version 4) lung toxicity. To our knowledge, cancer vaccine–induced granulomas have not been described previously in patients with melanoma. Interestingly, sarcoidosis was described in patients with melanoma treated with IFNα (21, 22) or ipilimumab (23, 24). Sarcoid-like reactions accompanying malignancy were reported in 0.42% of patients with melanoma (25), raising the alternative possibility that the patient's sarcoidosis could have developed incidentally and independently of immunotherapy.

Cancer vaccines are usually safe and display a low toxicity. However, with the increasing potential of new-generation and powerful vaccines, clinicians may face unexpected AEs, especially in patients with strong immune responses, such as the one presented here.

Disclosure of Potential Conflicts of Interest

No potential conflicts of interest were disclosed.

Authors' Contributions

Conception and design: L. Cagnon, D.E. Speiser
Development of methodology: D.E. Speiser
Acquisition of data (provided animals, acquired and managed patients, provided facilities, etc.): N. Bordry, L. Cagnon, S. Abed-Maillard, P. Baumgaertner, I. Letovanec, H. Bouchaab, E. Romano, O. Michielin, D.E. Speiser
Analysis and interpretation of data (e.g., statistical analysis, biostatistics, computational analysis): N. Bordry, C.-M. Costa-Nunes, I. Letovanec, R. Lazor, H. Bouchaab, E. Romano, O. Michielin, D.E. Speiser
Writing, review, and/or revision of the manuscript: N. Bordry, C.-M. Costa-Nunes, L. Cagnon, P.O. Gannon, S. Abed-Maillard, T. Murray, I. Letovanec, R. Lazor, H. Bouchaab, E. Romano, O. Michielin, D.E. Speiser
Administrative, technical, or material support (i.e., reporting or organizing data, constructing databases): N. Bordry, C.-M. Costa-Nunes, L. Cagnon, S. Abed-Maillard, I. Letovanec, N. Rufer, O. Michielin, D.E. Speiser
Study supervision: L. Cagnon, S. Abed-Maillard, D.E. Speiser

Acknowledgments

The authors thank the patient for his dedicated collaboration. They gratefully acknowledge L.J. Old, J. O'Donnell-Tormey, L. Harmer, and J. Skipper for support, and M.Swartz, R. Venhaus, L. Pan, D. Rimoldi, and the members of their groups for collaboration and advice.

Grant Support

This work was supported by grants from the Swiss National Science Foundation (grant no. 310030-135553), the Swiss Cancer League (grant no. 02836-08-2011), Ludwig Cancer Research (United States), the Cancer Research Institute (United States), and the Cancer Vaccine Collaborative (United States).

The costs of publication of this article were defrayed in part by the payment of page charges. This article must therefore be hereby marked *advertisement* in accordance with 18 U.S.C. Section 1734 solely to indicate this fact.

Received August 4, 2014; revised September 1, 2014; accepted September 14, 2014; published OnlineFirst October 2, 2014.

References

1. Sampson JH, Carter JH, Friedman AH, Seigler HF. Demographics, prognosis, and therapy in 702 patients with brain metastases from malignant melanoma. J Neurosurg 1998;88:11–20.
2. Wolchok JD, Kluger H, Callahan MK, Postow MA, Rizvi NA, Lesokhin AM, et al. Nivolumab plus ipilimumab in advanced melanoma. N Engl J Med 2013;369:122–33.
3. Attia P, Phan GQ, Maker AV, Robinson MR, Quezado MM, Yang JC, et al. Autoimmunity correlates with tumor regression in patients with metastatic melanoma treated with anti-cytotoxic T-lymphocyte antigen-4. J Clin Oncol 2005;23:6043–53.
4. Phan GQ, Yang JC, Sherry RM, Hwu P, Topalian SL, Schwartzentruber DJ, et al. Cancer regression and autoimmunity induced by cytotoxic T lymphocyte-associated antigen 4 blockade in patients with metastatic melanoma. Proc Natl Acad Sci USA 2003;100:8372–7.
5. Cormier JN, Salgaller ML, Prevette T, Barracchini KC, Rivoltini L, Restifo NP, et al. Enhancement of cellular immunity in melanoma patients immunized with a peptide from MART-1/Melan A. Cancer J Sci Am 1997;3:37–44.
6. Baumgaertner P, Jandus C, Rivals J-P, Derré L, Lövgren T, Baitsch L, et al. Vaccination-induced functional competence of circulating human tumor-specific CD8 T-cells. Int J Cancer 2012;130:2607–17.
7. Riker AI, Radfar S, Liu S, Wang Y, Khong HT. Immunotherapy of melanoma: a critical review of current concepts and future strategies. Expert Opin Biol Ther 2007;7:345–58.
8. Slingluff CL, Petroni GR, Chianese-Bullock KA, Smolkin ME, Hibbitts S, Murphy C, et al. Immunologic and clinical outcomes of a randomized phase II trial of two multipeptide vaccines for melanoma in the adjuvant setting. Clin Cancer Res 2007;13:6386–95.
9. Slingluff CL, Speiser DE. Progress and controversies in developing cancer vaccines. J Transl Med 2005;3:18.
10. Speiser DE, Liénard D, Rufer N, Rubio-Godoy V, Rimoldi D, Lejeune F, et al. Rapid and strong human CD8$^+$ T cell responses to vaccination with peptide, IFA, and CpG oligodeoxynucleotide 7909. J Clin Invest 2005;115:739–46.
11. Slingluff CL Jr. The present and future of peptide vaccines for cancer: single or multiple, long or short, alone or in combination? Cancer J 2011;17:343.
12. Tanaka S, Harada M, Mine T, Noguchi M, Gohara R, Azuma K, et al. Peptide vaccination for patients with melanoma and other types of cancer based on pre-existing peptide-specific ctotoxic T-lymphocyte precursors in the periphery. J Immunother 2003;26:357–66.
13. Itoh K, Yamada A, Mine T, Noguchi M. Recent advances in cancer vaccines: an overview. Japanese J Clin Oncol 2008;39:73–80.
14. Eggermont AMM. Therapeutic vaccines in solid tumours: can they be harmful? Eur J Cancer 2009;45:2087–90.
15. Yoshida K, Noguchi M, Mine T, Komatsu N, Yutani S, Ueno T, et al. Characteristics of severe adverse events after peptide vaccination for advanced cancer patients: analysis of 500 cases. Oncol Rep 2011; 25:57–62.
16. Rosenberg SA, Yang JC, Restifo NP. Cancer immunotherapy: moving beyond current vaccines. Nat Med 2004;10:909–15.
17. Slingluff CL, Petroni GR, Yamshchikov GV, Barnd DL, Eastham S, Galavotti H, et al. Clinical and immunologic results of a randomized phase II trial of vaccination using four melanoma peptides either administered in granulocyte-macrophage colony-stimulating factor in adjuvant or pulsed on dendritic cells. J Clin Oncol 2003;21:4016–26.
18. Agostini C, Adami F, Semenzato G. New pathogenetic insights into the sarcoid granuloma. Curr Opin Rheumatol 2000;12:71–6.
19. Spagnolo P, Sverzellati N, Wells AU, Hansell DM. Imaging aspects of the diagnosis of sarcoidosis - Springer. Eur Radiol 2014;24:807–16.
20. Miller BH, Rosado-de-Christenson ML, McAdams HP, Fishback NF. Thoracic sarcoidosis: radiologic-pathologic correlation. Radiographics 1995;15:421–37.
21. Heinzerling LM, Anliker MD, Müller J, Schlaeppi M, Moos von R. Sarcoidosis induced by interferon-α in melanoma patients: incidence, clinical manifestations, and management strategies. J Immunother 2010;33:834–9.
22. North J, Mully T. Alpha-interferon induced sarcoidosis mimicking metastatic melanoma. J Cutan Pathol 2011;38:585–9.
23. Eckert A, Schoeffler A, Dalle S, Phan A, Kiakouama L, Thomas L. Anti-CTLA4 monoclonal antibody induced sarcoidosis in a metastatic melanoma patient. Dermatology 2009;218:69–70.
24. Berthod G, Lazor R, Letovanec I, Romano E, Noirez L, Mazza Stalder J, et al. Pulmonary sarcoid-like granulomatosis induced by ipilimumab. J Clin Oncol 2012;30:e156–9.
25. Seve P, Schott AM, Pavic M, Broussolle C, Gilis L, Thomas L. Sarcoidosis and melanoma: a referral center study of 1,199 cases. Dermatology 2009;219:25–31.

3 Identification of melanoma cells and lymphocyte subpopulations in lymph node metastases by FTIR imaging histopathology

In this study, we created and used an FTIR imaging tool to automatically identify the main cell types and structures composing metastatic LNs and non-metastatic LNs. We established that cell types present in the LNs (e.g., melanoma cells and lymphocytes subpopulations) have different infrared spectral features and can be recognized by FITR imaging. In addition, we showed that a Parital Least Squares Discriminant Analaysis (PLS-DA) model was capable of predicting whether lymphocytes originated from invaded or non-invaded LNs. This project was predominantly carried out by Dr. Noémie Wald (Eric Goormaghtigh Group, Université Libre de Bruxelles, Bruxells, Belgique). I contributed to this work by gathering the FFPE samples of metastatic LNs and non-metastatic LNs, choosing the staining and identifying the different regions in the metastatic LNs. The manuscript has been submitted to *BBA-Molecular Basis of Disease* and is currently under review.

Identification of melanoma cells and lymphocyte subpopulations in lymph node metastases by FTIR imaging histopathology

N. Wald[1], N. Bordry[2], P.G. Foukas[2], D. E. Speiser[2] and E. Goormaghtigh[1]

[1] Laboratory for the Structure and Function of Biological Membranes, Center for Structural Biology and Bioinformatics, Université Libre de Bruxelles, Brussels, Belgium;

[2] Ludwig Center for Cancer Research, Department of Oncology CHUV, University of Lausanne, Lausanne, Switzerland

Keywords: IR spectroscopy, FTIR imaging, melanoma, lymphocytes, immune cells, metastases

Abbreviations

CGH, Comparative Genomic Hybridization; FISH, Fluorescence In Situ Hybridization; FPA, Focal Plane Array; FFPE, Formalin-Fixation Paraffin-Embedding; FTIR, Fourier Transform Infrared; HCA, Hierarchical Cluster Analysis; IR, Infrared; MCT, Mercury Cadmium Telluride, PCA, Principal Component Analysis; PC, Principal Component; PLS-DA, Partial Least Square Discriminant Analysis; S/N, Signal to Noise, TIL, Tumor Infiltrating Lymphocyte.

Abstract

While early stages of melanoma are usually cured by surgery, metastatic melanomas are difficult to treat because the widely available options have low response rates. Careful and precise diagnosis and staging are essential to determine patient’s risk and to select appropriate treatments. Fortunately, the recent progress in immunotherapy is very encouraging. In this context, it is important to characterize the intratumoral infiltration of immune cells in each patient, which is however not done routinely due to the lack of standardized methods. In this study, we used Fourier Transform Infrared (FTIR) imaging combined with multivariate statistical analyses to investigate non-metastatic and metastatic lymph nodes from melanoma patients. Our results show that the different cell types have different infrared spectral features allowing automated identification of these cell types. High recognition rates were obtained using a supervised Partial Least Square Discriminant Analysis (PLS-DA) model. Melanoma cells were recognized with 87.1% sensitivity and 85.7% specificity, showing that FTIR spectroscopy has similar detection power as immunohistochemistry. Besides, FTIR imaging could also distinguish lymphocyte subpopulations (B and T cells). Finally, we investigated the changes in lymphocytes due to the presence of metastases. Interestingly, specific features of spectra of lymphocytes present in metastatic or tumor-free lymph nodes could be evidenced by PCA. A PLS-DA model was capable of predicting whether lymphocytes originated from invaded or non-invaded lymph nodes. These data demonstrate that FITR imaging is capable to distinguish known and also novel biological features in human tissues, with potential practical relevance for histopathological diagnosis and biomarker assessment.

Introduction

Melanoma is the most aggressive form of skin cancer. It is responsible for approximately 80% of deaths caused by cutaneous malignancies [1,2]. While early stages of melanoma are usually cured by surgery, metastatic melanomas are difficult to treat because the widely available treatment options such as chemotherapy or radiotherapy do not show high response rates [3,4]. The prognosis of patients and treatment selection depend on disease stage, which is determined based on a series of parameters including primary tumor thickness, ulceration, mitotic rate, and metastases in lymph nodes and other organs [5,6]. Routinely, melanoma cells in tissues (for example in the sentinel lymph node) are detected by visual inspection under the microscope of the hematoxylin and eosin (H&E) stained sections of the resection by a trained pathologist. Detection of melanoma cells remains a challenge because they present a wide variety of histological features and patterns of spreading [7]. Moreover, the anatomopathological study of tissue sections is time consuming, and to some degree subjective with consequent inter-observer discrepancies [8]. For the identification of melanoma cells, some additional techniques are available. Confirmation of the presence of melanoma can be achieved by immunohistochemistry [9], Fluorescence In Situ Hybridization (FISH) or by Comparative Genomic Hybridization (CGH) [10–12].

In this last decade, the importance of stromal and infiltrating cells in tumor progression has been highlighted in numerous studies [13,14]. In particular, the presence of immune cells at the tumor site has been shown to play an important role in patient's outcome [13,15–17]. The presence of Tumor-Infiltrating Lymphocytes (TIL) in primary melanomas [18] and in metastatic lymph nodes [19] has been shown to positively correlate with survival. Furthermore, the presence of these TIL is also associated with successful outcome to immunotherapies such as with the CTLA-4 specific antibody ipilimumab [20]. Yet, it is also recognized that the immune system plays a dual role in cancer development and progression [17]. While some immune cells suppress tumor growth by killing or inhibiting tumor cell proliferation, other immune cell types can promote tumor progression. Thus, the final outcome depends on the subpopulations of immune cells present at the tumor site [21]. Cytotoxic T cells ($CD8^+$) and T helper-1 cells ($CD4^+$) both play an active role in tumor reduction while the function of B cells is less clear [21]. Several studies showed that B cell infiltration in primary melanoma and metastases correlated with survival advantage [22,23] whereas another study showed, in mice, that B cell depletion improves the immune destruction of the tumor [24].

It is now clear that characterization of tumor immune cell infiltration is important. Although this can be assessed by immunohistochemistry, this is not currently done because of the lack of standardized methods. Moreover, the current techniques for histopathological characterization can only assess a small number of proteins (immunohistochemistry) or genomic abnormalities (FISH). On the contrary, Fourier Transform Infrared (FTIR) imaging brings global information on the biochemical content of the cells and tissues. The technique was shown to be a useful tool to obtain unique fingerprints of different cell types. FTIR spectroscopy is a vibrational technique based on the interaction of an infrared beam with the covalent bonds of biological molecules. FTIR is sensitive to all molecules (proteins, lipids, nucleic acid, carbohydrates…) and particularly to protein secondary structure [25,26]. Moreover the IR spectrum reflects the nature, chain length and unsaturation of lipids [27,28]. In the study of prokaryotic and eukaryotic cells, FTIR has been shown to provide information about cell strain [29], cell cycle [30,31] and various metabolic perturbations caused by candidate anticancer drugs [32].

When coupled with a microscope device, this technique provides spatially resolved information on the biochemical content of the different cell types and structures present in tissue sections. FTIR imaging was recently recognized as an emerging tool for histopathological studies [33–35]. Particularly in cancer research, the technique has proven its value in various cancer types [36–38]. Nevertheless, few papers report on the study of melanoma [38–41] or lymphocytes [42,43] by FTIR imaging. Two studies have shown the possibility to differentiate benign nevi from malignant melanomas [38,41] while another study has demonstrated that FTIR imaging was sensitive enough to distinguish different subtypes of primary melanoma [44].

The present study demonstrates the potential of FTIR for the identification of main cell types present in melanoma metastases in lymph nodes. It focuses specifically on the identification of melanoma cells and the different subpopulations of lymphocytes that infiltrate the tumor. Multivariate statistical models were built to predict the identity of cell types in tissue sections of melanoma metastases. These models were established in training sets and then validated in tests sets of different patient sections.

Materials and Methods

1. Patient samples

Thirty-four biopsies of melanoma metastases in lymph nodes from 14 patients were collected by the Ludwig Cancer Research Center at the University Hospital of Lausanne, Switzerland. All the biopsies were formalin-fixed and paraffin-embedded (FFPE). These 34 FFPE-metastases were used for the first section of this article. Eight additional metastatic lymph nodes and eight non-metastatic lymph nodes from the same patients were used in the second section. Written informed consent was obtained based on the study protocol, approved by the ethical commission of the University of Lausanne.

2. Tissue handling and immunohistochemistry

Eight adjacent sections of 5 µm thickness were cut from each FFPE melanoma metastasis. One of them was deposited on a special microscope slide, transparent to infrared light (BaF_2 slides, ACM, Villiers St. Frederic, France) and was used for FTIR measurements. Tissue sections were first deparaffinized in xylene and rehydrated in an ethanol gradient. One section was stained with hematoxylin and eosin (H&E) and the six sections left were stained by immunohistochemistry. For this purpose, tissues were treated with 3% H_2O_2 in distilled water for five minutes or 0.5% H_2O_2 in methanol for 10 minutes to quench endogenous peroxidase activity. Antigen retrieval was carried out by heating the sections in a Tris–EDTA buffer (pH 9) for 1’30" in a steamer. Subsequently, the slides were incubated in Tris-HCL buffer (pH 7.6) for 15 minutes. Sections were incubated for 40 minutes at room temperature with the primary antibody for CD8 (clone C8/144B, Dakocytomation, Glostrup, Denmark), CD4 (clone 4B12, Novocastra, Newcastle Upon Tyne, UK), CD19 (clone BT51E, Novacastra, Newcastle Upon Tyne, UK), S100 (Novocastra, Newcastle Upon Tyne, UK), Melan-A (clone A103, Dako, Glostrup, Denmark) and melanosome (clone HMB45, Dakocytomation, Glostrup, Denmark) followed by a secondary anti-mouse antibody RTU/HRP ENVISION (K4001, Dakocytomation, Glostrup, Denmark) for 30 minutes. Diaminobenzidine (DAB) was used as a brown chromogen (K3468, Dakocytomation, Glostrup, Denmark) for CD8 and CD19 and 3-amino-9-ethylcarbazole (AEC) was used as a red chromogen (K3464, Dakocytomation, Glostrup, Denmark) for CD4, S100, Melan-A and melanosome. The slides were then counterstained with Hematoxylin (Merck 1.05175) for 5-8 seconds and mounted with xylol. Immunostaining with appropriate isotype control antibodies were used as negative controls. All stained sections were scanned with a NanoZoomer (Hamamatsu, Hamamatsu, Japan) and images were analyzed with NDPview program (Hamamatsu, Hamamatsu, Japan). The stained sections were analyzed with assistance of a trained pathologist.

3. FTIR measurements

The FTIR data were collected using a Hyperion 3000 FTIR imaging system (Bruker Optics, Ettlingen, Germany), equipped with a liquid nitrogen cooled 64x64 Mercury Cadmium Telluride (MCT) Focal Plane Array (FPA) detector, in transmission mode. The size of an image covers an area of 180x180 μm^2 and was composed of 4096 pixels of 2.8x2.8 μm^2 each. It must be noted that true spatial resolution can be significantly lower than the pixel size, depending on the wavelength. It took about 5 minutes to record an infrared image composed of 4096 spectra at a spectral resolution of 8 cm^{-1} and where each spectrum is the average of 256 scans. Larger images could be obtained by associating several unit images

(4096 spectra) side by side. Pixels can also be binned 2x2 to record larger images but this lead to a spatial resolution decrease (e.g. 5.6 µm pixel size for 2x2 binning).

4. Data analysis

4.1 Preprocessing

All spectra were preprocessed as follows. Water vapor contribution was subtracted as described previously [45,46] with 1956-1935 cm^{-1} as reference peak and CO_2 peak was flattened between 2450 and 2250 cm^{-1}. The spectra were baseline-corrected. Straight lines were interpolated between the spectra points at 3620, 2995, 2800, 2395, 2247, 1765, 1724, 1480, 1355, 1144 and 950 cm^{-1} and subtracted from each spectrum. Spectra were normalized for equal area between 1725 and 1481 cm^{-1} (amide I and II bands). The signal to-noise-ratio (S/N) was then systematically checked on every spectrum. It was required to be greater than 350 when noise was defined as the standard deviation in the 2000-1900 cm^{-1} region of the spectrum and the signal was the maximum of the curve between 1750 and 1480 cm^{-1} after subtracting a baseline passing through these two points.

4.2 Difference spectra

Difference spectra allow emphasizing the spectral variations between two distinct conditions. Difference spectrum was built by subtraction of the spectra of B cells from the spectra of the T cells.

4.3 Statistical analyses

Principal Component Analysis (PCA), as described previously [47], is an unsupervised multivariate method enabling variable reduction by building linear combinations of wavenumbers varying together, called Principal Component (PC). The first principal component explains most of the data variance. The second principal component, uncorrelated to the first one, accounts for most of the residual variance and so on. Usually 2 to 6 PCs are sufficient to explain the major proportion of the original variance of the data set and reducing the description of each spectrum to 2 to 6 numbers representing the projection (scores) of the spectra on the PCs. One advantage of the method is that it extracts the important information as a set of new orthogonal variables, the Principal Components (PCs) [48,49].

K-means clustering is an unsupervised analysis based on a nonhierarchical iterative algorithm. This analysis aims at partitioning n spectra into k clusters on basis of the spectral features. The process to organize spectra in clusters can be described as follows: each IR spectrum is defined by a point in a p-dimensional space (p being the number of data points of the spectra). In this space, k points are initially chosen randomly. They represent the origin of each cluster. The k parameter is chosen by the operator. The distances between these k points and all the spectra are then calculated. Each spectrum is then associated with a cluster to minimize its geometrical distance to the position of the origin of the cluster. Once every spectrum is assigned to a cluster, centroids of the clusters are calculated and the distances of the spectra to the centroids are again computed. The spectra are reorganized so that each spectrum is assigned to the cluster with the nearest centroid. The centroid positions are recalculated until none of the spectra needs to be reassigned to another cluster. The whole process is repeated several times with different starting points (k points). As a result of this analysis, spectra with similar features are in a same cluster and spectra within different clusters are as dissimilar as possible [50,51]. This analysis was applied here on spectra recorded on large area of tissue sections (c. a. 100 000 spectra). Images were colored so that each pixel was associated with a cluster and each cluster was associated with a color. To provide information about the similarities that exist among the different clusters, a dendrogram was built. This was performed in carrying a hierarchical clustering on the centroid of each cluster.

The Multivariate Analysis of the Variance (MANOVA) indicates whether one group among others is significantly different. The MANOVA was performed in this study using the score on the first 6 PCs obtained after a PCA on the series of spectra from B cells and T cells from the database.

Partial Least Square Discriminant Analysis (PLS-DA) is a supervised discriminant method based on the PLS regression models [52]. This analysis requires a priori knowledge about the classes of spectra. PLS-DA was used to extract latent variables of the data set that enable the construction of a factor allowing to predict a class.

From the confusion tables, sensitivity and specificity were calculated for each cell type class as follows. Sensitivity was calculated as S_v= TP/(TP+FN) and specificity as S_p=TN/TN+FP, where TP, FN, TN and FP correspond to True Positive, False Negative, True Negative and False Positive respectively [53].

Preprocessing (correction of the spectra for water vapor contribution, baseline subtraction and normalization), PCA, MANOVA, K-means clustering and PLS-DA were carried out by Kinetics, a custom made program, running under Matlab (Matlab, Mathworks Inc).

Results

1. Identification of the main cell types

Thirty-four biopsies of melanoma metastases invading lymph nodes from 14 different patients were analyzed by infrared spectroscopy. The main goal of the work was to characterize the infrared spectra of the major cell types composing these melanoma metastases and to create an automatic tool for spectral histopathological recognition. The workflow of the experiments is schematically represented in Figure 1. For each FFPE biopsy, eight adjacent sections were cut (step 1) and each one was stained with either H&E or one of the six different immunohistochemistry stainings selected or left unstained (step 2). Six different antibodies targeting four different cell types were used: anti-HMB45/anti-S100/anti-Melan-A to target melanoma cells, anti-CD4 to target helper T cells, anti-CD8 to target cytotoxic T cells and anti-CD19 to target B cells. One section remained unstained for infrared measurements and was deposited on a material transparent to infrared light (Barium fluoride (BaF_2) slide) (step 3).

The H&E stained section and the immunostained sections were used as references to localize the main cell types on the unstained section with the help of a pathologist. On the basis of this visual inspection, six main cell types were identified: the melanoma cells, the erythrocytes, the lymphocytes (T and B cells), the endothelial cells composing small capillaries and finally the connective tissue. This last category included the capsule and the wall of the vascular tissues. A database composed of spectra from the main cell types was built. The process to collect spectra from one cell type is illustrated in Figure 1 (step 4). Up to 500 FTIR measurements (4096 spectra each) were recorded in total. For each FTIR measurement, around one hundred spectra were selected. The composition of the spectral database is described in Table 1. This table lists, for each cell type category, the number of spectra, the number of biopsies and the number of patients from which spectra were acquired.

First of all, one mean spectrum was computed from all the spectra of each category. These mean spectra are represented in Figure 2. Visual inspection of these spectra already shows that some differences can be observed in some parts of the IR spectrum. For example, the erythrocyte category shows differences in the lipid region (3000-2800 cm^{-1}), the amide II band and the 1400-1000 cm^{-1} region.

Another way of analyzing the differences between the spectra and, at the same time, to reduce considerably the number of variables is the Principal Component Analysis (PCA). In order to obtain a reasonable number of spectra that can be visualized on a PCA score plot, we first averaged the c. a. 100 spectra selected per measurement. In turn, 500 mean spectra were obtained and the PCA was computed. The score plot resulting from this analysis is shown in Figure 3a. It can be observed that the main cell types cluster together. This separation between erythrocytes (in green), the connective tissue (in red), the melanoma cells (in orange) and the lymphocytes (in blue and purple) mainly occurs along PC1 and PC2. We also observed that endothelial cells and melanoma cells show similar spectra and are close in the score plot. Only partial separation occurs between T cells, B cells and B cells from the germinal centers in this plot. While p values, obtained after computation of a MANOVA on the projection of the spectra on the six first PCs, indicate that the mean spectra of lymphocyte subtypes are significantly distinct (p values <0.05, data not shown), only a trend to separation exists between these subpopulations of lymphocytes on a PCA score plot when individual spectra are considered. This separation can be better observed in the PCA including only spectra from lymphocytes (Figure 11). Accordingly, in a first step, all lymphocyte types were included in one category for the following analyses of this section.

The part b of Figure 3 depicts the first three principal components that represent about 84 % of the variance. They can give some clue about biochemical differences between the cell types that will be discussed later.

The results reported above obtained on representative mean spectra suggest that there is an intrinsic difference between the IR spectra of the main cell types found in melanoma invaded lymph nodes. Yet, they do not provide a robust tool to recognize individual spectra. In a second step, we used the Partial Least Square Discriminant Analysis (PLS-DA) to create a predictive model able to recognize these main cell types. Based on this supervised analysis, we built two successive models as represented in Figure 4. A first level model built on the 1800-1000 cm^{-1} spectral region was used to differentiate the epithelial cells, the erythrocytes, the lymphocytes and the connective tissue. The first class named epithelial cells included melanoma cells as well as endothelial cells. These two cell types were grouped in one class because of their spectral similarities even if, according to histology, endothelial cells are quite distinct from epithelial cells. Finally, a second level model, built on the two combined spectral regions; 3000-2800 and 1800-1000 cm^{-1}, was used to distinguish melanoma cells from endothelial cells. The spectral regions used for these two models were determined after building 10 PLS-DA models on 100 cm^{-1} range between 3000-2800 cm^{-1} and 1800-1000 cm^{-1} in order to determine which spectral region presented the best predictive power (data not shown).

To assess and validate these models, we divided our spectral database into two parts: a training set and a test set. Different patients were included in the training set and in the test set for external validation. Two different distributions, randomly assigned between these two sets, were tested. These distributions are described in Table 2. For the two distributions, biopsies from 8 patients were used in the training set whereas biopsies from 6 patients were used for the validation of the models.

Results of prediction for patients included in the test sets are shown in Table 3a and b. Table 3a shows the percentages of the spectra predicted by the first level model as belonging to one of each class: epithelial cells, erythrocytes, lymphocytes and connective tissue. The second table (3b) presents the confusion matrix obtained when the second level model was applied to the first class (epithelial cells) determined above. This second level model identified melanoma cells versus endothelial cells from the “epithelial cell” class spectra identified with the first level model. Globally, percentages of correct recognition, shown on the diagonal of the tables, range from 81.8 to 100 % for the first model. Similarly percentages for correct recognition of the second model range from 91.7 to 97.3 % for the melanoma cells and endothelial cells. Sensitivities and specificities of the model to identify each cell type were computed and are shown in Table 3.

As a supplementary control, we applied these two successive models to an infrared image of 2.2x2.2 mm recorded from the metastasis of a patient who was not included in the training sets described in Table 2a. The result of this prediction is shown in Figure 5 e. Each pixel of the infrared image is predicted by the first level model and receives a color according to its membership. Then spectra predicted as belonging to the epithelial cells class were reanalyzed by the second level model. To assess the quality of the prediction the same area of the tissue from the adjacent stained sections are shown (a, b, c and d). These stainings show the localization of the melanoma cells (HMB45$^+$), the helper T cells (CD4$^+$) and the B cells (CD19$^+$) and the capillaries are visible on the H&E section. A good correspondence can be observed between these 5 images (a, b, c, d and e). Interestingly, quantitative information can be immediately obtained from the IR images. In this area of the tissue section, 38.7 % of the area is occupied by melanoma cells while 37.9 % is composed of lymphocytes. 22.5 % is represented by the endothelial cells and capillaries and only 0.8 % was composed of pure connective tissue according to the model.

2. Identification of lymphocyte subpopulations

This second section of the paper aimed to differentiate and identify subpopulations of lymphocytes using immunohistochemistry as references. After visual inspection of the scans of the sections stained for CD4$^+$ T cells and CD8$^+$ T cells corresponding respectively to helper and cytotoxic T cells, these two subtypes of T cells were merged in one same group for our analyses. In practice, they were too mixed in the tissues and could not be identified with sufficient certainty on the adjacent unstained section used for IR imaging. In order to analyze the differences between subpopulations of lymphocytes, we recorded larger IR images (mappings) on areas containing both T cells and B cells. K-means clustering were applied on these different mappings (from different patients) and high levels of similarities were observed between immunohistochemistry and the cluster analysis. One example is represented in Figure 6 with a K-means clustering composed of 6 groups. In the IR clustering image (Figure 6d), there is a good match between clusters and cell types. The yellow cluster (number 4) clearly corresponds to the melanoma cells. The B cells are represented by cluster number 2 while the T cells correspond to cluster number 1. The dendrogram (**e**) shows that the spectra of these two subtypes of lymphocytes are very similar. A similar analysis was obtained for five different biopsies and, after referring to the corresponding immunohistochemistry, spectra from the 2 clusters corresponding respectively to B cells and to T cells were extracted. Difference spectra were obtained for each biopsy upon subtracting spectra corresponding to B cells from spectra corresponding to T cells. They are shown in Figure 7 for each biopsy.

Similar bands can be observed in the difference spectra, e.g. from 1500 to 1000 cm^{-1} and 1800-1700 cm^{-1} while the amide I region of the difference spectra is less reproducible (1700-1600 cm^{-1}). These difference spectra show a high level of resemblance among different patients, meaning that common spectral features can be found for B and T cells for different patients. As similar features appeared for all patients, we built a predictive model able to identify these two lymphocyte subpopulations in general. A model was trained with the individual spectra extracted from the previous cluster analysis on the 1800-1000 cm^{-1} spectral region. Spectra from 4 biopsies were used to build the model which was then validated on the remaining biopsy. One example of this external validation is shown in Figure 5f. The 3 PLS-DA models (2 successive levels) were applied on this infrared image: a first level model to identify epithelial cells, lymphocytes, erythrocytes and connective tissue, a second level model to identify melanoma cells and endothelial cells and another second level model that identify B and T cells (see also Figure 4). Importantly spectra from this patient were not included in any of the training sets of these three models. A good agreement was observed between the IR image and the two immunohistochemistry stainings corresponding to T cells (CD4^{+}) and B cells (CD19^{+}). Another example for a different patient is shown as supplemental data (Figure 12).

3. Comparison of lymphocyte populations from metastatic and non-metastatic lymph nodes

We have shown above that the IR spectrum of lymphocytes contains sufficient information to discriminate between B cells and T cells. It has been shown in a previous study that spectra of lymphocytes obtained from lymph nodes and tonsils could be easily separated into two classes called “activated” and “non-activated” [47]. The activation state was previously determined on the basis of a microscopic examination by a pathologist. Furthermore, these “activated” and “non-activated” lymphocytes were distinguishable from the lymphocytes infiltrating breast tumor [47]. It was therefore of interest to question the impact of melanoma metastases on the lymphocytes of an invaded lymph node, even in regions not in direct contact with the melanoma cells. In the last part of the study, we compared eight metastatic lymph nodes and eight non-metastatic lymph nodes from the same patient (16 lymph nodes in total). Six FTIR measurements (of 4096 spectra each) of T cells were recorded for each biopsy. For each measurement, a subset of 300 individual spectra was randomly selected and for each subset a mean spectrum was computed. All together, we obtained 80 mean spectra (5 per lymph node) and these were submitted to a PCA. The score plot of the PCA shows that a difference indeed exists between the lymphocytes present in lymph nodes invaded by a metastasis when compared to those without any metastasis (Figure 8a). The clustering between these two groups of lymphocytes arises from PC3, which is illustrated in Figure 8b.

In the PCA above, we analyzed mean IR spectra. However, if IR imaging is going to be applied on IR images of lymph nodes sections, it is also necessary to identify the spectra at the pixel level (i.e. individual spectra). We therefore performed PLS-DA to classify spectra of lymphocytes according to their localization in lymph nodes with or without metastases. One hundred individual spectra were randomly selected for each patient from their metastatic and non-metastatic lymph nodes. One lymph node (either metastatic or non-metastatic) was removed at a time from the training set, and the membership of the spectra from this lymph node was predicted. This was computed 16 times after removing the spectra of each lymph node at a time. The result of this prediction is represented in Figure 8, as a bar chart and corresponds to the percentage of spectra correctly predicted as belonging to the class (metastatic or non-metastatic lymph node). Overall, the spectra of 15 lymph nodes among the 16 were correctly predicted (93.75 % of the lymph nodes). One of the 15 correctly predicted lymph nodes was just at the limit for correct assignment (50% of the prediction of the spectra) and one lymph node among the 16 was a false negative.

Discussion

Results presented in this paper show that spectra from different cell types (erythrocytes, melanoma cells, endothelial cells, lymphocytes and connective tissue) in lymph nodes invaded by melanoma metastases have different spectral features. In turn, these cell types can be identified on the basis of their infrared spectra. Unsupervised multivariate statistics such as PCA do not require any *a priori* knowledge on the data. Yet, PCA score plots suggest that the global chemical composition of these main cell types present significant differences which dominate the sources of variance found through the data sets. Observation of the shape of the PCs can bring some clue on the chemical origin of the differences found among cell types. The separation between the main cell types occurs when projecting the spectra on the plane made by the first two PCs (Figure 3). The shape of the first two PCs in the amide I and amide II range is sigmoidal. In the amide I range, a minimum near 1620 cm^{-1} and a maximum near 1670 cm^{-1} are characteristic of a change in the secondary structure of the proteins [25,26]. A similar shift was observed in the amide II range, also suggesting a change in the secondary structure. This result means that proteins present in the different cell types may differ in their secondary structure content. This can be easily understood for the connective tissue composed of spectra from the capsule of the lymph node as well as from the wall of the different vascular tissues such as vessels and arteries. They all contain a large fraction of collagen fibers. Collagen is a very peculiar protein that forms triple helices which have an IR spectrum characterized by a maximum at 1638 cm^{-1} [26]. Differences between lymphocytes and the other cell types were mainly observed in the 1300-1000 cm^{-1} spectral region and more precisely near 1230 and 1080 cm^{-1} corresponding to the stretching of the phosphate groups (asymmetric and symmetric respectively) (Figure 2). As described previously, these two bands are mainly due to a contribution of nucleic acids [54,55] and could underline a difference in the nucleic acid content/state of lymphocytes (relative to the protein). Lymphocytes are small cells with a high nuclear-cytoplasmic (NC) ratio (size of the nucleus/size of the cytoplasm; 3:1) when compared to normal cells [56]. This could explain the difference between nucleic acid/protein ratio for lymphocytes when compared to endothelial cells or erythrocytes (cells without any nucleus). An increased NC ratio is also a characteristic observed in malignant cells and particularly in melanoma [57]. A high level of nucleic acid contribution was also observed here in the spectrum of melanoma cells.

High recognition rates were obtained using a supervised PLS-DA model. Running successive models instead of a one-step model was found to improve very significantly the correct recognition rates when large mapping were analyzed in external validation. The erythrocytes were best recognized with 100 % of correct assignment. This is in agreement with observations by PCA that erythrocytes are chemically very different from all other cell types. This difference is likely related to the absence of nucleus and presence of large hemoglobin content. FTIR imaging did not achieve perfect separation between lymphocytes and epithelial cells. A similarity between these two classes was already observed in the score plot of the PCA. An explanation could be that both lymphocytes and melanoma cells present high nucleus/cytoplasm (NC) ratios. Yet, melanoma cells were recognized with 87.1% sensitivity and 85.7% specificity. This is important because melanoma cells present a wide range of histological features. They can mimic epithelial, hematologic, mesenchymal and neural tumors [9]. As a result, they are difficult to recognize by visual inspection under a microscope, remaining one of the most challenging areas of pathology [7,10]. The sensitivity obtained here by FTIR spectroscopy is comparable to the one obtained with other methods used to identify melanoma cells in tissue sections. Immunohistochemistry is the primary tool to distinguish melanoma from other cell types, using antibodies specific for melanocytic specific antigens (e.g. Melan-A, S100 or HMB45). These antigens are also expressed in melanocytes, the normal counterpart of melanoma cells [9]. S100 is the marker with the highest sensitivity (97 to 100%) but shows a low specificity (75-87%) because this protein is also expressed by a variety of other cells. HMB45 is less sensitive (58-83% for metastatic melanoma and 77-100% for primary melanoma) but is more specific. The sensitivity of Melan-A ranges from 75 to 92 % while the specificity ranges from 95 to 100% [9]. This means that sensitivity and specificity obtained by FTIR spectroscopy are similar to the one obtained by current immunohistochemistry methods. Furthermore, usually more than one staining is required as the expression of melanocytic antigens (e.g. HMB45, Melan-A) decreases drastically as a function of the progress of the disease and is frequently absent in metastases [9,58]. A study showed that their expression is absent in more than 20% of melanoma lesions [58]. Other more recent techniques to identify melanoma cells are Fluorescence In Situ Hybridization (FISH) and Comparative Genomic Hybridization (CGH). They are respectively based on the detection of chromosomal alterations and on changes in DNA copy numbers on the entire genome [10,12,59]. Sensitivity and specificity of FISH reach 87% and 95%, respectively [11]. However, these two techniques are expensive and time-consuming and CGH does not bring information on the spatial distribution in the tissue as the DNA needs to be isolated and purified [10]. For FISH, only 4 probes can be used at a time, meaning that only 4 genomic alterations can be studied simultaneously. Overall, FTIR imaging appears as a promising technique to study lymph node histological sections.

Quite interestingly, FTIR imaging could make the difference between subpopulations of lymphocytes. The fact that B and T cells could be distinguished on the basis of unsupervised analysis (K-means) is very encouraging. It means that infrared spectroscopy is sensitive enough to highlight, in an unsupervised manner, subtle differences that exist between B cells and T cells. These lymphocytes have different functions but are similar concerning their hematopoietic origin and are expected to be relatively similar in their molecular composition. A good correspondence was observed between immunohistochemistry stainings of T and B cells and the FTIR images where a K-means cluster analysis was applied. Importantly, a supervised PLS-DA model built on spectra of some patients could be validated on spectra from other patients. These results are in agreement with results obtained in a previous study on human spleen sections [42]. Unsupervised analysis such as clustering was shown to be capable of identifying B and T cells in frozen sections of human spleen using the 1800-950 cm^{-1} spectral region. The difference between B and T cell spectra obtained in that study was quite consistent with the one obtained here, in particular in the region of the bands near 1240 and 1080 cm^{-1} corresponding to the asymmetric and symmetric stretching of PO_2^- groups. Another study on lymph nodes invaded by breast cancer [43] reported that it was possible, based on unsupervised analysis, to detect differences between B and T cells. Nevertheless, these two studies did not use immunohistochemistry to confirm the B or T cell origins and did not create predictive supervised models to generalize it to several patients.

At this point of the discussion, it is worth pointing out that tissues are complex structures and lymphocytes are often mixed with small capillaries or other immune cells such as macrophages or dendritic cells. Therefore spectra of lymphocytes could be affected by the surrounding tissue and could contain a mix contribution of different cell types. In Figure 10, different areas of five H&E stained sections containing mainly B cells and T cells are displayed. We can observe that lymphocytes are usually significantly mixed with other cell types and that it is particularly true for the T cell areas. A question can therefore be raised about the differences previously observed between T and B cells. This difference could arise either from T and B cells themselves or from a particular mix with stromal cell spectra. The possibility to distinguish T cells from B cells on the basis of their intrinsic molecular content only was established in previous studies where T and B cells were purified from blood samples [42,60]. This suggests that origin of the differences could be found in the subtle differences of the biochemical composition of these cells alone. Yet, we cannot rule out a contribution of the stroma.

The last part of the paper investigated the changes undergone by the lymphocytes when metastases are present in the same lymph node. Interestingly, features of spectra of lymphocytes present in invaded or non-invaded lymph nodes were quite significantly different. An analysis of the principal component describing this change indicated that the main differences occurred in the region of the spectra where the contribution of the nucleic acids is prominent. We also showed that supervised analysis such as PLS-DA was capable of predicting whether lymphocytes originated from invaded or non-invaded lymph nodes. These models were validated externally as the spectra of one lymph node were removed from the training set and the model was then validated on these spectra. Fifteen lymph nodes out of 16 were correctly predicted. We could not accurately decipher the reason for the difference but a hypothesis about the activation state of the lymphocytes can be proposed. So far, only few infrared studies about lymphocytes have been published.

Two groups have worked on lymphocyte activation and two studies have shown that it was possible to observe differences induced by activation of B cells [61,62]. The first study showed that lymphocyte activation *in vitro* by different stimuli could be detected by FTIR after 90 minutes only. The second study showed that B cells in the germinal centers of activated lymph nodes were spectroscopically different from the non-activated B cells in the mantle area of the follicles [61]. Moreover, a study carried out in our laboratory reported that lymphocytes from secondary lymphoid organ (tonsils and lymph nodes) present different IR spectra based on their activation state [47]. All together these publications indicate that the observed differences could be associated with activation. The results presented in this paper and the ones previously published [61,62] suggest a potential use of FTIR in the characterization of the activation state of lymphocytes. Nonetheless, further characterization of the activation and differentiation state of the lymphocytes in these tissue sections would be required for a more in-depth understanding (e.g. through the characterization and quantification of cytokine production). Clinically, this result also suggests that it could be possible to identify the presence of (micro-)metastases through the impact they have on lymphocytes. The success rate of such an approach remains to be established.

Potential applications of the results reported in this study are at least twofold. First, FTIR imaging can facilitate the detection of (micro-)metastases of melanoma in lymph nodes, and can therefore also contribute to disease staging [15,16,63]. The current limitation is the large size of the data when imaging large tissue sections. Yet, the technology is now just able to record and analyze images recorded on tissue sections in the cm^2 size. Secondly, FITR imaging allows the identification and the quantification of lymphocyte subpopulations in the tumor microenvironment, providing important additional information to evaluate cancer patients. Besides such practical applications, FITR imaging can provide novel insights into the complex biology of tissues, promoting research in e.g. immunology, metabolism and further fields of bio-medical sciences.

Acknowledgments

This research has been supported by grants from the Belgian National Fund for Scientific Research (FRFC 2.4527.10, 2.4526.12 and T.0155.13), the Swiss Cancer League (02836-08- 2011), the Foundation Theodor et Gabriela Kummer (Lausanne), and Ludwig Cancer Research (United States). E.G. is Director of Research with the National Fund for Scientific Research (FNRS) (Belgium), N.W. is Research Fellow supported by the Fund for Research and Education within Industry and Agriculture (FRIA) from the FNRS (Belgium).

The authors gratefully acknowledge Ms Susana Leubat, Ms Solange Gros, Ms Véronique Noguet, Ms Marie-Carmen Silva and Mr Alain Michel for the technical assistance.

References

[1] F.S. Hodi, S.J. O'Day, D.F. McDermott, R.W. Weber, J.A. Sosman, J.B. Haanen, R. Gonzalez, C. Robert, D. Schadendorf, J.C. Hassel, W. Akerley, A.J.M. van den Eertwegh, J. Lutzky, P. Lorigan, J.M. Vaubel, G.P. Linette, D. Hogg, C.H. Ottensmeier, C. Lebbé, C. Peschel, et al., Improved survival with ipilimumab in patients with metastatic melanoma, N. Engl. J. Med., 363 (2010) 711–23.

[2] A.J. Miller, M.C. Mihm, Melanoma, N. Engl. J. Med., 355 (2006) 51–65.

[3] V. Gray-Schopfer, C. Wellbrock, R. Marais, Melanoma biology and new targeted therapy, Nature, 445 (2007) 851–7.

[4] M.S. Soengas, S.W. Lowe, Apoptosis and melanoma chemoresistance, Oncogene, 22 (2003) 3138–51.

[5] C.M. Balch, J.E. Gershenwald, S.-J. Soong, J.F. Thompson, M.B. Atkins, D.R. Byrd, A.C. Buzaid, A.J. Cochran, D.G. Coit, S. Ding, A.M. Eggermont, K.T. Flaherty, P.A. Gimotty, J.M. Kirkwood, K.M. McMasters, M.C. Mihm, D.L. Morton, M.I. Ross, A.J. Sober, V.K. Sondak, Final version of 2009 AJCC melanoma staging and classification, J. Clin. Oncol., 27 (2009) 6199–206.

[6] F.L. Greene, L.H. Sobin, The staging of cancer: a retrospective and prospective appraisal, CA. Cancer J. Clin., 58 (2008) 180–90.

[7] U. Sundram, J.D. Harvell, R. V Rouse, Y. Natkunam, Expression of the B-cell proliferation marker MUM1 by melanocytic lesions and comparison with S100, gp100 (HMB45), and MelanA, Mod. Pathol., 16 (2003) 802–10.

[8] E.R. Farmer, R. Gonin, M.P. Hanna, Discordance in the histopathologic diagnosis of melanoma and melanocytic nevi between expert pathologists, Hum. Pathol., 27 (1996) 528–31.

[9] S.J. Ohsie, G.P. Sarantopoulos, A.J. Cochran, S.W. Binder, Immunohistochemical characteristics of melanoma, J. Cutan. Pathol., 35 (2008) 433–44.

[10] P. Gerami, A. Zembowicz, Update on fluorescence in situ hybridization in melanoma: state of the art, Arch. Pathol. Lab. Med., 135 (2011) 830–7.

[11] J. Song, W.J. Mooi, V. Petronic-Rosic, C.R. Shea, T. Stricker, T. Krausz, Nevus versus melanoma: to FISH, or not to FISH, Adv. Anat. Pathol., 18 (2011) 229–34.

[12] J. Bauer, B.C. Bastian, Distinguishing melanocytic nevi from melanoma by DNA copy number changes: comparative genomic hybridization as a research and diagnostic tool, Dermatol. Ther., 19 40–9.

[13] D. Hanahan, R.A. Weinberg, Hallmarks of cancer: the next generation, Cell, 144 (2011) 646–674.

[14] D. Hanahan, R.A. Weinberg, The hallmarks of cancer, Cell, 100 (2000) 57–70.

[15] F. Pagès, J. Galon, M.-C. Dieu-Nosjean, E. Tartour, C. Sautès-Fridman, W.-H. Fridman, Immune infiltration in human tumors: a prognostic factor that should not be ignored, Oncogene, 29 (2010) 1093–102.

[16] J. Galon, F. Pagès, F.M. Marincola, M. Thurin, G. Trinchieri, B.A. Fox, T.F. Gajewski, P.A. Ascierto, The immune score as a new possible approach for the classification of cancer, J. Transl. Med., 10 (2012) 1.

[17] R.D. Schreiber, L.J. Old, M.J. Smyth, Cancer immunoediting: integrating immunity's roles in cancer suppression and promotion, Science, 331 (2011) 1565–70.

[18] F. Azimi, R.A. Scolyer, P. Rumcheva, M. Moncrieff, R. Murali, S.W. McCarthy, R.P. Saw, J.F. Thompson, Tumor-infiltrating lymphocyte grade is an independent predictor of sentinel lymph node status and survival in patients with cutaneous melanoma, J. Clin. Oncol., 30 (2012) 2678–83.

[19] M.C. Mihm, C.G. Clemente, N. Cascinelli, Tumor infiltrating lymphocytes in lymph node melanoma metastases: a histopathologic prognostic indicator and an expression of local immune response, Lab. Invest., 74 (1996) 43–7.

[20] R.-R. Ji, S.D. Chasalow, L. Wang, O. Hamid, H. Schmidt, J. Cogswell, S. Alaparthy, D. Berman, M. Jure-Kunkel, N.O. Siemers, J.R. Jackson, V. Shahabi, An immune-active tumor microenvironment favors clinical response to ipilimumab, Cancer Immunol. Immunother., 61 (2012) 1019–31.

[21] W.H. Fridman, J. Galon, F. Pagès, E. Tartour, C. Sautès-Fridman, G. Kroemer, Prognostic and predictive impact of intra- and peritumoral immune infiltrates, Cancer Res., 71 (2011) 5601–5.

[22] A. Ladányi, J. Kiss, A. Mohos, B. Somlai, G. Liszkay, K. Gilde, Z. Fejös, I. Gaudi, J. Dobos, J. Tímár, Prognostic impact of B-cell density in cutaneous melanoma, Cancer Immunol. Immunother., 60 (2011) 1729–38.

[23] G. Erdag, J.T. Schaefer, M.E. Smolkin, D.H. Deacon, S.M. Shea, L.T. Dengel, J.W. Patterson, C.L. Slingluff, Immunotype and immunohistologic characteristics of tumor-infiltrating immune cells are associated with clinical outcome in metastatic melanoma, Cancer Res., 72 (2012) 1070–80.

[24] S. Inoue, W.W. Leitner, B. Golding, D. Scott, Inhibitory effects of B cells on antitumor immunity, Cancer Res., 66 (2006) 7741–7.

[25] E. Goormaghtigh, J.-M. Ruysschaert, V. Raussens, Evaluation of the information content in infrared spectra for protein secondary structure determination, Biophys. J., 90 (2006) 2946–57.

[26] E. Goormaghtigh, R. Gasper, A. Benard, A. Goldsztein, V. Raussens, Protein secondary structure content in solution, films and tissues: Redundancy and complementarity of the information content in circular dichroism, transmission and ATR FTIR spectra, Biochim Biophys.Acta-Proteins Proteomics, 1794 (2009) 1332–1343.

[27] A. Derenne, O. Vandersleyen, E. Goormaghtigh, Lipid quantification method using FTIR spectroscopy applied on cancer cell extracts, Biochim. Biophys. Acta, 1841 (2014) 1200–9.

[28] A. Derenne, T. Claessens, C. Conus, E. Goormaghtigh, Infrared spectroscopy of membrane lipids, in: Encycl. Biophys., 2013: pp. 1074–1081.

[29] D. Naumann, Infrared Spectroscopy in Microbiology, (2000) 102–131.

[30] S. Boydston-White, M. Romeo, T. Chernenko, A. Regina, M. Miljković, M. Diem, Cell-cycle-dependent variations in FTIR micro-spectra of single proliferating HeLa cells: principal component and artificial neural network analysis, Biochim. Biophys. Acta, 1758 (2006) 908–14.

[31] S. Boydston-White, T. Chernenko, A. Regina, M. Miljković, C. Matthäus, M. Diem, Microspectroscopy of single proliferating HeLa cells, Vib. Spectrosc., 38 (2005) 169–177.

[32] A. Derenne, R. Gasper, E. Goormaghtigh, The FTIR spectrum of prostate cancer cells allows the classification of anticancer drugs according to their mode of action, Analyst, 136 (2011) 1134–41.

[33] I.W. Levin, R. Bhargava, Fourier transform infrared vibrational spectroscopic imaging: integrating microscopy and molecular recognition, Annu. Rev. Phys. Chem., 56 (2005) 429–74.

[34] M. Diem, M. Romeo, S. Boydston-White, M. Miljkovic, C. Matthaus, A decade of vibrational micro-spectroscopy of human cells and tissue (1994-2004), Analyst, 129 (2004) 880–5.

[35] B. Bird, M. Miljkovic, M.J. Romeo, J. Smith, N. Stone, M.W. George, M. Diem, Infrared micro-spectral imaging: distinction of tissue types in axillary lymph node histology, BMC Clin. Pathol., 8 (2008) 8.

[36] D.C. Fernandez, R. Bhargava, S.M. Hewitt, I.W. Levin, Infrared spectroscopic imaging for histopathologic recognition, Nat. Biotechnol., 23 (2005) 469–74.

[37] R. Bhargava, Towards a practical Fourier transform infrared chemical imaging protocol for cancer histopathology, Anal. Bioanal. Chem., 389 (2007) 1155–69.

[38] Z. Hammody, R.K. Sahu, S. Mordechai, E. Cagnano, S. Argov, Characterization of malignant melanoma using vibrational spectroscopy, ScientificWorldJournal., 5 (2005) 173–82.

[39] S. Mordechai, R.K. Sahu, Z. Hammody, S. Mark, K. Kantarovich, H. Guterman, A. Podshyvalov, J. Goldstein, S. Argov, Possible common biomarkers from FTIR microspectroscopy of cervical cancer and melanoma, J. Microsc., 215 (2004) 86–91.

[40] E. Ly, N. Cardot-Leccia, J.-P. Ortonne, M. Benchetrit, J.-F. Michiels, M. Manfait, O. Piot, Histopathological characterization of primary cutaneous melanoma using infrared microimaging: a proof-of-concept study, Br. J. Dermatol., 162 (2010) 1316–23.

[41] A. Tfayli, O. Piot, A. Durlach, P. Bernard, M. Manfait, Discriminating nevus and melanoma on paraffin-embedded skin biopsies using FTIR microspectroscopy, Biochim. Biophys. Acta, 1724 (2005) 262–9.

[42] C. Krafft, R. Salzer, G. Soff, M. Meyer-Hermann, Identification of B and T cells in human spleen sections by infrared microspectroscopic imaging, Cytometry. A, 64 (2005) 53–61.

[43] B. Bird, K. Bedrossian, N. Laver, M. Miljković, M.J. Romeo, M. Diem, Detection of breast micro-metastases in axillary lymph nodes by infrared micro-spectral imaging, Analyst, 134 (2009) 1067–76.

[44] E. Ly, O. Piot, R. Wolthuis, A. Durlach, P. Bernard, M. Manfait, Combination of FTIR spectral imaging and chemometrics for tumour detection from paraffin-embedded biopsies, Analyst, 133 (2008) 197–205.

[45] E. Goormaghtigh, J.. Ruysschaert, Subtraction of atmospheric water contribution in Fourier transform infrared spectroscopy of biological membranes and proteins, Spectrochim. Acta, 50 (1994) 2137–2144.

[46] E. Goormaghtigh, FTIR Data Processing and Analysis Tools, in: A. Barth, P.I.Haris (Eds.), Adv. Biomed. Spectrosc. (Biological Biomed. Infrared Spectrosc., IOS Press, 2009: pp. 104–128.

[47] A. Benard, C. Desmedt, M. Smolina, P. Szternfeld, M. Verdonck, G. Rouas, N. Kheddoumi, F. Rothé, D. Larsimont, C. Sotiriou, E. Goormaghtigh, Infrared imaging in

breast cancer: automated tissue component recognition and spectral characterization of breast cancer cells as well as the tumor microenvironment, Analyst, 139 (2014) 1044–56.

[48] S. Wold, K. Esbensen, P. Geladi, Principal component analysis, Chemom. Intell. Lab. Syst., 2 (1987) 37–52.

[49] H. Abdi, L.J. Williams, Principal component analysis, Wiley Interdiscip. Rev. Comput. Stat., 2 (2010) 433–459.

[50] A. Benard, E. Goormaghtigh, Discrimination of breast tissue structures by FT-IR FPA imaging, in: n.d.

[51] P. Lasch, W. Haensch, D. Naumann, M. Diem, Imaging of colorectal adenocarcinoma using FT-IR microspectroscopy and cluster analysis, Biochim. Biophys. Acta, 1688 (2004) 176–86.

[52] L. Wang, B. Mizaikoff, Application of multivariate data-analysis techniques to biomedical diagnostics based on mid-infrared spectroscopy, Anal. Bioanal. Chem., 391 (2008) 1641–54.

[53] R. Kumar, A. Indrayan, Receiver operating characteristic (ROC) curve for medical researchers, Indian Pediatr., 48 (2011) 277–287.

[54] G. Bellisola, C. Sorio, Infrared spectroscopy and microscopy in cancer research and diagnosis, Am. J. Cancer Res., 2 (2012) 1–21.

[55] D.R. Whelan, K.R. Bambery, L. Puskar, D. McNaughton, B.R. Wood, Quantification of DNA in simple eukaryotic cells using Fourier transform infrared spectroscopy, J. Biophotonics, 6 (2013) 775–84.

[56] M.L. Turgeon, Clinical Hematology: Theory and Procedures, Lippincott Williams & Wilkins, 2005.

[57] A. Baldi, P. Pasquali, E.P. Spugnini, Skin Cancer: A Practical Approach, Springer Science & Business Media, 2013.

[58] N.J.W. de Wit, G.N.P. van Muijen, D.J. Ruiter, Immunohistochemistry in melanocytic proliferative lesions, Histopathology, 44 (2004) 517–41.

[59] C. Vanison, N. Tanna, A.S. Murthy, Comparative genomic hybridization for the diagnosis of melanoma, Eur. J. Plast. Surg., 33 (2010) 45–48.

[60] M. Verdonck, S. Garaud, H. Duvillier, K. Willard-Gallo, E. Goormaghtigh, Label-free phenotyping of peripheral blood lymphocytes by infrared imaging, Analyst, (2014).

[61] A.I. Mazur, J.L. Monahan, M. Miljković, N. Laver, M. Diem, B. Bird, Vibrational spectroscopic changes of B-lymphocytes upon activation, J. Biophotonics, 6 (2013) 101–9.

[62] B.R. Wood, B. Tait, D. McNaughton, Fourier-transform infrared spectroscopy as a tool for detecting early lymphocyte activation: a new approach to histocompatibility matching, Hum. Immunol., 61 (2000) 1307–14.

[63] D. Bogunovic, D.W. O'Neill, I. Belitskaya-Levy, V. Vacic, Y.-L. Yu, S. Adams, F. Darvishian, R. Berman, R. Shapiro, A.C. Pavlick, S. Lonardi, J. Zavadil, I. Osman, N. Bhardwaj, Immune profile and mitotic index of metastatic melanoma lesions enhance clinical staging in predicting patient survival, Proc. Natl. Acad. Sci. U. S. A., 106 (2009) 20429–34.

Tables

Histological class	Number of individual spectra	Number of biopsies N=34	Number of patients N=14
Melanoma cells	16139	33	13
Connective tissue	10343	28	12
T cells	6325	21	11
B cells	8675	27	12
Germinal center B cells	2935	14	9
Erythrocytes	6103	22	11
Endothelial cells	2853	9	6
TOTAL	**53358**		

Table 1: Description of the spectral database. For each cell type, the table indicates the number of individual spectra, the number of biopsies and the number of patients collected for this study.

a.

TRAINING SET	TEST SET
LAU 818 (6) LAU 371 (2) LAU 444 (1) LAU 672 (3) LAU 1022 (1) LAU 392 (7) LAU 936 (1) LAU 1129 (4)	LAU 321 (1) LAU 648 (3) LAU 1017 (1) LAU 205 (2) LAU 1015 (1)
8 patients/ 25 biopsies/ 38354 spectra	5 patients/ 8 biopsies/12151 spectra

b.

TRAINING SET	TEST SET
LAU 392 (7) LAU 936 (1) LAU 1129 (4) LAU 321 (1) LAU 648 (3) LAU 1017 (1) LAU 205 (2) LAU 1015 (1)	LAU 818 (6) LAU 371 (2) LAU 444 (1) LAU 672 (3) LAU 1022 (1)
8 patients/ 20 biopsies/30074 spectra	5 patients/ 13 biopsies/ 20431 spectra

Table 2: Repartition of the patients in the training set and the test set for the two PLS-DA models built for the recognition of the five main cell types identified in melanoma metastases: melanoma cells, erythrocytes, connective tissue, endothelial cells and lymphocytes (a and b, respectively, for the first and second model). Patients are represented by their code and the number of biopsies used for each patient is written in brackets. The total number of patients, biopsies and spectra used for each set are indicated below each column.

a.

		PREDICTED AS					
	%	Epithelial cells	Erythrocytes	Lymphocytes	Connective tissue	Sensitivity	Specificity
TRUE	Epithelial cells	**95,0 ± 2,1**	0,0 ± 0,0	2,0 ± 0,1	3,1 ± 2,0	95,0	85,7
	Erythrocytes	0,0 ± 0,0	**100,0 ± 0,0**	0,0 ± 0,0	0,0 ± 0,0	100,0	100,0
	Lymphocytes	18,2 ± 1,3	0,0 ± 0,0	**81,8 ± 1,2**	0,1 ± 0,1	81,8	98,8
	Connective tissue	10,5 ± 4,9	0,1 ± 0,1	0,0 ± 0,0	**89,5 ± 4,9**	89,5	98,6

b.

		PREDICTED AS	
	%	Melanoma cells	Endothelial cells
TRUE	Melanoma cells	**91,7 ± 5,8**	8,3 ± 5,8
	Endothelial cells	2,7 ± 1,7	**97,3 ± 1,7**

Table 3: Validation of the cell type recognition models: a. for the 4 main histological classes (epithelial cells, erythrocytes, lymphocytes and connective tissue) and b. for the 2 subclasses of epithelial cells (melanoma cells and endothelial cells). The confusion matrix was obtained by averaging the two matrices obtained on the two different test sets (see Table 1) and show the mean ± standard deviation.

Figures

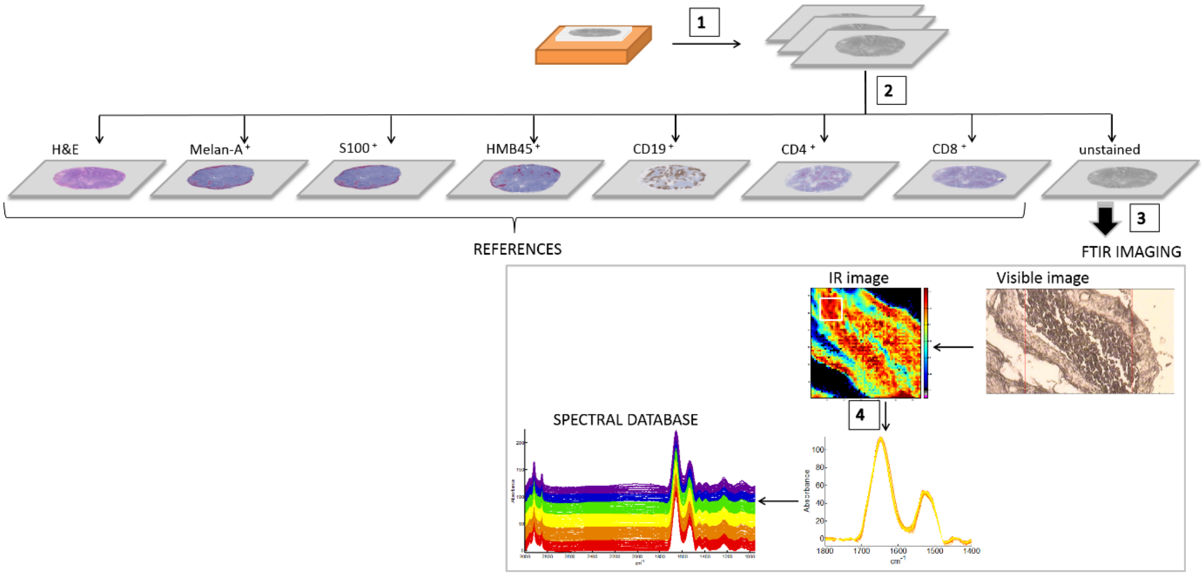

Figure 1: Schematic representation of the experimental workflow. 1. Each formalin-fixed and paraffin-embedded (FFPE) melanoma metastasis was cut in eight adjacent sections of 5 µm thickness. 2. The first section was H&E stained and six of them were immunostained with 6 antibodies (anti-HMB45, anti-S100, anti-Melan-A, anti-CD19, anti-CD4 and anti-CD8). The last one remained unstained and was used to record IR measurements. The stained sections were used as references to localize the areas of measurements. 4. For each infrared image (composed of 4096 spectra) one hundred spectra of a particular cell type were selected to build a spectral database.

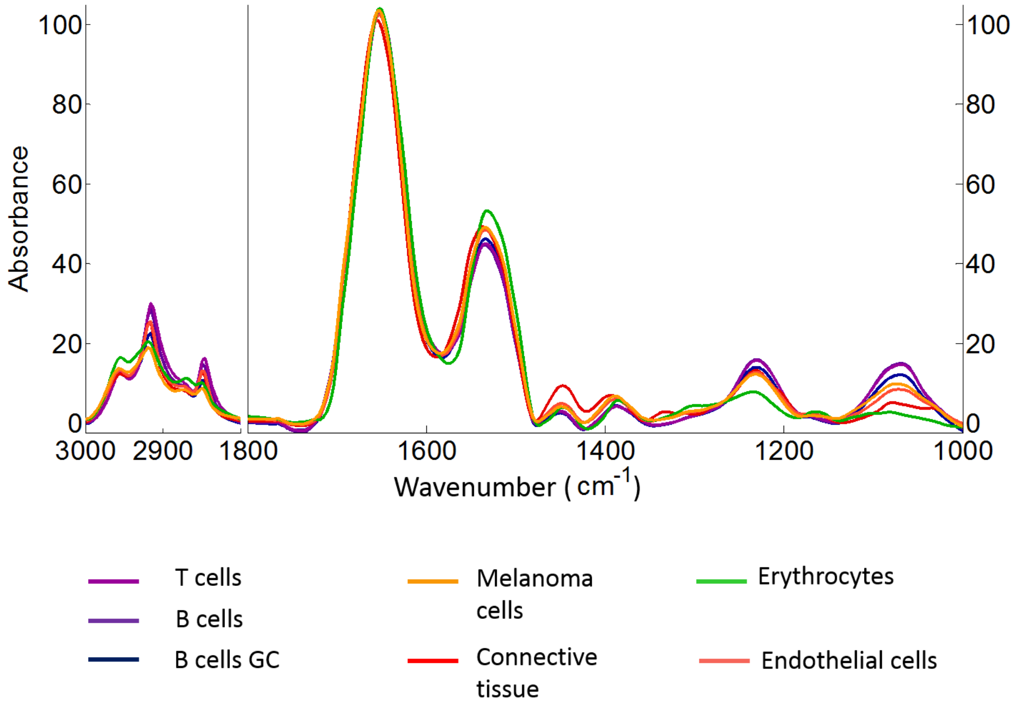

Figure 2: Mean IR spectra of the main cell types constituting melanoma metastases in lymph nodes. Each mean spectrum is the average of at least 2500 spectra.

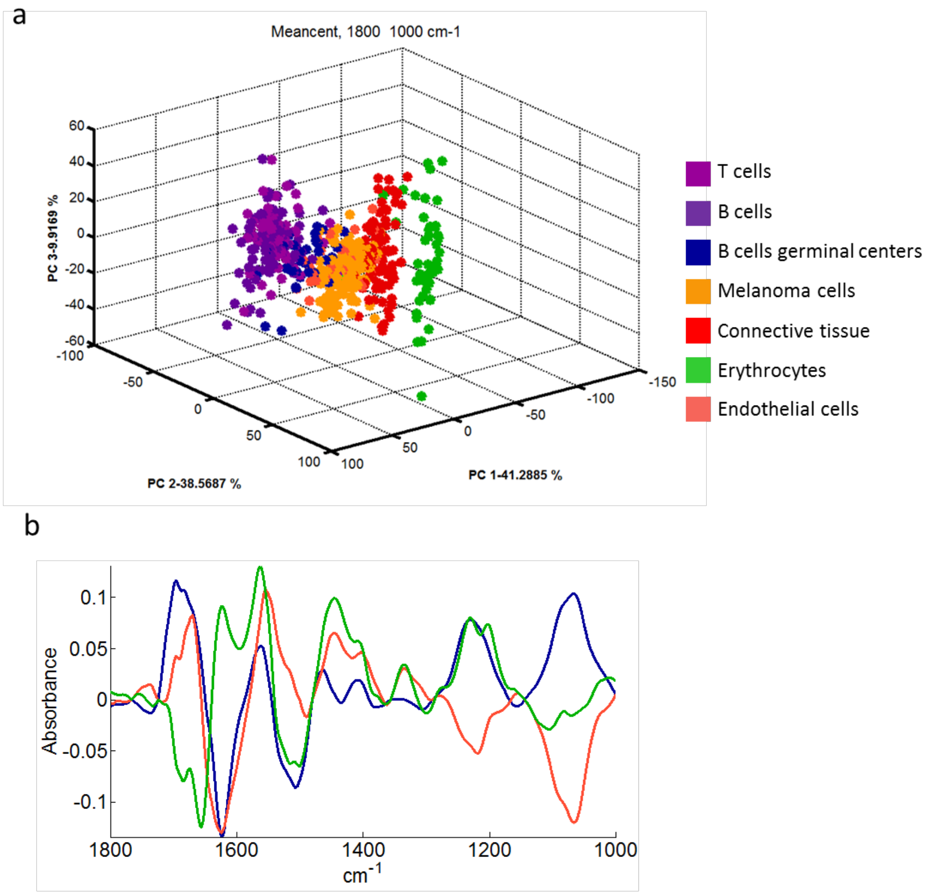

Figure 3: PCA analysis of the infrared spectra of various cell types. a. PCA score plot of the 500 mean spectra averaged each from around 100 individual spectra. b. Representation of the first three PCs: PC1 in blue, PC2 in red and PC3 in green (1800-1000 cm^{-1} range). The variance explained by each PC is indicated (in %) on the axes.

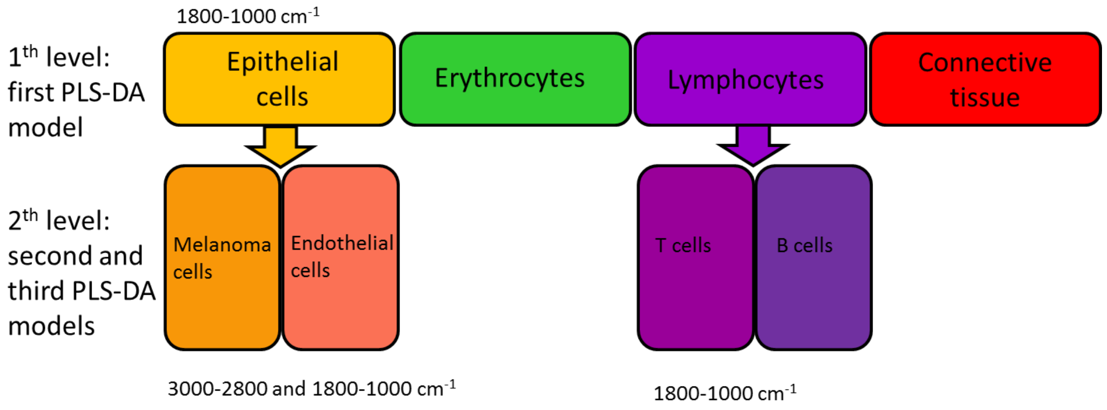

Figure 4: Schematic representation of the strategy used for spectral histopathology recognition. Three different PLS-DA models were built. A first level model discriminated the 4 main cell types: epithelial cells, erythrocytes, lymphocytes and connective tissue. A second level model distinguished the melanoma cells from the endothelial cells. Finally, a third model of second level identified subtypes of lymphocytes: T cells and B cells.

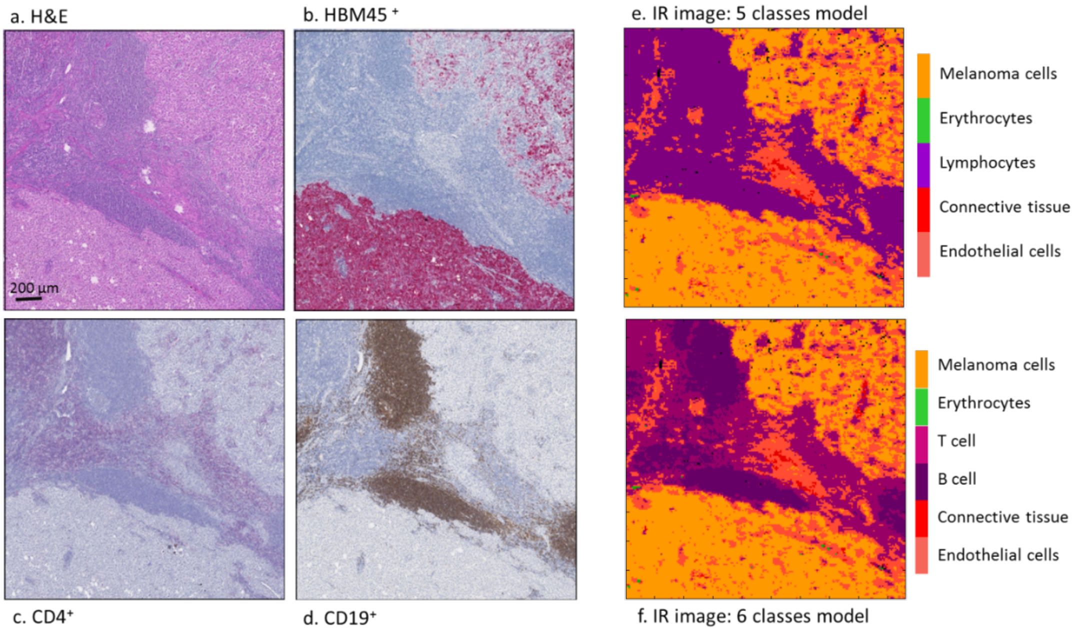

Figure 5: Application of two-level models for the identification of cell types. Visible images of a H&E stained section of a melanoma metastasis in a lymph node of 2.2x2.2 mm (a), HMB45$^+$ immunostained adjacent section (b), CD4$^+$ immunostained section (c), CD19$^+$ immunostained section (d) and IR images of the corresponding area of the unstained section from which the spectra where predicted with different PLS-DA models. e. A first level model was applied to predict the membership of the spectra to one of the 4 main classes and a second level model was then applied on the spectra predicted to the epithelial class to identify them as belonging to melanoma cells (orange) or endothelial cells (pink). f. Application of the third PLS-DA model to identify T cells and B cells. Pixels were 2x2 binned. The patient was not included in the training set of any of the three models.

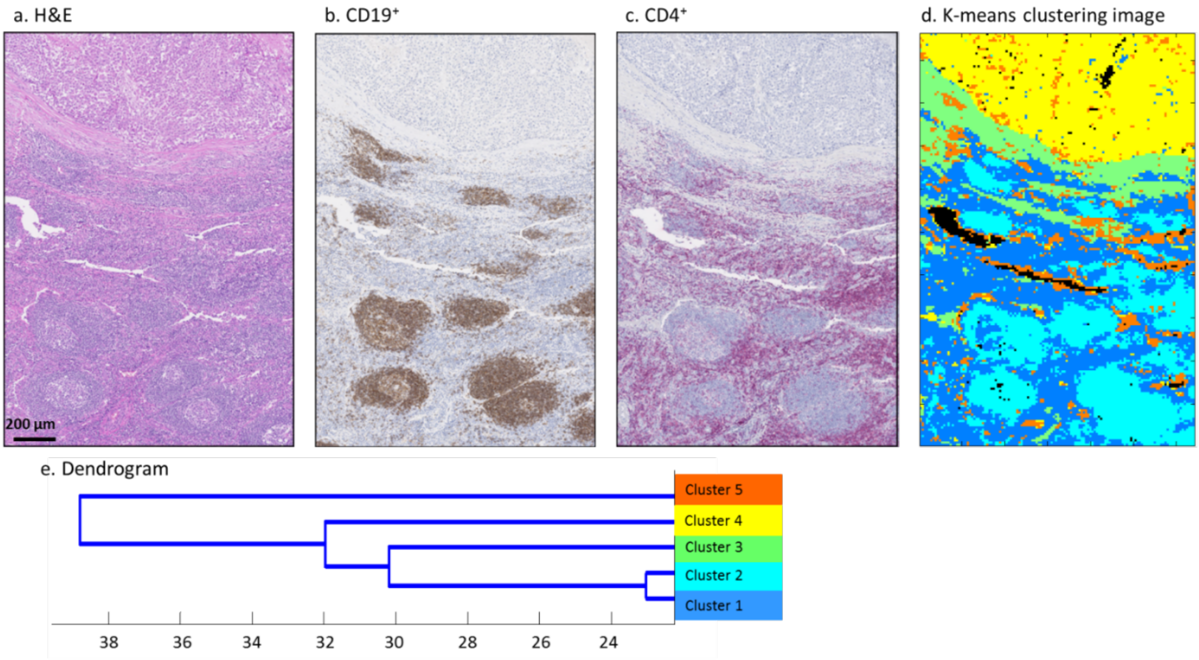

Figure 6: Identification of lymphocyte subtypes. a. Visible images of an H&E stained section of melanoma metastasis in lymph node. The field of view is 1.5x2.2 mm^2 (a), adjacent CD19+ immunostained section (b), adjacent CD4+ immunostained section (c), and infrared image of the unstained section (d). A K-means clustering analysis was applied on the centroids. Each cluster is represented by a color, with the corresponding dendrogram (e). Pixels were binned 2x2.

Figure 7: Difference spectra obtained in subtracting spectra of the cluster corresponding to B cells from the spectra of the cluster corresponding to the T cells for 5 different biopsies (a to e).

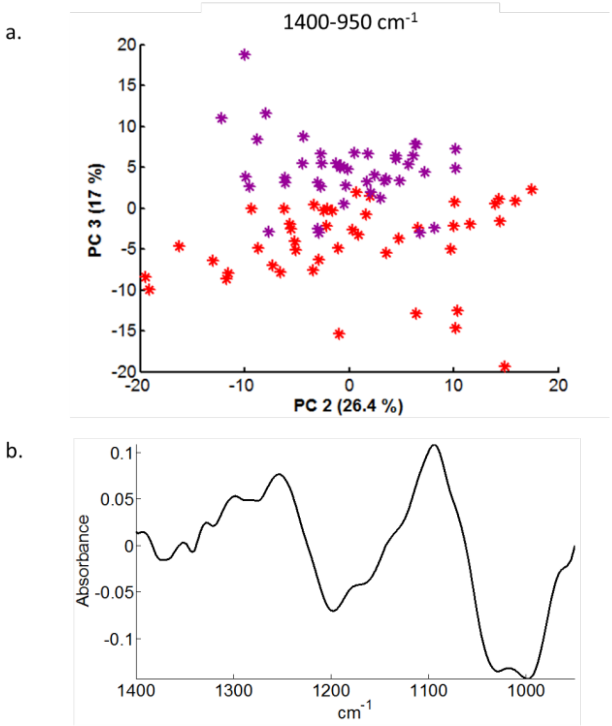

Figure 8: a. PCA score plot of the mean spectra of lymphocytes recorded from 8 metastatic lymph nodes (in red) and 8 non-metastatic lymph nodes (in purple) of 8 patients. b. Representation of the third principal component responsible for the discrimination.

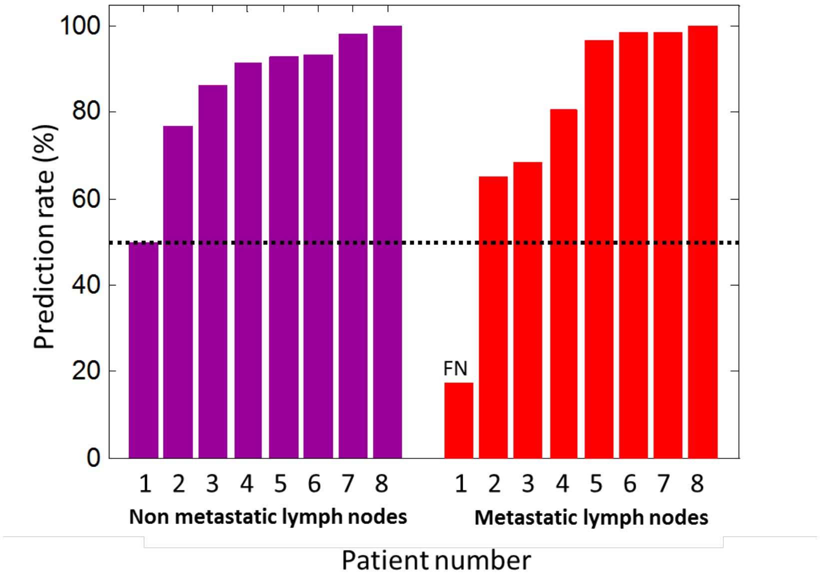

Figure 9: Validation of the PLS-DA model. Each bar of the chart corresponds to one of the 16 models built to recognize spectra of lymphocytes as belonging to metastatic or non-metastatic lymph nodes. The bar height corresponds to the percentage of spectra correctly predicted as belonging to one of the class. The PLS-DA models were trained on the 1800-950 cm^{-1}) spectral region.

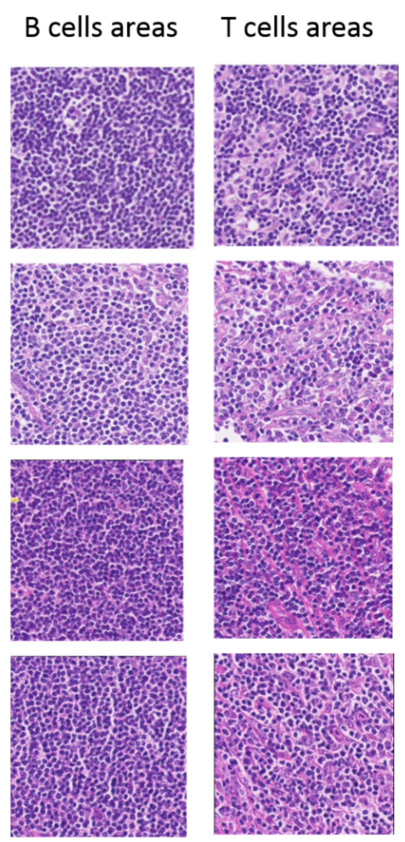

Figure 10: Images of H&E stained sections on areas composed mainly of lymphocytes from 5 different biopsies (corresponding to the 5 ones presented in Figure 7). The left column corresponds to B cells and the right column to T cells. The areas were identified based on the adjacent immunostained sections ($CD19^+$ for B cells and $CD4^+/CD8^+$ for the T cells). The size of each image is around 180 µm x 180 µm corresponding to the size of one IR image.

SUPPLEMENTARY DATA

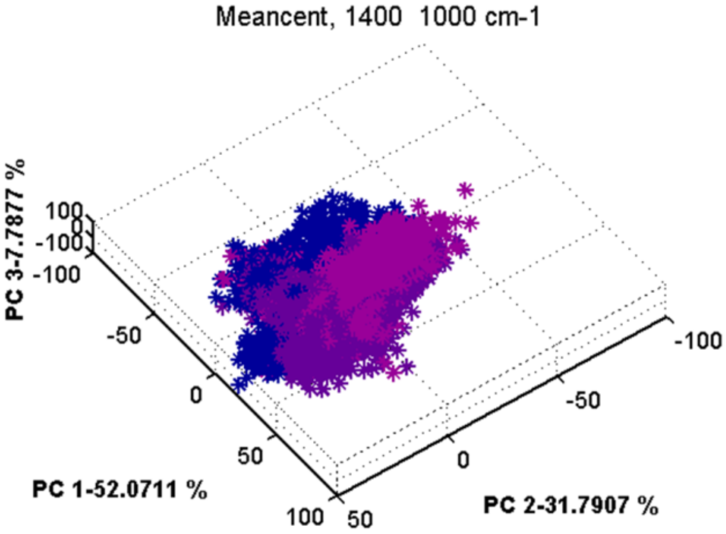

Figure S1: Score plot of the PCA calculated from individual spectra of T cells, B cells and B cells from the germinal centers from the database of spectra as described in Table 1.

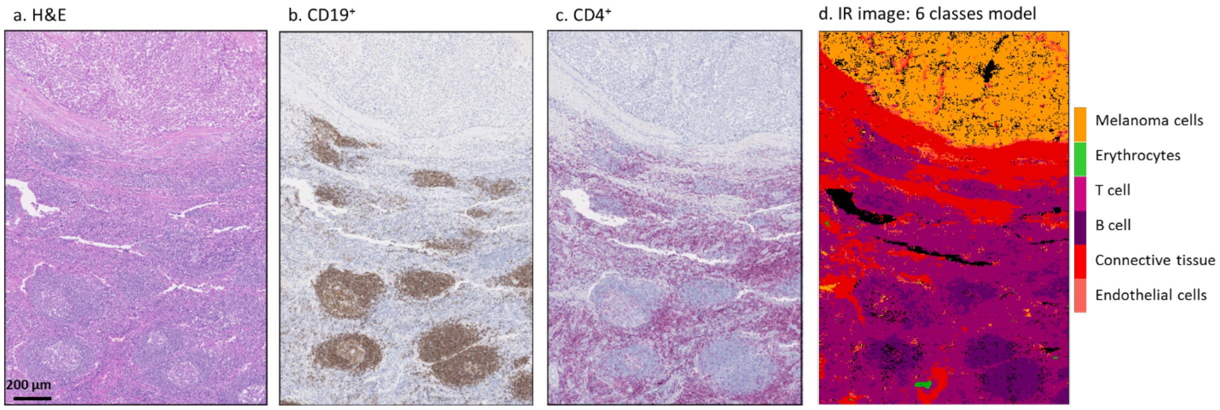

Figure S2: Identification of lymphocyte sub-types by infrared imaging. Visible image of an H&E stained section of a melanoma metastasis in lymph node. Image size is 1.5 x2.2 mm^2 (a), CD19$^+$ immunostained section (b), CD4$^+$ immunostained section (c), and IR image of the corresponding area of the unstained section from which the spectra where predicted with different PLS-DA models (d). A first level model was applied to predict the membership of the spectra to one of the 4 main classes, a second level model was then applied on the spectra predicted as “epithelial” to identify them as belonging to melanoma cells (orange) or endothelial cells (pink). Another second level model was applied to predict membership of lymphocytes to B or T cells. Pixels were binned 2x2. The patient was not included in the training set of any of the three models.

4 Adaptive immune resistance via CSF-1 produced by melanoma cells

In this study, we investigated the role of CSF-1 in modulating the anti-tumor response in ipilimumab-treated patients using IHC and *in vitro* co-cultures, revealing that melanoma cells produce CSF-1 via CTL-derived cytokines when attacked by CTLs, resulting in the recruitment of immunosuppressive monocytes. This work was performed in close collaboration with Natalie Neubert (Daniel Speiser Group). I contributed by gathering the FFPE tissues from ipilimumab treated patients, setting up the staining quantification method and analysing the results leading to Figure 3. I also performed CSF-1 quantification in the blood of these patients leading to Figure 1 and 4. None of the results presented here are published and should therefore be considered as preliminary and confidential.

Adaptive immune resistance via CSF-1 produced by melanoma cells

Natalie J. Neubert[1,2,*], Natacha Bordry[1,2,*], Sabine Hoves[3], Carola H. Ries[3], Petra Baumgaertner[1,2], Silvia A. Fuertes Marraco[1,2], Evdoxia Pavlidou[4], Periklis Foukas[5], Daniel E. Speiser[1,2]

*These authors contributed equally to this work.

1. Ludwig Cancer Research Center, University of Lausanne, Switzerland

2. Department of Oncology, Lausanne University Hospital (CHUV), Switzerland

3. Roche Innovation Center Penzberg, Oncology Division, Roche Pharmaceutical Research and Early Development, Penzberg, Germany

4. Roche Innovation Center Penzberg, Pathology Division, Roche Pharmaceutical Research and Early Development, Penzberg, Germany

5. Department of Pathology, Lausanne University Hospital (CHUV), Switzerland

Conflict of interest:

C.H. Ries and S. Hoves are employees of Roche Diagnostics GmbH and are inventors of granted and pending patent applications relating to RG7155. C.H. Ries holds stock and stock options in F. Hoffman La Roche. The other authors have no conflicts of interest in relation to this study.

Abstract

Colony stimulating factor-1 (CSF-1) is a key regulator of monocyte / macrophage migration and differentiation, and promotes their pro-tumorigenic functions. CSF-1-receptor (CSF-1R) blockade has shown promising results in the treatment of patients with tenosynovial giant cell tumors and in mouse models of cancer including melanoma. Here we investigated whether CSF-1 plays a role in patients with cutaneous melanoma. We first show that CSF-1 concentrations were significantly increased in the serum of 14 metastatic melanoma patients compared to healthy controls. Subsequently, our *in vitro* study demonstrates that CSF-1 remained undetectable in supernatant of melanoma cells, but reached high concentrations when co-cultured with melanoma-specific cytotoxic T lymphocytes (CTLs) or stimulated with tumor necrosis factor alpha (TNFα) and interferon gamma (IFNγ). Furthermore, immunohistochemical analysis of primary tumors and metastases revealed that CSF-1 and CSF-1R correlated with the frequencies of $CD8^+$ T cells and $CD163^+$ macrophages in the tumor microenvironment (TME). Finally, in peripheral blood mononuclear cells (PBMC) of these patients, CSF-1 concentrations correlated with $CD8^+$ T cell differentiation and the frequency of myeloid-derived suppressor cells (MDSC). Thus, CTLs attacking melanoma cells secrete TNFα and IFNγ, which in turn induce CSF-1 production by melanoma cells, resulting in the recruitment of immunosuppressive monocytes. These findings support the combined use of CSF-1R blockade with T cell based immunotherapy for melanoma patients.

Introduction

CSF-1 and its cognate receptor, CSF-1R, are known to regulate the migration, proliferation, differentiation and survival of monocytes, macrophages and their precursors (1). Triggering of CSF-1R also drives the recruitment of tumor-associated macrophages (TAMs) and promotes the differentiation of TAMs toward an immunosuppressive and pro-tumorigenic phenotype (2,3). TAMs represent key orchestrators of various tumor-promoting processes and have been identified as an independent poor prognosis factor in several cancer types (4). Indeed, clinical studies have shown that treatment with anti-CSF-1R antibody decreased CSF-1R$^+$CD163$^+$ TAMs and induces a shift toward higher CD8$^+$/CD4$^+$ T cell ratios in the TME of various tumor types (5). Furthermore, overexpression of CSF-1 has been correlated with poor prognosis in cancer of the reproductive system such as ovarian, uterine, breast and prostate cancers (6). Thus, there is ample evidence that in most types of solid tumors, TAMs are involved in tumor progression through their recruitment by CSF-1.

TAMs can suppress anti-tumor T cells in the TME (7). Recently, two reports using mouse melanoma models have observed that blockade of CSF-1R using the CSF-1R kinase inhibitor PLX3397 in combination with adoptive T cell therapy improves treatment efficacy as compared to single treatments (8,9). Both studies found a strong decrease in F4/80$^+$ TAMs as well as an increase of IFNγ secretion by tumor infiltrating CD8$^+$ T cells after combination therapy. Importantly, the anti-tumor effect of PLX3397 was dependent on CD8$^+$ T cells. Taken together these results suggest that CSF-1R blockade in combination with T cell therapy is a promising approach. However, it remains unclear, what triggers the CSF-1 production and whether CSF-1 also plays a role in human melanoma.

Here we investigated the role of CSF-1 in the context of anti-cytotoxic T-lymphocyte-associated protein-4 (CTLA-4) therapy (e.i. ipilimumab) in melanoma patients. We showed increased serum levels of CSF-1, and that melanoma cells themselves produced CSF-1.

Interestingly, melanoma cells did so only when attacked by CTLs, or when exposed to the CTL-derived cytokines TNFα and IFNγ.

Material and Methods

1. Patient population and samples

Human sample collection and use adhered to protocols approved by the Institutional Review and Privacy Board of the University Hospital of Lausanne (CHUV, Lausanne, Switzerland) (protocol N: 400/11-IPI-Biology) and the local ethics committee. All patients gave informed consent prior to study inclusion. Healthy volunteers or patients provided peripheral blood withdrawn by using tubes containing Li-heparin–coated beads (Sarstedt). Blood was centrifuged for 10 min at 210 × *g* for plasma preservation, followed by PBMC preparation by gradient centrifugation using Lymphoprep (Ficoll equivalent; Axis-Shield). All cells were used fresh or after cryopreservation. Viable cell recovery was consistently 85–100%. Patients in this study were diagnosed with metastatic melanoma and received a maximum of four cycles of 3 mg/kg ipilimumab intravenously every three week upon disease progression with at least one prior treatment. Blood samples were withdrawn at baseline, during treatment, 20 day after treatment, and then monthly for as long as 14 months after the last ipilimumab dose.

2. Cell culture

Melanoma cell lines were generated from metastasis or tumor-infiltrated lymph node specimens from HLA-A2$^+$ patients with histologically proven metastatic melanoma and were a kind donation from Donata Rimoldi. All melanoma cell lines were MLANA-positive (confirmed by FACS) and had dbeen cultured less than 6 months at the time of the experiments (<P26). Autologous or HLA-matched MLANA-specific CD8+ T cell clones (CTLs) were isolated from melanoma patient blood and amplified by restimulation with PHA, irradiated feeder cells, and hrIL-2 (10). The material originated from the following individuals: Melanoma patients listed in Figure 2A (melanoma cell lines), LAU1015 and LAU1185 (MLANA-specific CTLs), LAU5048 (yellow fever-specific CTLs), and healthy donors

(monocytes).

The complete Medium used was RPMI 1640 - GlutaMAX^{TM}-I, complemented with 10% heat-inactivated FCS, 1% non-essential amino acids (Gibco), 1% l-glutamine (Gibco), Hepes (10 mM), and 10,000 U/ml of penicillin/streptomycin (Gibco). Monocytes were enriched from whole blood by negative selection using the Rosette Sep (STEMCELL Technologies) (5) and cultured in RPMI 1640 - GlutaMAX^{TM}-I plus 10% fetal bovine serum (FBS), 4 mM L-glutamine with 100 ng/ml recombinant human (rhu)-CSF-1, or rhuGM-CSF for M2 or M1 macrophages, respectively (5). Melanoma culture supernatant was prepared in the same medium without additional CSF-1 or GM-CSF.

3. Flow cytometry

Data acquisition was performed with a Gallios flow cytometer (Beckman Coulter, 3-laser configuration) and the data were processed with FlowJo (Tree Star Inc., v9.7.7). The anti-human antibodies used were anti-CSF-1R (PE, clone 12-3A3-1B10, eBioscience) and the matched isotype control was rat IgG2a, kappa (PE, clone 12-4321-42, eBioscience).

4. ELISA

The CSF-1 concentration in culture supernatant and serum samples of ipilimumab-treated patients was determined using the human M-CSF Quantikine ELISA kit (R&D Systems) according to the kit instructions. The IFNγ concentration was measured by ELISA with anti-human IFNγ antibodies from Invitrogen (capture antibody: Cat. no. AHC4432; detection antibody: Cat. no. AHC4539).

5. mRNA analysis

mRNA was extracted from melanoma cells using the Pico Pure™ RNA isolation kit (Arcturus) according to the kit instructions and CSF-1 mRNA levels were determined with the NanoString nCounter™ technology at the iGE3Genomics platform, University of Geneva. The data analysis was done by Charlotte Soneson at the SIB.

6. IHC staining and quantification

IHC was performed on consecutive 4-µm paraffin sections from complete excisions of 8 primary melanoma and 13 cutaneous melanoma metastasis lesions from 15 patients. The tissue samples were acquired before inclusion of these patients in the ipilimumab clinical trial. The following primary antibodies were used: rabbit polyclonal anti-CSF-1 (Antigenix America), mouse monoclonal anti-CSF-1R (clone 29 pRED, Roche Penzberg), mouse monoclonal anti-CD8 (Ventana) and mouse monoclonal anti-CD163 (clone MRQ-26, Ventana). Slides were placed on a BenchMark XT slide stainer (Ventana; Roche), for deparaffinization, endogenous peroxidase quenching, and epitope retrieval. UltraView Universal DAB Detection Kit (Ventana) was used. All stains included a negative control with a matched antibody isotype, whereas staining of tonsillar sections served as positive controls for all antibodies.

Stained slides were scanned in a batch format by using the Vectra multispectral imaging system (Perkin-Elmer), and lower power field images of the entire tissue were first collected. Then, an average of 4 high power fields (HPF) (20x) was chosen in tumor regions with high and low infiltrating CD8$^+$ cells respectively (Figure S1). The same regions were selected for CSF-1, CD163 and CSF-1R staining. The selected 20× images were subsequently acquired and processed by using inForm tissue finder software (PerkinElmer). For unmixing of the images and analysis, the spectral libraries of hematoxylin and DAB were generated. For CSF-1 and CD8 staining, the HPFs selected were first segmented using the counterstained-based cell segmentation algorithm and the numbers of positive cells were then calculated through nuclei threshold analysis. For CSF-1R and CD163 staining, the HPFs were segmented using the object-based cell segmentation algorithm and the numbers of positive cells were also calculated through nuclei threshold analysis. Thresholds used to determine the cutoff for all four antibodies stains were set visually and approved by a trained pathologist.

7. Statistics

Correlation coefficients were computed using Spearman's non-parametric test or with linear regression. The non-parametric unpaired Mann–Whitney U test was used to assess statistical significance of differences between two data sets, and the non-parametric Wilcoxon sign rank test was used for paired samples. Data show the mean ± standard deviation of replicates, if not otherwise indicated. For all statistical analyses, asterisks indicate $^*P \leq 0.05$; $^{**}P \leq 0.01$; $^{***}P \leq 0.001$; $^{****}P \leq 0.0001$. Statistical tests in Figure 2 were done by David Barras (SIB, Lausanne, Switzerland).

Results

We analyzed serum samples from 15 patients with AJCC stage IV or unresectable stage III malignant melanoma. 12 healthy blood donors served as controls. Interestingly, in untreated melanoma patients, CSF-1 concentrations were statistically significantly increased as compared to healthy controls, demonstrating that metastatic melanoma triggers the production of CSF-1 (Figure 1A). In contrast, the comparison of patient's CSF-1 values before and after treatment with ipilimumab showed no difference (Figure 1B). However, a positive correlation trend was seen between baseline CSF-1 and lactate dehydrogenase (LDH) concentration in the serum of ipilimumab-treated patients (Figure 1C), suggesting that CSF-1 is increased with progressive disease.

We determined whether melanoma cells *in vitro* might contribute to the increased systemic CSF-1 levels observed in the blood of melanoma patients. CSF-1 remained low or undetectable in supernatants from melanoma cell cultures (Figure 2B). However, melanoma cells do not act in isolation *in vivo* but rather in interaction with the TME. Hence, we postulated that the immune microenvironment, particularly CTLs, could directly influence and induce melanoma cells to secrete CSF-1. Indeed, we found increased CSF-1 concentrations in co-cultures of melanoma cell lines with melanoma-specific CTLs, which was confirmed in all four cell lines tested. Co-cultures with yellow-fever-specific CTLs did not trigger melanoma

CSF-1 secretion, indicating that CTLs must be antigen-specific to trigger CSF-1 secretion by melanoma cells.

We subsequently assessed if the induction of CSF-1 secretion was dependent on a direct contact between CTLs and melanoma cells. This was not the case, since TNFα and IFNγ, two cytokines that are secreted by activated CTLs induced CSF-1 secretion by six different melanoma cell lines in absence of melanoma-specific CTLs (Figure 2C). These results indicate that CTL-derived cytokines alone are sufficient to trigger CSF-1 secretion in melanoma cells without the need of a direct cell-cell contact.

To establish the kinetics of this interaction, we then analyzed melanoma cells treated for different durations up to three days and using three different CTLs to melanoma cell ratios (Figure 2D and E). The more CTLs per tumor cells were seeded, the more IFNγ and CSF-1 was found in the supernatant. The highest IFNγ concentration in the co-culture was measured at 24h whereas the CSF-1 concentration still increased at 72h thus compatible with the notion that IFNγ induces CSF-1 secretion. TNFa concentrations in the co-culture remained low or undetectable supporting the hypothesis that IFNg is the main trigger for CSF1 secretion (data not shown).

To determine whether CSF-1 protein expression was regulated at the transcriptional level, we measured CSF-1 mRNA in melanoma cells after 24h of the above-mentioned different treatments. The results confirmed our findings at the protein level, since we found strong increases of CSF-1 mRNA in all four tested cell lines when cultured with melanoma-specific CTLs or the two cytokines TNFα and IFNγ, but not in presence of negative control CTLs (Figure 2F). These data show that the rapid and strong secretion of CSF-1 by melanoma cells is transcriptionally regulated.

Melanoma-derived CSF-1 might either act pro-tumorigenically in a direct manner, by autocrine signaling, or indirectly, via a third cell type in the tumor microenvironment. To test whether CSF-1 secreted by melanoma cells could potentially signal back into melanoma cells via CSF-1R, we analyzed the expression of CSF-1R on six different melanoma cell lines, untreated or cultured in the presence of TNFα and/or IFNγ. No CSF-1R could be detected on the melanoma cell lines under any of the tested conditions consistent with the idea that CSF-1 might not mediate autocrine signaling on melanoma cells (Figure S2).

To determine whether CSF-1 triggering by melanoma antigen-specific CTLs or CTLs derived cytokines may also occur *in vivo* in the TME, we quantified the expression of CD8, CSF-1, CSF-1R and CD163 in primary tumors and metastases from cutaneous melanoma patients. We found that tumor regions of high density of tumor-infiltrating $CD8^+$ T cells showed higher CSF-1^+, CSF-$1R^+$ and $CD163^+$ cells (Figure 3A and 3C-F) compared to regions of low density of tumor-infiltrating $CD8^+$ T cells within the same tumor (Figure 3G-J). Interestingly, these positive correlations were also observed when comparing different patients, i.e. the ones with high tumor-infiltrating $CD8^+$ T cells to those with low tumor-infiltrating $CD8^+$ T cells (Figure 3B).

Since the presence of activated T cells was associated with increased CSF-1 expression in the TME, we determined whether a similar association might also be detectable at the systemic level. Therefore we analyzed CSF-1 concentrations and T cell frequencies in the blood of patients after ipilimumab therapy. Indeed, CSF-1 concentrations correlated statistically significantly with the percentage of effector memory (EM) $CD8^+$ T cells (Figure 1A), and inversely with the percentage of effector memory RA (EMRA) $CD8^+$ T cells (Figure 1B), a population of T cells that arise in the absence of antigen (11). The concentrations of CSF-1 also correlated significantly with $ICOS^+$ $CD8^+$ T cells (Figure 4C). These cells have been shown to correlate with clinical outcome of patients treated with anti-CTLA-4 antibodies (reference). Finally, the concentrations of CSF-1 correlated negatively with Granzyme B^+ $CD8^+$ T cells (Figure 4D). Although difficult to interpret, these findings may suggest that the T cells are Granzyme low because of increased killing activity. Overall, our results indicate that specific and functional anti-tumor CD8$^+$ T cell responses trigger the secretion of CSF-1 by melanoma cells locally and systematically.

Discussion

In this study we demonstrated that melanoma patients have increased CSF-1 serum concentrations when compared to healthy donors. Exposure of melanoma cell lines to melanoma-specific CTLs or CTL-derived cytokines triggered their expression of CSF-1. This suggests that melanoma cells can contribute to the increased systemic CSF-1 levels and that this CSF-1 secretion is induced by T cell-derived IFNγ. In line with this observation, T cell-infiltrated tumor regions contained increased levels of CSF-1 and of CD163+ macrophages. Moreover, at the systemic level, increased levels of CSF-1 in patient serum correlated with an elevated frequency of CD8 effector memory T cells, a type of T cell that is increased in presence of its target antigen. In addition, CD8$^+$ ICOS$^+$ T cells and CD8$^+$ GrzB$^+$ T cells also showed correlations with CSF-1 plasma concentrations of melanoma patients. Taken together these findings suggest a model in which IFNγ is secreted by melanoma-specific T cells upon recognition of their target cells and then induces CSF-1 in neighboring melanoma cells. Then, the melanoma cell-derived CSF-1 leads to macrophage recruitment and differentiation.

The latter part of this hypothesis remains to be proven. Two recent reports have analyzed the influence of tumor-conditioned medium on macrophages, but their results are not conclusive. Solinas *et al.* found that the conditioned medium of only two out of 16 different cancer cell lines influenced monocyte differentiation towards the M2 type and these two pancreatic cancer cell lines showed CSF-1 concentrations similar to the concentrations in the supernatant of T cell- or cytokine-treated melanoma cells here (12). Three of the non-active supernatants in this study were also tested for CSF-1 concentration and showed undetectable CSF-1 levels. When CSF-1 was depleted from the supernatant or CSF-1R was blocked on monocytes, its differentiation activity was reduced or entirely abolished, suggesting that CSF-1 is the responsible molecule in the cancer cell supernatant for the differentiation of monocytes. In contrast, Wang *et al*. found that upon culture with melanoma-conditioned medium human monocytes expressed both M1 and M2 markers and neutralizing CSF-1 in the melanoma-conditioned medium did not influence the monocyte differentiation (13). To date it remains unclear whether melanoma derived factors influence human macrophages in a pro- or anti-tumorigenic manner. To shed light on the melanoma cell influence on macrophages in the context of immunotherapy, we now plan to culture human blood monocytes with supernatant of melanoma cells that had been treated with melanoma-specific T cells or T cell-derived cytokines.

In conclusion, our results support the development of melanoma therapy combining CSF-1R blockade with T cell immunotherapy. A clinical trial is currently recruiting patients with different tumor types, to study the combination of the CSF-1R kinase inhibitor PLX3397 and the anti-PD-1 antibody Pembrolizumab (NCT02452424).

Acknowledgements

Donata Rimoldi for melanoma cell lines. Susana Leuba, Katia Fortis, Esther Danenberg for tissue processing and IHC technical support. Sintia Winkler and Anne Wilson for flow cytometry support Olivier Michielin, Maurice Matter, Loredana Leyvraz, Laurène Cagnon, Samia Abed Maillard and Hélène Maby-El Hajjami for clinical (study) contributions. Mylène Docquier and her team at the iGE3Genomics platform, University of Geneva, for the support in conducting the NanoString experiment. Leon Pradel (Roche) for providing the protocol for CSF-1R FACS staining. Charlotte Soneson (SIB) for the analysis of the NanoString data and David Barras (SIB) for the statistical calculations in Figure 2.

Grant support

This work was supported by the ISREC Foundation, the Emma Muschamp Foundation (both Switzerland), the Cancer Research Institute, Ludwig Cancer Research (both USA), the

Wilhelm Sander-Foundation (Germany), and grants from Swiss Cancer Research (3507-08-2014), Swiss National Science Foundation (CRSII3_141879), and SwissTransMed (KIP 18)

Figure legend

Figure 1. CSF-1 concentration is increased in the blood of metastatic melanoma patients compared to healthy donors, and correlates with LDH levels. A) CSF-1 concentrations in sera of healthy donors (n=12) and in patients at baseline, i.e. before starting ipilimumab treatment (n=15). Mann-Whitney test. Error bars represent S.E.M **B)** Concentrations of CSF-1 before and after ipilimumab treatment (n=12); Wilcoxon test **C)** Linear regression of lactate deshydrogenase (LDH) concentrations in relation with CSF-1 concentrations measured at baseline in the serum of melanoma patients. Statistically significant differences are highlighted in bold when p values were < 0.05. (Ipi): ipilimumab

Figure 2. Melanoma cells produce CSF-1 when attacked by Melan-A-specific CTLs but not by irrelevant CTLs and this induction is mediated by TNFα and IFN. A) Melanoma cell lines were generated from surgery specimens of melanoma patients. **B, C and D)** CSF-1 protein concentrations and **E)** IFNγ protein concentrations in supernatants of melanoma cells cultured as indicated for (B) 24h, (C) 48h or up to (D and E) 72h. The co-cultures were seeded at the indicated CTL to melanoma cell ratio (x-axis), except from B, where a 1:1 ratio was seeded. **D)** Log2 CSF-1 mRNA expression of melanoma cells after 24h of the indicated treatment (n=3). Statistical tests: One-way Anova (B, F) and two-way Anova (C - E); *** P < 0.001, ** P < 0.01.

Figure 3. Tumor infiltrating CD8+ T cells are positively associated with CSF-1 expression and with an enhancement of CSF-1R$^+$ and CD163$^+$ cells in melanoma tissues. A) Spearman correlation of CD8 with CSF-1 (left panel), CSF-1R (middle panel) and CD163$^+$ cells/mm^2 (right panel) calculated per area. **B)** Spearman correlation of CD8 with CSF-1 (left panel), CSF-1R (middle panel) and CD163$^+$ cells/mm^2 (right panel) calculated per patient. Representative images of **(C)** CD8, **(D)** CSF-1, **(E)** CSF-1R and **(F)**

CD163 staining in a tumor region with high $CD8^+$ T cell infiltration and **(G)** CD8, **(H)** CSF-1, **(I)** CSF-1R and **(J)** CD163 staining in a tumor region with low $CD8^+$ T cell infiltration. Statistically significant differences are highlighted in bold, when p values were < 0.05.

Figure 4. CSF-1 serum levels correlated positively with effector memory (EM) $CD8^+$ T cells and negatively with effector memory $CD45RA^+$ (EMRA) $CD8^+$ T cells in blood of melanoma patients. Linear regression of average CSF-1 concentration in relation with average **(A)** EM, **(B)** EMRA, **(C)** ICOS and **(D)** Granzyme B $CD8^+$ T cell concentrations measured in the blood of patients during ipilimumab treatment. (EM): effector memory; (EMRA): effector memory $CD45RA^+$

Supplementary Figure S1. High and low tumor-infiltrating $CD8^+$ T cell regions defined in melanoma patient tissues using Vectra system (Perkin Elmer)

Supplementary Figure S2. No CSF-1R expression could be detected by flow cytometry on untreated or cytokine-treated melanoma cell lines. Six melanoma cell lines were left untreated (black non-solid line) or treated with TNFα and/or IFNγ for two days (red solid line). The peak with grey fill depicts the isotype control. Untreated monocytes enriched from human PBMCs were used as positive control.

References

1. Hume DA, MacDonald KPA. Therapeutic applications of macrophage colony-stimulating factor-1 (CSF-1) and antagonists of CSF-1 receptor (CSF-1R) signaling. Blood. 2012;119:1810–20.

2. Joyce JA, Pollard JW. Microenvironmental regulation of metastasis. Nat Rev Cancer. 2008;9:239–52.

3. Pyonteck SM, Akkari L, Schuhmacher AJ, Bowman RL, Sevenich L, Quail DF, et al. CSF-1R inhibition alters macrophage polarization and blocks glioma progression. Nat Med. 2013;19:1264–72.

4. Biswas SK, Mantovani A. Macrophage plasticity and interaction with lymphocyte subsets: cancer as a paradigm. Nat Immunol. 2010;11:889–96.

5. Ries CH, Cannarile MA, Hoves S, Benz J, Wartha K, Runza V, et al. Targeting Tumor-Associated Macrophages with Anti-CSF-1R Antibody Reveals a Strategy for Cancer Therapy. Cancer Cell. Elsevier Inc; 2014;25:846–59.

6. Pollard JW. Tumour-educated macrophages promote tumour progression and metastasis. Nat Rev Cancer. 2004;4:71–8.

7. Martinez FO, Helming L, Gordon S. Alternative Activation of Macrophages: An Immunologic Functional Perspective. Annu Rev Immunol. 2009;27:451–83.

8. Mok S, Koya RC, Tsui C, Xu J, Robert L, Wu L, et al. Inhibition of CSF-1 Receptor Improves the Antitumor Efficacy of Adoptive Cell Transfer Immunotherapy. Cancer Research. 2013.

9. Sluijter M, van der Sluis TC, van der Velden PA, Versluis M, West BL, van der Burg SH, et al. Inhibition of CSF-1R supports T-cell mediated melanoma therapy. PLoS ONE. 2014;9:e104230.

10. Speiser DE, Baumgaertner P, Voelter V, Devêvre E, Barbey C, Rufer N, et al. Unmodified self antigen triggers human CD8 T cells with stronger tumor reactivity than altered antigen. Proc Natl Acad Sci USA. 2008;105:3849–54.

11. Geginat J, Lanzavecchia A, Sallusto F. Proliferation and differentiation potential of human CD8(+) memory T-cell subsets in response to antigen or homeostatic cytokines. Blood. 2003;101:4260–6.

12. Solinas G, Schiarea S, Liguori M, Fabbri M, Pesce S, Zammataro L, et al. Tumor-Conditioned Macrophages Secrete Migration-Stimulating Factor: A New Marker for M2-Polarization, Influencing Tumor Cell Motility. J Immunol. 2010;185:642–52.

13. Wang T, Ge Y, Xiao M, Lopez-Coral A, Azuma R, Somasundaram R, et al. Melanoma-derived conditioned media efficiently induce the differentiation of monocytes to macrophages that display a highly invasive gene signature. Pigment Cell & Melanoma Research. 2012;25:493–505.

Figure 1

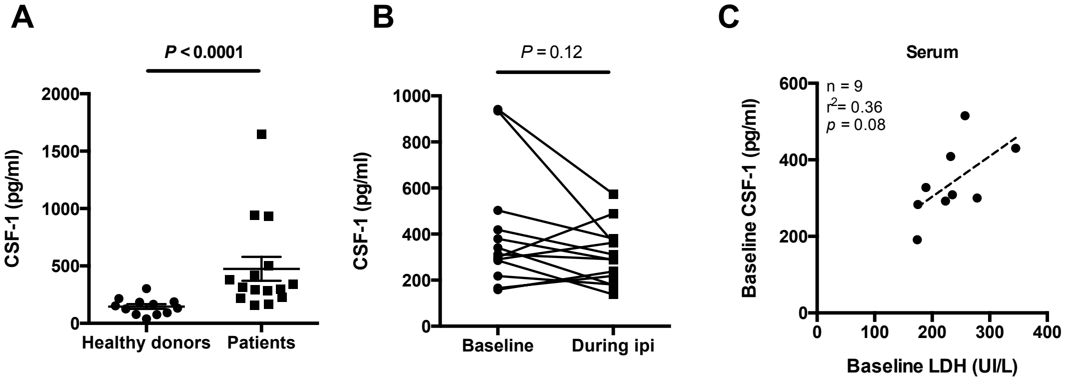
A
P < 0.0001
CSF-1 (pg/ml)
2000
1500
1000
500
0
Healthy donors
Patients
B
P = 0.12
CSF-1 (pg/ml)
1000
800
600
400
200
0
Baseline
During ipi
C
Serum
n = 9
r^2= 0.36
p = 0.08
Baseline CSF-1 (pg/ml)
600
400
200
0
0
100
200
300
400
Baseline LDH (UI/L)

Figure 2

A

Patient	Cell line	Gender	Source of cell line	HLA-A
LAU50	Me275	male	tumor-infiltrated lymph node	*02:01, *23:01
LAU203	Me290	female	tumor-infiltrated lymph node	1, *02:01
LAU444	T444C	female	metastasis	*02:01
LAU1013	T1013A	male	lymph node ing R	*02:01
LAU1015	T1015A	male	metastasis	*02:09, 32(19)
LAU1185	T1185B	female	metastasis	*02:01

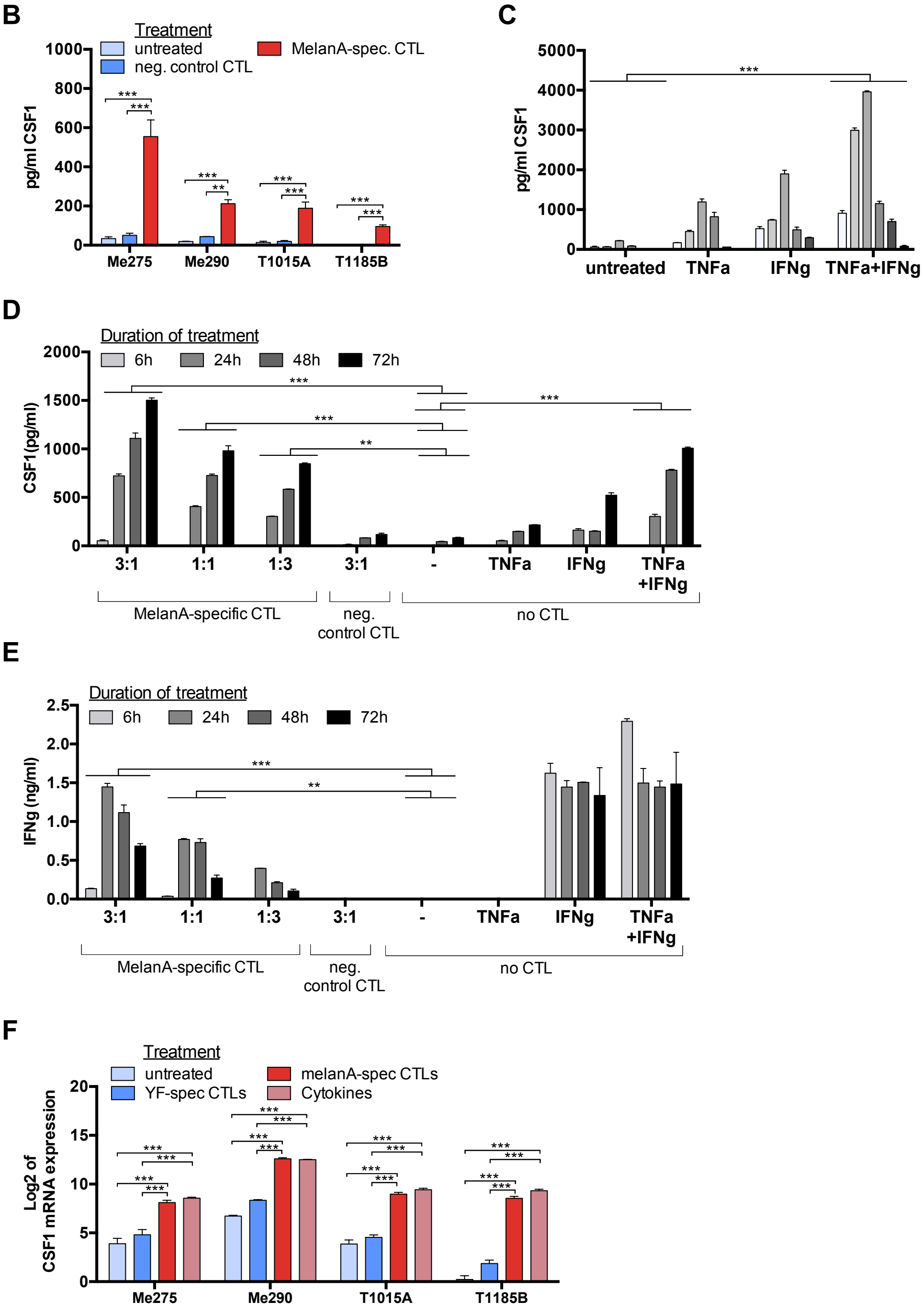

Figure 3

A

Per area

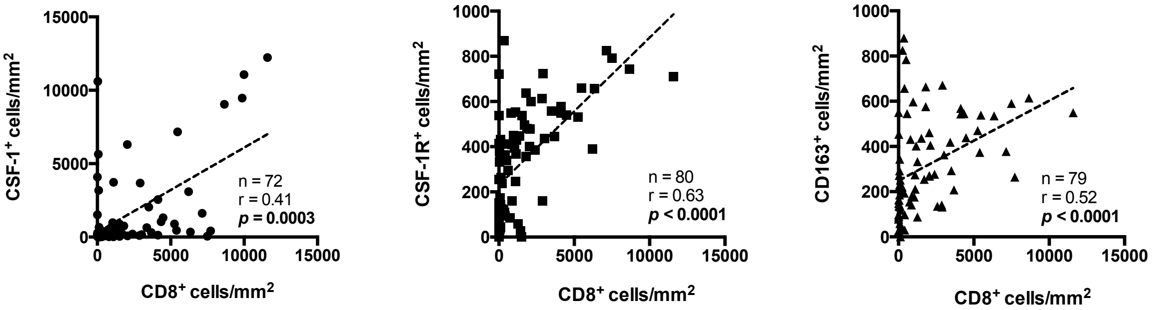

B

Per patient

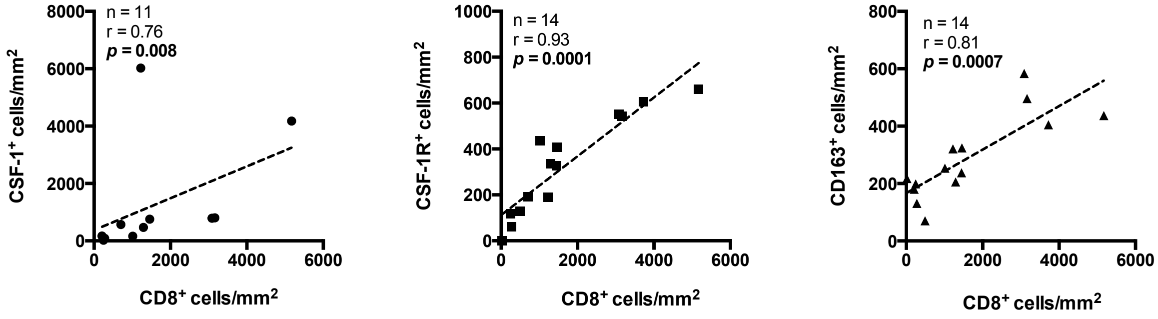

High tumor CD8 region

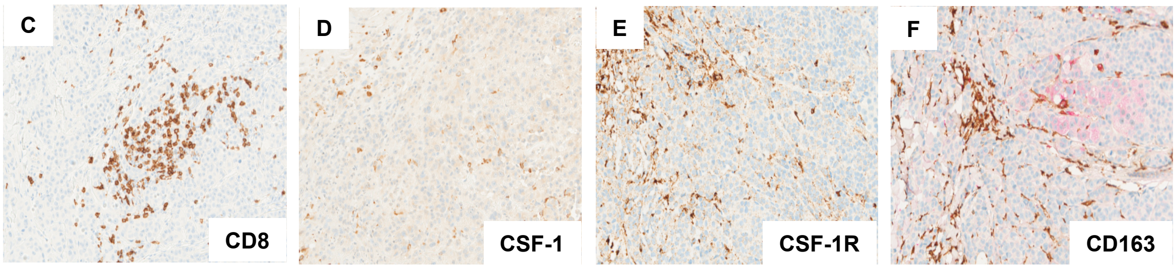

Low tumor CD8 region

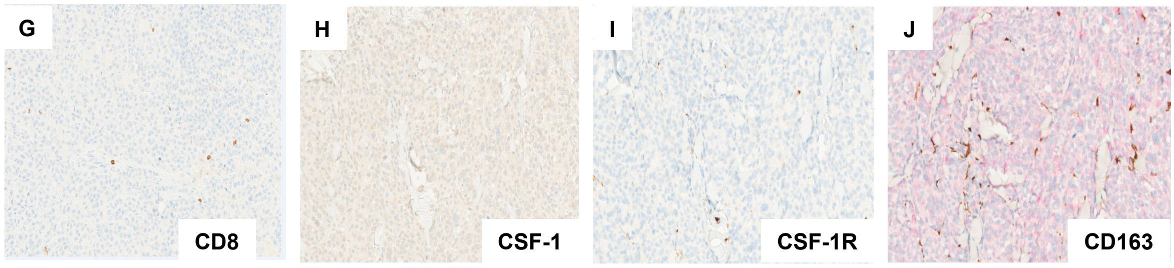

Figure 4

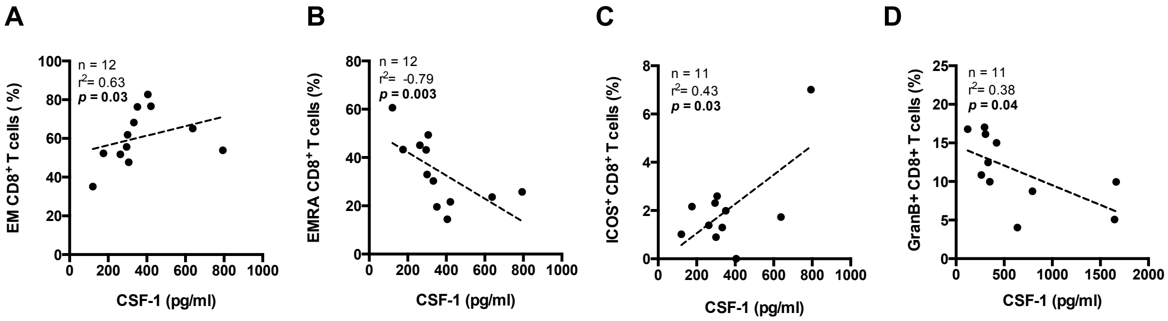
A
n = 12
r2= 0.63
p = 0.03
EM CD8+ T cells (%)
0
20
40
60
80
100
0 200 400 600 800 1000
CSF-1 (pg/ml)
B
n = 12
r2= -0.79
p = 0.003
EMRA CD8+ T cells (%)
0
20
40
60
80
0 200 400 600 800 1000
CSF-1 (pg/ml)
C
n = 11
r2= 0.43
p = 0.03
ICOS+ CD8+ T cells (%)
0
2
4
6
8
0 200 400 600 800 1000
CSF-1 (pg/ml)
D
n = 11
r2= 0.38
p = 0.04
GranB+ CD8+ T cells (%)
0
5
10
15
20
25
0 500 1000 1500 2000
CSF-1 (pg/ml)

Supplementary Figure 1

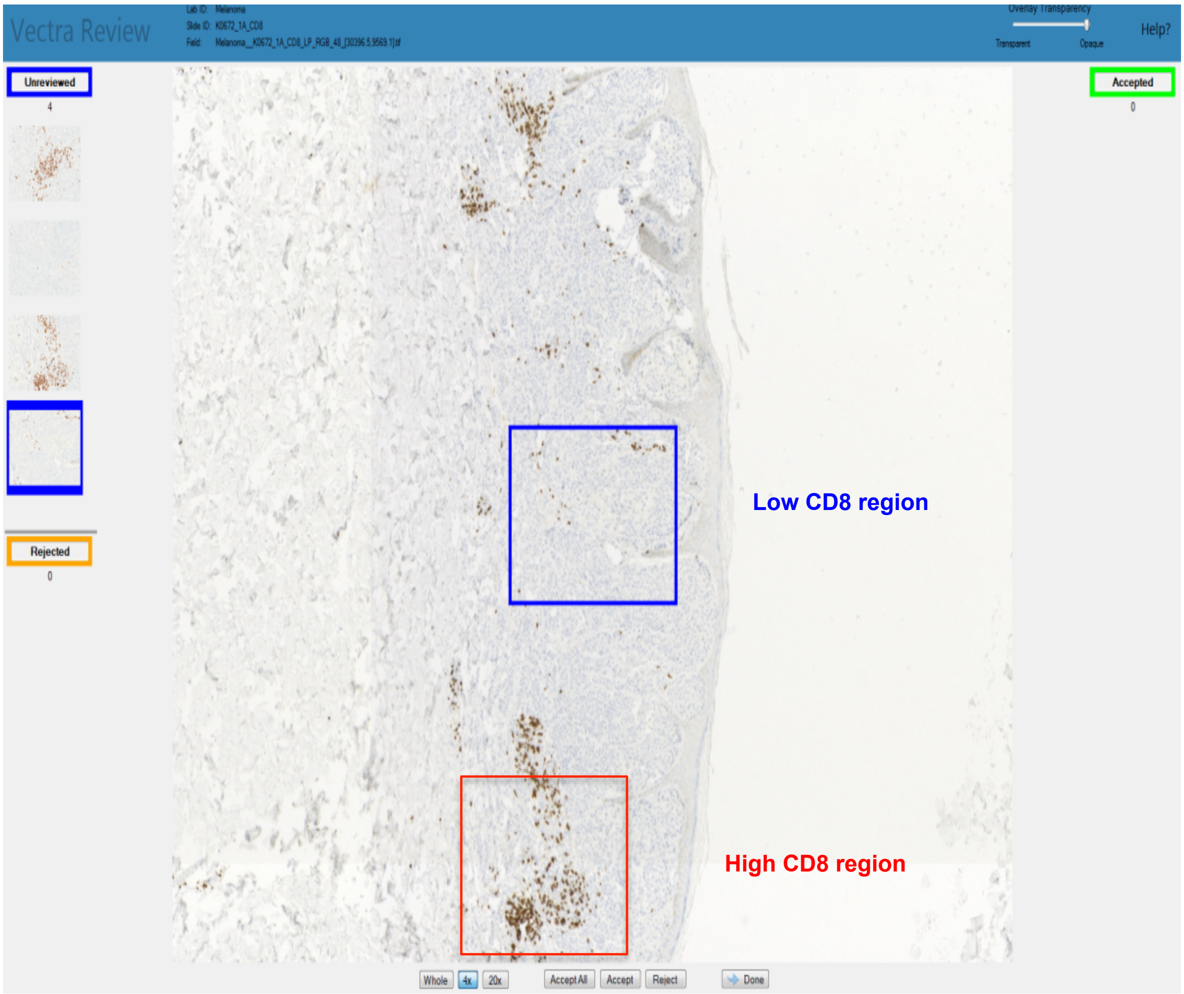

Lab ID: Melanoma
Slide ID: K0672_1A_CD8
Field: Melanoma__K0672_1A_CD8_LP_RGB_48_[30396.5,9569.1].tif

Supplementary Figure 2

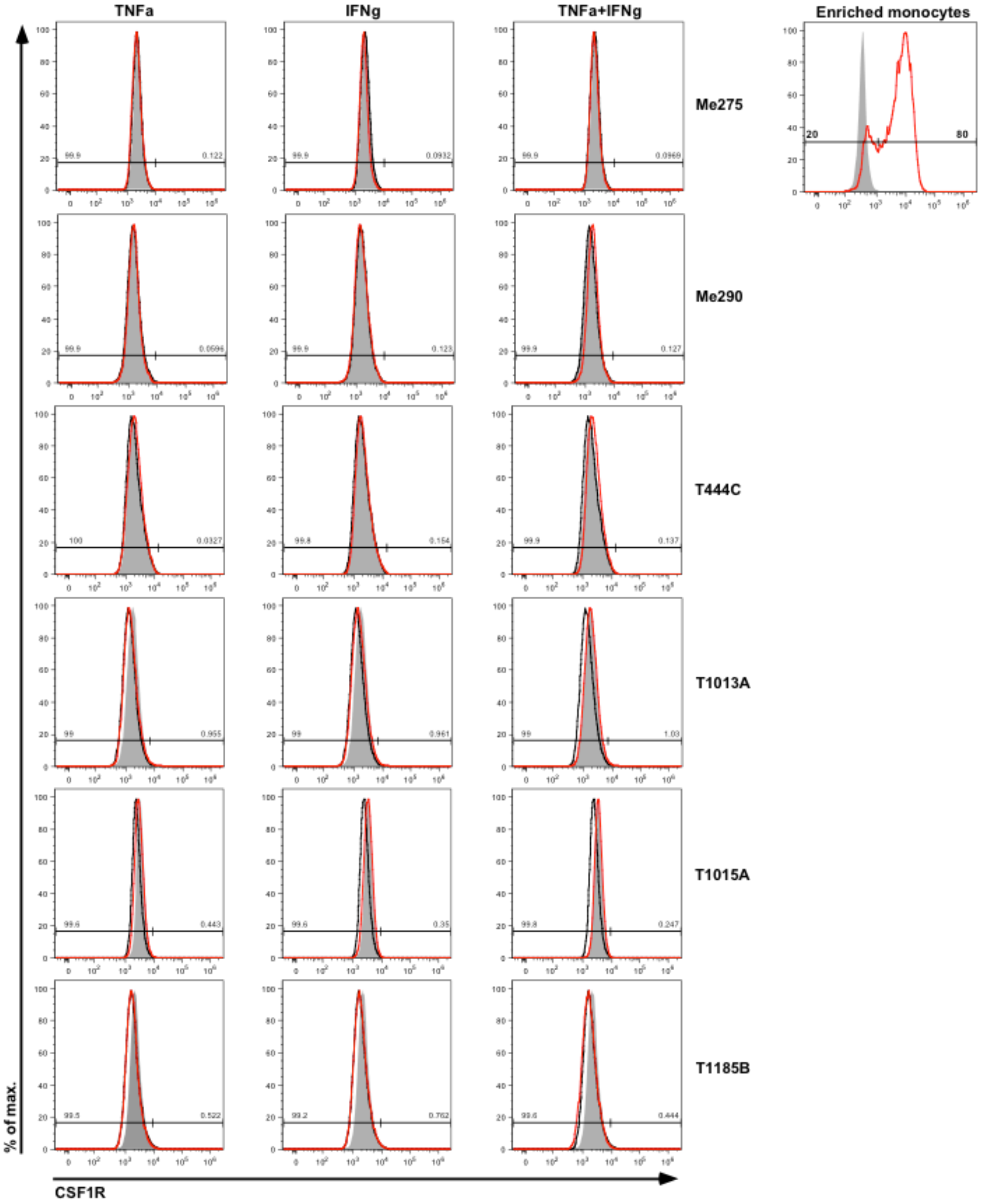

CONCLUSIONS AND PERSPECTIVES

This thesis provides multiple insights into the relationships between human melanoma cells and their environment.

In the first and primary objective of this thesis, our novel approach using modern imaging tools allowed us to study unusually large tissue areas and quantify the major TME components, providing novel data on potential roles of lymphatic vessels and immune cells in melanoma pathophysiology. However, our approach remained largely descriptive, and provided only limited information on the underlying mechanisms. Being fully aware of these limitations, we have proceeded by complementing our studies with collaborations (still ongoing) to tackle the local and systemic impact of lymphatic vessels on T cells. In strong concerted efforts, we have set in action sophisticated clinical investigation protocols, allowing us to obtain a variety of different tissues and fluids from melanoma patients, as described in more detail below.

Tumor-associated lymphatic vessels and their respective draining LNs are associated with the modification of the immune profile of the TME. The next step will be to determine how lymphatic vessels induce these changes. Many studies have identified alterations in both local and regional immune functions in mouse melanoma, which contribute to the expansion and metastasis formation. This immune modulation appears to be driven by factors derived from the tumor (e.g. VEGF-C, TGF-β) and the lymphatic vessels (CCL21/CCL19). We will therefore quantify CCL21 in various patient tissues in order to try to find links between VEGF-C and lymphatic vessels. We will also quantify VEGF-C and CCL21 in patient blood using ELISA. We hope that the analysis of *in situ* and systemic expression of these two key molecules will further our understanding on their cross-talk in the progression of human melanoma.

In order to recapitulate *in vivo* interactions, one must be able to analyze specific cell populations within the context of their heterogeneous tissue microenvironment. IHC techniques facilitate detection of *in situ* expression of specific cellular and molecular parameters. However, this technique is limited by the number of markers that can be co-analysed. It is, therefore, difficult to fully characterize the activation/maturation status of specific immune cell populations. Furthermore, fresh clinical tissue samples suitable for fluorescence-activated cell sorting (FACS) analysis are often difficult to obtain. Alternatively, Laser Capture Microdissection (LCM) can be used to address both questions simultaneously: *in situ* localisation and the quantification of expression of multiple molecular entities via real-time quantitative polymerase chain reaction (qRT-PCR), including properties that are directly indicative of cellular functions. LCM technology can harvest the cells of interest directly or can isolate specific cells by cutting away unwanted cells to give histologically pure and enriched cell populations. We will use LCM to further investigate FFPE tissues and quantify the expression of VEGF-C, TGF-β, CCL21 and CCL19, together with other genes that shape the TME (primary tumor, non metastatic and metastatic LNs) in addition to those markers already described in objective 1. We hope to obtain insightful data on immune cells as well as the surrounding TME of these patients and understand more precisely the local impact of lymphatic vessels on the TME.

Another step towards better defining the local anti-tumor immune response within the tissues of these patients would be to accurately characterize the phenotype and the functionality of tumor-infiltrating T cells. We have previously collected T cells from tumors of these patients and assessed their phenotype and functionality directly *ex vivo* using multiparameter flow cytometry. However, the number of samples for which we had matching tissues analyzed in this study was not sufficient for a meaningful evaluation.

To overcome this limitation, we developed two novel protocols of clinical investigation, with the aim to obtain and study several different TME components directly ex vivo upon surgical resection. Firstly, we are currently recruiting patients with primary melanoma (who have not received any treatment prior to surgery) and are collecting blood samples and primary tumors (fresh tissue and frozen tissues). We will then repeat the experiments described in objective 1. As the phenotype and functionality of tumor-infiltrating T cells, as well as transcriptome information on tumor and LECs has not been assessed in the LUD 00-018 study patients (because of the lack of fresh and frozen primary tissues), this protocol will allow us to complete this missing information. Thus far, 5 patients in total have been enrolled in this study.

Secondly, for more profound characterization of the TME and the lymphatic vessels, we have set-up a collaborative clinical investigation protocol. This protocol involves dedicated pathologists, surgeons, clinicians and researchers. A unique aspect of this protocol is the new and precise *in vivo* sampling method used directly in the operating theater. Apart from the collection of those tissues described above in protocol one, afferent lymphatic vessels and lymph fluid are collected during the SLNs procedure and LN dissection. We are determining the composition of the afferent lymph in terms of chemokines, growth factors and cytokines using proteomics, and looking at differences between patients with positive SLNs and patients with negative SLNs. We are also doing molecular and gene profiling on lymphatic vessels and LN tissues. Finally, we will perform IHC (with the same markers described in objective 1) on SLN tissues that will not be used for diagnosis. At present, we have already enrolled 116 melanoma patients.

This project joins clinicians and two parallel research laboratories focusing on preclinical (Melody Swartz group) and clinical melanoma research (Daniel Speiser group). The potential of this collaboration is to translate, from studies in mouse models of an intractable human cancer, new knowledge on disease mechanisms with a particular focus on better understanding the TME and the associated lymphatic microenvironment and potentially identifying targets for novel therapies.

In conclusion, the study of immune modulation in cancer is complex and no single method is sufficient to cover all aspects. In this thesis, we explored important questions to improve understanding and treatment of melanoma by employing diverse methods and biological specimens. Such an approach fosters better understanding of the cellular and molecular interactions between the different components of the TME and their roles in local and systemic immune modulation that drives melanoma formation and progression. Finally, this work emphasized the importance of integrative collaborative work between clinicians, pathologists and laboratory researchers to develop novel and effective therapies for melanoma patients.

REFERENCES

1. Sansonetti, P. J. 2006. The innate signaling of dangers and the dangers of innate signaling. *Nat. Immunol.* 7: 1237–1242.

2. Garboczi, D. N., P. Ghosh, U. Utz, Q. R. Fan, W. E. Biddison, and D. C. Wiley. 2010. *Structure of the complex between human T-cell receptor, viral peptide and HLA-A2. Nature. 1996. 384: 134-141*. :6394–6401.

3. Siegel, R., D. Naishadham, and A. Jemal. 2013. Cancer statistics, 2013. *CA Cancer J Clin* 63: 11–30.

4. Hanahan, D., and R. A. Weinberg. 2000. The hallmarks of cancer. *Cell* 100: 57–70.

5. Hanahan, D., and R. A. Weinberg. 2011. Hallmarks of cancer: the next generation. *Cell* 144: 646–674.

6. Cavallo, F., C. De Giovanni, P. Nanni, G. Forni, and P.-L. Lollini. 2011. 2011: the immune hallmarks of cancer. *Cancer Immunol. Immunother.* 60: 319–326.

7. Zitvogel, L., A. Tesniere, and G. Kroemer. 2006. Cancer despite immunosurveillance: immunoselection and immunosubversion. *Nat. Rev. Immunol.* 6: 715–727.

8. Dunn, G. P., L. J. Old, and R. D. Schreiber. 2004. The Three Es of Cancer Immunoediting. *Annu. Rev. Immunol.* 22: 329–360.

9. Penn, I. 1996. Malignant melanoma in organ allograft recipients. *Transplantation* 61: 274–278.

10. Lee, P. P., C. Yee, P. A. Savage, L. Fong, D. Brockstedt, J. S. Weber, D. Johnson, S. Swetter, J. Thompson, P. D. Greenberg, M. Roederer, and M. M. Davis. 1999. Characterization of circulating T cells specific for tumor-associated antigens in melanoma patients. *Nat. Med.* 5: 677–685.

11. Romero, P., P. R. Dunbar, D. Valmori, M. Pittet, G. S. Ogg, D. Rimoldi, J. L. Chen, D. Liénard, J. C. Cerottini, and V. Cerundolo. 1998. Ex vivo staining of metastatic lymph nodes by class I major histocompatibility complex tetramers reveals high numbers of antigen-experienced tumor-specific cytolytic T lymphocytes. *J. Exp. Med.* 188: 1641–1650.

12. Salgaller, M. L., A. Afshar, F. M. Marincola, L. Rivoltini, Y. Kawakami, and S. A. Rosenberg. 1995. Recognition of multiple epitopes in the human melanoma antigen gp100 by peripheral blood lymphocytes stimulated in vitro with synthetic peptides. *Cancer Res.* 55: 4972–4979.

13. Anichini, A., C. Vegetti, and R. Mortarini. 2004. The paradox of T-cell-mediated antitumor immunity in spite of poor clinical outcome in human melanoma. *Cancer Immunol. Immunother.* 53: 855–864.

14. Galon, J., A. Costes, F. Sanchez-Cabo, A. Kirilovsky, B. Mlecnik, C. Lagorce-Pagès, M. Tosolini, M. Camus, A. Berger, P. Wind, F. Zinzindohoué, P. Bruneval, P.-H. Cugnenc, Z. Trajanoski, W.-H. Fridman, and F. Pagès. 2006. Type, density, and location of immune cells within human colorectal tumors predict clinical outcome. *Science* 313: 1960–1964.

15. Senovilla, L., E. Vacchelli, J. Galon, S. Adjemian, A. Eggermont, W. H. Fridman, C. Sautès-Fridman, Y. Ma, E. Tartour, L. Zitvogel, G. Kroemer, and L. Galluzzi. 2012. Trial watch: Prognostic and predictive value of the immune infiltrate in cancer. *oncoimmunology* 1: 1323–1343.

16. Erdag, G., J. T. Schaefer, M. E. Smolkin, D. H. Deacon, S. M. Shea, L. T. Dengel, J. W. Patterson, and C. L. Slingluff. 2012. Immunotype and immunohistologic characteristics of tumor-infiltrating immune cells are associated with clinical outcome in metastatic melanoma. *Cancer Res.* 72: 1070–1080.

17. Galon, J., F. Pagès, F. M. Marincola, M. Thurin, G. Trinchieri, B. A. Fox, T. F. Gajewski, and P. A. Ascierto. 2012. The immune score as a new possible approach for the classification of cancer. *Journal of Translational Medicine* 10: 1.

18. Galon, J., B. Mlecnik, G. Bindea, H. K. Angell, A. Berger, C. Lagorce, A. Lugli, I. Zlobec, A. Hartmann, C. Bifulco, I. D. Nagtegaal, R. Palmqvist, G. V. Masucci, G. Botti, F. Tatangelo, P. Delrio, M. Maio, L. Laghi, F. Grizzi, M. Asslaber, C. D'Arrigo, F. Vidal-Vanaclocha, E. Zavadova, L. Chouchane, P. S. Ohashi, S. Hafezi-Bakhtiari, B. G. Wouters, M. Roehrl, L. Nguyen, Y. Kawakami, S. Hazama, K. Okuno, S. Ogino, P. Gibbs, P. Waring, N. Sato, T. Torigoe, K. Itoh, P. S. Patel, S. N. Shukla, Y. Wang, S. Kopetz, F. A. Sinicrope, V. Scripcariu, P. A. Ascierto, F. M. Marincola, B. A. Fox, and F. Pagès. 2014. Towards the introduction of the "Immunoscore" in the classification of malignant tumours. *J. Pathol.* 232: 199–209.

19. Pagès, F., J. Galon, M.-C. Dieu-Nosjean, E. Tartour, C. Sautès-Fridman, and W.-H. Fridman. 2010. Immune infiltration in human tumors: a prognostic factor that should not be ignored. *Oncogene* 29: 1093–1102.

20. Fridman, W.-H., R. Remark, J. Goc, N. A. Giraldo, E. Becht, S. A. Hammond, D. Damotte, M.-C. Dieu-Nosjean, and C. Sautès-Fridman. 2014. The immune microenvironment: a major player in human cancers. *Int. Arch. Allergy Immunol.* 164: 13–26.

21. Terheyden, P., C. Siedel, A. Merkel, E. Kämpgen, E. B. Bröcker, and J. C. Becker. 1999. Predominant expression of Fas (CD95) ligand in metastatic melanoma revealed by longitudinal analysis. *J. Invest. Dermatol.* 112: 899–902.

22. Yang, L., Y. Pang, and H. L. Moses. 2010. TGF-beta and immune cells: an important regulatory axis in the tumor microenvironment and progression. *Trends Immunol.* 31: 220–227.

23. Mellor, A. L., and D. H. Munn. 2004. Ido expression by dendritic cells: tolerance and tryptophan catabolism : Abstract : Nature Reviews Immunology. *Nat. Rev. Immunol.*

24. Bronte, V., P. Serafini, A. Mazzoni, D. M. Segal, and P. Zanovello. 2003. L-arginine metabolism in myeloid cells controls T-lymphocyte functions. *Trends Immunol.* 24: 302–306.

25. Marincola, F. M., E. Wang, M. Herlyn, B. Seliger, and S. Ferrone. 2003. Tumors as elusive targets of T-cell-based active immunotherapy. *Trends Immunol.* 24: 335–342.

26. Swartz, M. A., N. Iida, E. W. Roberts, S. Sangaletti, M. H. Wong, F. E. Yull, L. M. Coussens, and Y. A. DeClerck. 2012. Tumor microenvironment complexity: emerging roles in cancer therapy. In vol. 72. 2473–2480.

27. Zou, W. 2005. Immunosuppressive networks in the tumour environment and their therapeutic relevance. *Nat. Rev. Cancer* 5: 263–274.

28. Thompson, J. F., R. A. Scolyer, and R. F. Kefford. 2005. Cutaneous melanoma. *The Lancet* 365: 687–701.

29. Rigel, D. S., J. Russak, and R. Friedman. 2010. The evolution of melanoma diagnosis: 25 years beyond the ABCDs. *CA Cancer J Clin* 60: 301–316.

30. Tsao, H., M. B. Atkins, and A. J. Sober. 2004. Management of Cutaneous Melanoma. *N. Engl. J. Med.* 351: 998–1012.

31. Tucker, M. A., and A. M. Goldstein. 2003. Oncogene - Abstract of article: Melanoma etiology: where are we? *Oncogene*.

32. Elwood, J. M., and J. Jopson. 1997. Melanoma and sun exposure: an overview of published studies. *International Journal of Cancer*.

33. Miller, A. J., and M. C. Mihm Jr. 2006. Melanoma — NEJM. *New England Journal of Medicine*.

34. Takata, M., H. Murata, and T. Saida. 2009. Molecular pathogenesis of malignant melanoma: a different perspective from the studies of melanocytic nevus and acral melanoma. *Pigment Cell Melanoma Res* 23: 64–71.

35. Rigel, D. S., and R. J. Friedman. 1993. The rationale of the ABCDs of early melanoma. *J. Am. Acad. Dermatol.* 29: 1060–1061.

36. Clarkson, K. S. 2001. The usefulness of tyrosinase in the immunohistochemical assessment of melanocytic lesions: a comparison of the novel T311 antibody (anti-tyrosinase) with S-100, HMB45, and A103 (anti-melan-A). *Journal of Clinical Pathology* 54: 196–200.

37. Clark, W. H., D. E. Elder, D. Guerry, M. N. Epstein, M. H. Greene, and M. Van Horn. 1984. A study of tumor progression: the precursor lesions of superficial spreading and nodular melanoma. *Hum. Pathol.* 15: 1147–1165.

38. Emmett, M. S., K. E. Symonds, H. Rigby, M. G. Cook, R. Price, C. Metcalfe, A. Orlando, and D. O. Bates. 2010. Prediction of melanoma metastasis by the Shields index based on lymphatic vessel density. *BMC Cancer* 10: 208.

39. Criscione, V. D., and M. A. Weinstock. 2010. Melanoma thickness trends in the United States, 1988-2006. *Journal of Investigative Dermatology* 130: 793–797.

40. Balch, C. M., J. E. Gershenwald, S.-J. Soong, J. F. Thompson, M. B. Atkins, D. R. Byrd, A. C. Buzaid, A. J. Cochran, D. G. Coit, S. Ding, A. M. Eggermont, K. T. Flaherty, P. A. Gimotty, J. M. Kirkwood, K. M. McMasters, M. C. Mihm, D. L. Morton, M. I. Ross, A. J. Sober, and V. K. Sondak. 2009. Final version of 2009 AJCC melanoma staging and classification. *Journal of Clinical Oncology* 27: 6199–6206.

41. Morton, D. L., J. F. Thompson, A. J. Cochran, N. Mozzillo, R. Elashoff, R. Essner, O. E. Nieweg, D. F. Roses, H. J. Hoekstra, C. P. Karakousis, D. S. Reintgen, B. J. Coventry, E. C. Glass, and H.-J. Wang. 2006. Sentinel-Node Biopsy or Nodal Observation in Melanoma. *N. Engl. J. Med.* 355: 1307–1317.

42. Cuchet, E., N. Pinel, D. Corcella, J.-P. Vuillez, J. Lebeau, F. Moutet, M. Colonna, and M.-T. Leccia. 2007. Sentinel lymph node biopsy in cutaneous melanoma: outcome after 5-years follow-up. *Eur J Dermatol* 17: 387–391.

43. Fridman, W.-H., F. Pagès, C. Sautès-Fridman, and J. Galon. 2012. The immune contexture in human tumours: impact on clinical outcome. *Nat. Rev. Cancer* 12: 298–306.

44. Giraldo, N. A., E. Becht, R. Remark, D. Damotte, C. Sautès-Fridman, and W. H. Fridman. 2014. The immune contexture of primary and metastatic human tumours. *Curr. Opin. Immunol.* 27: 8–15.

45. Chapman, P. B., A. Hauschild, C. Robert, J. B. Haanen, P. Ascierto, J. Larkin, R. Dummer, C. Garbe, A. Testori, M. Maio, D. Hogg, P. Lorigan, C. Lebbe, T. Jouary, D. Schadendorf, A. Ribas, S. J. O'Day, J. A. Sosman, J. M. Kirkwood, A. M. M. Eggermont, B. Dréno, K. Nolop, J. Li, B. Nelson, J. Hou, R. J. Lee, K. T. Flaherty, G. A. McArthur, BRIM-3 Study Group. 2011. Improved survival with vemurafenib in melanoma with BRAF V600E mutation. *N. Engl. J. Med.* 364: 2507–2516.

46. Sosman, J. A., K. B. Kim, L. Schuchter, R. Gonzalez, A. C. Pavlick, J. S. Weber, G. A. McArthur, T. E. Hutson, S. J. Moschos, K. T. Flaherty, P. Hersey, R. Kefford, D. Lawrence, I. Puzanov, K. D. Lewis, R. K. Amaravadi, B. Chmielowski, H. J. Lawrence, Y. Shyr, F. Ye, J. Li, K. B. Nolop, R. J. Lee, A. K. Joe, and A. Ribas. 2012. Survival in BRAF V600-mutant advanced melanoma treated with vemurafenib. *N. Engl. J. Med.* 366: 707–714.

47. Romano, E., S. Pradervand, A. Paillusson, J. Weber, K. Harshman, K. Muehlethaler, D. E. Speiser, S. Peters, D. Rimoldi, and O. Michielin. 2013. Identification of multiple mechanisms of

resistance to vemurafenib in a patient with BRAFV600E-mutated cutaneous melanoma successfully rechallenged after progression. *Clin. Cancer Res.*

48. Sullivan, R. J., and K. T. Flaherty. 2013. Resistance to BRAF-targeted therapy in melanoma. *Eur. J. Cancer* 49: 1297–1304.

49. Long, G. V., D. Stroyakovskiy, H. Gogas, E. Levchenko, F. de Braud, J. Larkin, C. Garbe, T. Jouary, A. Hauschild, J. J. Grob, V. Chiarion Sileni, C. Lebbe, M. Mandalà, M. Millward, A. Arance, I. Bondarenko, J. B. A. G. Haanen, J. Hansson, J. Utikal, V. Ferraresi, N. Kovalenko, P. Mohr, V. Probachai, D. Schadendorf, P. Nathan, C. Robert, A. Ribas, D. J. DeMarini, J. G. Irani, M. Casey, D. Ouellet, A.-M. Martin, N. Le, K. Patel, and K. Flaherty. 2014. Combined BRAF and MEK inhibition versus BRAF inhibition alone in melanoma. *N. Engl. J. Med.* 371: 1877–1888.

50. Flaherty, K. T., J. R. Infante, A. Daud, R. Gonzalez, R. F. Kefford, J. Sosman, O. Hamid, L. Schuchter, J. Cebon, N. Ibrahim, R. Kudchadkar, H. A. Burris, G. Falchook, A. Algazi, K. Lewis, G. V. Long, I. Puzanov, P. Lebowitz, A. Singh, S. Little, P. Sun, A. Allred, D. Ouellet, K. B. Kim, K. Patel, and J. Weber. 2012. Combined BRAF and MEK inhibition in melanoma with BRAF V600 mutations. *N. Engl. J. Med.* 367: 1694–1703.

51. Larkin, J., P. A. Ascierto, B. Dréno, V. Atkinson, G. Liszkay, M. Maio, M. Mandalà, L. Demidov, D. Stroyakovskiy, L. Thomas, L. de la Cruz-Merino, C. Dutriaux, C. Garbe, M. A. Sovak, I. Chang, N. Choong, S. P. Hack, G. A. McArthur, and A. Ribas. 2014. Combined vemurafenib and cobimetinib in BRAF-mutated melanoma. *N. Engl. J. Med.* 371: 1867–1876.

52. Hodi, F. S., S. J. O'Day, D. F. McDermott, R. W. Weber, J. A. Sosman, J. B. Haanen, R. Gonzalez, C. Robert, D. Schadendorf, J. C. Hassel, W. Akerley, A. J. M. van den Eertwegh, J. Lutzky, P. Lorigan, J. M. Vaubel, G. P. Linette, D. Hogg, C. H. Ottensmeier, C. Lebbe, C. Peschel, I. Quirt, J. I. Clark, J. D. Wolchok, J. S. Weber, J. Tian, M. J. Yellin, G. M. Nichol, A. Hoos, and W. J. Urba. 2010. Improved Survival with Ipilimumab in Patients with Metastatic Melanoma. *N. Engl. J. Med.* 363: 711–723.

53. Robert, C., J. Schachter, G. V. Long, A. Arance, J. J. Grob, L. Mortier, A. Daud, M. S. Carlino, C. McNeil, M. Lotem, J. Larkin, P. Lorigan, B. Neyns, C. U. Blank, O. Hamid, C. Mateus, R. Shapira-Frommer, M. Kosh, H. Zhou, N. Ibrahim, S. Ebbinghaus, A. Ribas, KEYNOTE-006 investigators. 2015. Pembrolizumab versus Ipilimumab in Advanced Melanoma. *N. Engl. J. Med.*

54. Garon, E. B., N. A. Rizvi, R. Hui, N. Leighl, A. S. Balmanoukian, J. P. Eder, A. Patnaik, C. Aggarwal, M. Gubens, L. Horn, E. Carcereny, M.-J. Ahn, E. Felip, J.-S. Lee, M. D. Hellmann, O. Hamid, J. W. Goldman, J.-C. Soria, M. Dolled-Filhart, R. Z. Rutledge, J. Zhang, J. K. Lunceford, R. Rangwala, G. M. Lubiniecki, C. Roach, K. Emancipator, L. Gandhi, KEYNOTE-001 Investigators. 2015. Pembrolizumab for the Treatment of Non-Small-Cell Lung Cancer. *N. Engl. J. Med.*

55. Wolchok, J. D., H. Kluger, M. K. Callahan, M. A. Postow, N. A. Rizvi, A. M. Lesokhin, N. H. Segal, C. E. Ariyan, R.-A. Gordon, K. Reed, M. M. Burke, A. Caldwell, S. A. Kronenberg, B. U. Agunwamba, X. Zhang, I. Lowy, H. D. Inzunza, W. Feely, C. E. Horak, Q. Hong, A. J. Korman, J. M. Wigginton, A. Gupta, and M. Sznol. 2013. Nivolumab plus ipilimumab in advanced melanoma. *N. Engl. J. Med.* 369: 122–133.

56. Postow, M. A., J. Chesney, A. C. Pavlick, C. Robert, K. Grossmann, D. McDermott, G. P. Linette, N. Meyer, J. K. Giguere, S. S. Agarwala, M. Shaheen, M. S. Ernstoff, D. Minor, A. K. Salama, M. Taylor, P. A. Ott, L. M. Rollin, C. Horak, P. Gagnier, J. D. Wolchok, and F. S. Hodi. 2015. Nivolumab and Ipilimumab versus Ipilimumab in Untreated Melanoma. *N. Engl. J. Med.*

57. Curti, B. D. 2014. Rapid evolution of combination therapy in melanoma. *N. Engl. J. Med.* 371: 1929–1930.

58. Attia, P., G. Q. Phan, A. V. Maker, M. R. Robinson, M. M. Quezado, J. C. Yang, R. M. Sherry, S. L. Topalian, U. S. Kammula, R. E. Royal, N. P. Restifo, L. R. Haworth, C. Levy, S. A. Mavroukakis, G. Nichol, M. J. Yellin, and S. A. Rosenberg. 2005. Autoimmunity correlates with tumor regression in patients with metastatic melanoma treated with anti-cytotoxic T-lymphocyte antigen-4. *J. Clin. Oncol.*

23: 6043–6053.

59. Phan, G. Q., J. C. Yang, R. M. Sherry, P. Hwu, S. L. Topalian, D. J. Schwartzentruber, N. P. Restifo, L. R. Haworth, C. A. Seipp, L. J. Freezer, K. E. Morton, S. A. Mavroukakis, P. H. Duray, S. M. Steinberg, J. P. Allison, T. A. Davis, and S. A. Rosenberg. 2003. Cancer regression and autoimmunity induced by cytotoxic T lymphocyte-associated antigen 4 blockade in patients with metastatic melanoma. *Proc. Natl. Acad. Sci. U.S.A.* 100: 8372–8377.

60. Naidoo, J., D. B. Page, and J. D. Wolchok. 2014. Immune modulation for cancer therapy. *Br. J. Cancer* 111: 2214–2219.

61. Sapoznik, S., O. Hammer, R. Ortenberg, M. J. Besser, T. Ben-Moshe, J. Schachter, and G. Markel. 2012. Novel anti-melanoma immunotherapies: disarming tumor escape mechanisms. *Clin. Dev. Immunol.* 2012: 818214.

62. Robert, C., L. Thomas, I. Bondarenko, S. O'Day, J. Weber, C. Garbe, C. Lebbe, J.-F. Baurain, A. Testori, J. J. Grob, N. Davidson, J. Richards, M. Maio, A. Hauschild, W. H. Miller, P. Gascon, M. Lotem, K. Harmankaya, R. Ibrahim, S. Francis, T.-T. Chen, R. Humphrey, A. Hoos, and J. D. Wolchok. 2011. Ipilimumab plus dacarbazine for previously untreated metastatic melanoma. *N. Engl. J. Med.* 364: 2517–2526.

63. Rosenberg, S. A., and N. P. Restifo. 2015. Adoptive cell transfer as personalized immunotherapy for human cancer. *Science* 348: 62–68.

64. Speiser, D. E., and P. Romero. 2010. Molecularly defined vaccines for cancer immunotherapy, and protective T cell immunity. *Semin. Immunol.* 22: 144–154.

65. Cormier, J. N., M. L. Salgaller, T. Prevette, K. C. Barracchini, L. Rivoltini, N. P. Restifo, S. A. Rosenberg, and F. M. Marincola. 1997. Enhancement of cellular immunity in melanoma patients immunized with a peptide from MART-1/Melan A. *Cancer J Sci Am* 3: 37–44.

66. Baumgaertner, P., C. Jandus, J.-P. Rivals, L. Derré, T. Lövgren, L. Baitsch, P. Guillaume, I. F. Luescher, G. Berthod, M. Matter, N. Rufer, O. Michielin, and D. E. Speiser. 2012. Vaccination-induced functional competence of circulating human tumor-specific CD8 T-cells. *Int. J. Cancer* 130: 2607–2617.

67. Rosenberg, S. A., J. C. Yang, and N. P. Restifo. 2004. Cancer immunotherapy: moving beyond current vaccines. *Nat. Med.* 10: 909–915.

68. Lipson, E. J., W. H. Sharfman, S. Chen, T. L. McMiller, T. S. Pritchard, J. T. Salas, S. Sartorius-Mergenthaler, I. Freed, S. Ravi, H. Wang, B. Luber, J. D. Sproul, J. M. Taube, D. M. Pardoll, and S. L. Topalian. 2015. Safety and immunologic correlatesof Melanoma GVAX, a GM-CSF secreting allogeneic melanoma cell vaccine administered in the adjuvant setting. *Journal of Translational Medicine* 1–14.

69. Klebanoff, C. A., N. Acquavella, Z. Yu, and N. P. Restifo. 2010. Therapeutic cancer vaccines: are we there yet? *Immunol. Rev.* 239: 27–44.

70. Hodi, F. S., M. Butler, D. A. Oble, M. V. Seiden, F. G. Haluska, A. Kruse, S. Macrae, M. Nelson, C. Canning, I. Lowy, A. Korman, D. Lautz, S. Russell, M. T. Jaklitsch, N. Ramaiya, T. C. Chen, D. Neuberg, J. P. Allison, M. C. Mihm, and G. Dranoff. 2008. Immunologic and clinical effects of antibody blockade of cytotoxic T lymphocyte-associated antigen 4 in previously vaccinated cancer patients. *Proc. Natl. Acad. Sci. U.S.A.* 105: 3005–3010.

71. Wang, Y., and G. Oliver. 2010. Current views on the function of the lymphatic vasculature in health and disease. *Genes & Development* 24: 2115–2126.

72. Swartz, M. A., and M. Skobe. 2001. Lymphatic function, lymphangiogenesis, and cancer metastasis - Swartz - 2001 - Microscopy Research and Technique - Wiley Online Library. *Microscopy*

research and technique.

73. Aukland, K., and R. K. Reed. 1993. Interstitial-lymphatic mechanisms in the control of extracellular fluid volume. *Physiol. Rev.* 73: 1–78.

74. Christiansen, A., and M. Detmar. 2011. Lymphangiogenesis and Cancer. *Genes & cancer*.

75. Andrian, von, U. H., and T. R. Mempel. 2003. Homing and cellular traffic in lymph nodes. *Nat. Rev. Immunol.* 3: 867–878.

76. Fletcher, A. L., S. E. Acton, and K. Knoblich. 2015. Lymph node fibroblastic reticular cells in health and disease. *Nat. Rev. Immunol.*

77. Maby-El Hajjami, H., and T. V. Petrova. 2008. Developmental and pathological lymphangiogenesis: from models to human disease. *Histochem Cell Biol* 130: 1063–1078.

78. Wigle, J. T., and G. Oliver. 1999. Prox1 function is required for the development of the murine lymphatic system. *Cell* 98: 769–778.

79. Tammela, T., and K. Alitalo. 2010. Lymphangiogenesis: Molecular mechanisms and future promise. *Cell* 140: 460–476.

80. Joukov, V., T. Sorsa, V. Kumar, M. Jeltsch, L. Claesson-Welsh, Y. Cao, O. Saksela, N. Kalkkinen, and K. Alitalo. 1997. Proteolytic processing regulates receptor specificity and activity of VEGF-C. *EMBO J.* 16: 3898–3911.

81. Wissmann, C., and M. Detmar. 2006. Pathways Targeting Tumor Lymphangiogenesis. *Clinical Cancer Research* 12: 6865–6868.

82. Cao, Y., P. Linden, J. Farnebo, R. Cao, A. Eriksson, V. Kumar, J. H. Qi, L. Claesson-Welsh, and K. Alitalo. 1998. Vascular endothelial growth factor C induces angiogenesis in vivo. *Proc. Natl. Acad. Sci. U.S.A.* 95: 14389–14394.

83. Nagy, J. A., E. Vasile, D. Feng, C. Sundberg, L. F. Brown, M. J. Detmar, J. A. Lawitts, L. Benjamin, X. Tan, E. J. Manseau, A. M. Dvorak, and H. F. Dvorak. 2002. Vascular permeability factor/vascular endothelial growth factor induces lymphangiogenesis as well as angiogenesis. *J. Exp. Med.* 196: 1497–1506.

84. Oliver, G. 2004. Lymphatic vasculature development. *Nat. Rev. Immunol.* 4: 35–45.

85. Van der Auwera, I., Y. Cao, J. C. Tille, M. S. Pepper, D. G. Jackson, S. B. Fox, A. L. Harris, L. Y. Dirix, and P. B. Vermeulen. 2006. First international consensus on the methodology of lymphangiogenesis quantification in solid human tumours. In vol. 95. 1611–1625.

86. Clarijs, R., L. Schalkwijk, U. B. Hofmann, D. J. Ruiter, and R. M. W. de Waal. 2002. Induction of vascular endothelial growth factor receptor-3 expression on tumor microvasculature as a new progression marker in human cutaneous melanoma. *Cancer Res.* 62: 7059–7065.

87. Schledzewski, K., M. Falkowski, G. Moldenhauer, P. Metharom, J. Kzhyshkowska, R. Ganss, A. Demory, B. Falkowska-Hansen, H. Kurzen, S. Ugurel, G. Geginat, B. Arnold, and S. Goerdt. 2006. Lymphatic endothelium-specific hyaluronan receptor LYVE-1 is expressed by stabilin-1+, F4/80+, CD11b+ macrophages in malignant tumours and wound healing tissue in vivo and in bone marrow cultures in vitro: implications for the assessment of lymphangiogenesis. *J. Pathol.* 209: 67–77.

88. Stacker, S. A., M. G. Achen, L. Jussila, M. E. Baldwin, and K. Alitalo. 2002. Lymphangiogenesis and cancer metastasis. *Nat. Rev. Cancer* 2: 573–583.

89. Park, S. M., C. E. Angel, J. D. McIntosh, C. M. Mansell, C.-J. J. Chen, J. Cebon, and P. R.

Dunbar. 2014. Mapping the distinctive populations of lymphatic endothelial cells in different zones of human lymph nodes. *PLoS ONE* 9: e94781.

90. Pastushenko, I., C. Conejero, and F. J. Carapeto. 2015. Lymphangiogenesis: Implications for Diagnosis, Treatment, and Prognosis in Patients With Melanoma. *Actas Dermo-Sifiliográficas (English Edition)* 106: 7–16.

91. Skobe, M., T. Hawighorst, D. G. Jackson, R. Prevo, L. Janes, P. Velasco, L. Riccardi, K. Alitalo, K. Claffey, and M. Detmar. 2001. Induction of tumor lymphangiogenesis by VEGF-C promotes breast cancer metastasis. *Nat. Med.* 7: 192–198.

92. Karpanen, T., M. Egeblad, M. J. Karkkainen, H. Kubo, S. Ylä-Herttuala, M. Jäättelä, and K. Alitalo. 2001. Vascular endothelial growth factor C promotes tumor lymphangiogenesis and intralymphatic tumor growth. *Cancer Res.* 61: 1786–1790.

93. Skobe, M., L. M. Hamberg, T. Hawighorst, M. Schirner, G. L. Wolf, K. Alitalo, and M. Detmar. 2001. Concurrent induction of lymphangiogenesis, angiogenesis, and macrophage recruitment by vascular endothelial growth factor-C in melanoma. *Am. J. Pathol.* 159: 893–903.

94. He, Y., K. I. Kozaki, T. Karpanen, K. Koshikawa, S. Ylä-Herttuala, T. Takahashi, and K. Alitalo. 2002. Suppression of Tumor Lymphangiogenesis and Lymph Node Metastasis by Blocking Vascular Endothelial Growth Factor Receptor 3 Signaling. *JNCI Journal of the National Cancer Institute* 94: 819–825.

95. Dadras, S. S., B. Lange-Asschenfeldt, P. Velasco, L. Nguyen, A. Vora, A. Muzikansky, K. Jahnke, A. Hauschild, S. Hirakawa, M. C. Mihm, and M. Detmar. 2005. Tumor lymphangiogenesis predicts melanoma metastasis to sentinel lymph nodes. *Mod. Pathol.* 18: 1232–1242.

96. Van den Eynden, G. G., I. Van der Auwera, S. J. Van Laere, V. Huygelen, C. G. Colpaert, P. van Dam, L. Y. Dirix, P. B. Vermeulen, and E. A. Van Marck. 2006. Induction of lymphangiogenesis in and around axillary lymph node metastases of patients with breast cancer. *Br. J. Cancer* 95: 1362–1366.

97. Harrell, M. I., B. M. Iritani, and A. Ruddell. 2007. Tumor-induced sentinel lymph node lymphangiogenesis and increased lymph flow precede melanoma metastasis. *Am. J. Pathol.* 170: 774–786.

98. Hirakawa, S., L. F. Brown, S. Kodama, K. Paavonen, K. Alitalo, and M. Detmar. 2007. VEGF-C-induced lymphangiogenesis in sentinel lymph nodes promotes tumor metastasis to distant sites. *Blood* 109: 1010–1017.

99. Dadras, S. S., T. Paul, J. Bertoncini, L. F. Brown, A. Muzikansky, D. G. Jackson, U. Ellwanger, C. Garbe, M. C. Mihm, and M. Detmar. 2003. Tumor lymphangiogenesis: a novel prognostic indicator for cutaneous melanoma metastasis and survival. *Am. J. Pathol.* 162: 1951–1960.

100. Schietroma, C., F. Cianfarani, P. M. Lacal, and T. Odorisio. 2003. Vascular endothelial growth factor-C expression correlates with lymph node localization of human melanoma metastases - Schietroma - 2003 - Cancer - Wiley Online Library. *Cancer*.

101. Boone, B., W. Blokx, D. De Bacquer, J. Lambert, D. Ruiter, and L. Brochez. 2008. The role of VEGF-C staining in predicting regional metastasis in melanoma. *Virchows Arch.* 453: 257–265.

102. Mandriota, S. J. 2001. Vascular endothelial growth factor-C-mediated lymphangiogenesis promotes tumour metastasis. *EMBO J.* 20: 672–682.

103. Thiele, W., and J. P. Sleeman. 2006. Tumor-induced lymphangiogenesis: a target for cancer therapy? *J. Biotechnol.* 124: 224–241.

104. Massi, D. 2006. Tumour lymphangiogenesis is a possible predictor of sentinel lymph node status in cutaneous melanoma: a case-control study. *Journal of Clinical Pathology* 59: 166–173.

105. Gallego, E., L. Vicioso, M. Alvarez, I. Hierro, L. Pérez-Villa, A. Blanes, and A. Matilla. 2011. Stromal expression of vascular endothelial growth factor C is relevant to predict sentinel lymph node status in melanomas. *Virchows Arch.* 458: 621–630.

106. Straume, O., D. G. Jackson, and L. A. Akslen. 2003. Independent prognostic impact of lymphatic vessel density and presence of low-grade lymphangiogenesis in cutaneous melanoma. *Clin. Cancer Res.* 9: 250–256.

107. Pastushenko, I., P. B. Vermeulen, F. J. Carapeto, G. Van den Eynden, A. Rutten, M. Ara, L. Y. Dirix, and S. Van Laere. 2014. Blood microvessel density, lymphatic microvessel density and lymphatic invasion in predicting melanoma metastases: systematic review and meta-analysis. *Br. J. Dermatol.* 170: 66–77.

108. Achen, M. G., G. B. Mann, and S. A. Stacker. 2006. Targeting lymphangiogenesis to prevent tumour metastasis. *Br. J. Cancer* 94: 1355–1360.

109. Schoppmann, S. F., G. Bayer, K. Aumayr, S. Taucher, S. Geleff, M. Rudas, E. Kubista, H. Hausmaninger, H. Samonigg, M. Gnant, R. Jakesz, R. Horvat, Austrian Breast and Colorectal Cancer Study Group. 2004. Prognostic value of lymphangiogenesis and lymphovascular invasion in invasive breast cancer. *Ann. Surg.* 240: 306–312.

110. Liu, B., J. Ma, X. Wang, F. Su, X. Li, S. Yang, W. Ma, and Y. Zhang. 2008. Lymphangiogenesis and its relationship with lymphatic metastasis and prognosis in malignant melanoma. *Anat Rec (Hoboken)* 291: 1227–1235.

111. Rinderknecht, M., and M. Detmar. 2008. Tumor lymphangiogenesis and melanoma metastasis. *J. Cell. Physiol.* 216: 347–354.

112. Sahni, D., A. Robson, G. Orchard, R. Szydlo, A. V. Evans, and R. Russell-Jones. 2005. The use of LYVE-1 antibody for detecting lymphatic involvement in patients with malignant melanoma of known sentinel node status. *Journal of Clinical Pathology* 58: 715–721.

113. Förster, R., A. C. Davalos-Misslitz, and A. Rot. 2008. CCR7 and its ligands: balancing immunity and tolerance. *Nat. Rev. Immunol.* 8: 362–371.

114. Wiley, H. E., E. B. Gonzalez, W. Maki, M. T. Wu, and S. T. Hwang. 2001. Expression of CC chemokine receptor-7 and regional lymph node metastasis of B16 murine melanoma. *J. Natl. Cancer Inst.* 93: 1638–1643.

115. Günther, K., J. Leier, G. Henning, A. Dimmler, R. Weissbach, W. Hohenberger, and R. Förster. 2005. Prediction of lymph node metastasis in colorectal carcinoma by expressionof chemokine receptor CCR7. *Int. J. Cancer* 116: 726–733.

116. Mashino, K., N. Sadanaga, H. Yamaguchi, F. Tanaka, M. Ohta, K. Shibuta, H. Inoue, and M. Mori. 2002. Expression of Chemokine Receptor CCR7 Is Associated with Lymph Node Metastasis of Gastric Carcinoma. *Cancer Res.*

117. Shields, J. D., M. S. Emmett, D. B. A. Dunn, K. D. Joory, L. M. Sage, H. Rigby, P. S. Mortimer, A. Orlando, J. R. Levick, and D. O. Bates. 2007. Chemokine-mediated migration of melanoma cells towards lymphatics--a mechanism contributing to metastasis. *Oncogene* 26: 2997–3005.

118. Lanati, S., D. B. Dunn, M. Roussigne, M. S. Emmett, V. Carriere, D. Jullien, J. Budge, J. Fryer, M. Erard, F. Cailler, J. P. Girard, and D. O. Bates. 2010. Chemotrap-1: An Engineered Soluble Receptor That Blocks Chemokine-Induced Migration of Metastatic Cancer Cells In vivo. *Cancer Res.* 70: 8138–8148.

119. Carmeliet, P., and R. K. Jain. 2000. Angiogenesis in cancer and other diseases. *Nature* 407: 249–257.

120. Das, S., E. Sarrou, S. Podgrabinska, M. Cassella, S. K. Mungamuri, N. Feirt, R. Gordon, C. S. Nagi, Y. Wang, D. Entenberg, J. Condeelis, and M. Skobe. 2013. Tumor cell entry into the lymph node is controlled by CCL1 chemokine expressed by lymph node lymphatic sinuses. *Journal of Experimental Medicine* 210: 1509–1528.

121. Kim, M., Y. J. Koh, K. E. Kim, B. I. Koh, D. H. Nam, K. Alitalo, I. Kim, and G. Y. Koh. 2010. CXCR4 Signaling Regulates Metastasis of Chemoresistant Melanoma Cells by a Lymphatic Metastatic Niche. *Cancer Res.* 70: 10411–10421.

122. Lund, A. W., and M. A. Swartz. 2010. Role of Lymphatic Vessels in Tumor Immunity: Passive Conduits or Active Participants? *J Mammary Gland Biol Neoplasia* 15: 341–352.

123. Nevala, W. K., C. M. Vachon, A. A. Leontovich, C. G. Scott, M. A. Thompson, S. N. Markovic, Melanoma Study Group of the Mayo Clinic Cancer Center. 2009. Evidence of systemic Th2-driven chronic inflammation in patients with metastatic melanoma. *Clin. Cancer Res.* 15: 1931–1939.

124. Chen, Z., M. L. Varney, M. W. Backora, K. Cowan, J. C. Solheim, J. E. Talmadge, and R. K. Singh. 2005. Down-Regulation of Vascular Endothelial Cell Growth Factor-C Expression Using Small Interfering RNA Vectors in Mammary Tumors Inhibits Tumor Lymphangiogenesis and Spontaneous Metastasis and Enhances Survival. *Cancer Res.*

125. Kalkunte, S. S., T. F. Mselle, W. E. Norris, C. R. Wira, C. L. Sentman, and S. Sharma. 2009. Vascular endothelial growth factor C facilitates immune tolerance and endovascular activity of human uterine NK cells at the maternal-fetal interface. *J. Immunol.* 182: 4085–4092.

126. Takahashi, A., K. Kono, J. Itakura, H. Amemiya, R. Feng Tang, H. Iizuka, H. Fujii, and Y. Matsumoto. 2002. Correlation of Vascular Endothelial Growth Factor-C Expression with Tumor-Infiltrating Dendritic Cells in Gastric Cancer. *Oncology* 62: 121–127.

127. Shields, J. D., M. E. Fleury, C. Yong, A. A. Tomei, G. J. Randolph, and M. A. Swartz. 2007. Autologous chemotaxis as a mechanism of tumor cell homing to lymphatics via interstitial flow and autocrine CCR7 signaling. *Cancer Cell* 11: 526–538.

128. Issa, A., T. X. Le, A. N. Shoushtari, J. D. Shields, and M. A. Swartz. 2009. Vascular endothelial growth factor-C and C-C chemokine receptor 7 in tumor cell-lymphatic cross-talk promote invasive phenotype. *Cancer Res.* 69: 349–357.

129. Shields, J. D., I. C. Kourtis, A. A. Tomei, J. M. Roberts, and M. A. Swartz. 2010. Induction of lymphoidlike stroma and immune escape by tumors that express the chemokine CCL21. *Science* 328: 749–752.

130. Lund, A. W., F. V. Duraes, S. Hirosue, V. R. Raghavan, C. Nembrini, S. N. Thomas, A. Issa, S. Hugues, and M. A. Swartz. 2012. VEGF-C promotes immune tolerance in B16 melanomas and cross-presentation of tumor antigen by lymph node lymphatics. *Cell Rep* 1: 191–199.

131. Swartz, M. A., and A. W. Lund. 2012. Lymphatic and interstitial flow in the tumour microenvironment: linking mechanobiology with immunity : Abstract : Nature Reviews Cancer. *Nat. Rev. Cancer*.

132. Stack, E. C., C. Wang, K. A. Roman, and C. C. Hoyt. 2014. Multiplexed immunohistochemistry, imaging, and quantitation: A review, with an assessment of Tyramide signal amplification, multispectral imaging and multiplex analysis. *Methods* 70: 46–58.

133. Rubin, M. A., M. P. Zerkowski, R. L. Camp, R. Kuefer, M. D. Hofer, A. M. Chinnaiyan, and D. L. Rimm. 2004. Quantitative determination of expression of the prostate cancer protein alpha-methylacyl-CoA racemase using automated quantitative analysis (AQUA): a novel paradigm for automated and continuous biomarker measurements. *Am. J. Pathol.* 164: 831–840.

134. Väyrynen, J. P., J. O. Vornanen, S. Sajanti, J. P. Böhm, A. Tuomisto, and M. J. Mäkinen. 2012.

An improved image analysis method for cell counting lends credibility to the prognostic significance of T cells in colorectal cancer. *Virchows Arch.* 460: 455–465.

135. Gokhale, S., D. Rosen, N. Sneige, L. K. Diaz, E. Resetkova, A. Sahin, J. Liu, and C. T. Albarracin. 2007. Assessment of two automated imaging systems in evaluating estrogen receptor status in breast carcinoma. *Appl. Immunohistochem. Mol. Morphol.* 15: 451–455.

136. Ong, C. W., L. G. Kim, H. H. Kong, L. Y. Low, T. T. Wang, S. Supriya, M. Kathiresan, R. Soong, and M. Salto-Tellez. 2010. Computer-assisted pathological immunohistochemistry scoring is more time-effective than conventional scoring, but provides no analytical advantage. *Histopathology* 56: 523–529.

137. Hume, D. A., and K. P. A. MacDonald. 2012. Therapeutic applications of macrophage colony-stimulating factor-1 (CSF-1) and antagonists of CSF-1 receptor (CSF-1R) signaling. *Blood* 119: 1810–1820.

138. Biswas, S. K., and A. Mantovani. 2010. Macrophage plasticity and interaction with lymphocyte subsets: cancer as a paradigm. *Nat. Immunol.* 11: 889–896.

139. Ries, C. H., M. A. Cannarile, S. Hoves, J. Benz, K. Wartha, V. Runza, F. Rey-Giraud, L. P. Pradel, F. Feuerhake, I. Klaman, T. Jones, U. Jucknischke, S. Scheiblich, K. Kaluza, I. H. Gorr, A. Walz, K. Abiraj, P. A. Cassier, A. Sica, C. Gomez-Roca, K. E. de Visser, A. Italiano, C. Le Tourneau, J.-P. Delord, H. Levitsky, J.-Y. Blay, and D. Rüttinger. 2014. Targeting tumor-associated macrophages with anti-CSF-1R antibody reveals a strategy for cancer therapy. *Cancer Cell* 25: 846–859.

CURRICULUM VITAE

BORDRY Natacha
Address: 21, chemin de Rovéréaz
CH -1012 Lausanne
Tel: +41 (0)21 652 09 45
Mobile : +41 (0)79 443 32 27
Email : natacha.bordry@unil.ch

Date of birth: May 27th, 1987
Marital status: Single
Nationality: Swiss and French

Education

- **MD-PhD in Cancer Immunology** April 2012-present
  Role of lymphatic vessels in modulating anti-tumor immune response
  Thesis director: Daniel Speiser (UNIL) and Melody Swartz (EPFL)
  Laboratory of Clinical Tumor Immune Biology, UNIL, Lausanne, Switzerland and
  Lymphatic and Cancer Bioengineering Laboratory, EPFL, Lausanne, Switzerland

- **Federal Medicine Degree** October 2011
  Medical Faculty of the University of Geneva, Switzerland

- **Master in Medicine** 2008-2010
  Master thesis title: "Psychiatric impact of living-donor liver transplantation"
  Medical Faculty of the University of Geneva, Switzerland

- **Bachelor in Medicine** 2005-2008
  Medical Faculty of the University of Geneva, Switzerland

- **Scientific Baccalaureate with distinction** 2001-2005
  Rousseau secondary school, Geneva, Switzerland

Technical Skills

- **Computer skills:** Microsoft Office Package, GraphPad Prism, Aperio Imagescope, SPSS, Inform

- **Cellular biology and immunology techniques:** processing of human tumors and secondary lymphoid organs and cells isolation, isolation of peripheral blood mononuclear cells from blood samples (PBMCs), ELISA, ^{51}Chromium (Cr) Release Assay, Flow Cytometry, immunostaining

- **Mouse in vivo techniques:** basic knowledge of anesthesia, intra-peritoneal and intra-dermal tumor injection and immunization with different antigens and adjuvants.

Congress Participations

- **Selected oral presentation**
  - **Bordry N.,** P.O. Gannon, P.G. Foukas, M. Broggi, I. Letovanec, A. Legat, C. Meyer, P. Yan, E. Romano, M. Swartz and D.E. Speiser. *Immune and lymphatic vessel profiling of metastatic lymph nodes of melanoma patients.* **July 2014, The 3rd European MD-PhD meeting, Brunnen, Switzerland**

- **Poster presentations**
  - **Bordry N.,** P.O. Gannon, P.G. Foukas, M. Broggi, I. Letovanec, A. Legat, C. Meyer, P. Yan, E. Romano, M. Swartz and D.E. Speiser. *Immune and lymphatic vessel profiling of metastatic lymph nodes of melanoma patients.* **February 2015, Keystone Symposium Tumor Immunology - Multidisciplinary Science Driving Combination Therapy, Banff, Canada**
  - **Bordry N.,** P.O. Gannon, I. Letovanec, P.G. Foukas, A. Legat, C. Meyer, P. Yan, E. Romano, M. Swartz and D.E. Speiser. *Association of lymphangiogenesis with immune profiles in melanoma patients.* **February 2014, Cellular heterogeneity in the tumor microenvironment, San Diego, USA**

- **Bordry N.,** P. Baumgaertner, C.M. Costa-Nunes, S. Wieckowski, I. Luescher, N. Rufer and D.E. Speiser. *A novel method for the evaluation of the TCR affinity of antigen-specific CD8 T cells of vaccinated cancer patients*. **November 2011**, **Swiss MD-PhD meeting Solothurn, Switzerland**

- **Additional congress participations**
  - **11th International Congress of the Society of Melanoma Research**, **November 2014, Zurich, Switzerland**
  - **European society for medical oncology (ESMO) symposium on immune-oncology**: advances in cancer immunotherapy; from vaccines to antibodies and cell therapies, **November 2013, Geneva, Switzerland**
  - **5th International conference on tumor-host interaction and angiogenesis. June 2013, Ascona, Switzerland**

Publications

- **N. Bordry**, MA Broggi, K. De Jonge. PG. Foukas, E. Danenberg, P.O. Gannon, L. Cagnon, S. Abed Maillard, H. Maby-El Hajjami, I. Letovanec, P. Yan, E. Romano, M.A Swartz and D.E Speiser. *Local and distant immune modulation associated with lymphangiogenesis in melanoma patients* (manuscript in preparation)

- N. Wald, **N. Bordry,** P.G. Foukas , D. E. Speiser and E. Goormaghtigh. *Identification of melanoma cells and lymphocyte subpopulations in lymph node metastases by FTIR imaging histopathology* (Manuscript submitted to BBA-Molecular Basis of Disease)

- N. J. Neubert*, **N. Bordry*,** S. Hoves, C.H. Ries, P. Baumgaertner, S.A. Fuertes Marraco, E. Pavlidou, P. Foukas, D.E. Speiser. *Adaptive immune resistance via CSF-1 produced by melanoma cells* (manuscript in preparation)
  *This author contributed equally to this work

- **N.Bordry** et al, *Pulmonary sarcoid-like granulomatosis after multiple vaccinations of a long-term surviving metastatic melanoma patient,* Cancer Immunol Res. 2014 Dec; 2(12): 1148-53

- **N. Bordry**. *Agenda caché*, Revue Médicale Suisse, 6 octobre 2010; 265; 1892-1893

Prizes and Awards

- **American Association For Cancer Research (AACR) Scholar-In-Training Award** 2014
  Awarded to support attendance at this year's AACR conference in San Diego

- **Theodor and Garbiela Kummer Grant** 2012
  3 year grant awarded for the best young MD-PhD applicant

- **Special prize for the best report of clinical skills in outpatient care** 2008
  Awarded by the Faculty of Medicine of Geneva

Teaching

- **Biology and Medical Faculty of the University of Lausanne (UNIL)** 2012-present
  - Laboratory teaching assistant for medicine and biology undergraduates

- **Medical Faculty of the University of Geneva (UNIGE)**
  - Teaching assistant for the Programme of clinical skills 2010
    Revision course (physical examination of the adult) for 4th year students
  - Teaching assistant for the Programme of clinical skills 2008-2009
    Revision course (cardiology, neurology…) for 2nd and 3rd year students

Internships

- **Clinical internship in Medical Faculty of the University of NSW (Australia)** 2011
  - Four weeks rotation in the department of haematology in Saint-Vincent Hospital

- **Clinical internships in Medical Faculty of the University of Sydney (Australia)** 2011
  - Four weeks rotation in the department of neonatology in Royal Prince Alfred Hospital
  - Four weeks rotation in the department of infectious disease in Royal Prince Alfred Hospital

- **Laboratory of Lymphatic and Cancer Bioengineering, EPFL (Switzerland)** 2010
  Work on roles of tumor VEGF-C and CCL21 in immunological tolerance (four weeks)

- **Surgery internships in Medical Faculty of the University of Montreal (Canada)** 2009
  - Four weeks rotation in the department of cardiac surgery in Hotel-Dieu Hospital
  - Four weeks rotation in the department of orthopaedic surgery in Hotel-Dieu Hospital

- **Centre of the Charity Missionaries of Mother Teresa (Cuzco-Peru)** 2008
  - Immersion course in a community (four weeks)
    Health care and supervision of disabled children

Professional Experiences

- **Substitute Doctor in Geneva University Hospital (HUG)** 2012
  - Four weeks in the department of internal medicine

- **Centre for blood transfusion (Geneva)** 2009-2010
  - Training for doctors specialising in blood donation

- **Association for the Tutoring of Children (ARA, Geneva)** 2008-2010
  - Help in the department of paediatrics of the university hospital of Geneva (HUG)
    Pedagogical activities for the children who are in-patients

- **Cressy Santé Les Bains (Geneva)** 2007-2008
  - Health centre specialised in aquatherapy
    Help for disabled people

- **Association of the Medical Students in Geneva (AEMG)**
  - Member of the international section 2006-2007
    Organization and care of foreign students undertaking training
  - Organization of a workshop in humanitarian medicine (three months) 2006
    Finding funds, logistics and advertising

- **La Tour Hospital (Geneva)**
  - Auxiliary nurse in the maternity hospital (two weeks) 2007
    Reception and first aid given to patients
  - Auxiliary nurse in the department of orthopaedics (four weeks) 2005

- **Forum Meyrin Theatre (Geneva)** 2003-2008
  - Hostess

Languages

French	Mother tongue
English	Fluent (C1 European Language Scale)
German	Good academic standard
Spanish	Basic Knowledge

Interests

- **Travel**
- **Sports** (skiing, climbing, thai-chi, race and swimming)
- **Sciences**
- **Literature**